Structure and Sedimentology of the Dundas Group, western Tasmania.

by

David Selley

B.Sc. (Hons) (University of Adelaide)

Submitted in fulfilment of the requirements for the degree of

Doctor of Philosophy

University of Tasmania
Hobart

April, 1997

This thesis contains no material which has been accepted for the award of any other degree or diploma in any tertiary institution and, to the best of my knowledge and belief, contains no copy or paraphase of material previously published or written by another person, except when due reference is made in the text of the thesis.

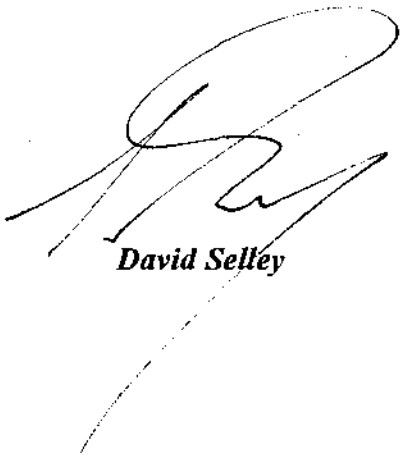

David Selley

ABSTRACT

Middle and Late Cambrian sediments and minor intrusives of the Dundas Group form the western most exposures in the Mt Read volcanic belt of western Tasmania. The Dundas Group comprise at least 2500 m of clastic sediments with rare pumice-bearing quartz and feldspar-phyric volcaniclastics, minor quartz-feldspar porphyritic intrusives and andesitic to dacitic lavas. Volcanogenic deposits become less abundant towards the western limits of the unit, where lithologies are characterised by thick polymict conglomerate packages which occur intercalated with mudstone and thinly bedded sandstone. Structural and stratigraphic complexities of the Dundas area, with particular emphasis on the Dundas Group, provide the focus of this study.

The provenance of the Dundas Group is linked to the presently exposed basement lithologies and coeval volcanics. These include the tholeiite dominated Crimson Creek Formation, boninites, gabbros and peridotites of the Serpentine Hill Complex, older mature meta-sandstones, and the volcanics of the Mount Read volcanic 'arc'. All these sources were detected in the conglomerates and sandstones of the Dundas Group. Suite 1 samples are dominated by Crimson Creek Formation with some contamination from mature sedimentary rocks and the mafic/ultramafic complexes. Suite 1B samples have been identified as Crimson Creek Formation rather than Dundas Group on the basis of their provenance. Suite 2 samples have been derived from the mafic/ultramafic complex and a felsic source. Suite 3 has a broad range of compositions consistent with thorough mixing of detritus derived from two or more sources. Suite 4 samples are mature sandstones which have a metasedimentary source. The distinction of Dundas Group suite 4 samples from the basement sandstones is very difficult with presence of distinctive traces of chromite very useful in recognising the younger Dundas Group sandstones. Suites 1B and 4 sandstones from the eastern zone have been tentatively identified as basement lithologies faulted up within the footwall of the Rosebery Fault.

Deposition of suite 3 siliciclastics occurred during the middle Middle Cambrian in the western area, but continued into the earliest Late Cambrian in the central area. During the latter period, suite 1A sediments were being deposited along the western margin of the basin, whereas coeval finer-grained suite 3 sediments occupied central or eastern portions of the basin. This asymmetry in lithofacies distribution from west to east reflects proximal derivation of suite 1A conglomerates and sandstones from rapidly uplifted basement sources to the west, with supply of thoroughly mixed sediment to the east.

The western-most exposures of the Dundas Group involve petrographically and chemically similar conglomerate-greywacke-mudstone successions which crop out at Dundas and at Que River to the north. These range in age from latest Middle Cambrian to probable Late Cambrian and represent a marked change in basin geometry characterised by rapid basement uplift. This phase of tectonism and associated sedimentation is coeval with the onset of thrusting and molasse-type Owen Conglomerate deposition further to the

east. In the western parts of the Mt Read volcanic belt, however, basin subsidence and quiescent marine sedimentation persisted until the middle late Cambrian. This asymmetry in facies architecture and basin evolution across the Mt Read volcanic belt corresponds to diachronous Late Cambrian E-W and downwarping of thin continental crust to the west of an advancing fold and thrust belt.

The earliest deformation recognised in the Dundas Group (D_1) is characterised by pre-lithification deformation features which include coherent slides along bedding parallel surfaces, chaotic zones of liquefaction, brittle fault zones and slump folds. These structures relate to syn-sedimentary seismic shock and/or gravitational collapse following basin-floor tilting.

Regional cleavage development and upright, open to tight folding correspond to the earliest phase of Middle Devonian orogenesis (D_2) . The S_2 cleavage is the dominant penetrative fabric developed throughout the Dundas region. Mesoscopic and macroscopic folds related to S_2 are upright to moderately inclined and shallowly to moderately plunging, however the trend of hinge lines is quite variable, ranging from NNW-SSE to NE-SW. The S_2 cleavage is almost always non-axial planar. The cleavage transection is interpreted to be the result of imposition of an ENE-WSW directed D_2 shortening axis on an earlier, pre-D_2 generation of NNE- to NE-trending mesoscopic and macroscopic folds. The pre-D_2 folds generation is tentatively correlated with a regionally developed phase of Late Cambrian E-W to NE-SW compression.

Structural relationships in the Dundas region are most complicated towards the east and culminate in tightly folded and disrupted strata positioned within the footwall of the Rosebery Fault. These rocks are characterised by the dissection of a N-S trending upright folds by an anastomosing array of steeply dipping shear zones. Where shear zones were developed in originally well stratified lithotypes with marked competency contrast, melange-type textures have formed. Domains of melange-type deformation are well exposed in the Ring River. The dominant texture common to all disrupted units is partially to completely fragmented sedimentary layers enclosed within a fine-grained and frequently fissile argillaceous matrix. Partitioning of strain and variation of deformation styles throughout the disrupted domains occurs primarily as a function of the original sedimentary lithotypes. Three broad mesoscopic styles are defined: i) "high strain" phacoid zones , ii) domains of large-scale boudinage and pinch-and-swell structure and iii) chaotic block-in-matrix structure. Bulk flattening-type strains in the Ring River melange is indicated by chocolate tablet boudinage structure and development of orthogonal extensional vein generations. The favoured interpretation for the development of the Ring River melange is the tightening and rotation of upright, shallowly plunging, NNE- to NE-trending pre-D_2 folds during oblique imposition of NNW to N striking D_2 slaty and spaced cleavages.

The melange textures formed under conditions of intense flattening strains, low effective confining pressure , marked competency contrast and relaxation of along strike boundary constraints to allow stretching in two directions. These conditions are common in accretionary environments but are not restricted to them. Similar conditions can occur in other upper crustal locations and produce melange from well-consolidated ancient rocks. The spatial relationships in the Ring River and throughout the eastern part of the Dundas region provide no support for the model that this melange was developed in an accretionary environment as suggested by Corbett and Lees (1987).

Four principal contentious issues are addressed here. Firstly the nature of the lower contact of the Dundas Group in the Ring River. This locality has been singled out as a critical test for one of the favoured tectonic models for western Tasmania. The work provided here indicates that this is a normal nonconformable contact as required by this model. The second major issue is the distribution of basement lithologies faulted into the eastern part of the map area. Major advances in the recognition of these blocks was produced by the detailed provenance studies. Thirdly, historical difficulty in constructing a coherent vertical and lateral stratigraphy in the Dundas region has been attributed to deposition within a series of sub-basins, which were periodically isolated from one another and derived material from different sediment dispersal systems. Finally the nature and significance of the melanges and disrupted zones along the Rosebery tectonic zone was given very detailed attention and the model that they are sufficient evidence to suggest a suture zone has been disproved.

Acknowledgments

The work presented here would not have been possible without the support and guidance of my supervisor Dr Ron Berry. Throughout the final year of this project, the amounted of time and energy Ron has dedicated to me will probably never be repaid. I give you my most warmest thanks. Thanks also go to the remaining academic staff of the Geology Dept., University of Tasmania for stimulating discussions and interest in my work. Particular acknowledgment must go to Drs Paul Kitto, Stuart Bull, Tony Crawford, Michael Roach and Richard Keele who have helped me significantly at various times during the course of this study.

To my dear friends from C461* - who I miss very much, thanks for helping make this a very pleasant period of my life.

Interest in my work from geologists at the Tasmanian Department of Mines has been greatly appreciated and in particular I would like to thank Drs Tony Brown and Keith Corbett who have provided me with their time and expertise on western Tasmanian geology.

Expert technical assistance from Simon Stevens, Nathan Duhig, June Pongratz, Nilar Hlaing, and Phil Robinson as well as the administrative brilliance of Christine Higgins, Peter Cornish and Jeanette Harris has made working here very pleasant.

Special thanks go to all my fellow students for their friendship support and encouragment over the years.

Finally, to my family: Corin, my parents, my brother and sister, whose love, understanding and faith has been absolute, I am always endebted.

TABLE OF CONTENTS

LIST OF FIGURES

LIST OF TABLES

Chapter 1
Introduction and Regional Geology

1.1 Aims and scope of study

The Middle to Late Cambrian Dundas Group represents a key element in the lithostratigraphic framework of western Tasmania. The complex structures and depositional patterns characterised by this succession of sedimentary rocks have been long reported and remain of considerable interest to geologists working in this region. Moreover, structural and stratigraphic relationships inherent to Dundas Group have been used to bolster a variety of geological models for the Early Palaeozoic evolution of western Tasmania. The aim of this project therefore is to document the structural and sedimentological aspects of the Dundas Group in order to test some of these evolutionary models and to better constrain depositional systems during Middle and Late Cambrian basin development. The Dundas region was chosen as the principal area of study, partly in that it contains a near complete section of richly fossiliferous Middle and Late Cambrian strata, but also in that relationships with older strata are well-represented.

The geographic location of the Dundas region and its position with respect to the major Late Proterozoic to Late Cambrian lithostratigraphic elements of western Tasmania are shown in Figure 1.1. Also shown are the locations of two smaller areas investigated during this study which involve northern and southern extensions of the Dundas Group.

Presented in this thesis are the results from mapping of the aforementioned areas at scales of between 1:200 and 1:25,000. Detailed mapping has been supplemented by a geochemical provenance study of Dundas Group sediments as well as a selection of pre-Dundas Group lithotypes. As the Dundas region has been extensively mapped by previous workers, certain key problems which have arisen from these studies were addressed in detail. Interest has focused on sediment dispersal patterns in the Dundas Group and the tectonic significance and conditions of deformation associated with domains of melange.

1.2 Access and Exposure

Field areas are characterised by rugged, densely vegetated terrain and outcrop is sparse. Fresh outcrop is generally restricted to river or creek sections and a few small cliff and ridge-top exposures. The section along the Ring River, located in the northern part of the Dundas region, in particular provided excellent exposure. Numerous

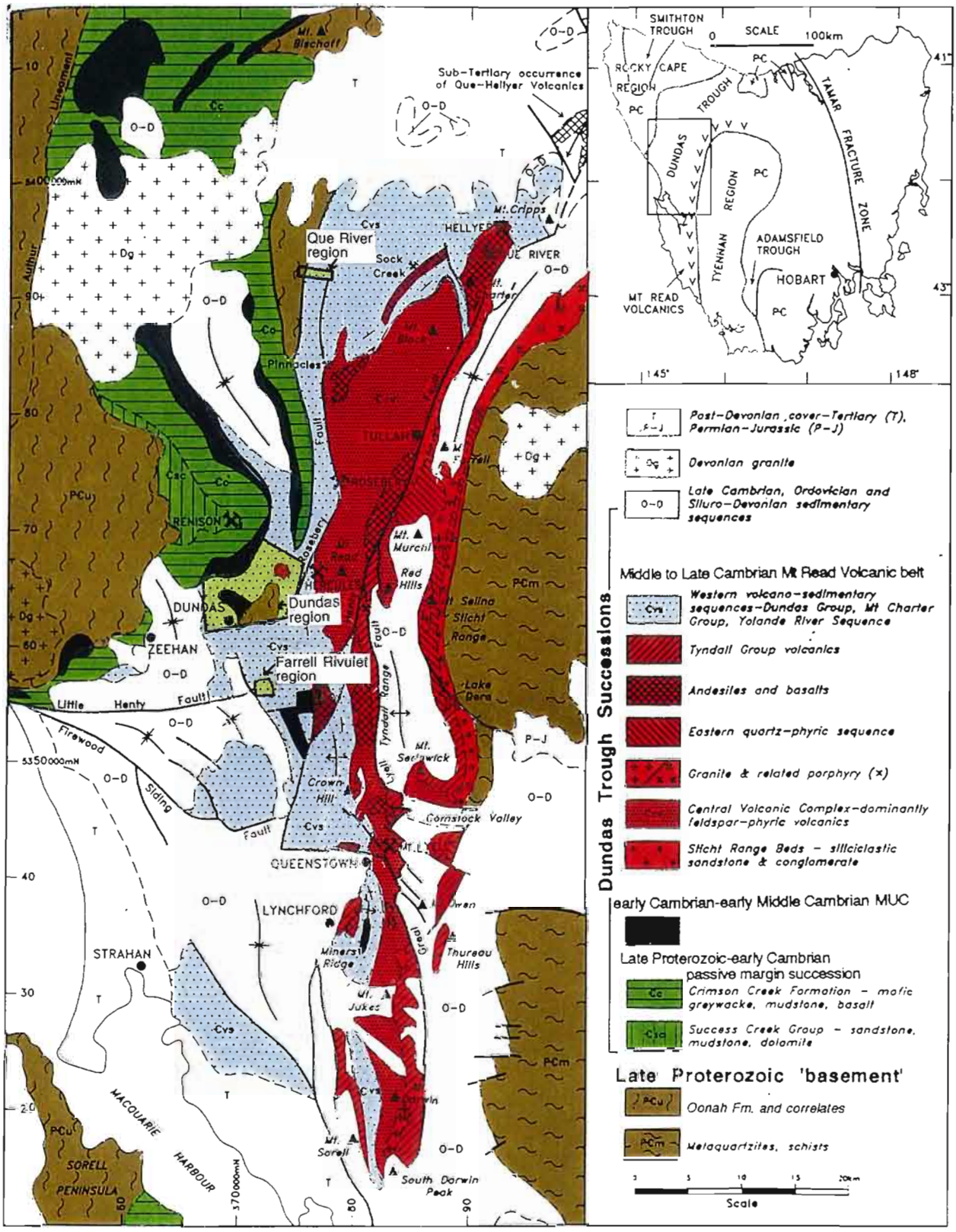

Figure 1.1 Map showing Late Proterozoic to Late Cambrian lithostratigraphic elements of the Dundas Trough. Field areas included in this study are highlighted in pale green: 1) Dundas region, 2) Que River region, 3) Farrell Rivulet region. (modified after Corbett, 1992)

exploration tracks and tram cuttings provide access and additional exposures, however these usually suffer from intense weathering.

1.3 Regional Geology

The geology of western Tasmania is very complex. Although there has been significance advances in our understanding of the Late Proterozoic - Early Palaeozoic lithostratigraphic and tectonic framework over the past 20 years, many aspects are still in contention. This summary is drawn from some of the more recent discussions and reviews (eg. Williams, 1978; Brown, 1986; Turner, 1989; Corbett, 1992; Crawford and Berry, 1992; Berry, 1994; Turner et al., 1994) and focuses primarily on the lithologic associations relevant to the western margin of the Dundas Trough. The Cambrian time-scale employed in this thesis is that presented in Laurie et al (1996).

1.3.1 Late Proterozoic elements ("basement")

Rocks of the Tyennan and Rocky Cape regions are situated to the east and west of the Dundas Trough respectively (Fig. 1.1) and have traditionally been considered to represent basement in western Tasmania. They involve poly-deformed and metamorphosed strata of dominantly sedimentary origin. Metamorphic grade is generally limited to lower greenschist facies, however upper greenschist to eclogite facies rock associations occur locally within the western portion of the Tyennan region (Fig. 1.1). Age constraints on the rock associations in these regions are based on radiometric dating. Rb-Sr model ages of 1100-1150 Ma from the less metamorphosed portion of the Tyennan region are likely to correspond to the depositional ages (Raheim and Compton, 1977). Only an upper limit for the age of shallow marine sediments of the Rocky Cape Group is available (760 ± 16 Ma), which is constrained by syn-orogenic granites which have intruded lithostratigraphic correlates on King Island (Turner et al., 1994). This date also represents the age of the oldest tectono-metamorphic event unequivocally recognised in rocks west of the Dundas Trough (Berry, 1994). Although uncertainty has existed, peak metamorphism and early deformation in the Tyennan region has been generally been attributed to the same period of deformation. However, a recently obtained ion probe zircon age of 502 ± 8 Ma for the timing of metamorphism in the high grade rock associations of the Tyennan region (Turner et al., 1994) has refuted this. The marked contrast in strain and metamorphic grade between these rocks and similarly aged sequences of the Dundas Trough has now led workers to suggest that either the high grade portions (Berry, 1994) or the entire Tyennan region is therefore exotic (Lees and Wright, 1994).

The Rocky Cape Group is unconformably overlain by younger Late Proterozoic proximal turbidites of the basal Ahrberg Group. Turner et al (1994) suggested these to be chrono-stratigraphic equivalents of deeper water turbiditic packages within the Oonah and

Burnie Formations. The latter is defined from north coast of Tasmania and its age is derived from synsedimentary dolerite dykes (Cooee Dolerite) which are dated by K-Ar at 725 ± 35 Ma (Crook, 1979). The Oonah Formation is most relevant to this study and crops out in the Pieman River and Zeehan districts where Brown (1986) recognised a 'lower' sandstone-mudstone succession and an 'upper' dolomitic-mudstone-volcanic succession. Correlates of the Oonah Formation have also been recognised as inliers within Dundas Trough sequences at Dundas (Blissett, 1962) and in the Ramsay River area (Brown, 1986). Up to six episodes of deformation occur locally, the first two of which involve recumbent isoclinal folding (Findlay, 1993). The recumbent fold generations within the Oonah Formation and its correlates have been attributed to the Penguin Orogeny. There is some argument however, as to the age of this event. Traditionally, the Penguin Orogeny has been considered to be of Late Proterozoic age as recumbent folding is not apparent in the overlying Late Proterozoic-Early Cambrian succession. Turner et al., 1994 on the other hand, regard the 500 ± 10 Ma metamorphic ages derived from Arthur Metamorphic Complex as representing the timing of the Penguin Orogeny.

1.3.2 Dundas Trough Successions

Sequences of the Dundas Trough are described herein in terms of a broad four-fold 'stratigraphy': 1) Late Proterozoic - Early Cambrian passive margin succession, 2) late Early to early Middle Cambrian mafic-ultramafic complexes, 3) Middle - Late Cambrian Mt Read volcanic belt, 4) Late Cambrian - Early Ordovician molasse-type succession (Owen Conglomerate and litho-stratigraphic correlates).

1.3.2.1 Late Proterozoic - Early Cambrian passive margin succession

The Success Creek Group and the conformably overlying Crimson Creek Formation form the basal sequence of the Dundas Trough (Fig. 1.1). They represent a period of passive margin sedimentation and tholeiitic volcanism during extension and rifting of the underlying continental crust (Crawford and Berry, 1992).

The relationship between the Success Creek Group and the underlying Oonah Formation is unclear. Whereas Brown (1986) has argued that the contact is unconformable, more recent mapping of the type area by Findlay (1993) has suggested that it is faulted. They do concur however, that generally higher degrees of structural complexity and grain suturing within the Oonah Formation provides evidence of a depositional and structural hiatus between the two units. The Success Creek Group passes upward through dominant micaceous quartz arenite with minor conglomerate and tuffaceous horizons into a shallow water succession involving thinly bedded siliceous siltstone, laminated mudstone, stromatolite-bearing dolomitic siltstone, chert and carbonate horizons. The latter provide the locus for Devonian tin mineralisation at the Renison Bell Mine. Deformation within at least one portion of this sequence has

produced a distinctive 'melange-type' fabric. Brown (1986) considered that part of this deformation occurred prior to sediment consolidation and argued that it indicated deposition on an unstable shelf, probably at the margin of a rapidly subsiding basin.

The transition from the Success Creek Group to the overlying Crimson Creek Formation is marked by the reduction of siliciclastic basement-derived detritus and the onset of tholeiitic volcanism. The latter consists of up to 5000 m of volcanogenic lithicwacke, basalt flows, laminated siltstone and mudstone (Brown, 1986). Gabbroic bodies with similar tholeiitic affinities to the lavas have been reported to intrude the sequence at the Renison Mine (Patterson, 1979). Evaporite pseudomorphs within several siltstone units indicate that the shallow water environment of the Success Creek Group continued during the deposition of the Crimson Creek Formation (Haines, 1991).

1.3.2.2 Late early Cambrian - early Middle Cambrian mafic-ultramafic complexes

Mafic-ultramafic complexes (MUC) crop out as discontinuous and commonly fault-bounded bodies throughout the western portion of the Dundas Trough (Fig. 1.1). They tectonically overlie correlates of the Crimson Creek Formation and at several localities exhibit basal mylonitic amphibolites which reveal consistent westward transport directions (Berry, 1989). They are dominated by serpentinised massive and layered cumulate assemblages, however two lava associations are also locally recognised; a low-Ti tholeiitic suite and a high-Mg andesite (boninite) suite (Brown, 1986). In the Heazlewood River MUC west of Waratah, these rock associations are intruded by tonalites, from which an ion probe zircon age of 510 ± 6 has been obtained (Kimbrough and Brown, 1992).

The significance of the MUC in terms of the Early Palaeozoic evolution of western Tasmania has long been in contention (see Corbett and Turner, 1989 for a review). The most recent and widely accepted model for their origin is that of Berry and Crawford (1988) (also Crawford and Berry, 1992), who proposed that the MUC represent slices of allochthonous intra-oceanic forearc crust that were emplaced onto the Late Proterozoic passive margin sequence during an arc-continent collisional event. A late Early to early Middle Cambrian age for this period of orogenesis is suggested from the first appearance of MUC-derived detritus within Middle Cambrian sedimentary rocks of the Dundas Group. This age also corresponds well with the iron probe zircon age of 502 ± 8 Ma for metamorphism in the high grade portions of the Tyennan region.

1.3.2.3 Middle and Late Cambrian sequences from the western Mt Read Volcanic belt

The Middle to middle Late Cambrian Mt Read volcanic belt occupies the eastern portion of the Dundas Trough and extends northward from Elliot Bay on the southwest coast to the Hellyer Mine region (Fig. 1.1). It involves a rapidly accumulated succession of basaltic to rhyolitic volcanic and intrusive rocks, which are flanked to the west by a

thick sedimentary rock-dominated sequence. Calc-alkaline trends characterise the greater volume of volcanic and intrusive rocks, which comprise transitional medium to high K, high K, and shoshonitic associations. Crawford et al (1992) have argued that these associations, and in particular the generation of shoshonitic basalts, are indicative of post-collisional magmatism. A volumetrically subordinate association of tholeiitic intrusive rocks and minor lavas (eg. the Henty dyke swarm) were emplaced during the waning stages of magmatism in the Dundas trough (Crawford et al., op cit.).

The geology of the belt is best known between Queenstown and Hellyer Mine, where it comprises four principal lithostratigraphic units (Corbett, 1992). Those which are restricted to the east of the Henty Fault include *Eastern quartz-phyric sequence* rhyolitic to dacitic lavas, volcaniclastics and quartz-feldspar porphyritic intrusives of probable middle Middle Cambrian age, and late Middle to early Late Cambrian volcaniclastics and minor rhyolitic lavas of the *Tyndall Group*. The central part of the belt is dominated by sub-aqueously deposited feldspar-porphyritic lava rich volcanics, pumiceous volcaniclastics and rare sedimentary horizons of the *Central Volcanic complex* (CVC). Flanking the western margin of the CVC is the *western volcano-sedimentary sequence* (WVS), parts of which form the principal focus of this study. The WVS comprises a lithologically diverse association of dominantly siliciclastic and volcaniclastic sedimentary rocks. Rapid lateral variations of sedimentary facies and provenance characteristics are common throughout this sequence and have historically hampered geologist's attempts to make regional litho-stratigraphic correlations. As a result, the WVS presently encompasses a series of litho-stratigraphically and geographically distinct rock packages, which have been grouped together primarily on the bases of their volumetrically significant component of sedimentary lithofacies and Middle to middle Late Cambrian fossil age control. Litho-stratigraphic units of the WVS include the Dundas Group (Elliston, 1954), the Huskisson Group (Taylor, 1954), the Rosebery Group (Taylor op cit.), the Yolande River sequence (no formal stratigraphic definition; name first introduced by Calver et al., 1987) and the Mount Charter Group (Corbett, 1992). A time-space diagram which illustrates the relative positions of these units as well as their relationship with underlying and overlying litho-stratigraphic units is shown in Figure 1.2. The Dundas Group includes western-most exposed strata of the Mt Read volcanic belt and is significant in that it unequivocally spans biostratigraphic stages from Undillan (Middle Cambrian) to Iverian (middle Late Cambrian). According to Elliston (op cit.), the Dundas Group includes all Middle to Late Cambrian rocks contained in the Dundas region (Fig. 1.1). More recent mapping in this area by Corbett and Lees (1987) has shown that the eastern margin of the Dundas region is defined by a major east-dipping fault which was active during Devonian orogenesis as a westerly-directed thrust (the Rosebery Fault). The Dundas Group comprises at least 2500 m of turbidite-dominated sedimentary rocks with rare pumice-bearing quartz and feldspar-phyric volcaniclastics,

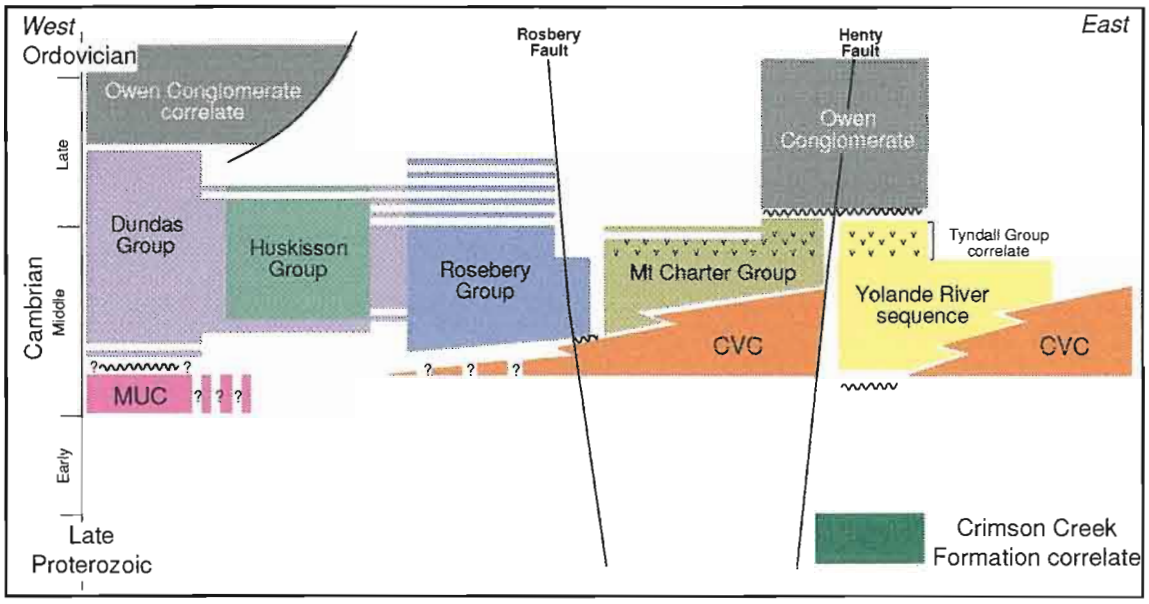

Figure 1.2 *Time-space diagram showing distribution of the western volcano-sedimentary sequence. Underlying and overlying packages for each litho-stratigraphic unit are show where demonstrable. Modified from Seymour and Calver (1995).*

minor quartz-feldspar porphyritic intrusives and andesitic to dacitic lavas. Volcanogenic deposits become less abundant towards the western limits of the succession, where lithologies are characterised by thick polymict conglomerate-massive sandstone packages which occur intercalated with mudstone and thinly bedded sandstone. In the west of the Dundas region, unfaulted contact relationships of the Dundas Group with both the underlying MUC and the overlying late Late Cambrian-Early Ordovician molasse-type succession are demonstrable (Fig. 1.2). The upper contact of the Dundas Group was considered by Brown (1986) to be gradational with overlying late Late Cambrian strata. The nature of the basal contact relationship with MUC is contentious and was considered by Rubenach (1974) as unconformable whereas more recent work by Brown (1986) documented an interfingering relationship between basal conglomerates of the Dundas Group and low-Ti lavas of the MUC. The significance of this basal relationship together with new data collected during this study are discussed in more detail in Chapter 2. Less complete sections of the Dundas Group occur to the east of the Dundas region, where boundary relationships are poorly constrained.

Immediately north of the Dundas region, bio- and litho-stratigraphic equivalents of the Dundas Group include the Huskisson and Rosebery Groups (Fig. 1.2), both of which were formally defined within the footwall of the Rosebery Fault. Corbett and Lees (1987) however, have mapped litho-stratigraphic equivalents of the basal formation of the Rosebery Group within the hangingwall of the Rosebery Fault south of Hercules Mine (Fig. 1.1). In contrast to the western exposures of the Dundas Group which lie upon an MUC basement, Corbett and Lees (op cit.) interpreted an unconformable relationship at the base of Rosebery Group correlates positioned east of the Rosebery Fault with underlying CVC. Although the base of the Rosebery Group is never exposed west of the

Rosebery Fault, the litho-stratigraphic correlation of the basal formation across this structure lends support to the inference that Middle to Late Cambrian strata positioned in the immediate footwall of the Rosebery Fault (including the eastern members of the Dundas Group) were laid down on a CVC substrate (Fig. 1.2).

The Mt Charter Group and Yolande River sequence are positioned west of the Henty Fault in the Que-Hellyer region and east of the Henty Fault in the Queenstown region respectively (Fig. 1.2). Both units can be distinguished from WVS units further to the west by their basal interdigitating relationships with the CVC and on a litho-stratigraphic basis by the presence of a thick volcaniclastic package towards their tops. The latter were considered by Corbett (1992) and White and McPhie (1996) to represent lithostratigraphic correlates of the Tyndall Group. Furthermore, appearance of the overlying molasse-type sequence occurs significantly earlier in these eastern regions, with gradational upper boundaries of the WVS indicated by fossil evidence as probable early Late Cambrian.

1.3.2.4 Late Cambrian - Early Ordovician molasse-type sequences

The Late Cambrian - Early Ordovician Denison Group is defined from the Denison Range in south-central Tasmania. Litho- and bio-stratigraphic correlates in the Dundas Trough include siliceous conglomerate and sandstone of the Owen and Zeehan Conglomerates which are distributed along the eastern and western margins of the Mt Read volcanic belt respectively. As alluded to in the previous section, the base of the conglomeratic succession is diachronous, younging from early Late Cambrian in the east, to late Late Cambrian in the west.

Deposition of the Owen Conglomerate and correlates reflects rapid emergence of Precambrian basement terrains, which form the principal sources of detritus in these units. Extremely rapid thickness changes in addition to local unconformities both at the base and within the Owen Conglomerate attest to the tectonically active environment of deposition.

1.3.3 Lower to Middle Palaeozoic tectonic development of the Dundas trough

The Early and Middle Palaeozoic succession of western and northern Tasmanian records at least two major periods of tectonic activity: 1) a prolonged and complicated Cambrian 'event', which pre-dated, was synchronous with, and post-dated the development of the Mt Read volcanic belt, and 2) the Middle Devonian Tabberabberan Orogeny.

1.3.3.1 Cambrian orogenesis

Over the past 10 years, focus has moved from the more obvious and widespread effects of Devonian orogenesis to rigorous analysis of the largely obscured Cambrian

deformation (Corbett and Lees, 1987; Berry and Crawford, 1988; Berry, 1989; Crawford and Berry, 1992; Leaman, 1992; Turner, et al. 1992; Woodward et al., 1993; Berry and Keele, 1993; Berry, 1994; Gray and Woodward, 1994; Lees and Wright, 1994). Analytical techniques employed by these workers to deduce the tectonic history during the Cambrian have been varied and have included mesoscopic and macroscopic structural analysis, gravity and magnetic geophysical modelling, analysis of geochronological data, investigation of igneous petrogenesis and sedimentological and volcanological facies architecture. The combined results of these studies has revealed a Cambrian 'event', which in its infancy at least, produced a thin-skinned structural framework and the amalgamation of Late Proterozoic to early Middle Cambrian allochthonous units and Late Proterozoic autochthonous continental basement during a phase of broadly W- to SW-directed thrusting.

Although a tectonically active setting for the development of the Mt Read volcanic belt is indicated by numerous, localised Middle and Late Cambrian unconformities (see Corbett and Turner, 1989), rapid vertical and lateral facies changes and ubiquitous soft sediment deformation, very few major structures have been identified which are unequivocally of Cambrian age. This problem of identifying Cambrian structures can be attributed principally to the strong tectonic overprint of the Middle Devonian orogeny and has fuelled contention surrounding the relative timing of shortening phases and the tectonic environment of the Dundas trough. Three recently proposed models for the tectonic evolution of the Cambrian succession in western Tasmania are outlined below.

I Dundas trough suture zone model (Green, 1983; Corbett and Lees, 1987)

Corbett and Lees (1987) proposed that the Middle to Late Cambrian portion of the Dundas trough developed as a forearc-arc sequence above an easterly dipping subduction zone between the Rocky Cape region to the west and the Tyennan region to the east. The 'Dundas Group' (WVS in the stratigraphic nomenclature used in this thesis) was considered as a forearc sequence accumulated within a depression flanking the Mt Read 'arc' to the east. Older Dundas trough sequences including the Crimson Creek Formation and MUC were interpreted as accreted remnants of an oceanic island arc which related to an older phase of westerly-directed subduction and in part formed basement to the younger Middle to Late Cambrian forearc sequence. Volcanism ceased during the Late Cambrian in response to collision of the Tyennan and Rocky Cape regions. Evidence of deformation associated with this E-W directed collisional event was thought to be manifested in a structurally anomalous high strain zone presently positioned within the footwall of the Rosebery Fault, involving tectonically interleaved slices of 'Dundas Group', Crimson Creek Formation, MUC and Precambrian basement. Corbett and Lees (op cit.) equated the structural style within this high strain zone with modern subduction-

related melanges and interpreted it to reflect underthrusting of the forearc sequence beneath the volcanic arc.

In general, this model no longer receives wide support, with criticisms including: i) lack of evidence for a pre-middle Middle Cambrian ocean basin that was wide enough to allow for the several hundred kilometres of subduction required to generate the Mt Read volcanic 'arc' (Corbett and Turner, 1989), ii) chemical affinities of the Mt Read volcanic 'arc' are inconsistent with those magmas produced in modern supra-subduction zone settings (cf. Crawford and Berry, 1992) and iii) the Late Cambrian timing for collision and emplacement of the MUC is inconsistent with the appearance of MUC-derived detritus in Middle Cambrian sedimentary rocks (Berry and Crawford, 1988). The nature and significance of the "melange-type" deformation within the footwall of the Rosebery Fault, however, has never been adequately addressed. As this structural domain represents one of the few documented of loci of Cambrian deformation in western Tasmanian, it clearly requires closer attention. Accordingly, examination of "melange-type" deformation in the Dundas region is a principal focus of this study, results of which are presented in chapter 5.

II Late Early-early Middle Cambrian arc-continent collisional model (or "allochthon model" of Berry and Crawford 1988)

At present, the most widely accepted interpretation for the development of the Cambro-Ordovician Dundas trough is based on a tectonic model originally presented by Berry and Crawford (1988), which has been progressively refined in a series of subsequent publications: Crawford and Berry (1992), Berry and Keele (1993), Crawford (1994) and Berry (1994). This model envisages a protracted history of orogenesis and basin development involving: i) late Early to early Middle oceanic island arc-continent collision during which allochthonous slices of MUC and high grade Precambrian terrains were emplaced above W- to later S-directed thrusts onto thinned, Late Proterozoic crust of the eastern Australian continent; ii) middle to late Middle Cambrian E-W extension which resulted in rapid subsidence of the Dundas trough, isostatic rebound of the Tyennan region and coeval post-collisional magmatism and VHMS mineralisation of the Mt Read volcanic arc; iii) Late Cambrian E-W compression and basin closure which resulted in inversion of middle Middle Cambrian growth faults, emergence of the Tyennan region and accumulation of the molasse-type succession within actively forming synclinal fold cores.

A fundamental problem with this model surrounds the proposed allochthoneity of the MUC. In order to explain the apparent interfingering relationship between the MUC and the basal Dundas Group interpreted by Brown (1986) (see section 1.3.2.3 and Chapter 2), Berry and Crawford (1988) argued that part of the Dundas Group may also be an exotic fragment of oceanic fore-arc material. Corbett and Turner (1989) however,

indicated that no conclusive evidence for allochthoneity of the Dundas Group exists and indeed, provenance characteristics of Dundas Group indicates that detritus was derived from autochthonous terrains.

III Middle to Early Ordovician foreland basin model (Lees and Wright, 1994)

A variation on the "allochthon model" was proposed by Lees and Wright (1994). These workers considered that shortening continued more or less continuously throughout the Early Cambrian-Late Cambrian and involved initial obduction of the MUC onto an autochthonous, rifted Late Proterozoic continental basement, followed by collision of the Tyennan region, which they also considered to be allochthonous. Formation of the Mt Read volcanic belt immediately followed the initiation of thrusting and accumulated in a foreland basin or possibly a series of piggy-back basins. The Late Cambrian molasse-type succession, they contested, heralds emergence of the Tyennan region, which was uplifted along a major mylonite zone at the eastern margin of the Mt Read volcanic belt.

The main differences then, between the model of Lees and Wright (1994) and Crawford and Berry (1988), surrounds the tectonic evolution of the Mt Read volcanic belt and the allochthoneity of the Tyennan region. Although Lees and Wright (op cit.) envisaged minor extensional phases during the late Middle Cambrian as evidenced by the emplacement of the tholeiitic Henty dyke swarm, an overall compressional setting was inferred. With limited constraints on the geometry and movement history on potential basin-bounding Cambrian faults, it is difficult to distinguish between a gross extensional or compressional environment for the development of the Mt Read volcanic belt. In support of an extensional setting is the persistence of sub-wave basin marine sedimentation and voluminous volcanism, neither of which are typical of collision-related foreland basin infills (cf. Allen et al., 1986; Miall, 1995). On the other hand, Allen et al. (op cit.) recognised that if collision followed a phase of significant crustal thinning (as was proposed in both models **II** and **III**), foreland basin sedimentation may remain sub-marine throughout the main period of basin development, with molasse-type sedimentation reflecting emergence of the orogenic belt, recorded only in the final stages.

1.3.3.2 Devonian Orogenesis

The principal phase of folding and cleavage development in the Mt Read volcanic belt occurred during Middle Devonian orogenesis (Williams, 1978; 1989; Seymour, 1980; Berry; 1994). Regional metamorphic grade associated with this period of orogenesis is prehnite-pumpellyite facies, however localised sub-greenschist facies metamorphism occurs adjacent to syn-orogenic granite bodies (Berry, op cit.). The structural style of the Middle Devonian orogen is complex and involves the interplay of major steeply- to moderately-dipping brittle-ductile fault zones and high wavelength upright to locally inclined, open to tight folds. Major faults form the loci for intense cleavage and brittle

fracture development, the latter recording prolonged and complex movement histories (eg. Berry, 1989). Those faults which have accumulated significant reverse and sub-ordinate strike-slip displacements during the Middle Devonian include the meridionally-striking Rosebery and Henty Fault zones which effectively dissect the Mt Read volcanic belt (Figs. 1.1 and 1.3). These two structures and have been interpreted by Berry and Keele (1993) to converge onto a common shallowly-dipping, W-directed sole thrust at approximately 5km depth. The structural domain between the Rosebery and Henty Fault zones has been uplifted during the Middle Devonian relative to neighbouring structural domains and presently exposes a window which contains the stratigraphic lowest portions of the Mt Read volcanic belt (predominantly CVC: Fig. 1.3). North of the Dundas region and approximately 5km west of the Rosebery Fault, a broad N-S striking zone of reverse faulting has emplaced inliers of Late Proterozoic strata and slices of MUC within the Lower Palaeozoic succession (Corbett and McNeill, 1988; Selley, 1992a; Berry and Keele, op cit.). E-W to WNW-ESE striking faults occur as major structures to the west and southwest of the Dundas region (Fig. 1.1).

The geometry and morphology of Middle Devonian folds are complex and variable. In the Dundas trough, major folds are oriented up to 30° clockwise and anticlockwise of a dominant NW- NNW-trend and possess sub-horizontal to sub-vertical plunges. They are characteristically non-cylindrical and are commonly transected (usually in an anticlockwise sense) by associated cleavages. Berry and Keele (1993) argued that the variation in fold orientation coupled with cleavage transected and non-cylindrical geometries were in part, at least, a consequence of non-coaxial interference between Middle Devonian (ENE-WSW compression) and pre-cleavage (probably Late Cambrian: E-W compression) strain axes. Rather than widespread nucleation of new folds during the earliest phase of Devonian orogenesis, these workers considered that many regionally developed folds were simply tightened Late Cambrian structures. An alternative explanation for variable fold orientation and cleavage transected fold geometries was offered by Selley (1992b). On the basis of detailed examination of progressively tightened and rotated mesoscopic folds adjacent to WNW-striking sinistral fault zones, Selley (op cit.) argued that larger scale folds were potentially nucleated, modified and ultimately cleavage transected during a single, non-coaxial (ie. rotation) deformation with an ENE-WSW directed far field maximum compressive stress.

Immediately following, or late in the phase of NW- to NNW-trending fold and cleavage development, the Dundas trough and younger sequences were intruded by relatively shallow level I- and S-type granitoids (Williams, 1989). Deformation associated with granite emplacement is relatively minor in western Tasmania, however a notable exception occurs immediately northwest of the Dundas region. Forceful emplacement of the largely unexposed Pine Hill Granite produced a complex domain of brittle extensional faults which provided conduits for magmatic-hydrothermal fluids and

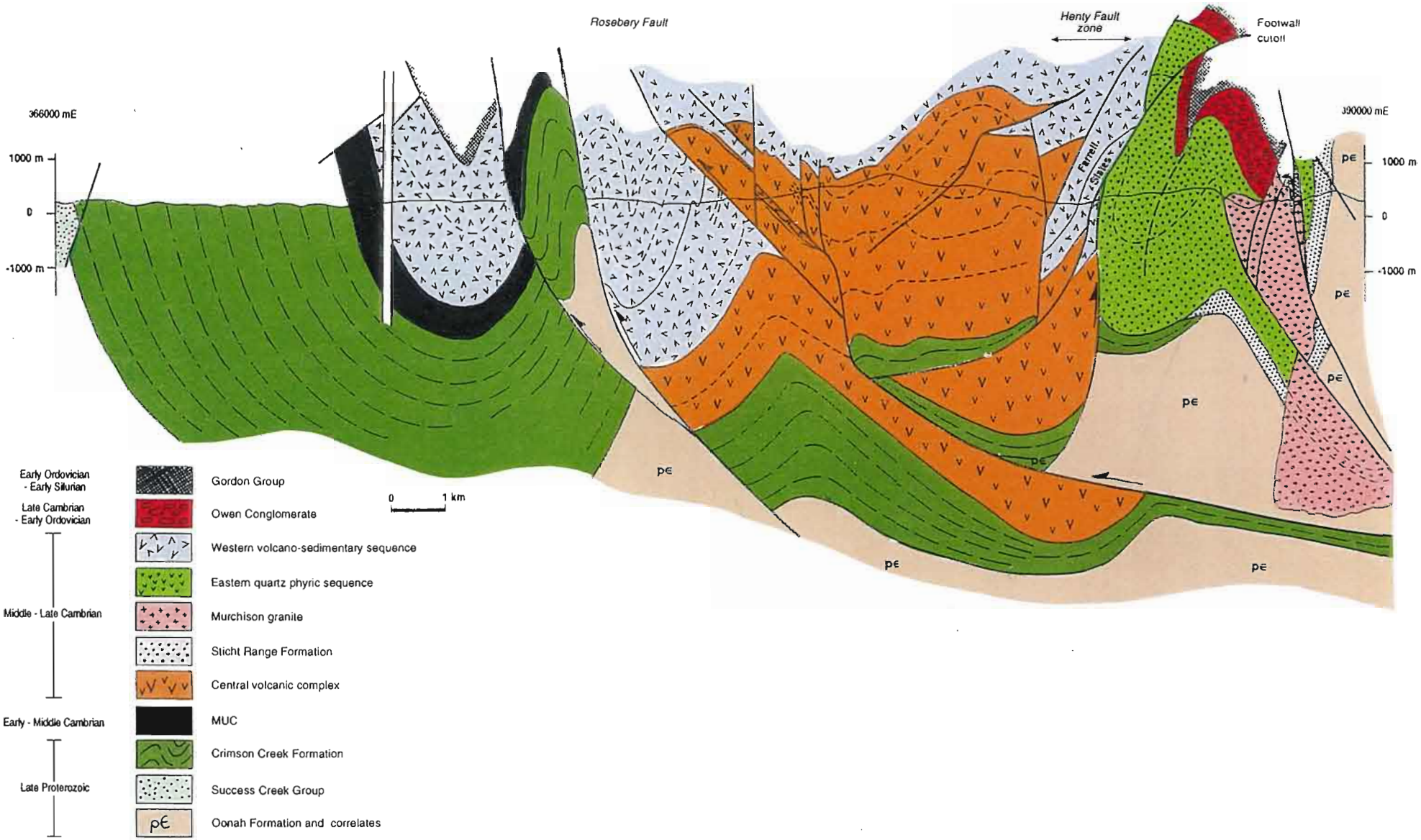

Figure 1.3 Interpretive cross section at 5374000mN (5 km north of Dundas region) across the Dundas trough showing down-dip geometry of major reverse faults. Modified from Berry and Keele (1993b) and Selley (1992b).

the formation of the Renison Bell tin deposit (Kitto, 1994). This phase of extensional fault development appears to be localised along the northern margin of the Pine Hill Granite and has not been recorded from the Dundas region.

The final phase of deformation during the Devonian orogeny, evidence of which is only sporadically recorded, involved NNE-SSW compression and the production of shallowly plunging WNW-trending folds in the south of the Mt Read volcanic belt (eg. Baillie and Williams, 1975) and sinistral wrench movement on the Henty Fault (Berry, 1989).

Chapter 2
Local Geology and Structural Relationships in Dundas Group Strata

2.1 Introduction

Over the last 45 years, the Dundas region has been mapped extensively by geologists from organisations including the Tasmanian Geological Survey and the University of Tasmania (eg. Elliston, 1954; Blissett, 1962; Corbett, 1984a; Brown, 1986). Their work has shown the geology to be complex and involve a diversity of rock types. Four main lithostratigraphic elements have been identified: 1) Late Proterozoic Concert Schist and correlates of the Oonah Formation, 2) Late Proterozoic to early Cambrian correlates of the Crimson Creek Formation, 3) ?early Middle Cambrian mafic-ultramafic complexes and 4) Middle to Late Cambrian Dundas Group and correlates. There has been considerable debate regarding the distribution and genetic relationships between these successions however, much of which can be largely attributed to the paucity of well-exposed and structurally conformable lithological contacts. With the exception of pristine sedimentary contacts between the Dundas Group strata and the MUC in the north of the region (Rubenach, 1974; Brown, 1986), the nature of which is also a controversial topic (see section 2.3), all contacts between various lithostratigraphic successions are faulted.

The geology of the Dundas region is shown in Figure 2.1. Marine meta-sediments and rare basaltic to felsic igneous rocks of the Dundas Group and correlates constitute the bulk of region. Older rocks (described herein as pre-Dundas Group succession) occur as fault-bounded inliers within the Middle to Late Cambrian sequence. The distribution and lithological characteristics of these successions are as follows.

2.2 Pre-Dundas Group successions

2.2.1 Concert Schist and correlates of the Oonah Formation

There is general agreement that the oldest rocks in the Dundas region comprise phyllite-dominated units of the Concert Schist (Blissett, 1962) and a less metamorphosed succession of quartz arenite and mudstone considered by Blissett (1962) as correlates of the Oonah Formation (Turner, 1979; Brown, 1986; Findlay, 1993). These successions crop out within a fault-bounded block (referred to as the 'Dundas Inlier' by Findlay, op cit.) located in south-central portions of the Dundas region (Fig. 2.1). Faulted contacts are shown with all younger lithostratigraphic

elements at different positions along the margin of the block. The Concert Schist consists of pale green to dark grey phyllitic rocks and less common psammites. Turner (op cit.) identified three main cleavage generations within this sequence of rocks, the second of which transposes bedding and has a schistose morphology involving segregated quartz- and mica-rich lamellae. Multiple sets (up to three) of crenulation cleavages have been observed in this study to overprint the dominant schistose fabric.

Correlates of the Oonah Formation consist of thick, commonly massive, amalgamated beds of quartz arenite, separated by dark grey mudstone units ranging in thickness from a few millimetres to tens of metres. The internal structure of some quartz arenite beds is indicative of deposition from turbidity currents, with preservation of Bouma Tabde divisions. Ripple laminated divisions are rare. The earliest phase of deformation in these rocks has produced tight upright to recumbent folds with associated slaty cleavage development. This cleavage has been subsequently folded about steeply to moderately plunging multi-hinged folds.

Blissett (1962) interpreted an unconformable relationship between the Concert Schist and correlates of the Oonah Formation on the basis of increased structural complexity within the former. However, detailed mapping of the boundary between these two sequences by Turner (1979) has indicated that the contact is structurally conformable, with no significant change in lithology and no evidence for erosion. Furthermore, Turner (op cit.) recognised a gradual increase in intensity of the early slaty cleavage developed in Oonah Formation correlates as the boundary is approached. On these bases, he considered the boundary relationship to be transitional in terms of strain and metamorphic grade. More recently, Findlay (1993) inferred that despite morphological differences between cleavages developed in either sequence, generations of structures are correlatable on the grounds that they possess similar geometries.

A detailed structural analysis of Late Proterozoic strata was not undertaken as part of this study and I am unable to confirm Findlay's (1993) hypothesis. Results from a litho-geochemical study of the rocks from this area however, indicate a subtle but consistent change in provenance signature between fine-grained rocks of the Oonah Formation correlate and the Concert Schist (see section 4.8). I therefore consider there to be fundamental lithological differences between the two sequences.

2.2.2 Correlates of the Crimson Creek Formation

Mapping by Blissett and Gulline (1962) indicated that much of the sedimentary succession which crops out to the east and northeast of the Late Proterozoic inlier at Dundas (from Moores Pimple northwards to the Ring River: Fig. 2.1) involves correlates of the Crimson Creek Formation. Their interpretation was based on supposed lithological affinities with rocks from the type section of the Crimson Creek Formation in the Pieman River and the assumption of a gradational contact with correlates of the

Oonah Formation. More recent work in this area (eg. Corbett, 1984a; Brown, 1986) has shown this interpretation to be largely erroneous, primarily through the recognition of 'acid' volcanic debris, which according to Brown (op cit.) is lacking in the dominantly mafic (tholeiitic) rocks of the Crimson Creek Formation. These geologists considered the sedimentary rocks in the eastern part of the Dundas area as lithostratigraphic correlates of the Dundas Group. Although my own mapping in this area has confirmed the presence of Dundas Group correlates, I agree with the interpretation of Blissett and Gulline (op cit.) that some of the rocks exposed in the east of the Dundas region have strong affinities with those of the Crimson Creek Formation. These rocks crop out in narrow, NNE-trending fault-bounded blocks situated in the Bather Creek - Ring River area (Fig. 2.1) which occur intercalated with inferred Middle or Late Cambrian strata of the Dundas Group. Smaller areas interpreted to comprise correlates of the Crimson Creek Formation have been identified along the eastern and southern margins of the Late Proterozoic inlier near CP73246370 and CP70906155 respectively (Fig. 2.1). In all cases, contacts with neighbouring lithostratigraphic units are faulted.

Correlation with the Crimson Creek Formation in this study is based on petrological and/or geochemical evidence (see Chapter 4: suite 1B). Over thirty thin sections of rocks from the type area of the Crimson Creek Formation (collected as a part of this study and from rock collections at the University of Tasmania and Tasmanian Department of Mines) were examined to determine the petrological characteristics of this succession.

Units correlated with the Crimson Creek Formation in the Dundas region consist of interbedded volcanogenic lithic sandstone and mudstone, with rare volcaniclastic sandstone deposits consisting primarily of texturally immature (first cycle) juvenile volcanic debris. No felsic volcanic detritus was identified from any of these units. Sandstone beds are either massive or normally graded and range in colour from purple to grey-green. The internal structure of volcaniclastic sandstone units is generally massive. Individual beds range in thickness from a few centimetres to 1.5m, however massive units possibly involving amalgamated depositional units were locally observed to exceed 20m in thickness. Mudstones are purple to grey and commonly closely laminated.

Petrologically, both framework components and matrix of volcaniclastic sandstones are extensively replaced by carbonate, chlorite and/or quartz in all samples. Relict euhedral crystal shapes are rare and the bulk of the framework comprises angular grains with ragged margins (Fig. 2.2a). Although intense alteration has obliterated internal textures in many grains, local preservation of vitric and lathwork textures, coupled with their irregular shapes are considered to indicate that they represent lithic fragments. Crystal morphologies normally associated with quench-textured mafic volcanics (eg. Bryan, 1972; Lofgren, 1974) are common within less altered lithic

Figure 2.2

(**a**) Basaltic volcaniclastic sandstone correlate of the Crimson Creek Formation. Framework comprises altered basaltic lithic fragments. Note the low degree of textural maturity and the preservation of vesicles in scoriaceous fragments. (sample 305)

(**b**) Basaltic hyaloclastite breccia contained in the lava succession from the upper part of the Serpentine Hill MUC. Coin is 23mm in diameter. (Sample 172)

(**c**) Sedimentary conglomerate from the upper part of the Serpentine Hill MUC. Monogenetic clast component consisting entirely of formerly glassy basaltic debris. Coin is 23mm in diameter. (sample 960)

(**d**) Polymict conglomerate from the basal member of the Dundas Group exposed on the northern slopes of Black Hill. The location of this sample is very close to that of (**c**). The two lithologies are clearly distinguishable however in terms of their clast compositions. Coin is 23mm in diameter. (sample 957)

(**e**) Sample showing a portion of the erosional contact between ?quench fragmented basalt of the Serpentine Hill MUC (lower part of sample) and overlying conglomerates of the Dundas Group situated on the northern slopes of Black Hill. (sample 346)

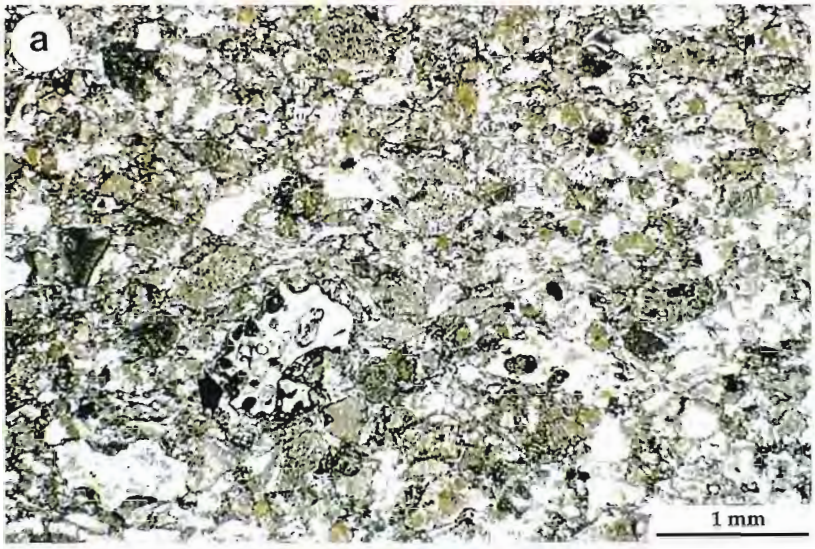
a
1 mm


b


c


d


e

fragments and include pilotaxitic, trachytic and in rare examples open bow-tie and radial spherulitic arrangements of microlites. Aphanitic vesicular fragments with margins defined by broken bubble walls are interpreted as scoria. Vesicles are uncompacted and in some cases are filled by secondary silica. Shards were less commonly observed, however this is probably a reflection of the intense alteration developed throughout the matrix. Fresh monomineralic detrital grains include abundant Fe-Ti oxides, rare Cr-spinel and subrounded quartz. Relict feldspar grains, partially altered to carbonate or silica and euhedral chlorite and epidote pseudomorphs after a ferromagnesian phase (probably clinopyroxene) were rarely recognised. The good preservation of mechanically unstable particles such as scoria and the lack of an internal structure in volcaniclastic deposits are interpreted to indicate either rapid deposition of volcanic debris synchronous with pyroclastic eruptions or redeposition of essentially unreworked material shortly after eruption.

The petrographic features of volcanogenic sandstone units are discussed in full in section 4.5.2.1 (see also Fig. 4.5h). These units are distinguished from volcaniclastic sandstones by a higher component of detritus of sedimentary origin (predominantly quartz grains of plutonic origin) and a lack of juvenile volcaniclastic material. The higher degree of textural maturity of volcanic particles in these sandstones, coupled with the inclusion of non-volcanic detritus is considered to indicate reworking of sediment prior to deposition.

2.2.3 Mafic-Ultramafic Complexes

Volumetrically significant mafic-ultramafic complexes (MUC) are situated in the western portion of the Dundas region (Fig. 2.1). The largest and most lithologically diverse of these complexes is the Serpentine Hill MUC, which contains a stratigraphically lower portion of layered cumulate rocks which is overlain by a succession of basaltic lava flows (Rubenach, 1974; Brown, 1986). Lenses of foliated amphibolite along the basal contact with underlying Crimson Creek Formation rocks (1km west of the study area) were interpreted by Berry (1989) to represent the sheared base of an allochthonous sheet emplaced during the ?early Middle Cambrian. The upper portion of the Serpentine Hill Complex crops out in the Ring River near CP719691 and on the northern slopes of Black Hill (Fig. 2.1). It consists predominantly of coarse- to fine-grained massive and pillowed flows of the low-Ti basalt suite with intercalations of hyaloclastite breccia (Fig. 2.2b) and texturally immature, unstratified basaltic conglomerate (Brown, 1986). Lithic fragments contained within sedimentary facies are almost exclusively basaltic in composition (Fig. 2.2c), however rare mudstone clasts were observed locally. No cumulate or gabbroic clasts were identified, indicating that lower levels of the MUC were unexposed during this period of sedimentation or at least were not actively supplying detritus to presently exposed depocentres.

Smaller, elongate fault-bounded lozenges occur in the central and eastern portions of the Dundas region as inliers contained within the Middle or Late Cambrian sedimentary succession. Most MUC are partially to completely serpentinised. Alteration to talc along the faulted margin the Dundas MUC has been described by Padmasiri (1974), whereas Corbett (1984a) indicated that the small MUC situated west of Moores Pimple is altered to carbonate and silica. For detailed descriptions of petrological and compositional affinities of the igneous rocks, the reader is referred to Rubenach (1967; 1973; 1974), Brown (1986) and Crawford and Berry (1992).

2.3 Relationships between the mafic-ultramafic complexes and the Dundas Group

Temporal and genetic relationships between the MUC and sedimentary rocks of the Dundas Group in the Dundas region have long been contentious issues. An early study by Elliston (1950) presented arguments for a intrusive relationship between the MUC and sediments of the Dundas Group on the basis of apparently transgressive contacts with Middle Cambrian strata. Blissett (1962) arrived at a similar conclusion, however he did not confirm Elliston's interpretation of a transgressive relationship and considered the MUC to have formed as large sill-like bodies emplacement between the base of the Dundas Group and the underlying Crimson Creek Formation. These interpretations of an intrusive mode of emplacement for the MUC were shown to be erroneous however, with the recognition of extrusive volcanic facies within the uppermost portion of the Serpentine Hill MUC (Rubenach, 1974). Furthermore, the discovery of MUC-derived detritus contained within basal conglomerates of the Dundas Group and apparent sedimentary contacts with the immediately underlying Serpentine Hill MUC, led Rubenach (op cit.) to propose that an unconformable relationship exists between these two sequences. This contact relationship is consistent with the currently accepted "allochthon model" (Berry and Crawford, 1988) for the early Palaeozoic tectonic evolution of western Tasmania in which the MUC are interpreted to have formed part of an allochthonous sheet emplaced during the Middle Cambrian (see Chapter 1).

Recent mapping by Brown (1986) however, has again placed doubt on the nature of this relationship. According to Brown (op cit.), interdigitating contacts between low-Ti basaltic lavas and basal conglomerate units of the Dundas Group are demonstrable along the margins of the Serpentine Hill MUC on the northern slopes of Black Hill and in the Ring River. If this interpretation is correct, a direct temporal and spatial relationship between sedimentation of the Dundas Group and MUC volcanism is indicated. As the compositional affinities of the basal Dundas Group indicate autochthoneity of this sequence (see Chapter 4; also Corbett and Turner, 1989), this clearly presents significant problems with the if the MUC are considered to be exotic (cf. Berry and Crawford, op cit.).

Presented below are the results from re-investigation of critical contact relationships described by Brown (1986) from the margins of the Serpentine Hill MUC.

Black Hill Area

As discussed in the previous section, conglomerate units occur intercalated with basaltic lava flows from the upper portion of the Serpentine Hill MUC. These conglomerate units are proximal to, or in rare cases directly overlain by coarse-grained lithofacies of the lower Dundas Group. Although these two rock-types appear similar in weathered outcrop, they are clearly distinguishable in terms of their provenance and texture. In contrast to the essentially monomict (ie. basaltic) character of conglomerates contained within the MUC, Dundas Group strata involve a diverse range of detrital constituents (compare Figs. 2.2c and d). Clast types in the latter include quartz arenite, dolomite, mudstone, volcanogenic greywacke and basaltic fragments interpreted to have been derived from both the MUC and the underlying Crimson Creek Formation (see Chapter 4 for a more detailed description). Furthermore, conglomerates of the Dundas Group are crudely stratified, with metre-scale bedding thicknesses, whereas those contained within the MUC are massive, unstratified and markedly laterally discontinuous. Despite extensive mapping in this region, I have not identified any examples of polymict conglomerate incorporated within the MUC, nor have I found monomict basaltic conglomerate or coherent lava included within Dundas Group strata.

Near CP69656635 a highly irregular contact was mapped out between the inferred base of the Dundas Group and underlying pillowed and brecciated basalt flows of the Serpentine Hill MUC. The exposed portion of this contact is traceable for only 5m. In detail it is seen as a rubbly surface forming the interface between ?quench-fragmented basalt and poorly sorted polymict conglomerate (Fig. 2.2e). The overlying sediments fill irregular depressions in the surface, however there is no evidence of grains having been incorporated in the underlying basalt. Moreover, some *rounded* basaltic clasts contained within the conglomerate are compositionally identical to the underlying basaltic sequence, indicating that the latter underlying sequence was being actively eroded (probably in a near-shore environment) during deposition of lower Dundas Group. In view of the features described above, this contact is interpreted an erosional surface.

Ring River

Where the eastern margin of the Serpentine Hill MUC is exposed in the Ring River (CP71956913), Brown (1986) described a complex sequence involving intermixed brecciated lava flows of the MUC and sedimentary flows positioned at the inferred base of the Dundas Group. Detailed mapping by myself at this locality shows that the contact between MUC basalt and Dundas Group sediments is faulted. The

intermixing of igneous and sedimentary material, considered by Brown (op cit.) as having formed during the collision of lava and unconsolidated sediment, is interpreted herein as blocks of MUC-derived talus breccia which have been re-deposited within muddy debris flows. A detailed stratigraphic section (Fig. 3.4) and description of the relevant lithofacies at this contact are given in section 3.2.3. Both the talus breccia units and the enclosing debris flow unit are considered to form part of the Dundas Group.

Although limited by lack of exposure, mapping along the margin of the Serpentine Hill MUC has revealed no examples for an interdigitating relationship with Dundas Group strata. Furthermore, the recognition of an inferred erosional contact between MUC lava sequences and overlying Dundas Group sedimentary rocks, combined with the presence of rounded MUC-derived detritus contained within the latter is considered to provide evidence in support of Rubenach's (1974) interpretation of an unconformable relationship between these rock packages.

2.4 Dundas Group and correlates

In the Dundas region, the Dundas Group and its correlates consist of a Middle to Late Cambrian turbidite-dominated succession. Felsic intrusive rocks and mafic lavas and/or shallow intrusive rocks form a minor part of the Dundas Group and are restricted in their distribution to central and eastern portions of the Dundas region. The sedimentary succession is lithologically diverse and possesses a highly complex internal structure characterised by rapid vertical and lateral facies changes. Facies variation occurs at the scale of tens to hundreds of metres, as shown for example by pinching out of laterally discontinuous conglomerate units. It is also recognisable on a macroscopic scale. From east to west across the study area, a crude asymmetric distribution of lithofacies is apparent (Fig. 2.1). In western areas, thick proximally-derived conglomerate units are a conspicuous lithotype and locally constitute up to 40% of the stratigraphy. Throughout the central portions of the study area however, finer-grained lithotypes dominate the succession, with conglomerate packages confined mainly to the lower portions of the stratigraphy. In addition, Brown (1986) identified an increase in the volume of acid to intermediate volcaniclastic material from west to east, a trend which has been confirmed through my own mapping. Along the eastern margin of the Dundas region, intense deformation has effectively dismembered the Middle to Late Cambrian succession. In this area, correlates of the Dundas Group occur as fault bounded blocks which are interpreted to be tectonically intercalated with older rocks (Crimson Creek Formation and MUC) (see section 2.2).

There is no simple method of classifying the Middle to Late Cambrian stratigraphy, partly due to the very poor exposure, but perhaps more importantly due to rapid lateral facies changes. For the latter reason in particular, the complex

stratigraphic sub-division proposed by Elliston (1954), which was based primarily on the incoming and outgoing of coarse-grained lithofacies, has been criticised by subsequent workers for its inapplicability away from the type section (eg. Blissett, 1962; Loftus Hills, 1964; Rubenach, 1967; Brown, 1986). Brown (op cit.) considered that only two lithologies (Red Lead Conglomerate and Razorback Conglomerate) were sufficiently distinctive to allow lithostratigraphic correlation and echoed Banks' (1956) comment that biostratigraphic evidence provides the only reliable technique of correlation. In this section, I summarise the published accounts of the stratigraphic sub-division of the Dundas Group in the type area. Detailed lithofacies analysis is presented in Chapter 3 and provenance characteristics in Chapter 4. Interpretations are drawn from these later chapters in modifying the previously described stratigraphy.

2.4.1 Type Area

The most complete section of Middle and Late Cambrian strata in the Dundas region occurs in the Dundas River (western area) and was defined by Elliston (1954) as the type section of the upper portion of the Dundas Group (Fig. 2.3). It involves a 2.5km thick, dominantly southwest facing succession which is richly fossiliferous and yields fossil ages from Undillan to Iverian (Laurie et al., 1995). The base of the succession is faulted against the Dundas MUC and the top is overlain by Late Cambrian sediments.

The oldest recorded fauna from the Dundas region (Templetonian age: Öpik, 1951) was collected from complexly faulted area approximately km SW of the Dundas River section at South Comet Creek. The unit from which the fossils are presumed to have been sourced (as the sample was collected from a loose boulder) was named the Judith Formation by Elliston (1950) and is generally considered to represent the base of the Dundas Group (Blissett, 1962a; Brown, 1986) (Fig. 2.3). It should also be noted that the sample was lost in a fire and the fauna has never been relocated (Laurie, et al., 1995). In view of these circumstances, the accepted age of the Judith Formation may be unreliable. Direct correlation between the South Comet section and the lower portion of the Dundas River section was interpreted by Blissett (op cit.) and Brown (op cit.) on the basis of the lithological similarity between a conglomerate package overlying the Judith Formation and the basal unit of the Dundas River section (Red Lead Conglomerate). Mapping from this study however, suggests that this correlation is possibly invalid as the clastic component of the two conglomerate units are distinct. Whereas the unit positioned in the South Comet Creek area consists predominantly of quartzite and chert clasts, the conglomerate at the base of the Dundas River section contains a high percentage of detritus derived from the MUC (eg. rounded fragments of basalt, rare serpentinite and abundant chromite grains; cf. Padmasiri, 1974). Although local changes in source characteristics may account for some variation in clast

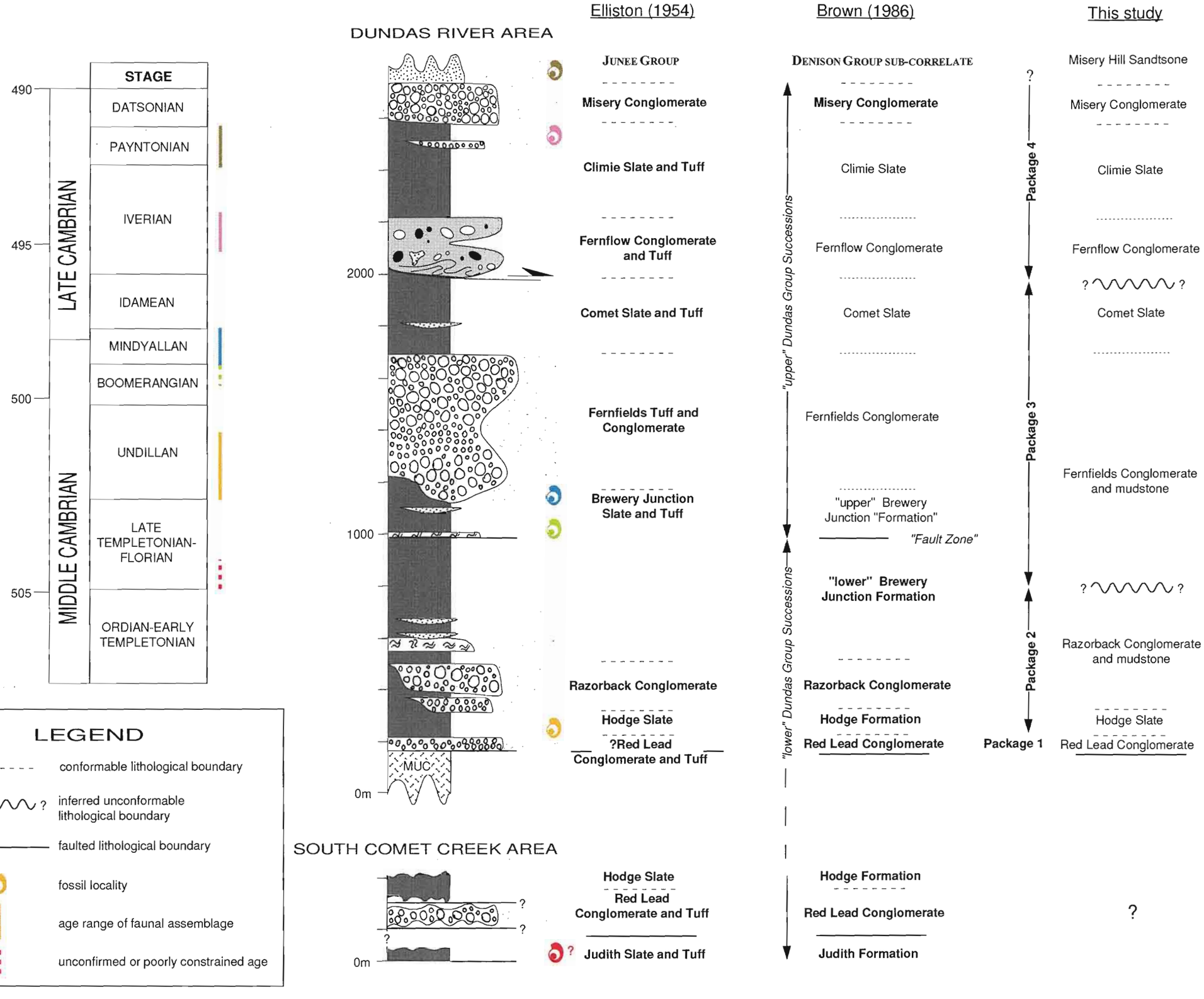

Figure 2.3. Stratigraphic relationships in the type area of the Dundas Group. Graphic log summaries data collected during this study. Fossil age chart is modified from Laurie et al. (1995) and Brown (1986).

composition, I consider that the two packages are sufficiently different to indicate that direct lithological correlation is at best tenuous. The stratigraphic position of the South Comet Creek section and its relationship to rocks in the Dundas River area must be placed in question. The following discussion is concerned only with the section exposed between the Dundas MUC and Misery Hill.

Previous stratigraphic sub-division and description of inferred unconformities

Elliston (1954) separated the section exposed between the Dundas MUC and Misery Hill into nine formations (Fig. 2.3). Brown (1986) partially rejected Elliston's (op cit.) sub-division (for the reasons discussed in the preceding section) and considered the Dundas Group in the type area as consisting of two distinct successions ("lower" and "upper" Dundas Group successions), now juxtaposed by a fault, but possibly originally representing a either a break in sedimentation or transition from below wave-base to shallow marine depositional environments at the top of the "lower" sequence. The faulted boundary was defined approximately 500m south of the Dundas River (CP696621) and was projected in a north-westerly direction to a stratigraphic position approximately 800m above the base of the type section (Fig. 2.3). Brown (op cit.) separated the "lower" Dundas Group sequences in the Dundas River area into four formations which approximately followed the terminology of Elliston (1950) but deviated slightly from the original stratigraphy in terms of their distribution: Red Lead Conglomerate → Hodge Formation → Razorback Conglomerate → "lower" Brewery Junction Formation. With the exception of the contact between the Hodge Formation and Razorback Conglomerate, which was inferred to be erosional, transitional boundary relationships were demonstrated between these units. Lithologies occur as alternating packages of conglomerate (up to 120m in thickness) and mudstone-dominated intervals, with rare acid to intermediate tuff horizons.

Litho-geochemical studies carried out as a part of this project indicate a marked change in provenance characteristics in the lower portion of the type section (see Chapter 4), lending support to Brown's (1986) hypothesis of a change in sedimentation within this part of the stratigraphy. However, the position of this chemo-stratigraphic boundary in the Dundas River section is approximately 200m below the previously suggested faulted contact (Fig. 2.3). Although there is slight angular discordance in bedding across this re-defined boundary, no evidence for major disruption due to faulting has been recognised. Furthermore, abundant pre-lithification deformation structures indicative of gravitationally-induced creep are contained within strata immediately underlying this boundary (see following section). These structures, coupled with angular discordance of bedding and change in provenance characteristics across the boundary, provide evidence for an unconformity within the lower portion of the type section.

Brown (1986) described the "upper" Dundas Group as "...sequences of randomly varying lenses and bedded units of coarse to fine-pebble conglomerate, grading to coarse-grained to fine-grained sandstone or lithic wacke with siltstone and mudstone interbeds.". He re-defined Elliston's (1950) six-fold stratigraphic sub-division of this succession on the basis that it is unique to the Dundas River section and thus not regionally mappable. Only the Misery Conglomerate was retained as a discrete formation and was considered to occur near the top of a continuous sedimentary cycle ranging in age from latest Middle Cambrian to very Late Cambrian.

Mapping of the "upper" Dundas Group sequences during this study has revealed a possible angular unconformity positioned approximately 1800m above the base of the type section. Exposed at the base of the Fernflow Conglomerate (Fig. 2.3) in the Dundas River is a shear zone approximately 10m in thickness. The fabric within this shear zone dips moderately to the SW and is defined by 'smeared out' bedding surfaces, compressional and extensional brittle fault surfaces oriented at low angles to relict layering. Strata both overlying and underlying the shear zone show abundant evidence for pre-lithification deformation including clastic dykes, ball-and-pillow structure and zones of chaotic liquefaction (*sensu* Decker, 1990). Positioned directly above the shear zone is the hinge and overturned limb of a large recumbent fold with sub-vertical plunge and a wavelength in the order of 40m. This shear zone and the fold are interpreted respectively as the basal detachment surface and a mega-slump fold contained within a large slide sheet. The overlying Fernflow conglomerate has upright stratigraphic facing and comprises 200m of matrix-supported intrabasinally-derived conglomerate, slide blocks with internally contorted strata and rare intercalations of apparently coherent strata. Bedding surfaces within coherent strata and overlying packages dip steeply to the WSW and are oblique to bedding situated below the shear zone by 10°-15°. This angular discordance of bedding and the sudden influx of coarse-grained disorganised sediment suggests that an interpretation of a localised (at least) angular unconformity is justified. Sedimentation is likely to have been nearly continuous across the contact and probably corresponds to tilting of the basin floor during basin development as opposed to a discrete orogenic episode. The timing of this event is poorly constrained bio-stratigraphically, with the inferred unconformity positioned approximately 900m above a fossil locality yielding Mindyallan ages and 800m below Iverian fauna. On the basis of this limited data, an early Late Cambrian age is suggested.

Although outcrop is extremely poor away from the Dundas River section, this inferred unconformity is tentatively interpreted on the bases of lithostratigraphic correlation and similar in bedding orientation, to be traceable in a NNW direction towards the Murchison Highway, a distance of approximately 3.5km (Fig. 2.1). In this area, a sequence of NNW-striking and steeply WNW-dipping strata consisting of debris

flows and interbedded turbiditic sandstone-mudstone units is interpreted as a lithostratigraphic correlate of the Fernflow Conglomerate. Below the inferred unconformity, laminated mudstones and rare clast-supported conglomerate strike WNW to NW and dip moderately southward. It must be emphasised however, that these two packages are separated by nearly 700m of non-exposure. Nevertheless, extrapolation of mapped bedding orientations towards the inferred boundary indicate an angular discordance of up to 45°. This very high angle would appear inconsistent with most examples of intrabasinal unconformities developed in extensional basins. Even in supra-detachment half graben basin infills, where intrabasinal angular unconformities are characteristically pronounced, angles of discordance across such surfaces usually occur between 10°-35° (eg. Dorsey and Becker, 1995; Forshee and Yin, 1995). If this interpretation of an unconformable relationship is correct, readjustment during post-depositional tectonic phases would appear necessary.

A further problem with the interpretation of an unconformity north of the Dundas River is the documentation of a Mindyallan faunal assemblage contained within the inferred correlate of the Fernflow Conglomerate (fossil locality: CP66836321) (Blissett, 1962; Banks, 1982). According to Banks (op cit.) this age is equivalent to or slightly older than the fauna positioned approximately 900m below the Fernflow Conglomerate in the Dundas River. Blissett (op cit.) describes the host lithology as a "slaty siltstone" and as such was probably deposited from hemipelagic fall-out or low density turbidity currents. Present exposure in this area is thickly overgrown and I have not been able to relocate the outcrop to confirm Blissett's description (it should also be noted that to my knowledge, the fauna has never been relocated). In consideration of his description however, it would appear unlikely that the fauna has been re-deposited as a result of reworking of older strata by turbidity currents. The nearest exposure to the fossil location occurs approximately 70m up section. It comprises a complex debris-flow association involving slide blocks and matrix-supported conglomerate, interbedded with more coherent, finer-grained units. The recognition of this facies association raises the possibility that the Mindyallan fauna may be contained within an olistolith comprising re-deposited older strata. This line of evidence is, however, weak and until more reliable lithological and fossil age data is collected, the positioning of the inferred unconformity in this northern region is considered tenuous.

Stratigraphic sub-division used in this study

For the purposes of description of the Dundas Group in this thesis, I have amended both Brown's (1986), and Elliston's (1950) stratigraphic sub-division. A simple four-fold sub-division (Packages 1-4: Fig. 2.3) is presented in which packages of strata are bounded by inferred unconformities, or changes in provenance. Although I agree with Brown's (op cit.) interpretation of change in sedimentation pattern within the

lower portions of the Dundas Group, I consider that the top of the "lower" sequence (Package 2 in this sub-division) is defined by the change in provenance characteristics described in the previous section. As the "Brewery Junction Formation" (*sensu* Elliston, op cit.) transgresses the top of this package, adherence to Elliston's original terminology becomes confusing. This term is therefore abandoned and strata previous ascribed to this 'formation' are included within neighbouring units (see Fig. 2.3). Furthermore, although some of the conglomerate units are lithologically distinctive, their lenticular geometry and appearance at slightly different levels of the stratigraphy and at different locations hinders their usefulness as regionally mappable formations. I retain most of the Elliston's original names however, but consider the relevant units as possessing a 'member' status rather than regionally mappable 'formations'.

Summarised below are the main lithological features of each package. Descriptions of the various lithotypes within each package relate to the graphic log shown in Figure 2.3.

Package 1

The stratigraphically lowest portion of the Dundas Group in the Dundas River area is named Package 1 and is faulted against the Dundas MUC north of Razorback Mine. It is very poorly exposed along the section which I mapped, where it consists of intercalated clast supported and open framework conglomerate. Samples collected from this package were not sufficiently fresh for geochemical provenance study, however petrographic evidence indicates a significant clastic input from the MUC. Undillan faunal assemblages contained in the immediately overlying Package 2 mudstone rocks provide an upper age limit for Package 1. A minimum of 50m is estimated for this Package.

Package 2

This package is estimated at 580m in thickness and comprises an association of mudstone, thinly bedded turbiditic sandstone-mudstone couplets (some of which show evidence for bottom current reworking), massive sandstone, 'chert' clast conglomerate and vitriclastic sandstone. Coarse-grained lithofacies are broadly contained within channels which cut down into underlying marine mudstones. Siliciclastics are derived principally from mature basement sources, with minor to moderate input from the MUC and felsic volcanic sources.

Package 3

Package 2 is overlain by structureless and parallel laminated mudstone of Package 3. The boundary between these two sequences is defined by the change to a basaltic provenance with dominant input of detritus sourced from the Crimson Creek

Formation in Package 3. The thickness of Package 3 is estimated at 1225m. Mudstone facies pass laterally and vertically into turbiditic sediments including thinly bedded sandstone-mudstone couplets, massive and graded sandstones and disorganised to crudely stratified closed-framework conglomerate. One volcaniclastic unit was identified in this package and occurs approximately 150m above the base. Coarse-grained bodies are laterally discontinuous and comprise a thick (450m) sequence within middle and upper stratigraphic levels of the package exposed in the Dundas River. The middle portion of the package is richly fossiliferous and contains faunal assemblages ranging Boomerangian to Mindyallan stages.

Package 4

Package 4 is inferred to overlie mudstone rocks of Package 3 with angular unconformity. The basal 200m of the succession comprises mainly intrabasinally-derived open framework conglomerate and slide sheets. Most of the detritus is interpreted to have been sourced from underlying Package 3 strata and thus is likely to inherit the "Crimson Creek Formation source signature" of the latter. This lower conglomeratic succession is overlain with apparent conformity by a substantial thickness of mudstone-dominated units with rare thinly bedded turbidites, slide sheets, thin debris flows and mudstone-bounded disorganised clast-supported conglomerate units towards the upper portions of the succession. Provenance characteristics of the mudstone-dominated succession indicate a change from intrabasinally-derived material to an extrabasinal, mature basement source terrain. Iverian fauna occur close to the top of this succession.

The uppermost portion of the Package 4 contains disorganised to crudely stratified clast-supported conglomerate and sandy turbidites Well-rounded quartzite and silicified mudstone are the dominant clast litho-types in conglomerates implying rapid uplift of mature basement source terrains.

2.4.2 Black Hill area

Brittle faulting and poor exposure has complicated stratigraphic relationships in this region. A relatively coherent section is exposed on the northern and western slopes of Black Hill (Fig. 2.1), involving a southerly facing succession which can be broadly correlated both bio- and litho-stratigraphically with the lower portion of the type section (Packages 1-3, ranging Undillan to Mindyallan stages). The basal conglomerate unit lies with erosional contact on pillowed and brecciated lava facies of the MUC (see section 2.2). It consists primarily of crudely stratified, closed-framework conglomerate with subordinate sandstone and occupies a similar stratigraphic position to Package 1 of the type area. Conglomerate units are distinguished however by an additional component of coarse-grained detritus derived from the Crimson Creek

Formation in the unit exposed on Black Hill. Package 2 correlates in the Black Hill area are dominated by thick units of 'chert' conglomerate which cut down into black structureless mudstone, thinly to medium bedded turbiditic mudstone-sandstone couplets and rare debris flows. The bottom current reworked facies recognised in the type area is not well represented in the Black Hill area.

Correlates of Package 3 are exposed in the area around Grand Prize Mine and along the western slopes of Black Hill (Fig. 2.1). Lowermost strata contained in this package are generally coarser-grained compared to those positioned at similar stratigraphic levels in the type area and comprise intercalated clast-supported conglomerate and thinly bedded, mudstone-dominated turbidites. Layer-parallel slide surfaces were commonly observed from this part of the succession, with transport directions indicated from slumped or sheared strata indicating a westward-dipping palaeoslope.

A succession of interbedded mudstone, pebbly mudstone and slumped strata occurs on the southern slopes of Black Hill (Fig. 2.1) and is tentatively correlated with the lower portions of Package 4 from the type area. These rocks are very poorly exposed however and the stratigraphy is complicated by brittle faulting.

2.4.3 Central area

The central area of the Dundas region extends eastward from the Serpentine Hill MUC to the Fahl Mine and southeast to the spur track which connects Bonnie Point and Moores Pimple (Fig. 2.1). Middle to Late Cambrian strata in this region are dominantly east-facing and have been complexly folded about large-scale upright closures and brittlely dismembered by movement along NW to NNE striking faults. The oldest part of the succession is faulted against the Serpentine Hill MUC and unfossiliferous, but was correlated on a lithostratigraphic basis with the lower portion of the type area of the Dundas Group by Brown (1986). Strata involve a thick and lithologically diverse sequence of intercalated clast-supported polymict conglomerate, rock-fall breccia, pebbly mudstone, massive sandstone and thinly interbedded mudstone and siltstone. The provenance characteristics of these sediments indicate a significant contribution from the MUC and as such are comparable with Package 1 of the Dundas Group type section. There is marked lithological contrast between these two successions however, particularly in view of the abundance of fine-grained lithofacies in the central area section. Furthermore, the thickness of the package in the central area is estimated at 750m (200m of which comprises conglomerate facies), compared to 50m thickness of Package 1 strata in the type area.

In the area between the Great Northern Fault and Bonnie Point (Fig. 2.1), lithofacies are comparable with Package 2 of the Dundas Group type section and include intercalated 'chert' clast conglomerate, pebbly mudstone, massive sandstone,

bottom current reworked sandstone-mudstone couplets, thinly bedded muddy turbidites and felsic volcaniclastic deposits. Overlying this sequence at Bonnie Point are fossiliferous strata of Mindyallan age, indicating that the sequence is of similar age or slightly younger that Package 2 strata from the type area. A similar biostratigraphic correlation between this part of the succession exposed in the central area and the Dundas Group type area was inferred by Brown (1986). Brown (op cit.) also recognised the similarity in lithotypes between the two areas, however he considered that an apparent increase in the volume of volcaniclastic units in the central area relative to the type area of the Dundas Group meant that direct lithostratigraphic correlation was invalid.

Lithostratigraphic correlates of Package 3 are absent in the central region. Occurring at a similar biostratigraphic level to Package 3 however, are units exposed at Bonnie Point and Barker Creek (west of Carbine Hill: Fig. 2.1). These units and inferred overlying strata consist predominantly of fine-grained lithologies with interbedded pebbly mudstone, massive quartzose sandstone and rare clast-supported conglomerate. Chaotic units, with deformation possibly related to slumping or *in situ* liquefaction are also common at this level of the stratigraphy.

2.4.4 Eastern area

Lithostratigraphic correlates of the Dundas type section are absent in the region east of Fahl Mine and the spur track connecting Bonnie point and Moores Pimple. Fault bounded slivers of probable Middle or Late Cambrian strata involve massive and pebbly sandstones with sub-ordinate thinly bedded sandstone-mudstone couplets and thick volcaniclastic debris flows of intermediate composition.

Fault-bounded packages of tholeiitic basalt-derived turbidites and volcaniclastic sandstone occur in Bather Creek and on the western slopes of Moores Pimple are interpreted as basement inliers of Crimson Creek Formation (see section 2.2.2). Highly tectonised slivers of interbedded mature quartz sandstone and mudstone may also represent basement lithologies (Oonah Formation or Success Creek Group), or finer-grained equivalents of the Stitt Quartzite (see Chapter 4).

2.5 Structural relationships of the Dundas Group

At least three phases of deformation are demonstrable in Dundas Group strata.

D_1: Pre-lithification deformation

A variety of small-scale structures related to pre-lithification deformation have been identified throughout all stratigraphic levels of the Dundas Group. These structures predate development of the regional cleavage associated with D_2 and include:

1) coherent slides along bedding parallel surfaces

2) extensional structures related to creep: ie. boudinage, pull-aparts

3) surfaces along which detachment has occurred: ie. thrusts, shear zones, listric normal faults with associated roll-overs
4) chaotic zones of liquefaction: possibly related to seismic events of mass sliding: ie. ball-and-pillow, pseudonodules, thick zones of liquefaction, clastic dykes
5) brittle fault zones: ie. domains associated with numerous brittle faults - developed best in mudstones but close spatial association with liquefaction zones
6) folds: ie. mesoscopic folds which contain no axial planar fabric and are related to near surface gravitational collapse

D_2 Regional cleavage development and upright, open to tight folding

Late D_2: Brittle faulting and fracture cleavage development

D_2 structures possess morphological and geometric affinities with those developed during the earliest, E-W to ENE-WSW compressional phase of Middle Devonian orogenesis (cf. Seymour, 1980; Brown, 1986; Berry and Keele, 1993b). Analysis of structures related to this phase of deformation is the focus of results presented below.

D_3 Kink and crenulation cleavage developed

The effects of D_3 are not widespread, with best evidence observed locally within western parts of the Dundas region. They are related to the latest N-S phase of Middle Devonian compression identified in other regions of the Dundas trough, eg. Baillie and Williams (1975), Berry (1989) and Kitto (1994).

2.5.1 Mesoscopic D_2 structures

2.5.1.1 S_2 cleavage

The S_2 cleavage is the dominant penetrative fabric developed within Middle to Late Cambrian rocks of the Dundas region. In outcrop, it is most easily identified within the finer-grained portions of well-bedded sedimentary rock packages where it occurs as a moderately to steeply-dipping mesoscopic foliation spaced from 0.1-3mm. It becomes more widely-spaced and in general, less readily identifiable in sandstone lithotypes. In conglomerates however, S_2 is commonly manifested by a strong dimensional fabric defined by the preferred alignment of lithic fragments. Flattened clasts contain brittle fractures oriented sub-parallel to their shortest axis (hence sub-perpendicular to S_2: Fig. 2.4a). These fractures appear to have accumulated little or no shear displacement are consequently interpreted as extensional features which developed synchronously with S_2.

In thin section, the morphology of the S_2 cleavage varies according to the rock's composition and grainsize as well as the degree of strain. Rock-types, in which the coarse-grained detrital component is dominated by quartz, possess a slaty cleavage

Figure 2.4 Morphology of the S_2 cleavage

(a) S_2 cleavage in conglomerate defined by the flattening and strong alignment of clasts. Note the development of extensional fractures oriented perpendicularly to the long axes of clasts (CP72066919)

(b) Photomicrograph of S_2 in quartz-rich lithotype. The cleavage is defined by continuous phyllosilicate films in mudstone (to right) and shorter, more widely spaced seams in sandstone. Grain alignment is poor. (sample 897)

(c) Strong cleavage development in altered felsic volcaniclastic unit. Well-developed shape preferred orientation in quartz grains and quartz-mica beards extending from grain terminations. Intracrystalline strain in quartz grains is generally low. Incipient deformation band development in the large grain in centre of field of view. (sample 318)

(d) Strong shape preferred orientation in basaltic volcanogenic sandstone. (Sample 210)

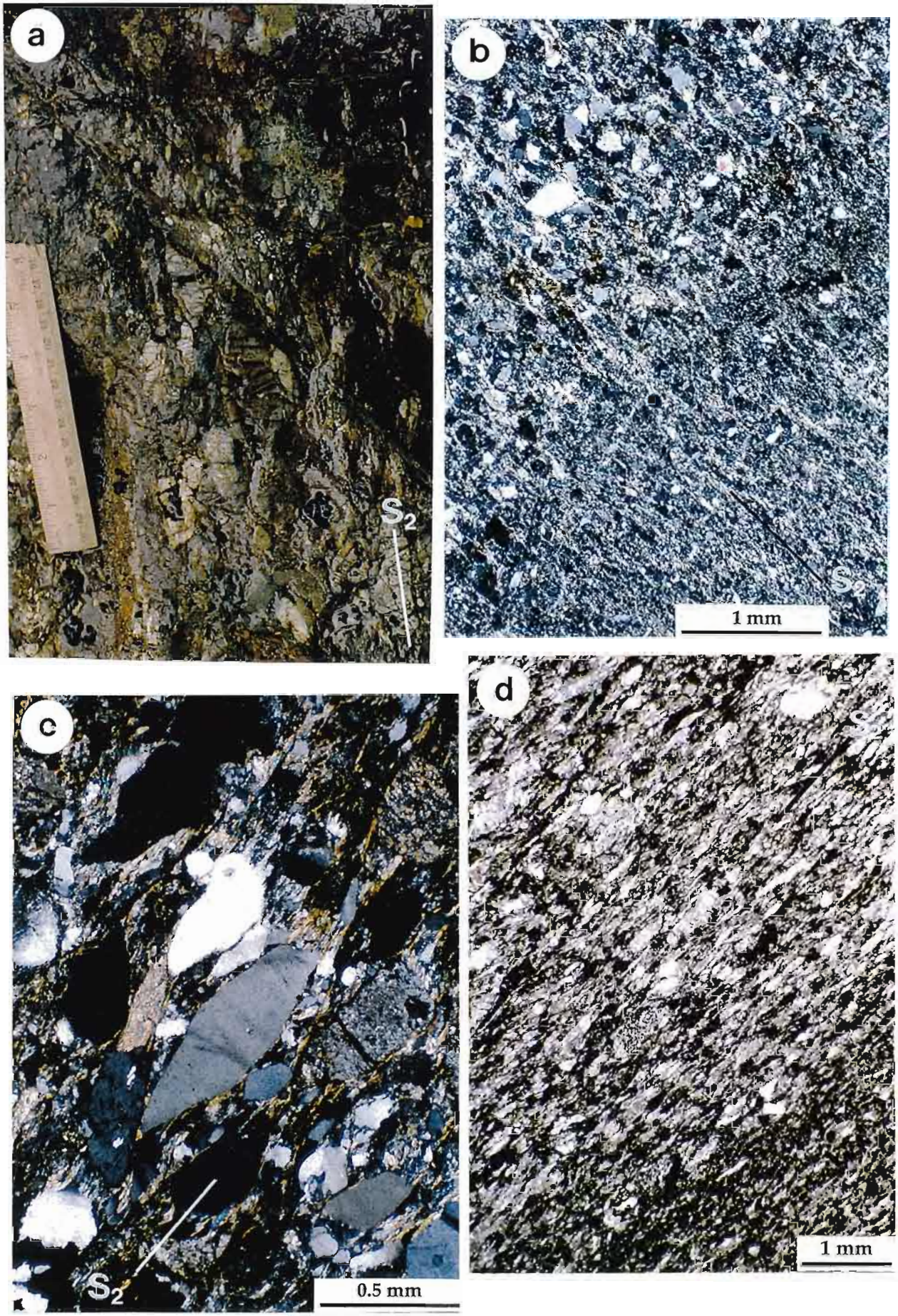
a
S_2
b
1 mm
c
S_2
0.5 mm
d
1 mm

defined by closely-spaced lamellae consisting of extremely fine-grained recrystallised layer silicate grains (usually white mica, but in some cases chlorite). These layer silicate lamellae are parallel and semi-continuous in mudstone lithotypes, but in coarse-grained equivalents, form shorter, more widely spaced segments concentrating along the faces of detrital grains oriented parallel to bulk S_2 (Fig. 2.4b). Dark pressure solution films were also observed to anastomose about detrital grains in some sandstones, with fibrous overgrowths or 'mica beards' commonly extending from the faces of detrital grains oriented at high angles to bulk S_2 in 'inter-film' domains. With increasing strain, a preferred dimensional orientation of detrital grains and localised development of intragranular microstructures becomes apparent (Fig. 2.4c). Medium to coarse-grained micas are kinked or rotated into parallelism with S_2, whereas quartz and feldspar grains have suffered little or no rotation with a general flattening of grains imposed by dissolution along faces parallel to bulk S_2. In extreme cases (ie. with the highly strain portions of melange terrains: see Chapter 5), deformed detrital grains have attained aspect ratios in the order to 10:1. Intragranular microstructures include brittle microfractures, deformation bands, deformation lamellae and rare sub-grain development. Accommodation of intragranular strain by crystal plastic processes (ie. dislocation creep) becomes increasingly important as grainsize increases.

Growth of phyllosilicate grains in association with S_2 development is generally lacking in sedimentary rocks with mafic and/or lithic-rich compositions. In moderately strained mudstones, S_2 is defined by closely spaced (0.01-0.08mm) sub-parallel to weakly anastomosing dissolution films consisting of a dark, irresolvable residue. Sandstones of equivalent composition show discontinuous wavy dissolution seams or a very weak cleavage defined by the crude alignment of scattered lithic fragments. At higher levels of strain, a strong grain alignment fabric is developed (Fig. 2.4d).

2.5.1.2 Mesoscopic Folds

Mesoscopic folds related to the S_2 cleavage are rare and were observed only from the central and eastern portions of the study area. Good examples are exposed in the section of the Ring River between CP68187332 and CP67637418 (near Fahl Mine: Fig. 2.1). Descriptions of fold morphologies is given below.

Fold morphology and hinge-cleavage relationships

Mesoscopic folds in the Fahl Mine area are mostly upright to moderately inclined and shallowly to moderately plunging. The trend of hinge lines is variable however and ranges from NNW-SSE to NE-SW (Fig. 2.5a). The majority of folds with inclined axial surfaces show W to NW vergences, however a minor proportion verge towards the SE. Although a few relatively open, NNW-SSE to N-S trending structures possess an S_2 axial planar fabric (and thus may be considered as simple F_2 folds), the

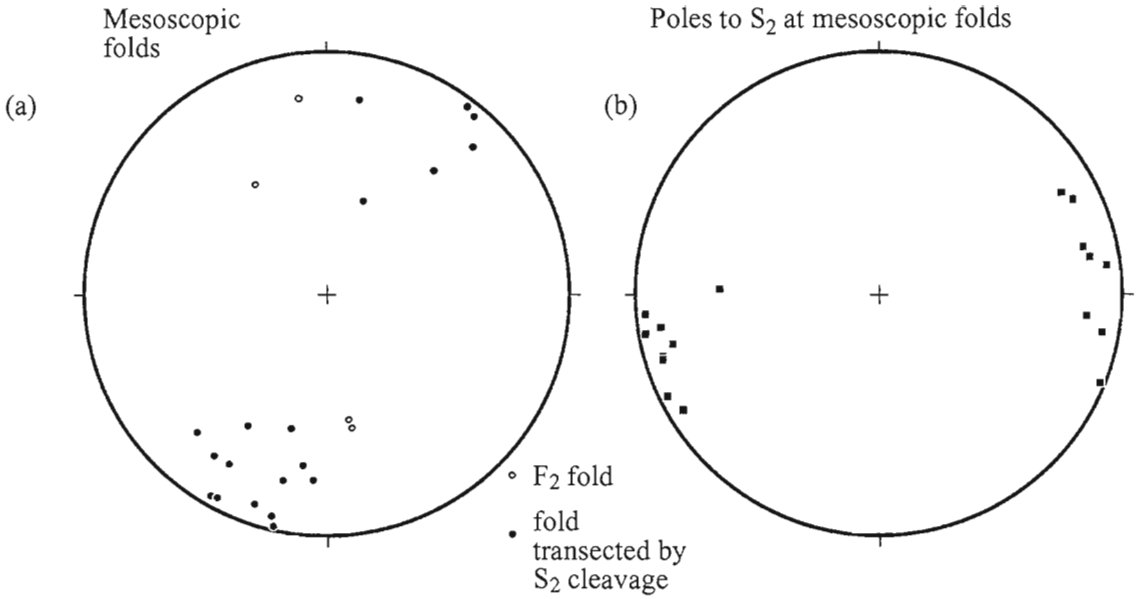

(c) Coaxial superposition of folds

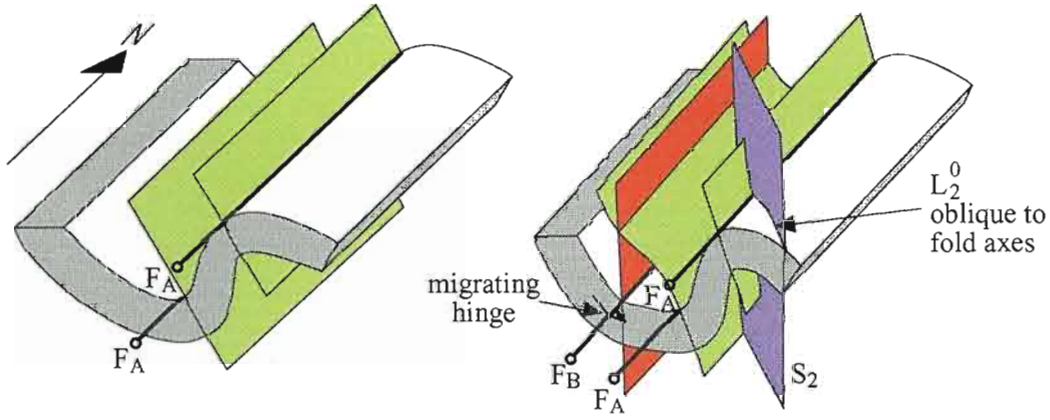

(d) Non-coaxial superposition of folds

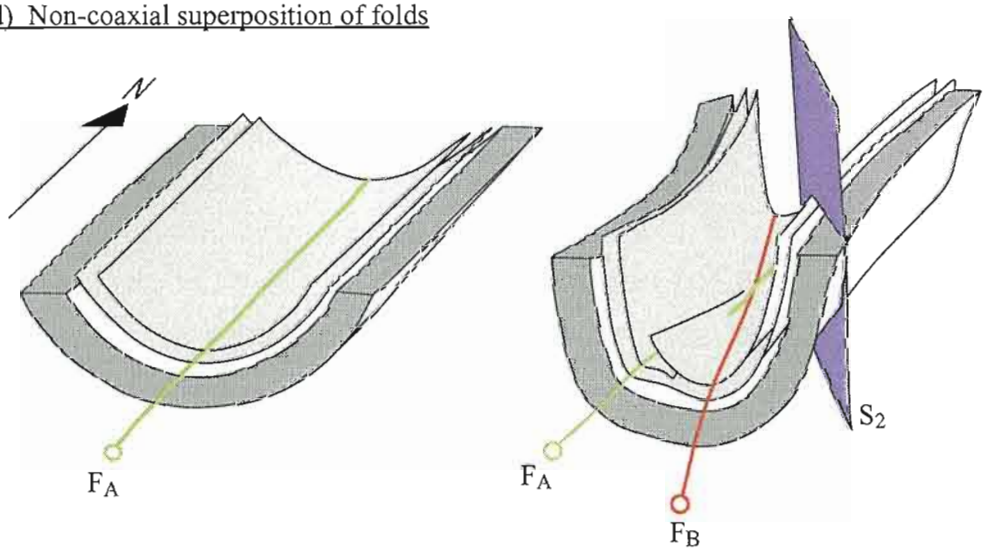

Figure 2.5. Geometry of cleavage transected and superimposed folds from the Fahl Mine area. (a) Most folds have moderate to shallow NNE to SSW plunges and are transected in an anticlockwise sense by the S_2 cleavage. A few have NNW or SSE plunges and are considered as simple F_2 folds. (b) S_2 cleavage measured at the hinge of mesoscopic folds. (c) mechansim of coaxial superposition of folds, producing box-type closures transected by the S_2 cleavage. F_B generation is imposed upon an earlier structure and migrates towards the latter with increasing strain (cf. Figs. 2.6b, c). (d) Non-coaxial superposition of fold generations. Note that both generations are transected by the S_2 cleavage (cf. Fig. 2.6a).

finite geometry of most folds appears to have been strongly influenced by pre-existing heterogeneities in the folded layers. Examples of the latter display both cylindrical and non-cylindrical geometries and the S_2 cleavage is almost always non-axial planar. Folds exhibit a variety of profile shapes including singular sub-rounded closures and less commonly, complex double-hinged closures with crude box-type geometries (Figs. 2.6a and b). In cases where limbs are sub-vertical, folds are characteristically strongly flattened, with evidence for extension in directions both parallel and perpendicular to the fold axis indicated by conjugate extensional shear fracture arrays with lines of intersection plunging down-dip and sub-horizontally. Evidence for buckling is shown by quartz and calcite-filled radial tension gashes in competent layers. In some closures, small thrusts, which are themselves folded, have formed along the inner arcs of competent layers (Fig. 2.6c). Figure 2.6b shows a double-hinged syncline involving a minor gentle closure (F_B) to the left of the major hinge (F_A) (the hinges are coaxial). In the minor hinge, thrusts appear to have been folded and displaced from the core of the fold to the steepened limb where local reactivation as extensional shear fractures has occurred. This geometry is interpreted to indicate migration of the minor hinge towards F_A, resulting in progressive unfolding of the original thrusted core. On close inspection, the S_2 cleavage was observed to parallel the axial trace on the profile plane of F_B, but cross-cut that of F_A (Fig. 2.5c). S_2 does however, transect both hinge axes as shown by the opposing plunges of the L_2^0 intersection lineation on opposite limbs of the structure (cf. Borradaile, 1978; Woodcock, 1990). There is no curving or bending of the trace of S_2 in the vicinity of the inferred migrated hinge however, indicating that the cleavage developed late in the folding history. I interpret these cleavage-fold relationships to indicate that despite their coaxiality, both hinges did not develop simultaneously, but rather reflect superposition of two discrete generations of folds. Imposition of flattening (manifest by S_2) oblique to the axial surface of an early fold generation (F_A), has resulted in local unfolding about a coaxial hinge axis (F_B) and transection of both structures by S_2 (Fig. 2.5c). Box-shaped closures are thus considered to result from refolding of initially single-hinge structures. With continued flattening and migration of newly developed hinge towards the older closure, it may be possible that F_A folds become completely replaced by F_B to again produce a single-hinge structure.

Non-cylindrical box-shaped folds have also been observed (Figs. 2.6a, 2.5d). As with the previous example, two distinct closures are apparent, however the hinge-lines are non-coplanar, with refolding of F_A about F_B (Fig. 2.5d). The resultant Type 1 interference pattern (Ramsay, 1967) produces a sinuous F_A fold axis, whereas the hinge-line of F_B is nearly straight. Only two examples of this style of interference pattern have been recognised and in both cases, F_B trended anticlockwise of F_A.

Poles to the S_2 cleavage associated with mesoscopic folds are shown in Figure 2.5b. This fabric is steeply dipping either side of vertical and a moderate spread in

Figure 2.6 Morphology of mesoscopic folds from the Fahl Mine area.

(a) Non-cylindrical multi-hinged closure with crude box-type geometry. Tightening oblique to the hinge line of an early fold generation (F_A) has resulted in refolding about F_B closure. (CP73506805)

(b) Cylindrical multihinged closure. Radial tension gashes occur within the competent sandstone horizon indicating buckling. Thrusts have been displaced from the hinge of the small closure (F_B) and are reactivated as extensional fractures in the steepened limb. (sample 498)

(c) One hinge of a large box-type fold. Folding of thrusts formed along the inner arc of the fold are interpreted to indicate buckling with migration of the hinge towards the right in reponse to progressive tightening. (sample 31)


a
F_A
F_B

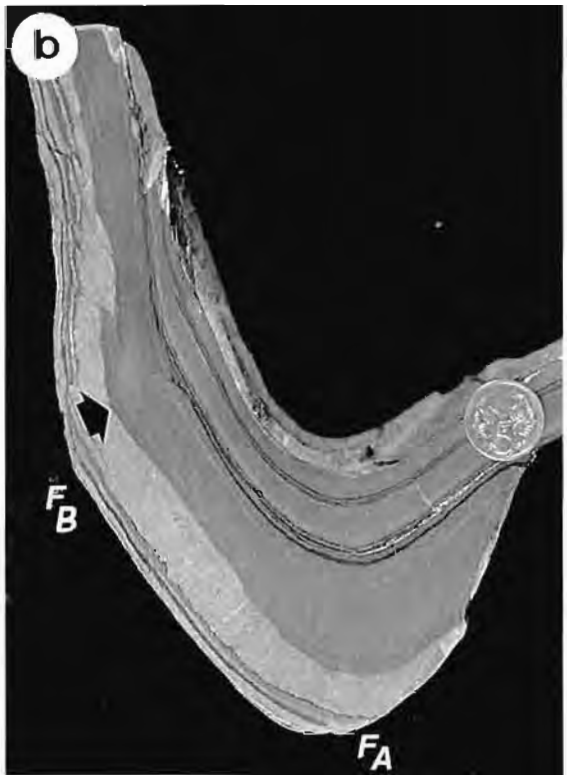
b
F_B
F_A

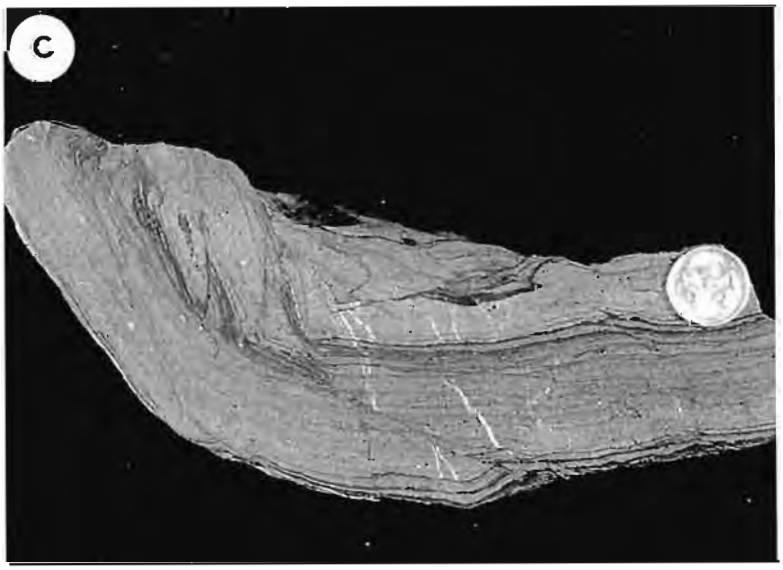
c

strike is shown, with the majority of the data striking NW to N (av: 348/89°E). Three measurements of S_2 involve NNE strikes. Despite this spread of data, the transection of individual folds by S_2 when viewed perpendicular to the hinge and parallel to the axial surface is consistently in an anticlockwise sense. The angle of transection measured from the fold hinge to the cleavage plane varies from only 1° or 2° in simple F_2 folds, and from 5° to 46° in the remainder. In cases where the angle of the transection was slight, or if the cleavage was not well-developed, transected folds were readily distinguished from simple F_2 structures in the field by the opposing plunge of the L_2^0 intersection lineation on either limb. In no cases have I found clear evidence to suggest that the cleavage was folded.

Significance of cleavage transection

Discussions of mechanisms involved in the development cleavage transected folds have been presented by Borradaile (1978) and briefly by Gray (1983). These workers provided examples by which folds are developed i) synchronously with the transecting cleavage and ii) asynchronously with the cleavage, but during the same deformation event. Clearly then, determination of the age of transected folds with respect to S_2 is not simple. Even in examples such as that shown in Figure 2.5d, where closures are non-cylindrical, double-hinged and the relative ages of fold generations can be established, each fold does not necessarily represent a discrete deformational event. Three possible modes of fold development should be considered in view of style of structures described above, each of which involves markedly contrasting strain histories. In addition to considering the two cleavage transection mechanisms outlined above, I investigate the possible effects of superimposed fold generations.

Mode 1: Cleavage transection and multiple non-colinear fold generations formed during a single deformation with bulk non-coaxial strain path

Cleavage transected folds of this type form during strong non-coaxial deformations in which fold axes initiate close to the maximum principal stretching direction but become progressively tightened and rotated towards the bulk shearing plane as strain increases (Powell, 1974). If the initiation of cleavage development lags behind the nucleation and rotation of folds (due to initial accommodation of strain at the grain-scale by non-cleavage forming processes), non-axial planar cleavage relationships will result (Borradaile, 1978; Woodcock, 1990) (Fig. 2.7a). Examples of this style of fold development have been documented from major transpressive shear zones (eg. LaFrance, 1989; Mosher and Berryhill, 1991) in which multiple generations of folds and cleavages can occur within a single deformation event. Mosher and Berryhill (op cit.) argued that the superposition and consistent younging directions shown by successive generations of structures provide accurate kinematic indicators. In the

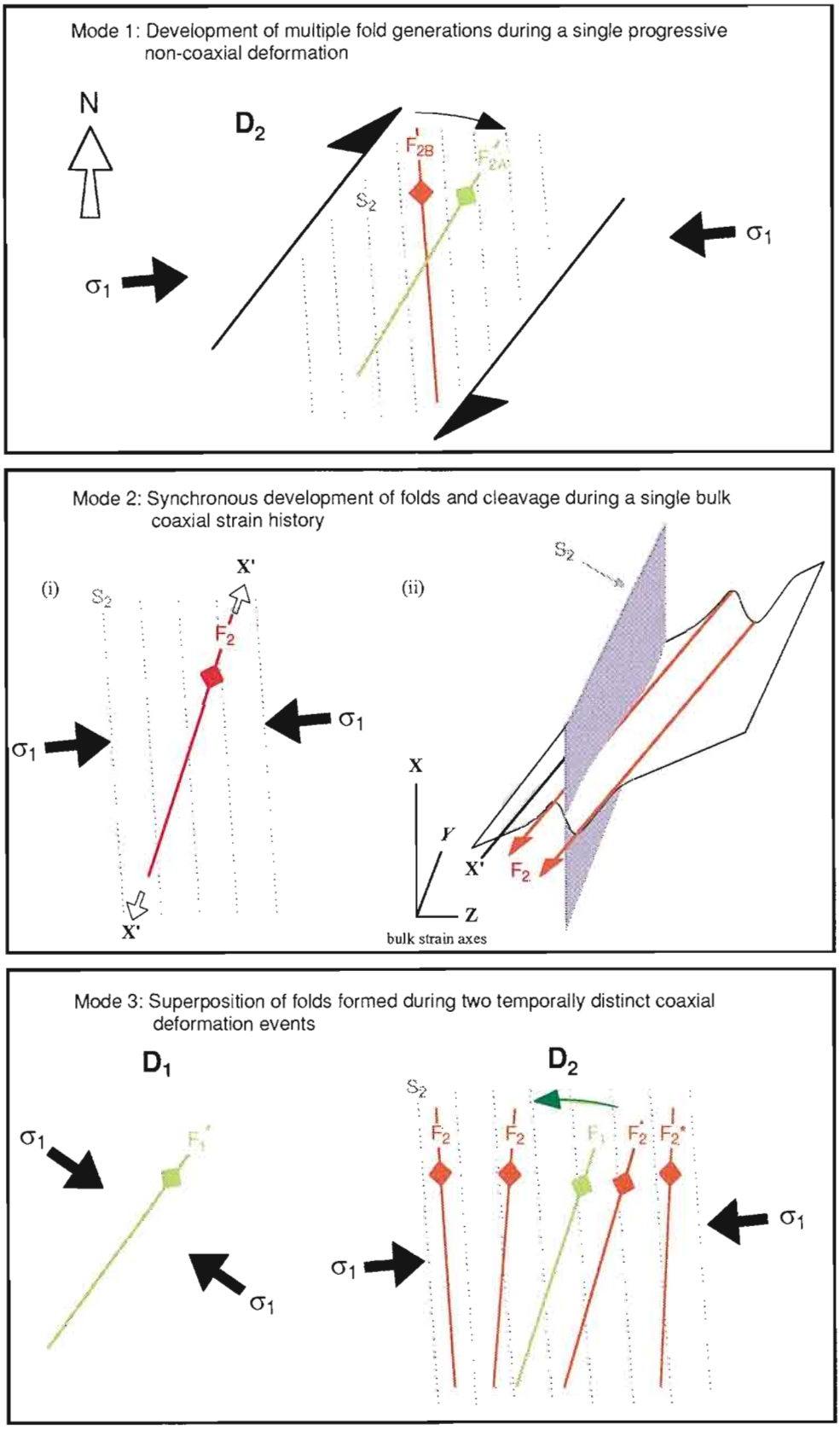

Figure 2.7. Three possible mechanisms for the generation of cleavage transected folds (see text for further discussion). **Mode 1** involves a non-coaxial strain path. For genetically related cleavage to transect folds, it must form after the nucleation and rotation of early folds (F_{2A}). With increasing increasing strain, folds (and cleavages) are rotated in a clockwise sense for the example shown. (modified after Mosher and Berryhill, 1991).

Mode 2 involves synchronous folding and cleavage development in a layer inclined with respect to the bulk strain ellipsoid. Fold axial planes nucleate obliquely to the bulk XY plane and parallel to the maximum extension direction in the folded layer (X'): (i) 2-dimensional view looking down on the folded surface, (ii) 3-dimensional view showing obliquity of F_2 and X' to the bulk strain axes (modified after Borradaile, 1978).

Mode 3 involves two discrete generations of folds with bulk coaxial strain paths. Imposition of a compressive force oblique to the early generation of folds results in hinge migration of F_1 closures to form F_2* closures or development of F_2 folds with axial surfaces oblique to the bulk flattening plane of D_2. With increasing strain, folds tighten and rotate in an anticlockwise fashion towards the bulk XY plane.

example of structures formed in a dextral system shown in Figure 2.7a, younger generations of folds and the 'delayed' cleavage display anticlockwise overprinting relationships.

A mode 1 origin for cleavage transected folds mapped along the Ring River section is unlikely however. The very high angles of cleavage transection shown by some folds (up to 46°) would require the folds to have rotated into parallelism with bulk shear plane if a classical simple shear model is adopted. Folds in this orientation would be expected to have tightened to near isoclinal (cf. Mawer and Williams, 1991) and experienced extreme hinge-parallel elongation. In contrast, many folds which display high angles of transection also display relatively low strains, with open to close morphologies and little evidence for substantial stretching parallel to the hinge. If a transpressive system is considered, then such high angles of transection would be impossible as both folds and cleavages would be required to form at angle considerably less than 45° to the bulk shear plane (cf. Sanderson and Marchini, 1984).

Mode 2: Synchronous fold and cleavage development where principal axes of strain within a deformed layer are oblique to those of the bulk strain ellipsoid

A mechanism by which non-coplanar fold and cleavage generations could develop synchronously during a single phase of deformation was proposed by Borradaile (1978). This model is based on the notion that fold nucleation on a planar surface will be influenced primarily by the state of strain *within* that surface, rather than the shape and orientation of the bulk strain ellipsoid. Specifically, Borradaile (op cit.) argued that folds will form sub-parallel to the maximum extension direction within a deformed layer (X'), regardless of the orientation of the XY plane of the bulk strain ellipsoid. On the other hand, cleavage development would be expected to track the XY plane of the bulk strain ellipsoid and could thus be considered as a 'principal plane fabric'. Thus, if X' in a deforming layer did not lie within the bulk XY plane, folds would nucleate oblique to the associated cleavage (Fig. 2.7). In this manner, cleavage transected folds could potentially develop during a single bulk coaxial strain path.

Duncan (1985) however, criticised Borradaile's model on the basis that certain assumptions were invalid or at least too simplistic to be readily applied to the deformation of natural geological materials. In particular, he found fault with Borradaile's assumption that folding of a layer could be considered in isolation of the mechanical effects imposed by neighbouring layers (and thus strain could be considered as homogenous on the scale of the enveloping surface of a single folded layer). Rather than the state of strain within an individual layer, Duncan (op cit.) argued that differences in stress and strain relationships between successive layers, which relate to contrasting mechanical properties, are more influential in terms of fold nucleation (cf. Lister and Williams, 1983).

Regardless of the uncertainties surrounding Borradaile's model of fold nucleation, a mechanism involving synchronous fold and cleavage development is untenable for at least for those structures investigated in this study which possess multi-hinged geometries. Even if the problems of producing non-coaxial fold generations during a single phase of deformation involving a homogenously strained rock package are ignored, the lack of deformation of the S_2 fabric requires that cleavage could not have actively developed throughout the entire history of folding. For example, if S_2 had initiated synchronously with early F_A folds, then the subsequent refolding of F_A by F_B must also have resulted in deformation of S_2.

Mode 3: Superposition of oblique fold generations

Multiple-hinged and cleavage transected single-hinged folds may form during superposition of non-colinear fold generations, each of which is related to distinct compressional events involving bulk coaxial strain paths (eg. Duncan, 1985). Experimental studies of two superimposed folding events involving buckling (Ghosh and Ramberg, 1968; Odonne and Vialon, 1987; Ghosh et al., 1992) have demonstrated that a variety of fold morphologies and interference patterns can develop which depend upon the tightness of the initial fold generation and degree of obliquity between successive compressional directions. Potential deformation paths indicated by these workers are shown in Figure 2.7b and include: 1) tightening and rotation of the early generation of folds (F_1) towards the bulk XY plane of the second deformation ($D_{2)}$, with no growth of new structures (Type 0 interference pattern of Ramsay and Huber, 1987); 2) refolding of F_1 by F_2 to produce typical Type 1 interference geometries; and 3) migration or "rolling" of F_1 fold axes during D_2 folding to produce single-hinged F_2 structures (Type 0 interference geometries) Of considerable importance is that even in cases where new folds (F_2) develop (either as a result of superposition or hinge migration), their axial surfaces rarely coincide with the XY plane of the D_2 bulk finite strain ellipsoid and are instead strongly influenced by the geometry and orientation of the pre-existing fold generation. As such F_2 folds occupy a position intermediate between XY and the original orientation of F_1. In fact, Odonne and Vialon (op cit.) have shown where the compressional directions of the successive deformation events deviate by less than 45°, F_2 folds are likely to develop sub-parallel to F_1. Consequently, a broad range in orientations is predicted for F_2. Moreover, if a cleavage develops during the second phase of deformation which faithfully tracks the bulk XY plane during D_2, all folds, regardless of age will be transected by the S_2 cleavage.

The mechanisms of superimposed fold development derived from the experimental studies outlined above best explain the fold-cleavage relationships identified in the Ring River section. Incompatibilities with modes 1 and 2 such as anomalously high angles of cleavage transection (ie. > 45°) and late-stage cleavage

development can be adequately explained by superposition of two oblique fold generations. The association of a single, undeformed S_2 cleavage with polyphase fold geometries however, indicates that D_2 was imposed on an early (ie. pre-D_2) fold generation that lacked an associated penetrative fabric. Folds formed during D_2 potentially resulted from tightening and modification of pre-D_2 structures or nucleated during D_2 either parallel or oblique to the bulk XY plane. Without the aid of overprinting cleavage relationships, however, coupled with the potential for both pre-D_2 folds, syn-D_2 folds to have nucleated obliquely to the S_2 cleavage, the relative age of individual closures cannot be unequivocally determined. Single hinged closures which are transected by the S_2 cleavage, for example, could represent either shape- and orientation-modified pre-D_2 folds or syn-D_2 folds. Only where rare multi-hinged closures are preserved can folds related to pre-D_2 and syn-D_2 generations be distinguished. In such cases (eg. Fig. 2.5c and d; Fig 2.6 a and b) F_A closures are interpreted as pre-D_2 structures, whereas F_B closures are interpreted as syn-D_2, cleavage transected F_2 folds.

In consideration of the absence of cleavage associated with pre-D_2 folds, their origin could be related to slumping or gravitational creep whilst sediments were unlithified (in which case they could be defined as F_1 folds), an interpretation which is supported by abundant D_1 structures throughout the Ring River section. The consistent anticlockwise sense of cleavage transection, however, indicates that pre-D_2 folds originally possessed a systematic geometry, which may be considered as evidence for a tectonic origin. Although it is recognised that regular fold geometries alone are not diagnostic of tectonic deformation (cf. Elliot and Williams, 1988), the fact that small-scale cleavage transected folds are not restricted to a narrow stratigraphic interval, but occur throughout a thick interval of late Middle Cambrian strata, leads me to favour a tectonic origin for pre-D_2 folds.

As all cleavage transected closures, both pre- and syn-D_2, exhibit consistent senses of transection, constraints can be placed on the original orientation of pre-D_2 folds. Although Type 1 interference geometries (ie. dome-and-basin structures) can develop where the obliquity of maximum shortening direction between successive fold phases (ie. $\angle Z_1\ Z_2$) occurs up to 90°, cases in which pre- and post-D_2 folds are coaxial require that $\angle Z_1\ Z_2$ is considerably less than 90°. The experiments of Odonne and Vialon (1987) showed that cases in which $\angle Z_1\ Z_2 < 45°$, syn-D_2 folds deviated significantly from the bulk XY plane of D2 and formed sub-parallel to pre-D_2 fold trends . Similarly, Ghosh et al (1992) showed that new F_2 folds did not nucleate where the angle between Z_1 and Z_2 was less than 40°, but rather Type 0 interference patterns resulted from modification of F_1 folds. Angles of roughly 40°-45° can therefore be assumed to represent the maximum obliquity between pre-D_2 and D_2 shortening directions in cases where Type 0 geometries (ie. single-hinged cleavage transected

folds) or coaxial fold couples are developed. Considering the consistent anticlockwise sense of fold transection then and taking the average S_2 orientation (348/89°E) as an approximation of the bulk XY plane of the D_2 finite strain ellipsoid, pre-D_2 structures would theoretically have trended up to 45° anticlockwise of 033. This is in reasonable agreement with the azimuths of measured cleavage transected fold axis data, which range from 008 to 045. Those folds which trend clockwise of the predicted 033 orientation may reflect Type 1 refolding of pre-D_2 structures, or they may indicate that some pre-D_2 folds originated at higher angles than 45° to the D_2 XY plane. Alternatively, NE-trending folds could reflect post-D_2 structural modification. As all folds which nucleated obliquely to Z_2 would be expected to rotate in anticlockwise fashion towards the bulk D_2 XY plane with increasing strain (cf. Lister and Williams, 1983), those folds which are presently oriented at high angles ($\approx 45°$) to S_2 would be expected to most accurately reflect the original orientation of pre-D_2 folds. In view of the geometric and mechanical constraints outlined above, the most favoured approximation of original pre-D2 fold orientations is 030.

2.5.2 Macroscopic structure: analysis by subarea

Recognition of macroscopic structures, in particular large-scale fold closures, is greatly hampered by the poor exposure and the limited information which can be gained from photo geology techniques. Furthermore, due to the rapid vertical and lateral variations in sedimentary facies, in particular distinctive and weathering-resistant litho-types such as conglomerate, potential marker units are commonly not traceable across fold hinges. This problem is further enhanced towards the east of the study area, where it is suggested that the hinges and limbs of tight folds have been faulted out such that it is almost impossible to match lithologies across closures. Reliance on the distribution of litho-types as the principal tool for establishing macroscopic fold geometry is therefore likely to be very misleading if used in isolation of stratigraphic facing directions or unambiguous vergence relationships.

The most informative structural data is gained from a limited number of sections along rivers and tracks which traverse the dominant structural grain. In the western portion of the study area, the majority of that data was collected from a single NE-SW traverse along the Dundas River, whereas grossly E-W trending traverses along the Ring River and NE Dundas Tramway provide most data from the central and eastern areas. In these latter areas, exposure between principal E-W sections is largely restricted to N or NNE trending creeks and exploration tracks which parallel the dominant structural grain and tend to follow major faults. Consequently, projection of fold axial traces away from the E-W traverses and correlation of individual closures over distances of 1km or more is largely interpretive.

In view of the problems outlined above, the investigation of macroscopic structural relationships presented herein is based primarily on the integration of domain analysis and mesoscopic structural analysis. Rocks of the Dundas Group and correlates of the Crimson Creek Formation are separated into three geographically distinct domains, within each of which the dominant structural grain (defined principally on the basis of bedding orientation) is grossly homogeneous: 1) Dundas Township domain, 2) Black Hill domain and 3) northeast Dundas domain (Fig. 2.8). Each domain is then sub-divided into a number of sub-areas. The boundary of sub-areas is defined in some cases by major faults, inferred unconformities or distinct changes in macroscopic structural geometry.

2.5.2.1 Dundas township domain

Rocks contained within the Dundas township domain include Middle and Late Cambrian portions of the Dundas Group. The eastern margin of the domain is defined by the faulted contact with the Dundas MUC (Fig. 2.8). This fault is sub-vertical in most places but locally dips steeply to the east. Reverse displacement (E-side up) is indicated by slicken-fibre orientation and S-C fabrics in serpentinite along N-striking segments of the fault, with an additional wrench component (sinistral sense) becoming important as the structure swings towards the NW.

The macroscopic structure of the Dundas township domain is relatively simple, with the bulk of the data positioned on the eastern limb of a major D_2 syncline which plunges shallowly towards the SSW and verges to the E. Stratigraphic facing in the eastern limb of the fold is to the SW and W, with a flip to easterly-facing and dipping beds in the SW corner of the domain defining the core of the structure (Fig. 2.8). The inferred axial trace of the syncline appears to die out rapidly northwards of the Dundas River. The reason for this geometry is unclear due to the lack of outcrop is this area, however I tentatively suggest that the closure has been displaced sinistrally across a brittle cross-fault.

A more detailed analysis of the structural geometry requires sub-division of the Dundas township domain into smaller sub-areas. The relatively simplicity of D_2 structures in this domain and preservation of a near complete stratigraphic section provides a unique opportunity to investigate the variation in macroscopic structural geometry inherited during basin development and sedimentation.

Sub-area DT1

Poles to bedding (S_0) plot diffusely about a great circle which strikes WNW and dips moderately to the NNE (Fig. 2.9a). This distribution of S_0 data tends to indicate open folding on moderately SSW-plunging axes, oblique to the shallow SSE-plunge of the major syncline. Although the trace of bedding is very difficult to map out due to

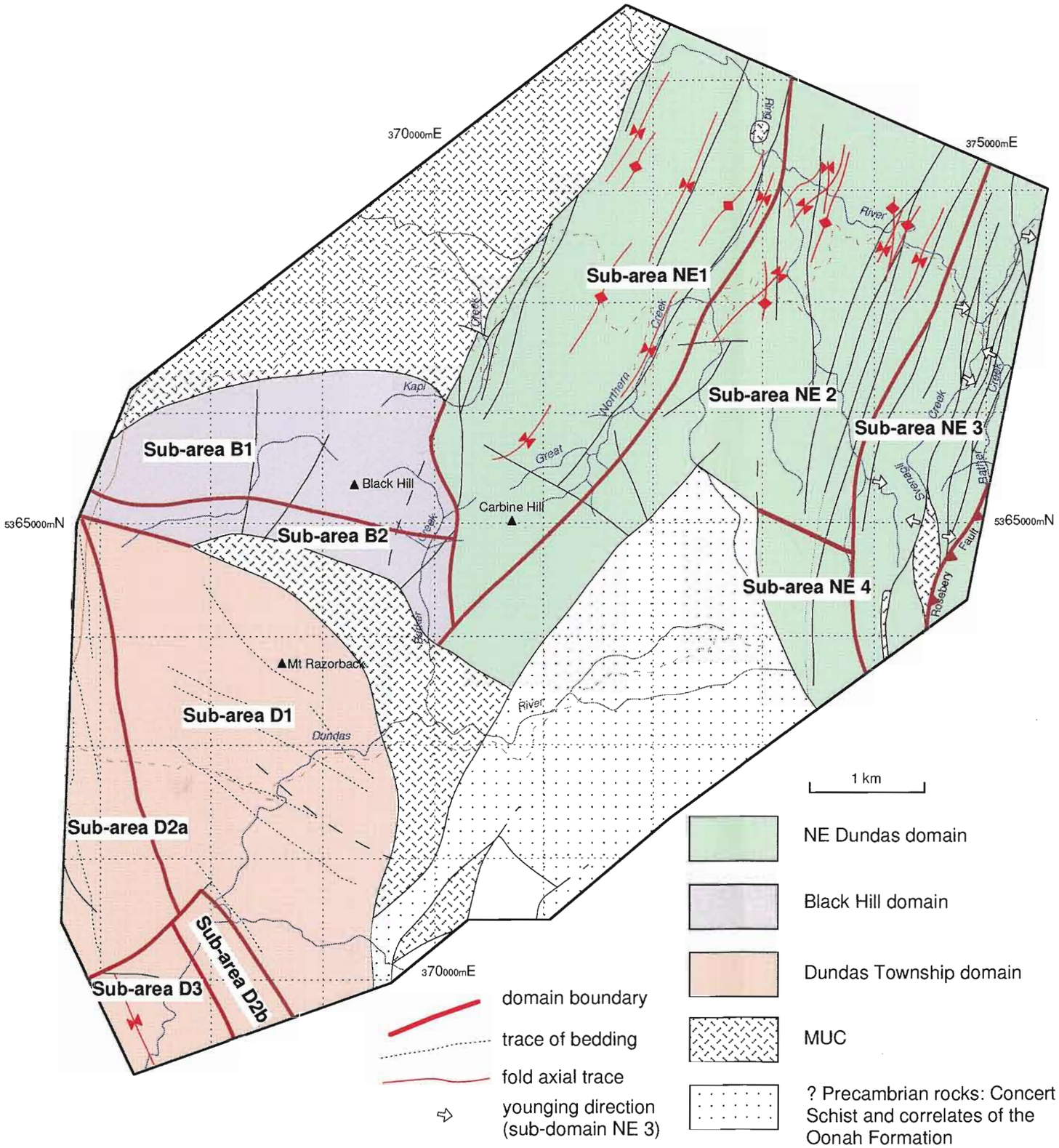

Figure 2.8. Structural domain map of the Dundas region

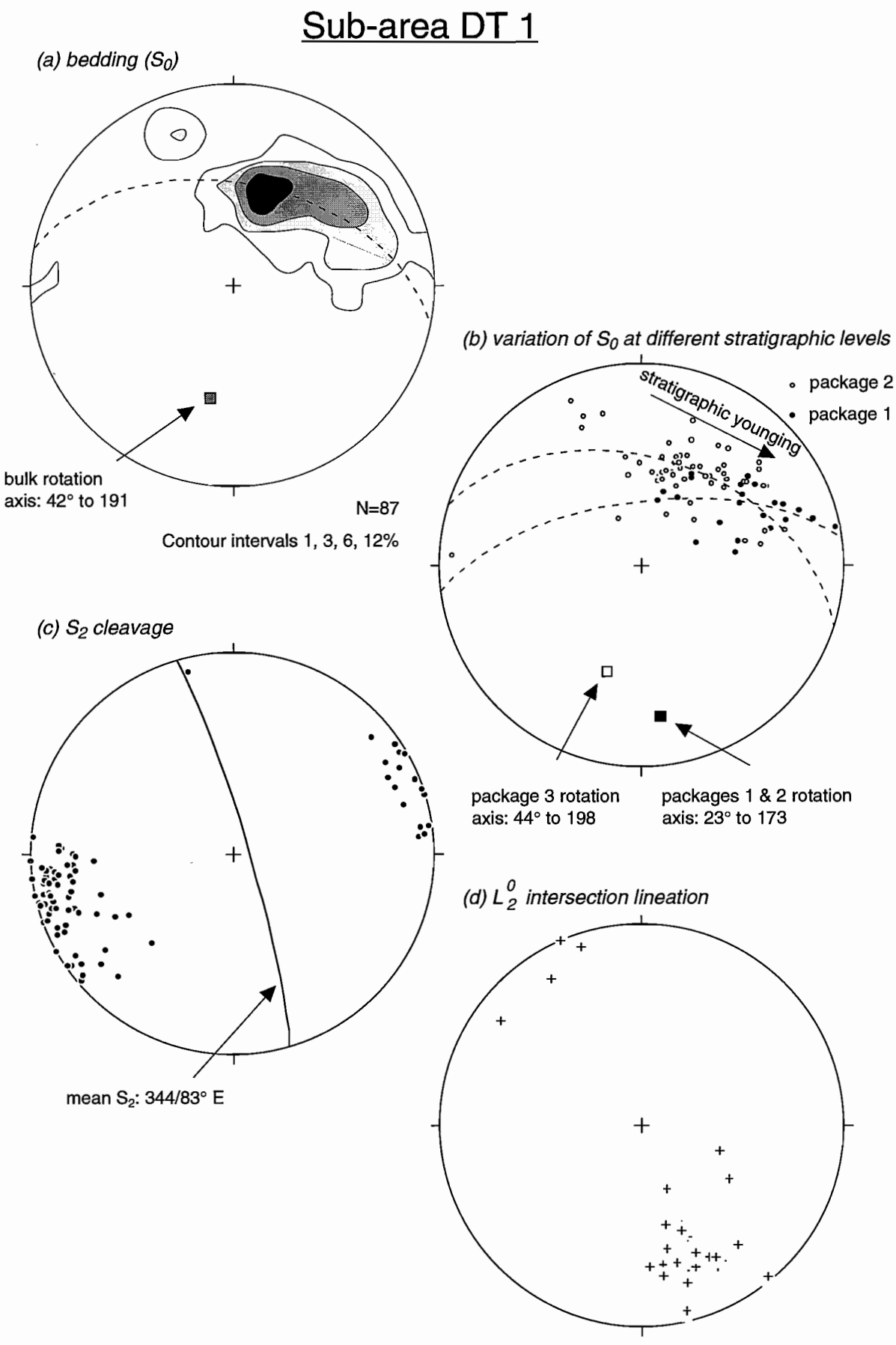

Figure 2.9. Equal area projections of structural data from sub-area DT 1.

lack of exposure away from the main river traverse, the few lines which can be constructed do not appear consistent with a simple folding geometry. Bedding traces within most units are only mildly curved, with the apparent fold geometry indicated from plot of bedding data possibly reflecting a crude "fanning" of S_0 (Fig. 2.8). Moving southward and up stratigraphy throughout the sub-area, there is a subtle rotation from dominantly WNW-striking, moderately SSW-dipping strata to more steeply dipping beds striking NNW. The lower most stratigraphic units (Packages 1 and 2) deviate from this trend, however, and exhibit flexuring of S_0 about a shallowly SSE-plunging rotation axis (Fig. 2.9b). The orientation of the rotation axis of S_0 at higher stratigraphic levels (Package 3) plot well away from the mean regional cleavage plane (S_2) (Fig. 2.9c). Note however that L_2^0 data plunge moderately to shallowly towards the SSE (Fig. 2.9d) in accordance with the attitude of the major synclinal fold axis. Importantly, there is little evidence for rotation of S_2 about shallowly or moderately plunging rotation axes as poles to this fabric are relatively tightly clustered and positioned close to the primitive circle. The slight spread of poles around the perimeter of this plot may, however reflect rotation on a sub-vertical axis. The geometric relationship between S_0 and the regional cleavage suggests that S_2 has been imposed upon, or transects a pre-existing (ie. pre-D_2) structure.

Sub-area DT2

Sub-area DT2 involves strata from the lower portions of Package 4. The structural geometry in this sub-area is distinguished from that of sub-area DT1 by an increase in bedding dip and a change in the dominant strike of S_0 to NNW orientations. The obliquity of S_0 between sub-areas DT1 and DT2 is most significant in the north of the domain, but becomes less apparent further to the south (Fig. 2.8).

The macroscopic structure is discussed below in terms of two smaller, structurally homogenous regions: DT2a and DT2b. Poles to S_0 in sub-area DT2a are shown in Figure 2.10a. This diagram indicates a concentration of bedding orientations which dip steeply to the ENE and strike towards the NNW. Additional scatter of data about a shallowly-dipping great circle is suggestive of gentle to open folding about sub-vertically dipping axes which is also likely to account for the 45° variation in strike of S_2 (Fig. 2.10b). This phase of gentle folding is therefore considered to post-date the development of S_2 and probably corresponds to refolding of the major D_2 synclinal closure on steeply-plunging F_3 warps and kink axes.

Mapping of the section along the Dundas River in sub-area DT2b has revealed a complex association of D_1 structures including large-scale slump folds and slide sheets (see section 2.3). These structures are considered to account for the more randomly oriented poles to S_0 in this region (Fig. 2.10d). In contrast to bedding data however,

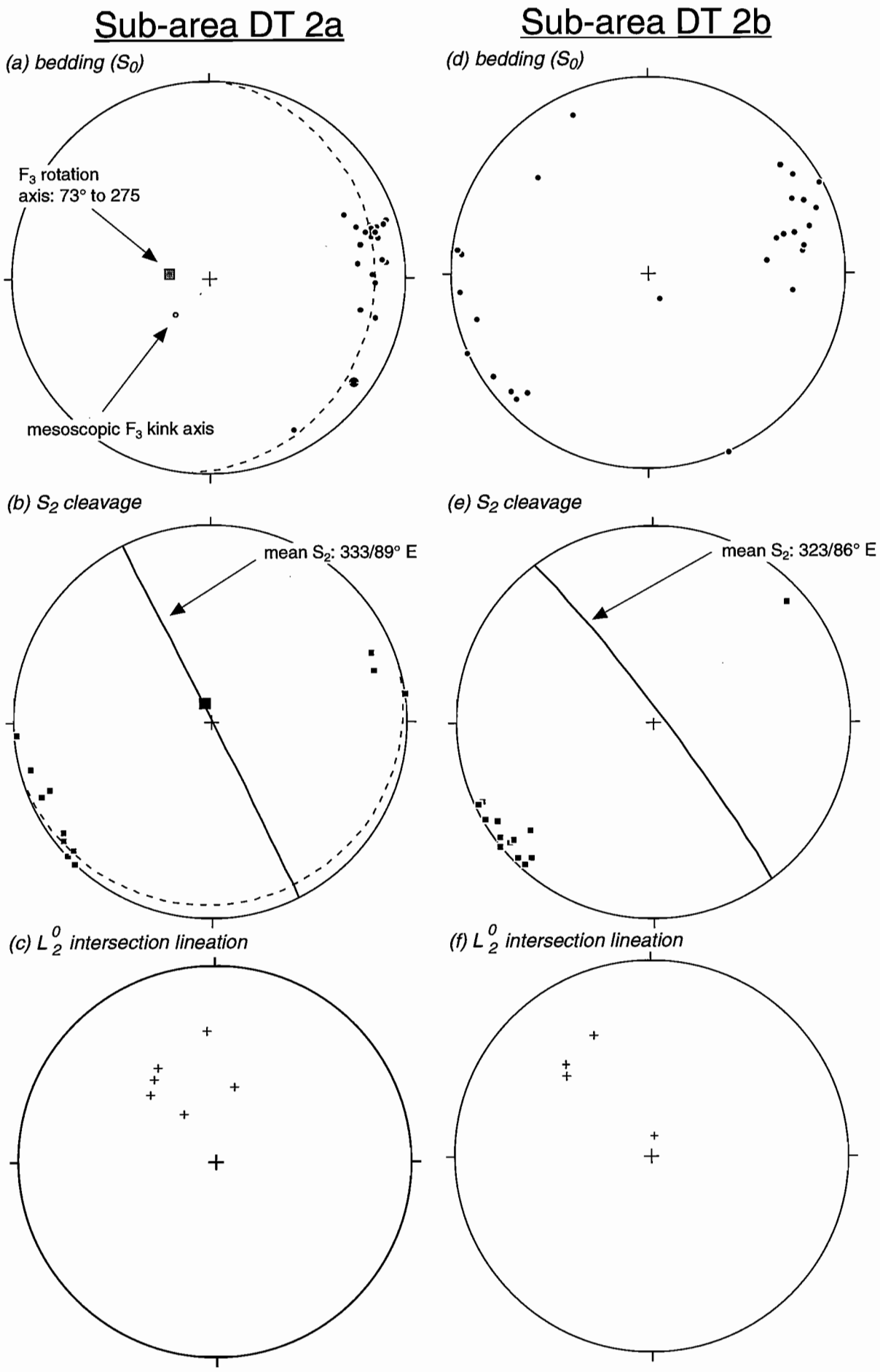

Figure 2.10. Equal area projections of structural data from sub-area DT 2.

poles to S_2 are tightly clustered (Fig. 2.10e) indicating that post-D_2 deformation in this sub-area is insignificant.

Throughout sub-area DT2 the L_2^0 intersection lineation consistently trends NW to N (Fig. 2.10c and 2.10f). The variation in plunge of this element from subvertical to horizontal cannot however, be explained by F_3 folding of both S_0 and S_2 about sub-vertical axes and is considered to indicate development of S_2 on pre-folded, or at least inclined bedding surfaces. Moreover, the flip of L_2^0 from dominantly SSW-plunges in sub-area DT1 to NW- or N-plunges in sub-area DT2, both of which are positioned on the same limb of the major D_2 syncline, provides good evidence for fundamental differences in the structural geometries of these two sub-areas prior to the development of the S_2 cleavage.

Sub-area DT3

Sub-area DT3 involves the uppermost (middle Late Cambrian) portion of the Dundas Group and occupies the core of the major F_2 syncline. Bedding on the eastern limb is generally steeply W-dipping to locally overturned, whereas strata positioned on the western limb dips moderately to the E. Poles to S_0 reflect the shallow SSE-plunge of the syncline with some spread of data away from the mean profile plane indicating that the total structure has a grossly non-cylindrical geometry (Fig. 2.11a). The spread of bedding data on the eastern limb of the fold is comparable to that shown in sub-area DT2a and is considered to be at least partly related to refolding on steeply plunging F_3 kink axes. Slight anticlockwise transection of the major structure by the S_2 cleavage is indicated by obliquity between the mean F_2 fold axis and the mean S_2 surface as well as the flip in plunge of L_2^0 from NNW on the eastern limb of the fold to SSW on the western limb (Figs. 2.11b and c). The apparent non-cylindrical geometry of folding in this sub-area may therefore also be attributable to a mild interference of F_2 folds with pre-D_2 irregularities in S_0 orientation.

2.5.2.2 Black Hill Domain

An overall E-W structural grain, defined by the orientation bedding, distinguishes this domain from the Dundas township domain.

Sub-area B1

Stratigraphic facing in this sub-area is dominantly towards the south, with poles to S_0 spread slightly about a rotation axis which plunges moderately to the SSW (Fig. 2.12a). This rotation axis coincides with relatively tightly clustered L_2^0 data (Fig. 2.12c), suggesting that the spread shown in bedding data is mainly due to gentle F_2 folding. Both the trend of F_2 fold axes and the steep ENE-dip of the S_2 cleavage are comparable with temporally analogous structures in the Dundas township domain.

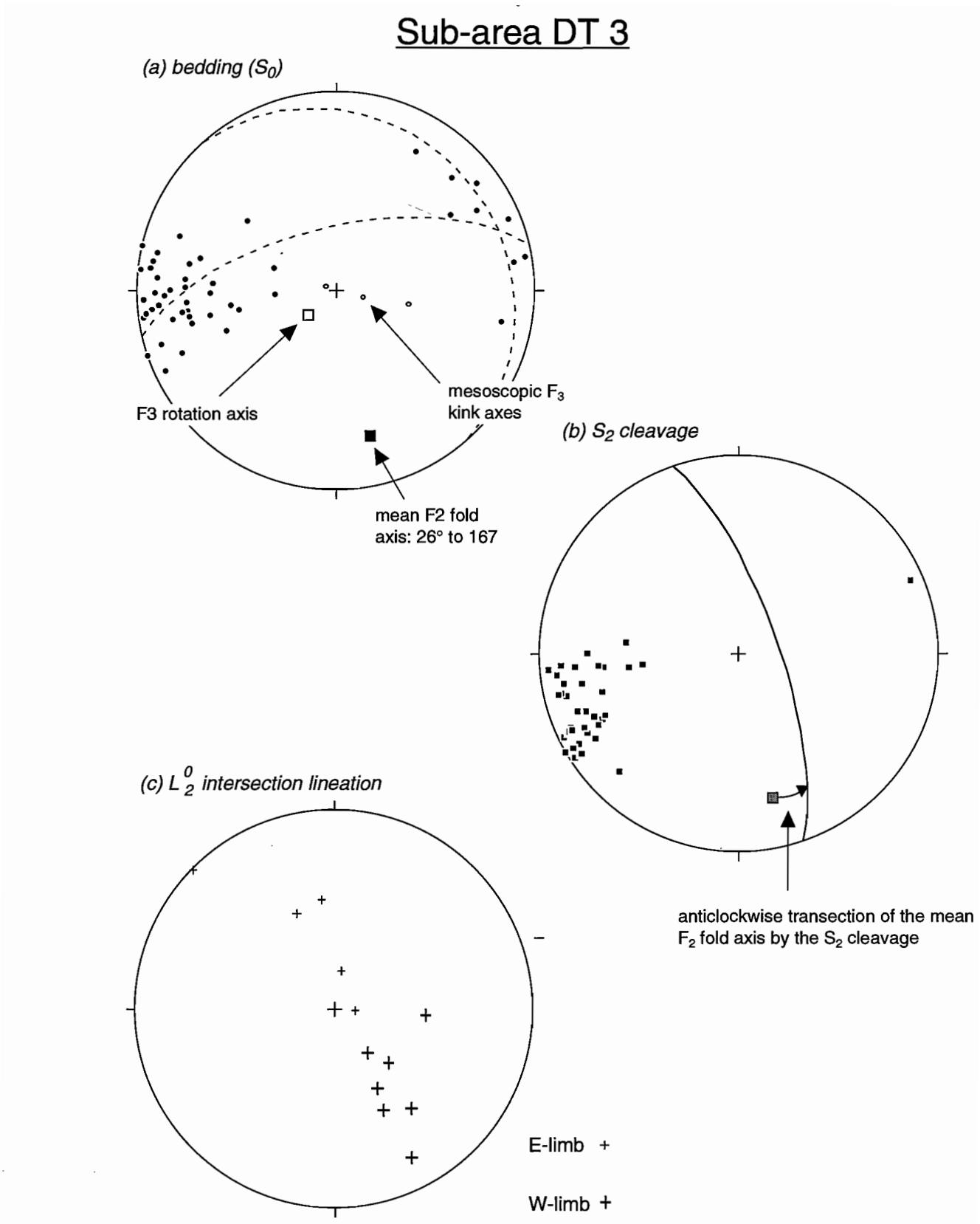

Figure 2.11. Equal area projections of structural data from sub-area DT 3.

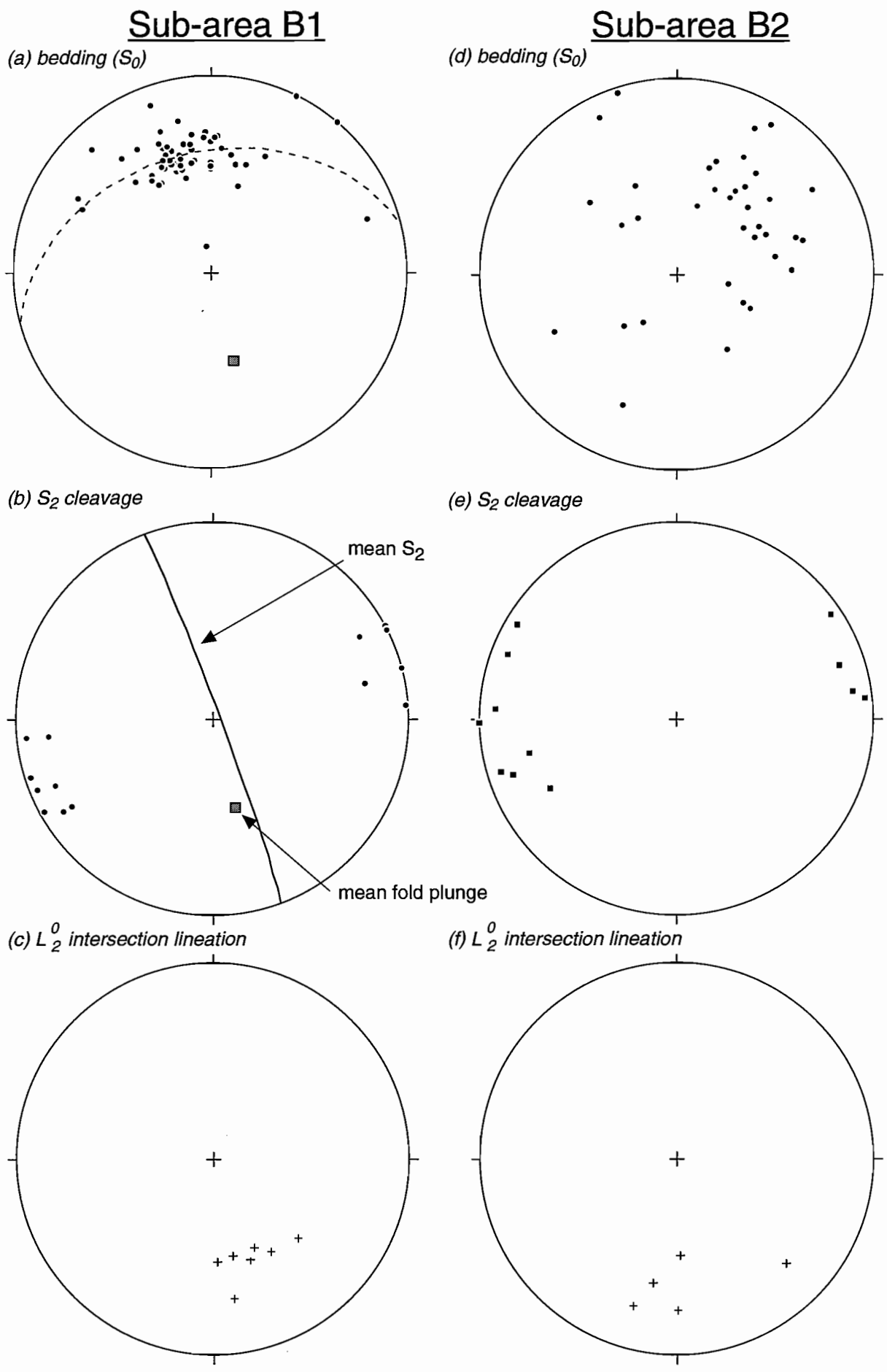

Figure 2.12. Equal area projections of structural data from Black Hill Domain.

Whether F_2 fold axes in sub-area B1 are transected by the S_2 cleavage however (as suggested in the Dundas township domain), is unclear. This uncertainty is mainly due to the combination of large F_2 interlimb angles and the moderate S-dip of bedding in this region. Even if S_2 was not truly axial planar to folds with this geometry, variation in the orientation of L_2^0 would be minor and thus insensitive to non-axial planar cleavage-fold relationships.

Little evidence exists for post-D_2 folding as indicated by the relatively consistent orientation of S_2 (Fig. 2.12b). The slight variation in strike of this fabric is probably attributable to lithologically controlled cleavage refraction or minor block rotation during late-stage brittle faulting. In the absence of significant post-D_2 modification of folds, the increase in plunge of F_2 in sub-area B1 compared to the Dundas township domain, is most likely a primary geometric feature resulting from folding of inclined strata.

Sub-area B2

The plot of bedding data for sub-area B2 shows a rather random distribution of poles, with a weak concentration indicating dominantly WNW to N strikes (Fig. 2.12d). No systematic structural geometry has been identified in this sub-area, due mainly to poor exposure, coupled with both complex rotation of blocks associated with late-stage brittle faulting and the involvement of thick packages of massive or contorted strata. Although the orientations of the S_2 cleavage and L_2^0 data show some deviation from those of sub-area B2 (compare Figs. 2.12b, e and c, f), the degree of rotation is only minor and apparently directed on steeply plunging axes. The bulk of variation in bedding data is therefore considered to be inherited from a pre-S_2 deformation.

2.5.2.3 Northeast Dundas domain

With the exception of sub-area NE3, the structural grain of the northeast Dundas domain possesses a N to NE trend. This structural grain is manifest by the inferred axial traces close to tight macroscopic folds. Both the tightness of folds and the density of faulting increases towards the east of the domain, where fault-bounded slivers of basement lithologies (MUC and Crimson Creek Formation) are tectonically intermingled with Cambrian strata.

Sub-area NE1

The western margin of sub-area NE1 is for the most part, defined by a faulted contact with pillowed basalts and plutonic rocks of the Serpentine Hill MUC (Fig. 2.8). The eastern margin is defined by a gross change in structural style from relatively simple fold morphologies to highly non-cylindrical geometries in sub-area NE 2. Strata is closely folded about a series upright closures which plunge shallowly to moderately

to the SSW. Although it is difficult to trace hinge lines for any significant distance on the ground, projection of the same closure between successive exposures reveals sinuous traces. Some structures cannot be traced between adjacent traverses and appear to die out along the length of their hinge lines. This non-cylindrical geometry of folds indicated from field observations is confirmed by the plot of poles to S_0 (Fig. 2.13a). Bedding data is distributed about a diffuse WNW-ESE girdle, with considerable spread increasing from shallow dipping hinge regions to the steepened limbs. The steeply-dipping S_2 cleavage is similarly effected, with strikes spread between NW and NNE, indicating rotation about a sub-vertically-plunging axis (Fig. 2.13b). Although the geometry of post-S_2 deformation resembles that related to F_3 folding in the Dundas township domain, no steeply plunging mesoscopic F_3 closures have been identified in this domain. Deflection of S_2 may therefore relate to block rotation during brittle faulting or it may in part reflect original heterogeneities in the orientation of the XY strain plane.

Figures 2.13c and d show the relative orientations of the L_2^0 intersection lineation and mesoscopic fold axes. There is good agreement between SSW-plunging mesoscopic folds and approximately 40% of L_2^0 data. The remainder shows significant deviation with progressive steepening as the lineation rotates towards SE-NW trends. It is considered unlikely the distribution of L_2^0 is solely attributable to rotation of major folds and S_2 about a sub-vertical rotation axis as this mechanism would be expected to produce a scatter of L_2^0 close to the primitive circle, rather than the observed increase in plunge. A more plausible explanation, especially in consideration of fold-cleavage relationships described in the previous section, is that the S_2 cleavage is not always axial planar to the major folds.

Sub-area NE 2

Sub-area NE 2 is characterised by strongly non-cylindrical fold geometries and complex interference of at least two generations of folds is locally demonstrable. Considerable scatter is shown by poles to S_0 (Fig. 2.14a), however a very crude N- to NE- trending structural grain is still weakly discernible and enhanced by the orientation of mesoscopic fold axes (Fig. 2.14d). Despite the rather random distribution of S_0 data, the NNW to NNE strike of S_2 remains comparable with that observed in sub-area NE 1 (Fig. 2.13b), indicating that post-D_2 deformation (either brittle faulting or folding) cannot account for the geometry of bedding. Obliquity of the regional cleavage to the structural grain defined by S_0 and major fold axes is shown by systematic distribution of L_2^0 around the mean S_2 plane, forming a NNW striking great circle (Fig. 2.14c). The bedding-cleavage relationships displayed within this sub-area are interpreted to indicate that S_2 has been imposed upon an earlier generation of folds with probable NNE to NE trends. Brown (1986) arrived at a similar conclusion on the basis of form surface

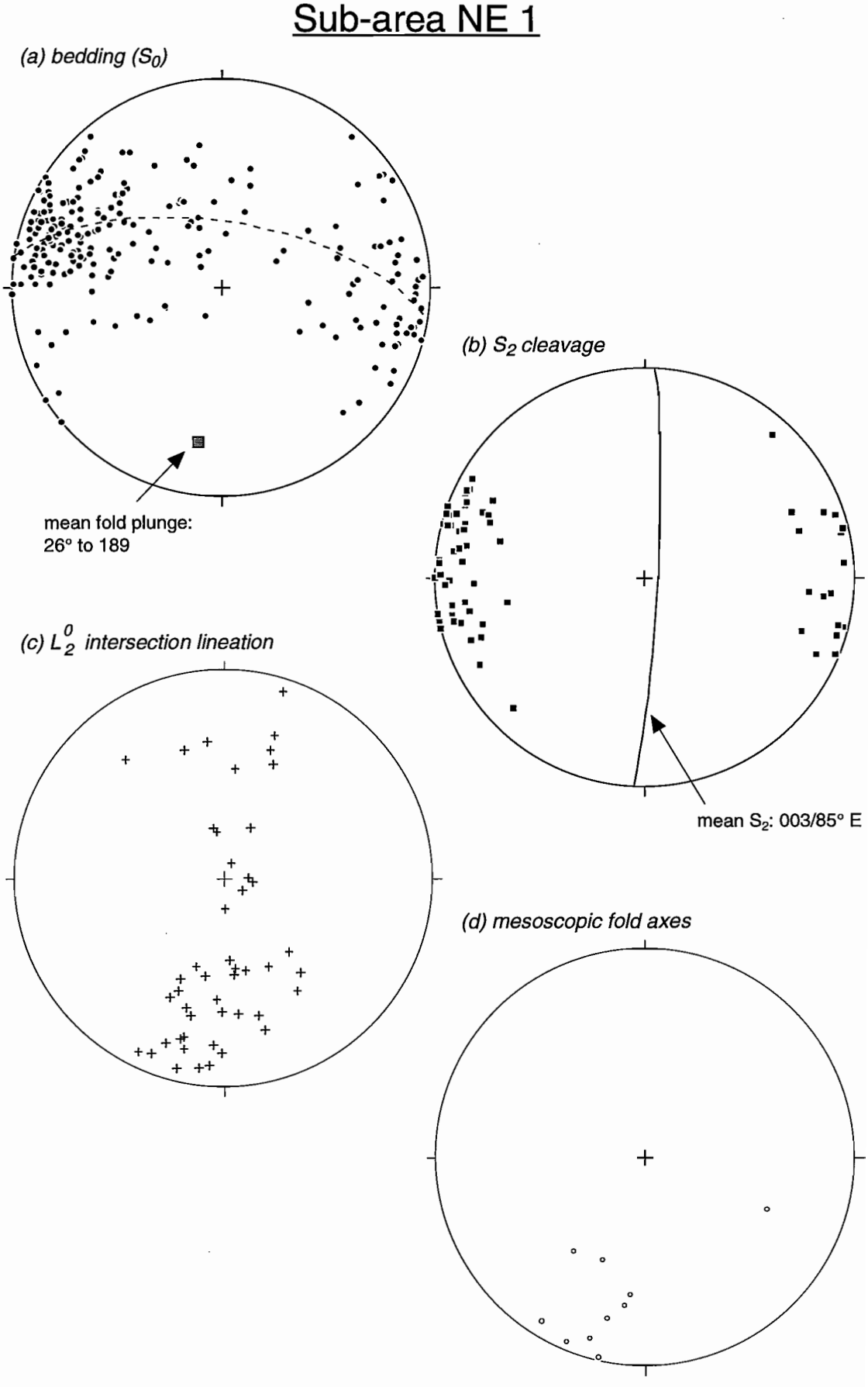

Figure 2.13. Equal area projections of structural data from sub-area NE 1.

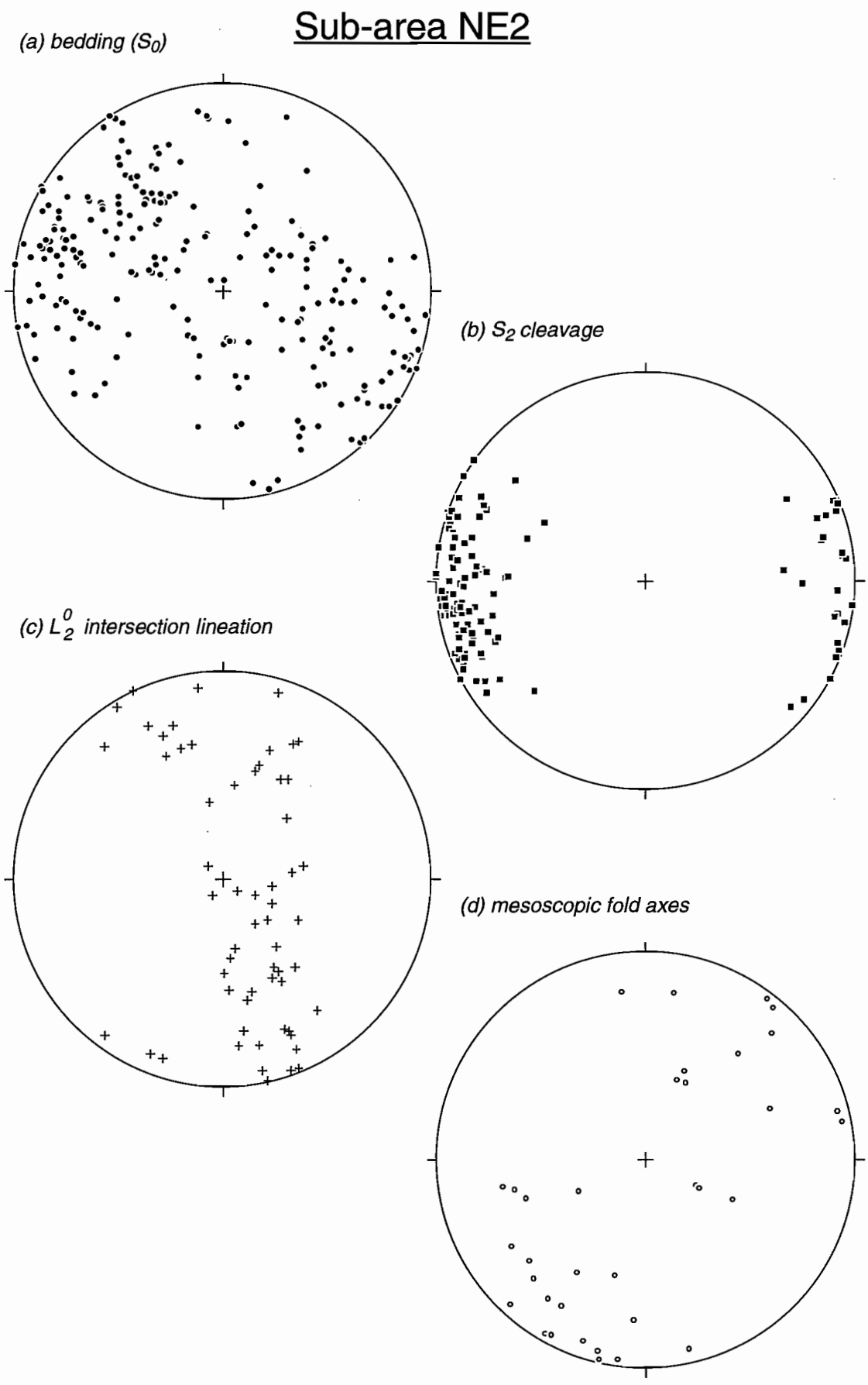

Figure 2.14. Equal area projections of structural data from sub-area NE 2.

mapping in an area north of the Ring River (around 730690) where he demonstrated complex fold morphologies and clear transection of fold axes by the regional cleavage.

Sub-area NE 3

Sub-area NE 3 is distinguished from sub-areas NE1 and NE2 by increased tightening of folds as shown by the predominantly steep to sub-vertical attitude of bedding (Fig. 2.15a). Strong tectonic dismemberment of upright folds during movement on syn- to late-D_2 NNW to NE striking faults and ductile shear zones has resulted in the annihilation of hinge regions and shearing out of limbs. The original geometry of folds is thus highly modified, with the position of relict closures indicated by flips in stratigraphic facing from E to W across faults and shear zones. Where relict axial surfaces of folds can be inferred, stratigraphic mis-match is shown between the opposing limbs, indicating that displacement along the intervening structures is considerable. Intense flattening has occurred in sub-vertically dipping strata, with localised transposition of bedding by the S_2 fabric and development of tectonic melange within originally well-stratified mudstone-dominated lithotypes.

Little evidence exists for the interference of multiple fold generations and the spread of poles to S_0 is comparable with, or slightly anticlockwise of steeply-dipping strata contained in sub-area NE 1 (compare Figs 2.15a and 2.13a). The spread of bedding data may be partly attributable to a pre-faulting non-cylindrical fold geometry, however in view of the strong disruption of folds, the effects of limb rotation during faulting are also likely to be important. Rotation of S_2 was observed at the outcrop scale along widely-spaced extensional shear band sets (S_{2C}) and mesoscopic brittle shear fractures. As these fabrics are best developed in massive lithotypes, it is unclear as to whether they have significantly effected the orientation of S_0.

Mean S_0 strikes a few degrees E of N and only slightly (4°) anticlockwise of the mean S_2 plane . Scatter of L_2^0 around the great circle defining mean S_2 and is considered to indicate anticlockwise cleavage-transection of major folds. No mesoscopic folds were recognised in this sub-area.

Subarea NE 4

Subarea NE 4 is anomalous in that bedding strikes NNW to N (Fig. 2.16a). Bedding dips are subvertical and comparable in orientation with the S_2 cleavage. Slight transection of folds is indicated by the scatter in L_2^0 however. The consistency of S_0 and S_2 data compared to other regions may indicate that the rocks in this subarea record only the effects of the D_2 deformation.

Sub-area NE3

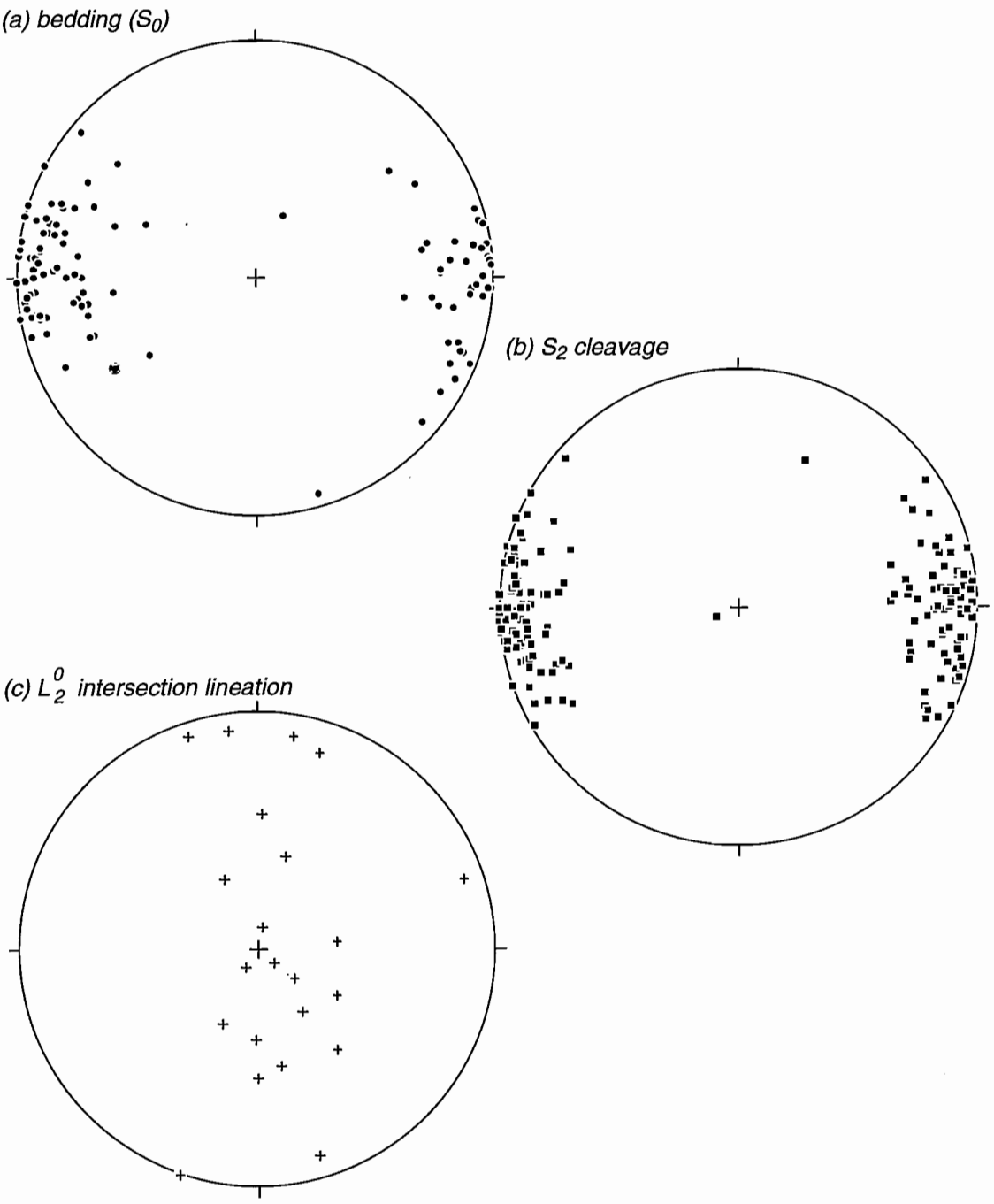

Figure 2.15. Equal area projections of structural data from sub-area NE 3.

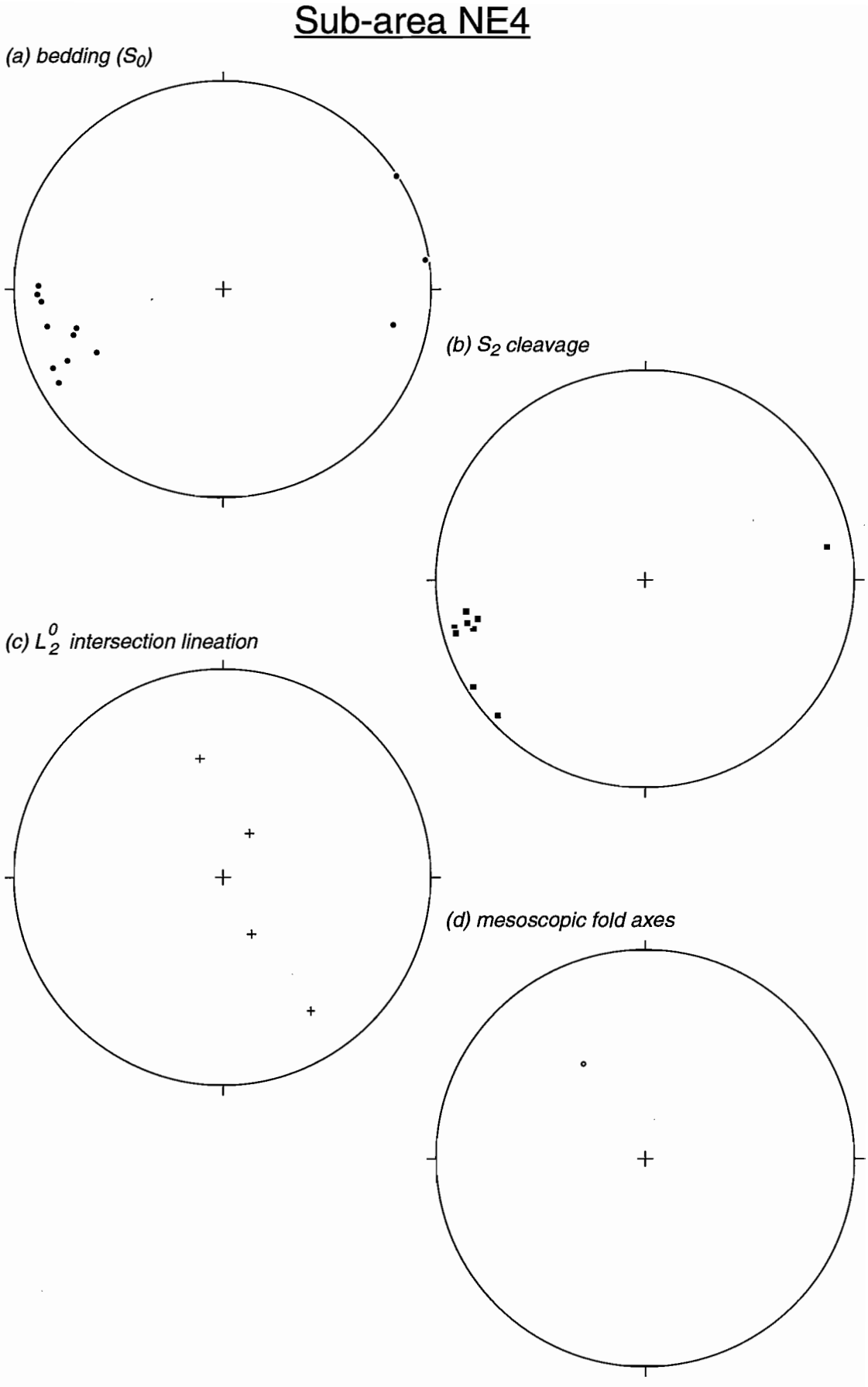

Figure 2.16. Equal area projections of structural data from sub-area NE 4.

2.5.3 Summary of D_2 and implications for early (pre-D_2) deformation

Mesoscopic and macroscopic analysis of D_2 structures reveals a complex geometry involving predominantly NNW to NE structural trends. Macroscopic F_2 folds are characteristically non-cylindrical and the variation in L_2^0 orientation provides evidence of transection of large-scale folds by the S_2 cleavage. This departure from simple fold morphologies is most evident in central and eastern parts of the Dundas region (northeast Dundas domain in particular), wherein the average S_2 cleavage orientation strikes anticlockwise of N- to NNE-trending F_2 hinge lines. Within the northeast Dundas domain, there is also considerable variation in structural style, with cleavage morphology, degree of fold tightness and fold dismemberment indicating a gross eastward increase in strain during D_2. The complex macroscopic cleavage-fold relationships within this region are also reflected in the geometry of mesoscopic folds. Anticlockwise transection and rare multi-hinged morphologies associated with mesoscopic folds are best interpreted to have resulted from the superposition of oblique pre-D_2 and syn-D_2 fold generations. On the bases of fold morphology and transection angle, the original orientation of the mesoscopic pre-D_2 fold generation is constrained to a NNE trend. If the mesoscopic fold history is applied to the macroscopic structural geometry of the northeast Dundas domain, a large-scale pre-D_2 NNE-trending fold generation, previously unrecognised in the Dundas region, can be interpreted. The most likely regional event associated with this folding is the Late Cambrian compressive phase which produced major upright, open N-trending folds and reverse faults (cf. Berry, 1994).

Although evidence also exists throughout the Dundas township domain for the influence of pre-D_2 'irregularities' in S_0 orientation on the morphology of the major F_2 syncline (shown mainly in the variable plunge of L_2^0), the effects of this pre-existing geometry appear most pronounced in sub-area DT1. This is most clearly shown by the obliquity of both S_0 and L_2^0 between sub-areas DT1 and DT2. The anomalous bedding geometry developed in sub-area DT1 cannot be attributed to post- or late-D_2 modification of the F_2 fold as the mean orientation of S_2 remains relatively consistent throughout the entire domain. In view of these structural relationships, I suggest that sub-area DT1 records an early phase of deformation (D_1 or at least pre-D_2) which did not involve, or was at best only weakly developed in younger (Upper Cambrian) strata positioned in sub-areas DT2 and DT3. This change in bedding geometry is consistent with the interpretation of an angular unconformity between Packages 3 and 4 (see section 2.3.1).

The rotation axis indicated by the distribution of bedding data from package 3 in the Dundas township domain roughly coincides with the pre-D_2 NNE-SSW fold trend interpreted within the northeast Dundas domain. However two lines of evidence are considered to indicate that this latter phase of folding does not account for the structural

geometry exhibited in the Dundas township domain. Firstly, rotation of bedding about a SSW-plunging rotation axis identified in sub-domain DT1 is not pervasive and has not effected rocks older than those contained within package 3 (ie. packages 1 and 2). Unless a large-scale bedding-parallel detachment is inferred at the base of package 3 (evidence of which has not be observed) it is difficult to resolve the difference in structural geometry between packages 3 and older strata in terms of a post-depositional fold generation. Secondly, individual bedding traces within package 3 remain relatively straight and are not folded about a SSW-plunging axis. Only when the bedding trace patterns is viewed in its entirety is a distinct "fanning" geometry revealed, with a rotation axis or "pivot point" positioned close to the western margin of sub-domain DT1. The pre-D_2 structural geometry in sub-domain DT1 is best explained by either lateral thickness variation or slumping within package 3 related to syn-depositional basin-floor rotation, possibly associated with extensional block tilting and half graben development. The lack of marked pre-D_2 deformation in sub-domains DT2 and DT3, which contain younger (Upper Cambrian) strata, indicates that if basin-floor tilting was active during Dundas Group deposition, it had ceased prior to package 4 sedimentation, or is at least is not manifest by the depositional geometry of Upper Cambrian strata.

Chapter 3
Sedimentary Facies of the Dundas Group

3.1 Introduction

Five main sedimentary facies have been recognised from the Dundas region. The characteristics and preferred interpretation of depositional process for each are outlined in Table 3.1. The main sedimentological attribute used in this classification scheme is grainsize (ie. facies 1-4), however the style of organisation of depositional units and/or provenance characteristics have also been considered in distinguishing facies 5 (volcaniclastics). This scheme follows the general outline of facies-classification proposed by Pickering et al. (1989), but with some simplifications: eg. their facies classes D-E (silts, silty muds and >95% mud-grade sediment) are amalgamated into facies 4 in this study, and a two-tier classification scheme is employed instead of their detailed three-tier scheme. In addition, it is considered that *immature volcaniclastic deposits* (facies 5) are sufficiently distinctive in terms of their provenance (ie. a large component of essentially unreworked volcanic debris) to require the addition of a unique facies class. Second-order classification is defined for most facies types on the bases of textures such as particle shape, degree of internal organisation and the presence or absence of distinctive sedimentary structures.

3.2 Facies 1: Conglomerates

Conglomerates are perhaps the most distinctive lithologies in the Dundas region. This is principally due to their greater resistance to weathering compared to finer-grained lithologies. Consequently in previous mapping studies of this region, conglomerates have been employed as lithostratigraphic markers.

They occur as very thick, laterally discontinuous bodies and less commonly as isolated thin to medium bedded units contained within finer-grained successions. Although conglomeratic deposits are recognised throughout the Dundas region, they are most voluminous in western areas. A variety of conglomerate types have been distinguished on the basis of clast morphology and degree of organisation. The vertical and lateral distribution of each sub-facies along with their sedimentary characteristics are discussed below.

Table 3.1. Sedimentary lithofacies of the Dundas Group and correlates

Facies	Sedimentary Features	Transport and Sedimentation	Biostratigraphic ranges
1	**Conglomerates**		
1A	*Clast-supported conglomerate* • clast-supported granule to cobble grade conglomerate, usually lacking internal organisation, with reverse and normal clast size grading locally developed • channelling, parallel- and cross-stratification developed in more organised deposits • thin to very thick bedded • clasts generally well rounded	High density turbidity current or grain flow deposit	Middle Cambrian to Latest Cambrian (?Undillan - ?Payntonian)
1B	*Disorganised matrix-supported conglomerate* • matrix-rich conglomerate and pebbly mudstone lacking internal organisation and stratification • poorly sorted with clasts ranging 1mm-3m • diversity of clast-types and shapes including well rounded particles similar to those contained in subfacies 1A and irregular intraclasts comprising mudstone, sandstone and conglomerate	Cohesive debris flow	?Middle Cambrian to early Late Cambrian
1C	*Open- to closed-framework mafic/ultramafic clast breccia* • disorganised, unstratified and laterally discontinuous • generally poorly sorted, angular to moderately rounded fragments ranging <1mm to 1m diameter • monogenetic provenance, with clasts derived from MUC	Rock-fall, with localised redeposition as cohesive debris flow	?Middle Cambrian
2	**Sandstones**		
2A	*Thick-bedded poorly organised sandstone* • thick- to very thick-bedded (≥ 40cm) fine to very coarse-grained sandstones • sharp tops and bases of beds • sorting poor to moderate • lacking internal organisation; massive with weak normal grading near bases • angular mudstone intraclasts dispersed throughout some beds • tractional features near tops of some beds, commonly distorted as a result of liquidization/fluidization	Sandy debris flows transitional to high-density turbidity currents; possible reworking of the tops of beds by bottom current activity	Middle Cambrian to early Late Cambrian
2B	*Parallel-stratified lithic-rich sandstones* • medium to thick bedded • complex vertical grainsize variations with normal, reverse and symmetrically graded bands • basal surfaces are planar to irregular (erosive) • thin Bouma-type intervals preserved at the tops of some beds	Traction carpet sedimentation from high-density turbidity currents; probable oscillating current velocities resulting from interaction of flow with sea-floor topography	?Middle to Late Middle Cambrian

Table 3.1 (cont.)

Facies	Sedimentary Features	Transport and Sedimentation	Biostratigraphic ranges
3	**Sandstone-mudstone couplets**		
3A	*Normally graded sandstone-mudstone couplets* • very thin to medium bedded, with sandstone-mudstone ratio ranging from approximately 1:5 to 2:1 • normal grading common with Tabcde, Tbcde, Tbce and Tbe Bouma sequences • load structures and pseudonodules common	High- to low- concentration turbidity currents	Middle Cambrian to Late Cambrian
3B	*Ripple-laminated sandstone-mudstone couplets* • very thin to medium bedded • fine to medium grained sandstone • moderate to good sorting • generally lacking systematic vertical sequence • complex lamination textures in many sandstones: parallel-, wavy-, lenticular-, cross-laminated • rare sandstones appear internally structureless or show weak normal grading • erosional surfaces at base and top of some sandstone layers; others show gradational basal contacts and sharp tops • internal erosional surfaces common • coarse basal lags • pre-lithification disturbance of primary sedimentary structures common	Strong traction current sedimentation, probably in response to bottom current activity. Possible reworking of fine-grained sand introduced into basin as sandy debris flows.	Middle Cambrian to early Late Cambrian
4	**Fine-grained sediments** • structureless mudstone, mudstone with delicate, parallel siltstone laminations, and ripple-laminated mudstone-siltstone couplets • sufficiently thick siltstone horizons and lenses show evidence of traction current sedimentation with erosional bases and parallel to cross-laminated interiors • Bouma Tc-Te divisions preserved in many mudstone-siltstone couplets	Structureless mudstone accumulating from hemi-pelagic fall-out. Parallel- and ripple laminated sediments depositing from low concentration traction currents (ie. turbidity or bottom currents)	Middle to Late Cambrian

Table 3.1 (cont.)

Facies	Sedimentary and compositional features	Mode of emplacement	Biostratigraphic ranges
5	**Immature volcaniclastic deposits**		
5A	*Feldspathic crystal-rich sandstone* • very thick depositional units (≥30m) • sharp planar base, possibly erosional • internal structure defined by massive, normally graded basal division and fine-grained, thinly bedded upper division • liquefaction features conspicuous particularly within upper division • detritus consisting mainly of rapidly redeposited, texturally unmodified juvenile volcanic debris: crystals, rare pumice fragments and ?ashy material in fine-grained tops • ?accidental volcanic and sedimentary lithic fragments concentrated towards base • matrix consists of chlorite- and/or albite-altered ?formerly glassy material	Basal division deposited from a single high density turbidity flow. Upper division deposited as either continuous suspension fall out from a surging low density turbulent flow or more episodic sedimentation following reworking of fine-grained material stored temporarily at higher positions on the basin slope.	?Middle Cambrian
5B	*Felsic vitriclastic sandstone* • very thickly bedded, crudely stratified, with normal grading of dense lithic particles • reverse grading defined by concentration of pumice fragments occurs towards the top of some beds (density grading) • shards and streaky pumice fragments are the main vitriclasts; crystals comprise the remainder of the juvenile volcanic component • possible phenocrystal Cr-spinels are contained within some vitriclasts	Syn-eruptive products of large-scale explosive events deposited from high density turbidity currents.	late Middle Cambrian
5C	*Quartz-feldspathic crystal-rich sandstone* • poorly organised crystal-rich sandstones with mud or less commonly formerly glassy matrices • coarse-fraction grading was identified at the base of one unit • large, rounded and fractured quartz crystals are a conspicuous detrital component • coarsely porphyritic ?pumice blocks appear up to 50cm in diameter	Sedimentation from cohesive to incohesive debris flows or high concentration turbidity currents. Initial fragmentation mode probably resulting from large scale explosive eruption.	late middle Cambrian
5D	*Basalt fragment-bearing mud-matrix breccia* • matrix-supported, disorganised, unstratified and very poorly sorted • large blocks of vitriclastic sandstone with intermixed basaltic debris occur randomly distributed throughout unit • basalt fragments are quench-textured, dense or vesicular and show globular or blocky outlines • delicate commingling of basaltic debris with both vitriclastic sandstone and non-volcanogenic mudstone hosts	Cohesive debris flow containing redeposited volcaniclastic and sedimentary debris; fragmentation and mingling of basaltic lava clasts via interaction of hot lava with unlithified sediment - ie. resedimented peperite	latest Middle Cambrian-early Late Cambrian

3.2.1 Subfacies 1A: Clast-supported conglomerates

Clast-supported, crudely- to well-stratified conglomerates comprise the bulk of the coarse-grained facies. Stratigraphic units included in this subfacies are the Red Lead, Razorback, Fernfields and Misery Hill conglomerates of previous workers (Elliston, 1954; Rubenach, 1967; Brown, 1986). As many of these stratigraphic names are only applicable to the type section in the Dundas River area, they are abandoned for the purposes of this discussion. The thickest accumulations of this lithotype are mappable at scales of up to 1:50000. On the facies distribution map (Fig. 2.1) they are shown as broadly lensoidal bodies, none of which can be traced along strike with confidence for more than a couple of hundred metres. Although this is partly due to structural complications and poor exposure, it is considered here to reflect an overall primary lenticular facies geometry.

The geometric and textural features of depositional units are summarised in the graphic sections shown in Figure 3.1 and supplemented by hand specimen and field photographs in Figure 3.2. Least organised units exhibit poor sorting (Fig. 3.2a), with clast sizes sometimes ranging < 1cm to 40cm within a single bed. The degree of clast roundness is moderate to good. Sandstone and mudstone intraclasts comprise a minor constituent of some beds. Clasts are usually in grain contact but sometimes are separated by medium- to coarse-grained sandy matrix. The matrix content and clast size can vary laterally within beds as shown in Figure 3.1b, where discontinuous 'pockets' of pebbly sandstone occur enclosed by clast-supported conglomerate. Grading is generally absent in disorganised conglomerate (Fig. 3.1a), however narrow zones of reverse and normal grading were observed at the bases and tops of a few beds (Fig. 3.2c). With increasing degree of internal organisation, normal grading, that may be present only in the upper portion of the beds or throughout the entire bed, becomes conspicuous (Figs. 3.1c-e). Thin, parallel stratified sandstone horizons may occur close to the top of such beds. In general, organised conglomerates show better sorting (moderate to good) and smaller clast-sizes (Fig. 3.2b).

Amalgamation of disorganised conglomerate beds is common. Stratification is indistinct in such cases, resulting in massive units with apparent thickness of up to 30m. Where individual beds are distinguishable, they exhibit planar, sharp boundaries. Common irregularities along basal surfaces are due to penetration of clasts into underlying finer-grained lithologies (eg. Fig. 3.1a). Upper surfaces may be draped by thin veneers of mudstone or show sharp contacts with massive sandstone. Channelling is not obvious on outcrop scales (maximum trace along strike is 10m), however a few beds have undulatory or very broad convex downward bases.

Normally graded conglomerates have sharp bases and sharp to transitional upper surfaces (Figs. 3.1c, d). In the latter case, progressively finer-grained conglomerate passes upward into coarse- to medium-grained sandstone. This sandstone is either

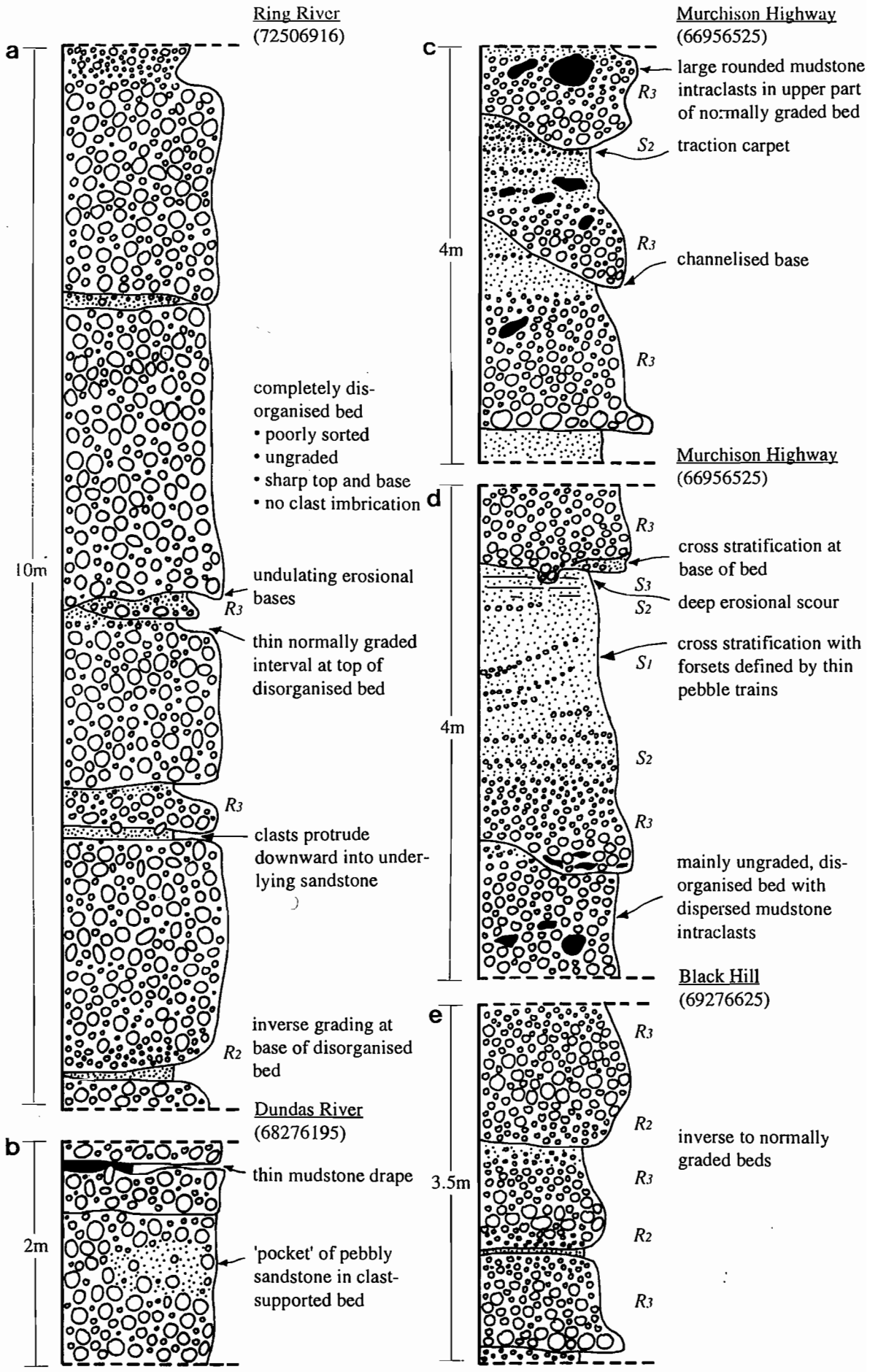

Figure 3.1. Graphic logs depicting various degrees of organisation in subfacies 1A conglomerates. **(a)** thickly bedded, disorganised conglomerate with rare, thin, inversely-graded intervals at base and normally graded tops; **(b)** amalgamated, sharply bounded disorganised conglomerate beds; **(c)** channelised normally graded conglomerate with abundant mudstone intraclasts in upper parts of beds; **(d)** interbedded disorganised and normally graded, stratified conglomerate; **(e)** crudely stratified conglomerate with inverse to normal grading or normal grading throughout. R2-S3 correspond to divisions of Lowe (1982) for deposits from high-density turbidity currents. X-axis of graphic logs is a schematic grainsize scale with grainsize increasing to right.

Figure 3.2. Examples of textures and bed organisation in subfacies 1A.

(**a**) Well-rounded, poorly sorted, polymict clast assemblage in hand specimen sampled from disorganised conglomerate bed. Matrix is composed of medium- to coarse-grained lithic sand. Diameter of coin is 23mm. (Sample 350)

(**b**) Increased degree of sorting accompanied by closer-packing in chert-dominated conglomerate. Additional clasts include angular black mudstone. Diameter of coin is 20mm. (Sample D152)

(**c**) Thin (5cm) normally graded interval at top of very thick (1.5m) disorganised conglomerate bed. An abrupt grain-size reduction is shown at the contact of the disorganised interval and the overlying normally graded interval (thick arrow), with the latter displaying typical T_a and T_b Bouma divisions (S_3 and T_t respectively of Lowe (1982)). The base of the overlying disorganised conglomerate bed is poorly sorted, but shows a subtle inverse size-grading. The basal surface is sub-planar with minor scouring of underlying sandstone to the left of the figure and local downward protrusion of rounded clasts. Length of pencil is 15cm. (Ring River: 72006913)

(**d**) Upper part of moderately organised conglomerate bed with parallel stratification defined by inversely graded, laterally continuous to lensoidal pebble conglomerate intervals within massive sandstone. The unit youngs toward the left. Length of hammer is 30cm. (Dundas River: 68136180)

(**e**) Crude, low angle cross-stratification in pebbly sandstone interval contained within disorganised conglomerate. Length of hammer is 30cm. (Black Hill: 69686649)

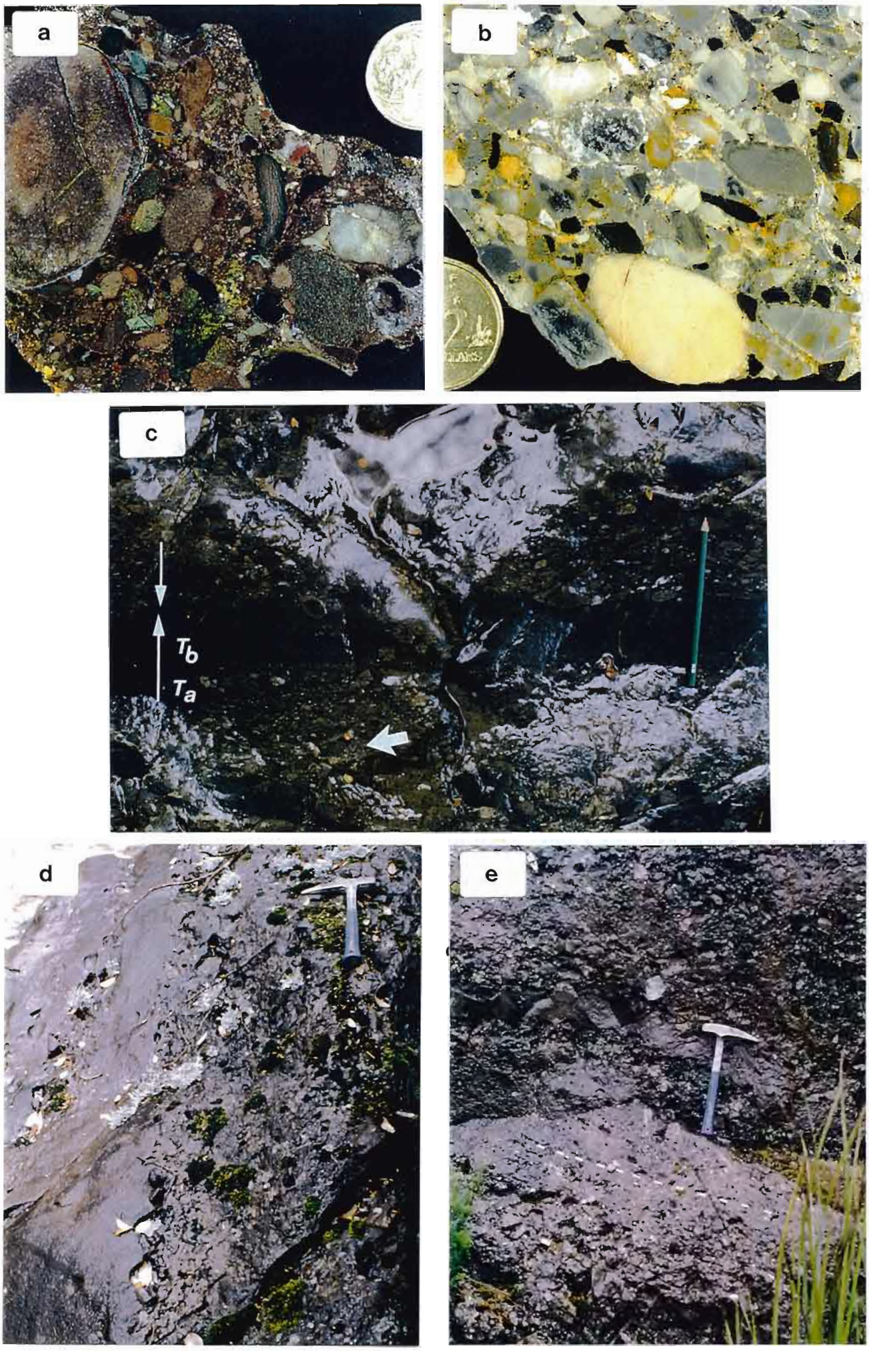
a
b
c
T_b
T_a
d
e

massive or parallel- or large-scale cross-stratified: stratification is defined by thin granule or pebble trains (Figs. 3.1d and 3.2d, e). In rare examples, cross-stratification was observed in lower portions of conglomerate beds. Evidence for erosion at the bases of these conglomerates is common, with scours filled by coarse-grained conglomerate measuring up to 50cm across (Fig. 3.1d). Larger scale channels show smooth convex downward to steeply-sided geometries (Fig. 3.1c). Irregularly shaped intraclasts are common close to the base of channellised conglomerates but may also occur in higher portions of the beds. Intraclasts range in dimension from cm-sized wisps to partially dismembered rafts up to 3m in length.

Transport and depositional processes

The variation in internal organisation of subfacies 1A conglomerates is interpreted to have resulted from differences in transport and depositional mechanisms. The largely ungraded, disorganised units are considered to have deposited from highly concentrated debris flows which were mainly cohesionless: ie.. particles were kept buoyant and suspended in the flow mainly by the dispersive pressure exerted by grain interactions (cf. Bagnold, 1956; Stauffer, 1967; Lowe, 1982; Shanmugam et al., 1995). That reverse grading is limited to the lowermost portions of only a few beds presumably indicates that fall out rates from suspension were too high to allow the formation of thick traction carpets. Deposition occurred by *en masse* settling of grains from a poorly sorted and essentially ungraded flow due to frictional freezing (cf. Lowe, op cit.). The presence of matrix-rich 'pockets' of pebbly sandstone within disorganised deposits is interpreted to indicate that transport processes were complex in some flows, with clast-support mechanisms including both grain dispersive pressure and matrix support.

The low volumes of sand associated with disorganised conglomerates may indicate that finer-grained material (ie populations 1 and 2 of Lowe, 1982) was separated from the pebble and cobble fraction and deposited further downslope. It is probable therefore that the conglomerate beds represent only part of the material incorporated in the depositing flows. In gravelly high density turbidites, detritus can be effectively fractionated according to grainsize and flow-type, with coarse-grained material transported by debris flows processes within the lower part of the flow and progressively finer-grained detritus transported by turbulent flow in upper portions (Lowe, op cit.). Deposition of material from lower and upper portions of the flow may occur independently and at different locations on the slope. Disorganised clast-supported conglomerates would be expected to comprise the most 'proximal' deposits formed from flow-types of this sort. Heterogenous deposits involving both clast- and matrix-supported domains could represent situations where turbulent flow was not sufficiently evolved to allow complete separation of fine and coarse-grained detritus prior to deposition.

The presence of normal size grading in more organised conglomerates indicates that flow turbulence was an important particle-support mechanism (Cas, 1979; Lowe, 1982). Many beds of this type show internal geometries consistent with R2→S3 divisions characterised by gravelly and sandy high density turbidites of Lowe (op cit.) (Fig. 3.1d). Apparently inconsistent with turbulent flow however, are the large 'floating' intraclasts which occur well above the base of some beds. According to Stauffer (1967), Hein (1982) and Shanmugam et al. (1995), 'floating' intraclasts are difficult to explain in terms of deposition from turbulent flow as they would tend to disintegrate during turbulent activity and due to their large size, would be expected to settle rapidly towards the base of the flow. Flows may not have been fully turbulent therefore and may in part have involved particle-support, matrix strength or buoyancy processes. This interpretation is consistent with the positioning of intraclasts within massive portions of beds, however they are sometimes observed in portions of units which show distinct normal grading and hence necessitate deposition from turbulent flows. A possible solution to this problem could involve introduction of intraclasts into the conglomerates during progressive deposition of particles rather than during transport. Considering the highly erosive nature of these depositing currents, rafts of channel-margin strata could easily become detached and included at any level of a progressively depositing conglomerate bed. Due to the turbulent action of the current close to the depositional surface, intraclasts would be expected to show some reworking and dismemberment.

3.2.2 Subfacies 1B: Disorganised matrix-supported conglomerate

Matrix-supported conglomerates were recognised at several stratigraphic levels ranging from probable middle Middle Cambrian to early Late Cambrian in age. In the type section of the Dundas Group however, this subfacies is essentially restricted to Late Cambrian strata. The thickness of individual depositional units ranges < 30cm to at least 25m, with the most significant accumulations in terms of volume occurring close to the western limits of present Dundas Group distribution. Other volumetrically significant deposits of this type occur close to the eastern margin of the study area (ie. within the belt of rocks extending northward from Moores Pimple to the Ring Valley Mine: Fig. 2.1), with a few thin units (< 5m thick) also recognised to the west of these positions in the region of Fraser Creek. Those units which have previously been given formal stratigraphic names include the Fernflow Conglomerate (type area of the Dundas Group) and the Salisbury Conglomerate (Rosebery Group correlate).

Bed geometries are tabular to highly irregular. In the few examples where primary depositional contacts were observed, bounding surfaces were usually sharp with non-erosive bases and irregular, hummocky tops. The Fernflow Conglomerate is an exception in that it has a transitional base with underlying slumped strata (Fig. 3.3a;

Figure 3.3. Subfacies 1B

(**a**) Schematic graphic log showing textural gradation from chaotically folded, slumped strata to overlying matrix-supported pebbly mudstone (approximately 40m mark) near the base of the Fernflow Conglomerate (Dundas River: 67806135). X-axis of graphic logs is a schematic grainsize scale with grainsize increasing to right.

(**b**) Pebbly mudstone containing scattered well-rounded, 'extrabasinally'-derived clasts supported by silty mudstone matrix. Clast-types include quartzite with subordinate lithic sandstone and mudstone. This outcrop forms part of the Fernflow Conglomerate exposed in the Dundas River (typical quality of exposure) and is positioned at 47m mark in (**a**). Hammer handle is 30cm in length.

(**c**) Polymict mud-supported conglomerate containing a rounded clast of close-packed pebble conglomerate (C), irregular pale grey mudstone clasts (M), well-rounded 'extrabasinally'-derived clasts (arrow) and angular igneous fragments (basalt and gabbro) inferred to have been sourced from the MUC (I). Pen is 13cm in length. (Ring River: 71956918)

(**d**) Tabular and wedge-shaped blocks of mudstone contained in matrix-supported conglomerate. Long margins of blocks (oriented horizontally in the photograph) are planar and oriented parallel to undisturbed internal laminations. The terminations of blocks are ragged and locally transitional with the enclosing muddy matrix. Notebook is 13cm in width. (Ring River: 71956918)

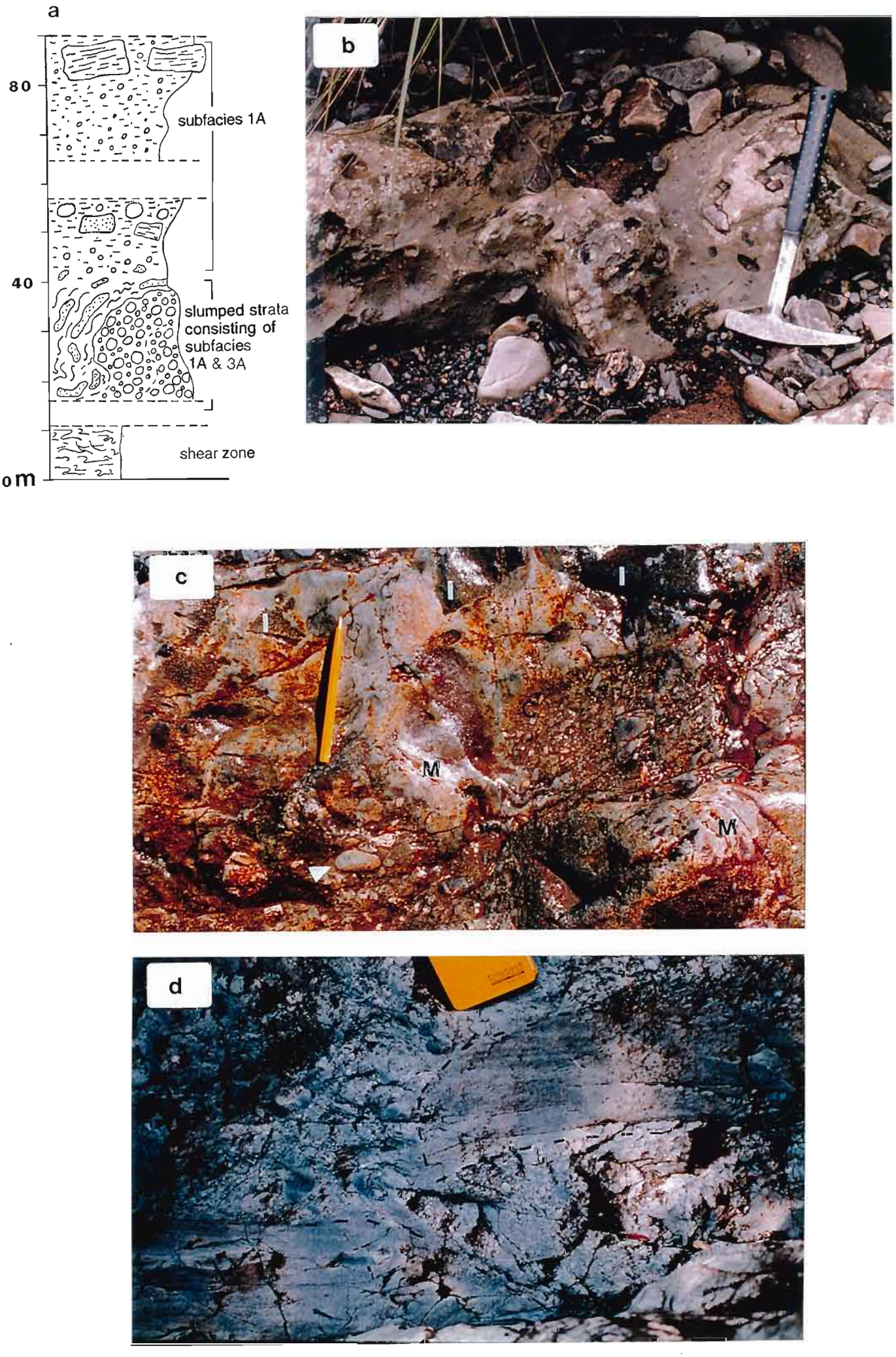
a
80
40
0 m
subfacies 1A
slumped strata consisting of subfacies 1A & 3A
shear zone
b
c
M
M
d

see also Section 2.1.5). The underlying unit consists of a recumbently folded interval of intercalated subfacies 1A conglomerate, normally graded sandstone (subfacies 3A) and laminated mudstone (sub-facies 5).

Determination of the lateral extent of sub-facies 1B deposits is hampered by limited exposure. 20m was the maximum distance any particular bed could be traced along strike, however units comprising several amalgamated flows are likely to extend over 100m or more. Internally, depositional units are disorganised, unstratified, extremely poorly sorted and the clast/matrix ratio can vary significantly throughout a single bed. Where the latter was observed, clasts were commonly arranged in 'nests' with crudely defined margins. Particles contained in these 'nests' may be dominated by a particular clast-lithotype and morphology.

In general, no preferred alignment of clasts was seen in these conglomeratic units. In cases where a planar fabric is developed however, clasts are enclosed by an anastomosing spaced cleavage and show evidence of internal brittle disruption. This alignment of clasts is therefore interpreted to reflect post-depositional tectonic flattening. Clast-size ranges from < 1mm up to 3m (in their longest dimension) in the thicker flows. Matrices are usually mudstone, however coarser material including poorly-sorted medium-grained sandstone occurs locally.

Rare normally graded granule conglomerate to coarse-grained sandstone horizons (up to 1m in thickness) occur intercalated with disorganised matrix-supported conglomerate in the package exposed 1km north of Moores Pimple (CP744652). These beds show moderate sorting, clast-support, internal planar stratification and erosional bases. Compositionally, normally graded beds are indistinguishable from the enclosing conglomerate.

Clast types consist of a diverse range of lithologies and morphologies. Those which are considered likely to have ultimately been derived from an extrabasinal source, clast sizes ranging from granules to boulders, appear indurated at the time of incorporation within the conglomerate and show moderate to high degrees of roundness (Fig. 3.3b). These are similar to clasts contained in subfacies 1A conglomerates. Of probable intrabasinal origin are irregular clasts and blocks of mudstone, sandstone and conglomerate (facies 1A) which appear texturally and compositionally similar to other penecontemporaneous lithofacies of the Dundas Group (Fig. 3.3c, d). Clasts of this type show blocky, rounded and irregular morphologies. They are distinguished from 'extrabasinally'-sourced clasts by the presence of soft sediment deformation features. Such features include 'flamey' margins which intermingle with the surrounding matrix, folded and contorted internal lamination (with no axial planar cleavage) and partial disaggregation of particles along the rounded margins of coarse-grained clasts. Some particularly large mudstone rafts (≈ 3m in length) show little evidence for ductile deformation however, with sharp planar margins and internal brittle microfaults.

Evidence for an intrabasinal origin for these clasts is based solely on compositional similarities with neighbouring packages of coherent mudstone. In the thick conglomerate exposed in the Ring River near CP720692 (Fig. 2.1), an additional clast-type, highly angular mafic lava and mafic-ultramafic plutonic fragments, was observed. These are also interpreted to have been sourced from within the basin and are considered to be reworked talus debris which was shed from fault scarps (see subfacies 1C).

Transport and Depositional Processes

Features including dominantly muddy matrix-support of clasts, lack of internal organisation, very poor sorting, inclusion of intrabasinal clasts (some of which exceed 3m in length) and sharp upper and lower bounding surfaces are typical of cohesive debris flows (Middleton and Hampton, 1973; Lowe, 1979; 1982; Postma, 1986). The dominant mechanism of particle support in such flows is provided by the cohesive strength of the clay-water matrix (Lowe, 1982). Leigh and Hartley (1992) argued that this process is capable of supporting only relatively small particles (ie. up to coarse-grained sand) and to explain the transport of larger clasts requires additional components of particle dispersive pressure and/or bouyancy induced by elevated pore-fluid pressures beneath outsize clasts. Similar combinations of simultaneously active support mechanisms have been invoked for the transport of clasts up to 20m across in the subaqueously deposited Parnell Grits (early Miocene), northern New Zealand (Ballance and Gregory, 1991). Localised intercalation of normally graded, organised horizons within compositionally analogous disorganised conglomerate is interpreted to indicate that portions of the flows sometimes became turbulent. This transformation of flow-type probably resulted from ingestion of water, presumably at the head of the transporting mass.

The general lack of internal stratification in these deposits is interpreted to indicate that deposition occurred *en masse* via frictional freezing during flow deceleration (Lowe, 1982). Upper portions of flows which were possibly turbulent may have become separated from the underlying cohesive mass and travelled further downslope from high-density turbidity currents.

In consideration of the abundance of deformed sedimentary clasts which resemble other Dundas Group lithotypes, it is suggested that these debris flow deposits were intrabasinally derived. The inclusion of clasts of extrabasinal origin could have resulted from minor direct input from a basin-margin feeder system, but they were perhaps more likely to have been derived during disaggregation and redeposition of subfacies 1A conglomerate units. This latter interpretation is supported by the vertical transition at the base of the 'Fernflow Conglomerate' from an inferred slump deposit containing deformed subfacies 1A units to the overlying debris flow deposit which

contains scattered, well-rounded and indurated clasts. Textural gradation from slumps (or slides) to debris flows have been described by Middleton and Hampton (1973), Naylor (1981) and Gawthorpe and Clemmey (1985) and have led these and other workers to suggest a genetic relationship between these two depositional facies. Naylor (op cit.) for instance considered that the 530m thick succession of debris flows (or 'olistostromes' in his terminology) in the Casanova areas of the Northern Appenines was derived entirely from the disaggregation of slumps or slides. The processes which lead to the transformation of slumps to debris flows however, are less well understood. A combination of mechanical disaggregation of strata as a result of layer rotation and/or extension (cf. Gawthorpe and Clemmey, op cit.) and mixing with water at the head of the translating mass (cf. Shanmugam et al., 1995) would seem likely.

3.2.3 Subfacies 1C: Open- to closed-framework mafic/ultramafic clast breccia

The distribution of this lithofacies is mainly restricted to the western limits of Dundas Group exposure: specifically along the eastern margin of the Serpentine Hill MUC at CP719692 and CP718686 (Fig. 2.1), where they occur close to the base of the local stratigraphy. Breccias are exposed in the Ring River at the northern locality and intersected in drill core at the southern locality. Another very poorly exposed conglomerate unit situated 1km SE of Godkin Ridge at CP716653 is tentatively included within this facies-type. The descriptions given below involves data collected principally from the former localities.

The breccia units form discrete, laterally-impersistent bodies which occur intercalated with both subfacies 1A and 1B conglomerates (Fig. 3.4a). They range in thickness from 7-28m and have sharp or less commonly transitional contacts with enclosing sedimentary rocks. In most cases however, the margins of breccia units are either unexposed or faulted. Internally, units exhibit a disorganised fabric and lack evidence of stratification (Fig. 3.4b). Some breccias have closed-framework textures whereas others are matrix-supported. In both cases however, sorting is very poor and the matrix is fine-grained, comprising mudstone or sandy mudstone. Closed-framework breccias involve clasts ranging in size from 5mm to 1m, and in degree of roundness from highly angular to sub-angular. They exhibit tabular, polygonal and splinter shapes (Fig. 3.4c). Clasts may be in direct contact with their neighbours, however they are more commonly enclosed entirely by matrix. In general, as the matrix content increases, grain-size is reduced whereas the degree of clast-roundness is enhanced, with clasts sometimes showing moderately rounded morphologies.

The lack of organisation and in particular the matrix-support shown by some of these breccias resembles textures characterised by units included in subfacies 1B. The main distinguishing feature of the two lithofacies is clast composition. Whereas subfacies 1B involves polymict clast assemblages which include abundant

Figure 3.4. Facies relationships and textures associated with subfacies 1C.

(**a**) Graphic log showing facies relationships from exposures in the Ring River near 719692. An easterly facing succession of conglomerate units is depicted, with intercalation of subfacies 1A-C. The lower subfacies 1C unit comprises closed- to moderately-open framework, unstratified conglomerate which contains angular clasts sourced from the MUC. Angular MUC-derived clasts are also found in enclosing sub-facies 1B conglomerate. The uppermost subfacies 1C unit is lensoidal, and contains angular to sub-rounded, matrix-supported igneous fragments. The base of the succession is in faulted contact with low-Ti basaltic lavas of the Serpentine Hill MUC.). X-axis of graphic logs is a schematic grainsize scale with grainsize increasing to right.

(**b**) Boulder of subfacies 1C conglomerate situated 100m downstream from the base of the section depicted in (**a**). Clasts appear as recessions in the rock surface and exhibit extremely poor sorting, moderately close packing and predominantly angular habits. The disorganised fabric and lack of stratification shown in this figure is typical of subfacies 1C. Length of hammer is 80cm.

(**c**) Poorly sorted, angular to sub-rounded plutonic fragments. The clast assemblage is almost monomict and consists of micro-gabbro. Clasts include tabular, polygonal and splintery habits. At the right of figure, clasts are in grain contact, whereas to the left individual clasts are completely enclosed by matrix.

(**d**) 1.5cm thick shear zone developed within micro-gabbro clast (margin highlighted by dotted line). Note that the shear zone terminates abruptly at the margins of the clast.

(**e**) Photomicrograph of mylonitised micro-gabbro clast shown in (**d**). A mylonitic foliation developed in the upper half of the figure is defined by the alignment of winged porphyroclasts of saussuritized feldspar (F), set in a groundmass of recrystallised pyroxene (now replaced by actinolite). The lower half of the shear zone is weakly foliated, but intensely recrystallised with relict, randomly oriented porphyroclasts. Crystal grain-size shows crude, but non-uniform increase towards the outer margins of the shear zone (upper and lower margins of figure). The margin of the clast is shown by the vertically oriented, irregular surface at the left of the figure (sedimentary matrix labelled M). (crossed polars) (Sample 96-001)

(**f**) Photomicrograph of matrix-rich portion of subfacies 1C breccia. Micro-gabbro clast outlines are enhanced by dotted lines. Matrix consists of poorly sorted, angular crystal fragments set in dark brown ?muddy groundmass. Crystals include actinolized pyroxene, most of which exhibit intra-crystalline strain (arrowed crystal fragment has kinked diallage parting), feldspar and unstrained quartz (q). (crossed polars) (Sample D170)

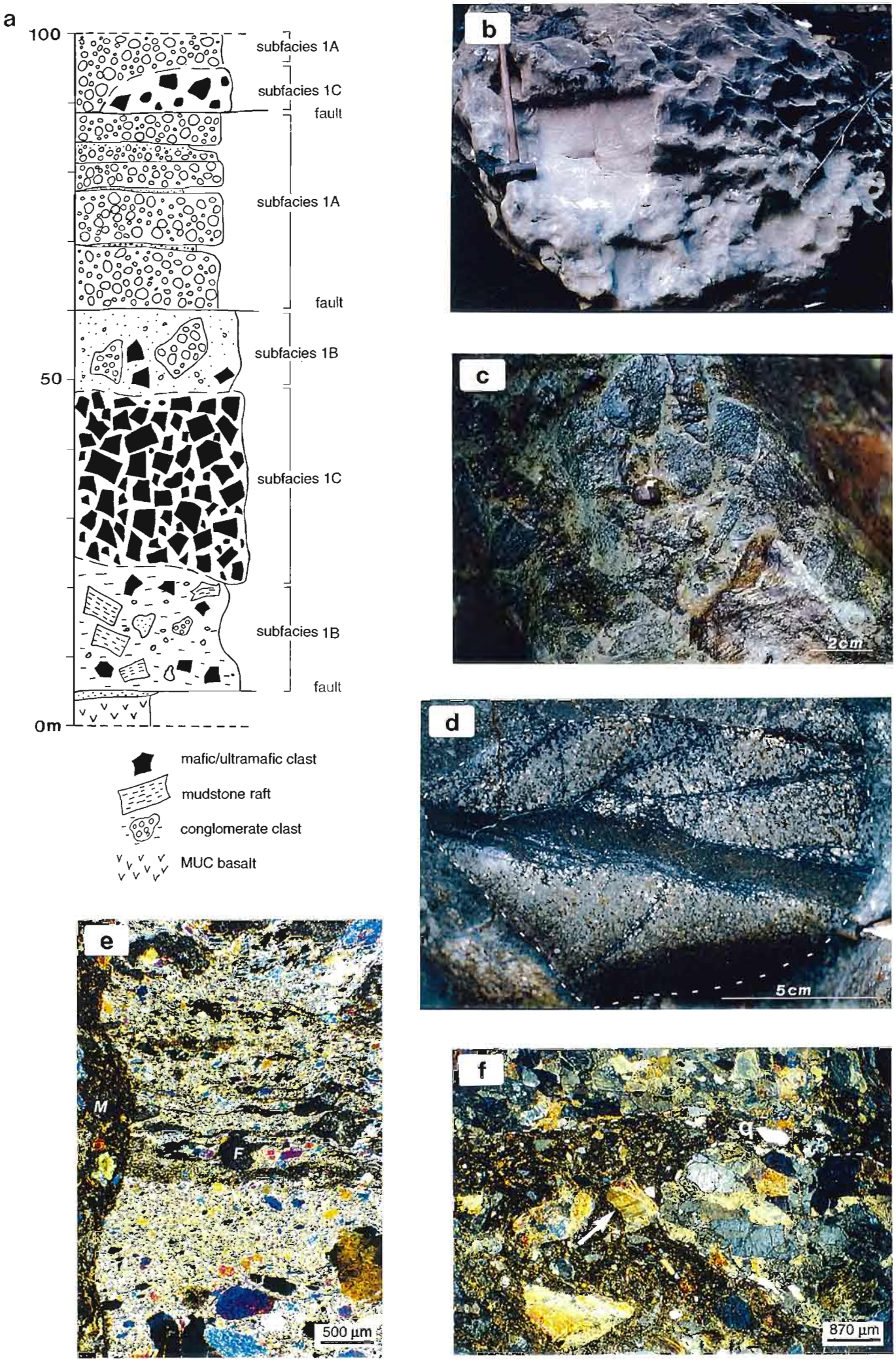
a
100
50
0m
subfacies 1A
subfacies 1C
fault
subfacies 1A
fault
subfacies 1B
subfacies 1C
subfacies 1B
fault
mafic/ultramafic clast
mudstone raft
conglomerate clast
MUC basalt
b
c
2cm
d
5cm
e
M
F
500 µm
f
q
870 µm

intrabasinally-derived sedimentary fragments, subfacies 1C comprises clasts which are largely monogenetic and lacking in sedimentary material. Clast-types are mainly of igneous origin and involve lithologies which are consistent with derivation from the MUC: massive and layered gabbro, micro-gabbro, serpentinised pyroxenite and basalt. Thus although a single dominant source is interpreted for these breccias, clast-types are not strictly monomict and involve both plutonic and extrusive lithotypes. Furthermore, microstructural evidence from some clasts indicates that the source rock was intensely deformed prior to fragmentation. An example of the high strains exhibited within these clasts is shown in Figures 3.4d and 3.4e, where a narrow mylonitic shear zone penetrates a fine-grained gabbroic fragment (flaser-gabbro) but terminates abruptly at the clast margin.

Sedimentary clast-types are a minor component and include mudstone, siltstone and chert. Whereas the latter are generally rounded, mudstone and siltstone fragments are irregular, with wispy margins and contorted internal laminations (where preserved). They are also commonly impinged upon by neighbouring rigid igneous clasts.

The matrix (Fig. 3.4f) includes material derived from both igneous and sedimentary sources. The fine-grained fraction (silt to mud) consists of randomly oriented needles and splinters, interpreted to have been derived from disaggregated pyroxene crystals, set in a very fine-grained chloritised groundmass. The groundmass is probably composed of mud, as there is no evidence to indicate that it was formerly glassy. Coarse-grained pyroxene, saussuritised plagioclase, hornblende and rare chromite crystal fragments were observed as part of the sand-sized fraction. Many of these grains are strained, with development of mechanical twins in feldspar and kinking of diallage cleavage in relict pyroxene. Ferromagnesian crystal fragments are now all replaced by amphibole and chlorite. Additional sand-sized particles contained in the matrix include unstrained quartz (possibly of volcanic origin) and mudstone lithic fragments.

Interpretation

Subfacies 1C exposures in the Ring River were originally mapped as intrusions of gabbro or fine-grained pyroxenite (Blissett, 1962; Rubenach, 1967). More recently they were described as fragmented basalt flows which collided and mixed with sedimentary flows (Brown, 1986: see also Section 2.1.4). The first of these interpretations can be discounted considering that: 1) the units are clearly clastic in nature, 2) clast assemblages are polymict and 3) deformation features in some clasts indicate intense strains prior to fragmentation. The second interpretation, which presumably invokes some sort of autobrecciation process, would also appear unlikely from points 2) and 3) and due to the abundance of fragments of plutonic origin. Although it might be argued that clasts derived from plutonic rocks were entrained

within parental basalt flows as xenoliths, they would be expected to comprise only a very minor volume of the lava. However, within any portion of the breccias, basalt fragments were never observed to comprise more than about 10% of the clastic component. Furthermore, there is no evidence to indicate that the matrix comprises fine-grained basaltic debris, which would be expected if the breccias were derived largely from fragmentation of basalt flow.

Although some clasts contain a strong deformational fabric and margins to the breccias may be faulted, a tectonic origin (ie. fault breccia) is also difficult to reconcile in view of the fact that units are laterally impersistent, enclosed by sedimentary rocks and primary depositional contacts are sometimes preserved along their margins. Moreover, the matrix is essentially undeformed and clasts are not cross-cut by a tectonic fabric.

The association of the features outlined above is considered to favour a sedimentary origin for the breccia units. Their disorganised fabric, immature clast shapes, restricted distribution and monogenetic provenance (the source is inferred as the presently adjacent MUC) are each considered to provide support for deposition proximal to the source. It is suggested that clasts were initially eroded from a steep topography (probably a fault scarp) wherein both plutonic and volcanic portions of the MUC were exposed. Transport of clasts occurred via rock-fall processes, with subsequent accumulation of talus deposits in either a piedmont position or on terraces positioned on the slope. Fabrics possessed by such deposits would be expected to include clast-support, poor sorting, angular clasts and internal disorganisation (cf. Tanner and Hubert, 1991). Infiltration of mud derived from fine-grained particles settling from suspension and sand-sized particles derived mainly from disaggregation of igneous fragments filled voids between the clasts and provided a binding matrix. In periods of relative stability on the slope (ie. tectonic quiescence), mud could have accumulated as thin blanket layers on breccia deposits. With renewed ?fault activity and wasting of the slope, rapid settling of blocks would be expected to contort and dismember fine-grained sedimentary layers.

Talus breccias which accumulated on or at the base of unstable slopes were likely sources of matrix-supported breccias which are considered to have deposited from cohesive debris flows (cf. subfacies 1B).

3.3 Facies 2: Sandstones

3.3.1 Subfacies 2A: Thick-bedded poorly organised sandstone

This facies comprises poorly to moderately well sorted, coarse- to fine-grained sandstones which have a compositional range from relatively clean quartzo-feldspathic to less abundant lithic-bearing varieties comprising subrounded to angular sand- to granule-sized particles of pale to dark grey mudstone, chert and rare volcanogenic material. They are best represented from eastern parts of the Dundas region where they were observed to occur in association with finer-grained sediments (usually sub-facies 4 laminated mudstone), chaotic units (facies 5) and less commonly granule conglomerate (subfacies 1A-1C). Units have also been recognised from the western domain, where they occupy relatively low biostratigraphic levels (middle Middle- to late Middle Cambrian) and occur interbedded with subfacies 1A, 3B and 4.

Individual depositional units range in thickness from 30cm to at least 2m. Most beds are disorganised, lack a well-defined internal stratification and show sharp upper and lower bounding surfaces. The latter commonly include planar amalgamation surfaces resulting in extensive, poorly structured sandstone packages which exceed 20m in thickness. In other cases, beds are separated by thin (< 5cm), parallel laminated or structureless mudstone. Grading is very rare and is usually confined to the lowermost portions of beds where it is defined by a subtle upward decrease in grainsize from granule conglomerate to coarse-grained sandstone. Faint, discontinuous mud lamellae occur near the tops of some beds. In most cases, lamellae appear to have been dismembered prior to complete lithification of the enclosing sand, however relict, undeformed parallel- or cross-laminated intervals were observed rarely.

Angular mudstone intraclasts (5-100mm in diameter) are a conspicuous component in some beds, especially those which comprise 'cleaner' sandstones. They occur randomly dispersed throughout the beds and appear to be suspended by the enclosing sand.

Interpretation

Sandstone units exhibit features which suggest depositional mechanisms transitional between debris-flows and high-density turbidity currents. Stauffer (1967) and Shanmugam et al. (1995) have interpreted thick, massive sandstone beds which involve textural and structural similarities to those investigated in this study, including sharp bounding surfaces and 'floating' mudstone intraclasts, as deposits from non-turbulent, high grain concentration sediment gravity flows. Shanmugam et al. (op cit.) defined these flows as 'sandy debris flows', which involve a range of particle support mechanisms including matrix strength, grain dispersive pressure and bouyancy. Deposition from these flows probably occurred *en masse* by frictional freezing.

The presence of localised intervals of normal grading within some beds and uppermost intervals of laminated sandstone are possibly indicative of transformation from debris flows to high-density turbidity currents. Alternatively, tractional features such as cross-lamination could have resulted from reworking of the tops of sandy debris flows by bottom currents. That these structures were recognised from only a few beds could indicate that their genesis is not directly related to the deposition of the underlying massive interval, which in turn lends support to the interpretation that they resulted from a post-depositional process. Furthermore, some sub-facies 2A sandstones exhibit a close spatial relationship to subfacies 3B sandstone-mudstone couplets, which as it will be shown later in this chapter, are inferred to have been deposited during periods of bottom current activity.

Rapid deposition of subfacies 2A sandstones is likely to have resulted in entrapment of significant volumes of pore fluid (cf. Middleton, 1970). Elevation of pore fluid pressures during burial or perhaps seismic activity would promote liquidization and/or fluidisation of the beds which could account for the dismembered form of mudstone lamellae near the tops of some beds.

The relatively 'clean' quartz-dominated composition exhibited by many sub-facies 2A units is in marked contrast to the lithic-rich composition of most other sandy lithotypes recognised from the Dundas region (ie. sub-facies 2B, 3A). The inferred rapid emplacement of subfacies 2A as debris flows however, would not have involved significant reworking of the clastic component. Redeposition of an already mature quartzose sandstone is therefore required. Similarly low proportions of labile constituents were documented by Stauffer (1967) in massive sandstones of Lower Tertiary age from the Santa Ynez Mountains, California. Stauffer (op cit.) considered the mature compositions of the sands to indicate winnowing and abrasion in a shelf environment prior to redeposition along the basin slope. A similar sedimentation history may be applicable to subfacies 2A.

3.3.2 Subfacies 2B: Parallel stratified sandstones

Parallel stratified lithic-rich sandstones were commonly recognised in association with subfacies 1A conglomerates. Sandstone units are generally volumetrically subordinate to the enclosing conglomerates, however locally they were observed to comprise the dominant lithology. The best examples of this lithofacies occur in the western domain, in particular as part of the coarse- to very coarse-grained package exposed in the Dundas River between CP683623 and CP681616 (Fernfields Conglomerate). Other good examples were found on the Murchison Highway at CP670651, where they occur in association with normally graded and disorganised sub-facies 1A conglomerate (see figure 3.2c, d).

Sedimentation units range from 5-40cm in thickness, with stratification defined by alternating bands of fine-sand to granule-sized particles (Fig. 3.5). Discrete bands are tabular to slightly lensoidal and range in thickness from 2-100mm. Contacts between successive fine- and coarse-grained bands are usually gradational, with rare sharp contacts possibly representing amalgamation surfaces. Grading within beds is usually complex and no systematic vertical variation in grain-size was observed. Individual coarse-grained bands are commonly symmetrically graded, passing with inverse size grading from underlying finer-grained bands to normally graded tops. Uppermost surfaces of beds are invariably planar, except were eroded by younger depositional units and range from sharp to transitional. An example of the latter is shown in Figure 3.5 where normal graded coarse-grained sandstone passes upward through a thin interval of parallel-laminated fine-grained sandstone, into ripple-laminated siltstone and finally structureless mudstone. In cases where subfacies 2B overlies conglomerate, basal surfaces vary from sharp to gradational. Sharp lower contacts are planar or demonstrably erosional with concave upward surfaces which incise up to 10cm into the underlying unit.

No evidence of bioturbation was observed in association with subfacies 2B, however layer disturbance inferred to have resulted from sliding and/or slumping is common.

Interpretation

The internal stratification in subfacies 2B is grossly analogous to progressive 'freezing' of inversely-graded traction carpets developed in high-density sandy turbidites (Hiscott and Middleton, 1979; Lowe, 1982). Unlike the typical sharply-topped, inversely-graded bands described by these and other workers however, many examples observed in this study involved symmetrically graded bands. This structure would tend to indicate that depositional processes fluctuated between traction carpet and suspension sedimentation during the history of the flow (ie. S2 and S3 of Lowe (op cit.) respectively: Fig. 3.5). Flow conditions involving oscillating current velocities (ie. repetitive accelerating and decelerating currents) could possibly account for the lack of a systematic vertical sequence of bed forms in these cases. Vertical grain-size variations corresponding to changing flow conditions is considered likely to have resulted from interaction of the flow with the sea-floor topography (cf. Kneller, 1995).

'Classical' normally graded Bouma-type intervals developed at the tops of some layers are inferred to have deposited from residual high- to low-density turbidity (ie. Tt-Te of Lowe (op cit.)). That these intervals are generally thin and poorly developed suggests that the bulk of these residual flows have bypassed the sites of sub-facies 2B deposition and have either continued downslope or spilled over the margins of channels, the latter confining the distribution of coarse-grained facies.

Figure 3.5 Parallel stratified sandstone beds of subfacies 2B. Individual bands show reverse, normal or symmetrical grading. Deposition of these beds is interpreted to have resulted from alternating episodes of traction carpet (S2, Tt) and suspension (S3, Te) sedimentation. See text for discussion. 1mm divisions on scale to right. (Sample 328).

Figure 3.6 Normally graded sandy portion of subfacies 3A sandstone-mudstone couple. Tb to Te Bouma divisions, deposited from a single waning turbidity current, are well developed. Few examples of subfacies 3A have the near complete 'classical' Bouma sequence shown in this specimen. Arrow points to 'fading ripple' (Tc division) which passes laterally into silty trough. Coin is 20mm in diameter. (Sample 430)

Lowe (1982)

S_3 ? amalgamation surface

S_3

S_2

S_2

? S_2

S_3

T_e

T_t S_3

S_2

? S_3 suspension sedimentation

S_2 traction carpet sedimentation

? S_3

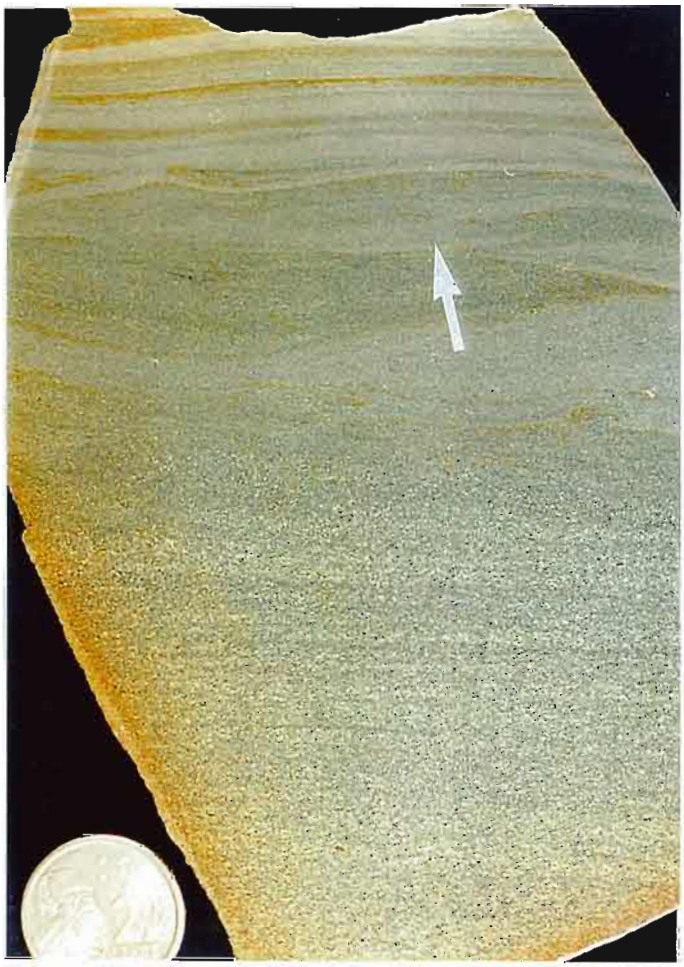

Bouma (1962)

T_e

T_d

T_c

T_b

3.4 Facies 3: Sandstone-mudstone couplets

Facies 3 consists of couplets of alternating coarse- to fine-grained sandstone and mudstone. Alternation between these lithologies occurs on the scale of centimetres to tens of centimetres and packages may be either sandstone- or mudstone-dominated. This facies is widespread throughout the Dundas region, forming packages in excess of 100m in thickness in both western and central areas. Significant thicknesses of this facies are less common in the eastern area, however this is likely to be an artefact of structural complexity and poor exposure in this region. Units have a weak spatial correlation with packages comprising dominantly coarse-grained lithologies (ie facies 1 and 2) but are usually contained within finer-grained mudstone-dominated packages. The thickest deposits were usually recognised as lateral extensions of conglomerate facies, but were also observed to envelope, or occur as intercalations within the latter.

The internal structure of sandstone-mudstone couplets shows a wide diversity, however two broad styles have been distinguished. The first of these, subfacies 3A, involves regular vertical sequences of structures which compare well with those described from classical turbidites (eg. Bouma, 1962). Subfacies 3B on the other hand lacks this vertical sequence in most instances, and involves a more complex and diverse array of sedimentary features. There are some features which are common to both sub-facies, and each may be present within a single depositional package. A continuum of depositional processes may therefore exist between the two subfacies.

3.4.1 Subfacies 3A: normally graded sandstone-mudstone couplets

This facies comprises laterally persistent tabular to slightly lenticular beds which range in thickness from 3-20cm. Gross normal grading from medium- to fine-grained sandstone at the base of beds to structureless or delicately laminated mudstone at the top is ubiquitous. Sorting is poor to moderate. Internally, depositional units exhibit a range of vertical sequence of structures which conform to Ta-e Bouma sequences in very rare cases, and more commonly involve Tbcde, Tbce and Tbe divisions (in many cases the Ta division is absent). Contacts between successive divisions are generally well defined but transitional. Exceptions occur where the Tc and/or Td divisions are absent, resulting in a sharp surface between the lower sandstone-dominated interval(s) and the overlying mud-rich interval(s). The upper surface of Tc ripple-laminated divisions are commonly wavy, below which thick lensoidal fine-sandstone or siltstone lamellae pass laterally into muddy troughs (Fig. 3.6). This form of ripple lamination closely resembles 'fading ripples' of Stow and Shanmugam (1980). Basal surfaces of beds are sharp and planar to irregular with the latter punctuated by scours, load casts and psuedonodules. Many examples of planar to concave upward detachment surfaces oriented at a low angle to bedding were also recognised. These are interpreted as slide

surfaces which developed prior to lithification of the sediment. Evidence of bioturbation was not observed.

Interpretation

Subfacies 3A is interpreted to have been deposited from waning high- to low-concentration turbidity currents. They probably represent finer-grained, lateral (ie. inter-channel deposits) or perhaps distal equivalents of coarse-grained sub-facies 1A and 2B. Kneller (1995) argued these types of 'classical' turbidites form in unrestricted depositional settings. Considering the close lateral and vertical relationships with 'proximal' coarse-grained facies, an inter-channel setting rather than a distal base-of-slope environment is considered most likely in this case.

3.4.2 Subfacies 3B: Ripple-laminated sandstone-mudstone couplets

This sub-facies was recognised at several localities throughout the western and central areas. It occurs in association with a number of different facies-types: fine-grained lithotypes (ie. facies 4 mudstone) are the most common facies association, however massive sandstone (subfacies 2A) and volcaniclastic units (subfacies 6B, 6C and 6D) were also observed together with subfacies 3B at some localities. Turbiditic sandstone-mudstone couplets (subfacies 3A) and subfacies 1A conglomerate (sub-facies 1A) occur in immediately adjacent packages, but not as discrete interbedded units. Packages consisting almost entirely of subfacies 3B occur up to 100m in thickness, and contain both mudstone- and sandstone-dominated intervals. Sandstones are generally medium- to fine-grained, moderately- to well-sorted and 'clean', consisting predominantly of quartz with subordinate feldspar, mica, heavy minerals and lithic fragments.

Subfacies 3B sandstone-mudstone couplets are immediately distinguishable from those of subfacies 3A by their lack of features typically associated with turbiditic emplacement. In particular, normal grading is absent, or at best weakly developed in a small percentage of sandstones. Furthermore, the upper surfaces of sandstone beds are invariably sharp and in some cases erosional. It is considered unlikely therefore, that successive sandstone and mudstone beds were deposited from a single turbulent sediment pulse.

Sandstone beds range in thickness from <1-20 cm and exhibit tabular (traceable along strike for at least 15m) to discontinuous lensoidal geometries. Internally, they are usually finely-laminated with sedimentary structures indicating transport via tractive processes. Flaser-, wavy- and lenticular bedding are common, with some sandstone horizons exhibiting ripple lamination throughout (Fig. 3.7a). Ripple geometries are not always constant throughout a bed, suggesting that palaeocurrents were unsteady and multi-directional. Laminae are mud-rich and probably represent periods of suspension

Figure 3.7 Polished hand specimens depicting textural characteristics of subfacies 3B.

(**a**) Portion of flaser-bedded sandstone unit. Ripple forms show opposing dip-directions at different intervals within the unit (arrows), indicating variable palaeocurrent directions. Diameter of coin is 23mm. (Sample 859)

(**b**) Sandstone-mudstone couplets showing planar-, ripple- and low angle cross-lamination. Individual sandstone layers have diffuse lower contacts with mudstone and grainsize varies non-uniformly throughout. Note mud-draped erosional surface within lower sandstone layer (white arrow). The upper surface of this layer appears locally constructional (development of very small lenticular ripples: white arrow head) and locally erosional (low angle truncation of mud lamellae: black arrow head). Height of photographed section is 5cm. (Sample 95-011)

(**c**) Rippled sandstone unit with flaser-bedded lower portion passing abruptly into parallel- and cross-laminated sandstone. Foresets in the latter are thin, tangential with underlying strata and oriented at low angles to topsets. Palaeocurrent is from right to left. (Sample 858)

(**d**) Sandstone-mudstone couplets with four repetitive upward coarsening 'cycles'. The base of each 'cycle' involves structureless or thinly laminated mudstone, which passes vertically with gradational contact into parallel laminated sandstone. The coarser-grained upper portion of sandstone layers were probably originally ripple-laminated, but have been modified by partial homogenisation and folding. The upper surface of each 'cycle' is sharp. (Sample 144)

(**e**) Interbedded mudstone containing thin, irregular silty lamellae and structureless sandstone layers with sharp upper contacts. The bases of sandstone layers load into the underlying mudstone (indicating originally sharp contacts), with complete disruption of lower-most horizon which now appears as a string of dispersed pseudonodules and an isolated tabular 'block'. (Sample 450)

(**f**) Stratally disrupted ripple-laminated sandstone-mudstone couplets. The thin muddy seam in the lower part of the figure (arrow) truncates relict lamellae in both overlying and underlying strata and is interpreted as a pre-lithification glide surface. Sandstone layers show partial homogenisation and annihilation of primary depositional fabrics. Rotated clastic dykes indicating consistent dextral sense of shearing occur in the upper portion of the figure. Diameter of coin is 23mm. (Sample 73)

(**g**) Mottled upper portions of laminated sandstone layers resulting from bioturbation. Numerous escape burrows are well-preserved in the right hand specimen. (left sample 73; right sample 70)


a


b


c


d


e

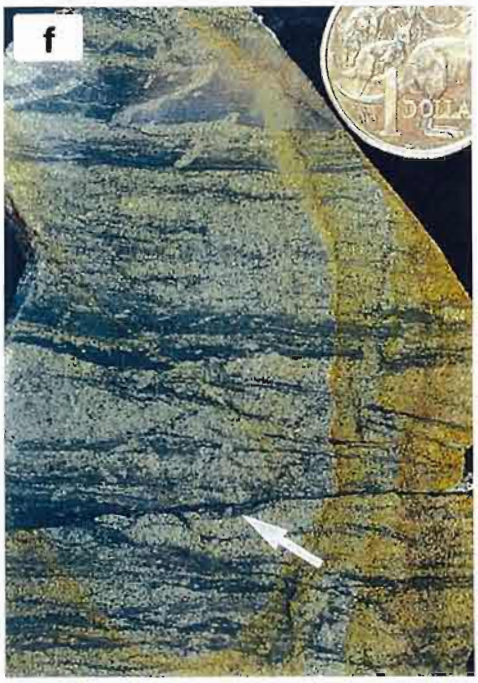
f


g

sedimentation. They thicken in ripple troughs and pinch out over ripple crests. In some cases, mud lamellae drape erosional surfaces which truncate lamellae in the underlying rippled strata. As noted earlier, erosional surfaces occur at the tops of some sandstone layers, however they have also been observed as internal truncation surfaces (eg. Fig. 3.7b). Planar cross-stratification is less common and involves thin, low angle foreset beds (Fig. 3.7c). The abundant ripple-laminated textures in sub-facies 3B sands are in contrast to sub-facies 3A wherein Tc divisions were only rarely developed.

Very thin, parallel, planar to lensoidal laminae of silt- or fine-grained sandstone occur throughout mudstone intervals, but are commonly concentrated toward the lower portions of many sandstone layers. The gradual upward increase in density of laminae in some cases gives an impression of a transitional bottom contact with the underlying mudstone interval (Figs. 3.7b, d). Inverse size grading within sand layers was also recognised with fine- to very fine-grained parallel-laminated sandstone overlain by slightly coarser, sharply topped ripple- or convolute-laminated sandstone. The grain-size break between the parallel- and ripple-laminated intervals is usually abrupt. Pseudonodules and other load features were not recognised below the 'bases' of sandy intervals in these units, supporting the interpretation that the upward transition from mudstone to sandstone is gradual, with no distinct grain-size (and hence density) contrast. Vertical repetitions of sandstone-mudstone couplets which exhibit this structure have been observed in packages which exceed 10m in thickness.

Thinly bedded, structureless sandstone-mudstone couplets form a minor component of sub-facies 3B. They occur as discrete interbeds within the ripple and planar laminated facies or form rhythmically bedded packages up to 8m in thickness. Sandstone beds have sharp bounding surfaces and are internally massive (Fig. 3.7e). Evidence of liquidization/fluidisation within the sandstone beds is ubiquitous, with crude development of dish and pillar structure, fluidisation pipes and loading of sand into underlying mudstone layers. In some cases, layers have disaggregated entirely to form a mass of pseudonodules (see lower portion of Figure 3.7e).

Pre-lithification deformation has also been important in modifying depositional textures in ripple laminated units (Fig. 3.7f). Many sandstone beds show partial homogenisation, convolute lamination or truncation by muddy detachment surfaces. Clastic dykes protruding from the tops of sandstone layers are commonly inclined as a result of layer-parallel shearing. In addition, disruption resulting from bioturbation is common, particularly in units from the central domain around CP734682 and CP717654. Bioturbation occurs in the upper-most portions of relatively thick sandstone layers (up to 20cm) but has disrupted entire beds in some cases. It involves partial to complete annihilation of primary sedimentary structures with local preservation of trace fossils (Fig. 3.7g).

Interpretation

In recent times, detailed studies of thinly bedded sequences deposited in sub-wave base marine environments, have revealed that the structure of sandstone-mudstone couples often do not conform with the regular vertical sequence of structures defined in 'classical turbidites' (cf. Kneller, 1995). In these situations, workers have been forced to abandon the relatively simple models proposed by Bouma (1962), Stow and Shanmugam (1980) and Lowe (1982) for turbidites which involve deposition from waning turbulent currents. The most popular interpretation for this deviation from 'classical' turbidite sedimentation involves reworking of sediment by bottom currents (commonly contour-following currents) (eg. Stanley 1988; 1993; Shanmugam et al., 1993; 1995). Many of the structural criteria considered by these workers (and others including Stow and Lovell, 1979; Stow and Holbrook, 1984; Gonthier et al., 1984) to be diagnostic indicators of bottom currents activity are shown in sub-facies 3B. These include: 1) abundance of structures produced by tractional currents (ie. parallel-, ripple- and cross-lamination), 2) inversely graded sand layers, 3) sharp grain-size breaks between sandstone layers and successive mudstone layers, 4) internal erosional surfaces, 5) good sorting of sand-sized particles, 6) lenticular form of sandstone bodies, 7) multiple palaeocurrent directions within individual beds and 8) evidence of bioturbation.

Although it is attractive to attribute the assemblage of sedimentary features shown in sub-facies 3B to bottom current activity, it should be noted that recent work on turbidite deposits has indicated that many of these may not be unique to the former process. Kneller (1995), has argued, principally on theoretical and experimental grounds, that the structure of deposits from turbidity currents can be strongly modified by fluctuations in the hydrodynamic properties of the transporting fluid. These are mainly influenced by seafloor topography and the initiation mechanism of the flow and could possibly result in structures which are grossly comparable with many of the criteria listed above for the recognition of bottom current reworked deposits. For instance, inversely graded sandstone deposits could result from the acceleration of turbulent currents at a particular point with time (waxing flow), resulting in progressively coarser grained material becoming transported to the site of deposition. Tractive depositional processes could persist to the tops of beds under such conditions. Inversely graded deposits produced from bottom current activity have been interpreted in a similar fashion by Shanmugam et al. (1993), who suggested that accelerating bottom currents capable of transporting progressively coarser-grained particles were responsible for this texture. Stanley (1988) on the other hand, attributed inverse-grading in bottom current reworked sands to the progressive downward erosion and redeposition of initially normally graded turbidite sands. In the first two processes

therefore, inverse grading corresponds to an increase in energy conditions, whereas the latter requires modification of a pre-existing depositional sequence.

Although the possibility that sub-facies 3B involved deposition from turbidity currents is not totally discounted, the more traditional interpretation of the characteristic textures associated with these deposits as having formed from bottom current activity is preferred. The strongest evidence for this interpretation is based mainly on the observation that 'classical' turbidite deposits do not occur in direct association (ie. interbedded) with sub-facies 3B. If turbidite sedimentation was the principal process involved in the deposition of this facies, then at least a small percentage of units consisting of 'normal' Bouma-type sequences would be expected.

It is inferred then, that bottom current activity provided an important mechanism for localised erosion and redeposition of sediment, however it was unlikely to have been responsible for supply of clastic material to the basin. Medium- to coarse-grained sediment was probably initially transported to the basin via gravity flow processes (ie. turbidity currents and/or debris flows). Possible relict precursors to bottom current deposits could include interbedded massive sandstone beds (facies 2A) or volcaniclastic units initially emplaced as high-density turbidites or debris flows (see section 3.6). Many of these units exhibit ripple laminated tops or upper erosional surfaces. Rare packages and discrete interbeds of thinly bedded, liquefied, fine-grained sandstone (Fig. 3.7e) could also represent relict primary deposits. Their sharp upper and lower bounding surfaces and massive, structureless interiors are consistent with deposition from grain flows. The apparent paucity of turbidite deposits found in association with facies 3B suggests that sedimentation occurred away from the main feeder-channel systems, possibly in inter-channel slope regions.

3.5. Facies 4: Fine-grained sediments

Included in this facies are mudstones and thinly interbedded siltstones. Facies 4 is widely distributed and voluminous throughout the Dundas region and occurs in association with all other facies types. Intervals dominated by facies 4 range from less than 2m to in excess of 350m in thickness. Relatively thin deposits occur enclosed within coarser-grained facies as laterally discontinuous mudstone drapes at the top of clast-supported conglomerate beds (subfacies 1A). Thicker accumulations of facies 4 are punctuated by narrow intervals of sandstone-mudstone couplets (facies 3) and centimetre- to metre-scale beds of disorganised mud-supported conglomerate (subfacies 1B). In western areas where modification of the original stratigraphy by Devonian tectonism is relatively minor, thick packages of mudstone-dominated sediment appear to envelop thick coarse-grained sequences. This is shown by the alternating depositional pattern of these facies in vertical section and by the occurrence of facies 4

as lateral equivalents to large lensoidal bodies of conglomerate. The richly fossiliferous character of many facies 4 units indicates marine sedimentation.

Textural variation occurs within facies 4 , with subfacies types including structureless mudstone, delicately laminated mudstone and current-rippled mudstone-siltstone couplets. The latter resemble Bouma Tc to Te divisions and are likely to have been deposited from fine-grained turbidity currents. Bottom current activity may also have played a role in depositing or modifying pre-existing fine-grained sediments. Structureless mudstone is in most cases considered to be the product of hemi-pelagic deposition, however localised association of this subfacies with slumped units may indicate that the apparent structureless character resulted from liquefaction and annihilation of original textures.

The appearance of thick, laterally continuous packages dominated by facies 4 are likely to reflect periods of relatively low sediment input into the basin. However, the more common occurrence of facies 4 as lateral equivalents of coarser-grained facies indicates that fine-grained sediment was actively depositing even during periods of high sediment influx. In these cases, turbidity flows supplying coarse-grained detritus to the basin would have been largely confined to channels incised within the muddy basin slope and fine grained material elutriated out during turbulent flow would contribute to the hemi-pelagic sedimentation.

3.6 Facies 5: Immature volcaniclastic deposits

Volcaniclastic facies comprise a volumetrically minor but distinctive association of sedimentary deposits. They have a wide spatial distribution throughout the Dundas region, but are restricted to low biostratigraphic levels: ie. pre-earliest Late Cambrian. Individual units have a range of textural styles, however they are grouped due to presence of abundant juvenile volcanic debris as a conspicuous detrital constituent. Volcanic particles are diverse, including juvenile crystals, altered pumice fragments, glass shards and texturally immature dense volcanic fragments. The composition of the volcanic fraction is also variable, ranging from basaltic to rhyolitic. Due to the labile nature of the constituents, units are poorly exposed in many cases and their internal structure and overall geometry are commonly indeterminable. The main features used in defining the following classification are sedimentary and volcanic textures combined with compositional characteristics.

3.6.1 Subfacies 5A: Feldspathic crystal-rich volcaniclastic sandstone

This facies crops out in the Ring River near the Ring Valley mine (Fig. 2.1) and comprises two thickly bedded volcaniclastic sandstone units interbedded with laminated dark grey mudstone. The two beds are compositionally and texturally identical and are positioned either side of a fault. It is probable that they represent structural repetition of

the same unit. The unit contained within the hangingwall of the fault (located east of the fault) is particularly well exposed and provides the bulk of the data in the descriptions below. Boulders of a similar lithotype were observed in Bather Creek approximately 1.25km to the ESE of the Ring Valley Mine, however their source was not located.

Internal structure

The original geometry and internal organisation of this unit have been modified to various degrees by an episode of post-depositional liquefaction. The effects of this disruption are most evident within the fine-grained upper portions of the unit where large blocks (some at least 15m in diameter) of chaotically deformed thinly bedded mudstone occur enclosed within a homogeneous 'matrix' of very fine-grained volcaniclastic siltstone (Fig. 3.8a). Despite this disruption, a moderately uniform internal structure defined by an upward decrease in particle size and the localised preservation of conformable contacts are considered to indicate that a relict primary organisation is present. A minimum estimate of the total thickness of the unit is 30m.

The internal structure of the unit and lithological variations are shown in Figure 3.8a. Moderately to poorly sorted lithic-crystal conglomerate occurs at the base and exhibits a sharp, weakly erosive, sub-planar contact with underlying laminated mudstone (Fig. 3.8e). Small-scale load features are locally developed along the contact. Close to the base (ie. within 5m above the basal contact) are blocks of contorted thinly bedded volcanogenic mudstone with cross sectional areas ranging 0.5-25m^2. They may represent rip-up clasts eroded from the unlithified substrate, blocks slumped into the flow from the margins of channels, or perhaps material which has sunk through the unit during post-depositional liquefaction. The conglomeratic base passes upward with transitional contact into medium-grained crystal-rich sandstone (Fig. 3.8d). This sandstone division is massive, unbedded and comprises the bulk of the unit. It has a closed to moderately open framework and sorting is poor to moderate. Lithic fragments comprise a minor framework component. Progressive but abrupt reductions in grainsize occur near the top of the unit where massive crystal-rich sandstone passes upward into homogenous very fine-grained crystal-vitric sandstone and finally into well-bedded (but disrupted) intervals of pale grey 'ash' and moderate to dark grey non-volcanogenic mudstone (Figs 3.8 c and b respectively).

Petrographic features

Clasts contained within the basal conglomeratic division include juvenile crystals and angular to rounded lithic fragments, the latter ranging in diameter from 3-20mm. Lithic fragments are almost exclusively of volcanic origin and include felsic to intermediate quartz-feldspar and feldspar porphyritic lithotypes. Wispy mudstone clasts

Figure 3.8 Textural and compositional variation within a well-exposed crystal-rich volcaniclastic unit near Ring Valley Mine (subfacies 5A).

(**a**) Graphic log depicting normally graded structure of the deposit. X-axis of graphic logs is a schematic grainsize scale with grainsize increasing to right. Polished hand specimens with representative compositional and textural features from various levels within the deposit are shown on the right.

(**b**) Interbedded normally graded pale grey silty mudstone and parallel-laminated grey mudstone, interpreted to have deposited from dilute turbidity currents which trailed the main body of the flow. Diameter of coin is 20mm. (Sample 980)

(**c**) Homogenous crystal-poor siltstone from massive interval positioned towards the top of the basal division. Diameter of coin is 20mm. (Sample 985)

(**d**) Feldspathic crystal-rich sandstone from unstratified, subtly normally graded interval; a pseudoclastic texture is developed as a result of patchy chlorite (dark green) and albite-chlorite (pale green) alteration of the matrix (1mm divisions in scale at bottom of figure). (Sample 982)

(**e**) Lithic-rich base of unit, with weak distortion of lamellae in underlying mudstone probably resulting from rapid emplacement and loading of dense volcanic debris; lithic fragments contained in the conglomerate are angular to sub-rounded, evenly porphyritic dacite and andesite. Large rounded quartz crystals (arrows) form a minor component. (Sample 981)

(**f**) Photomicrograph of crystal-rich sandstone (**c**) from lower division of the unit. The framework consists almost exclusively of fragmented feldspar crystals, with subordinate magnetite. Very low quartz abundance is typical of this unit. The matrix is extensively altered to chlorite and is interpreted to have originally been composed of glassy detritus. (Sample 982)

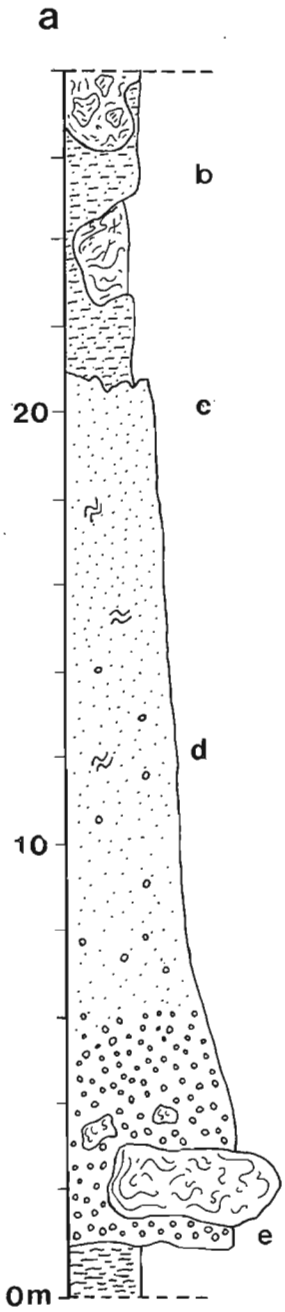

contorted mudstone

volcanic lithic fragment

relict pumice

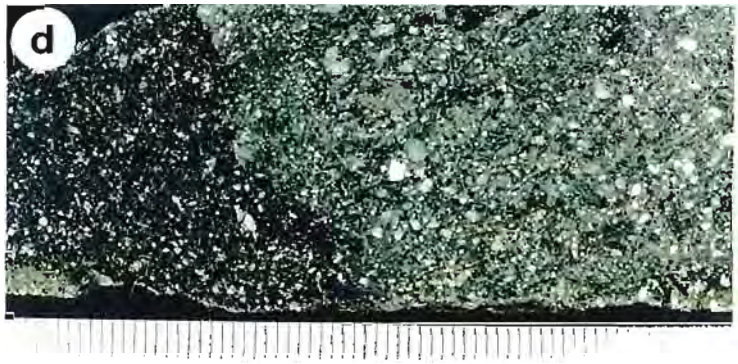

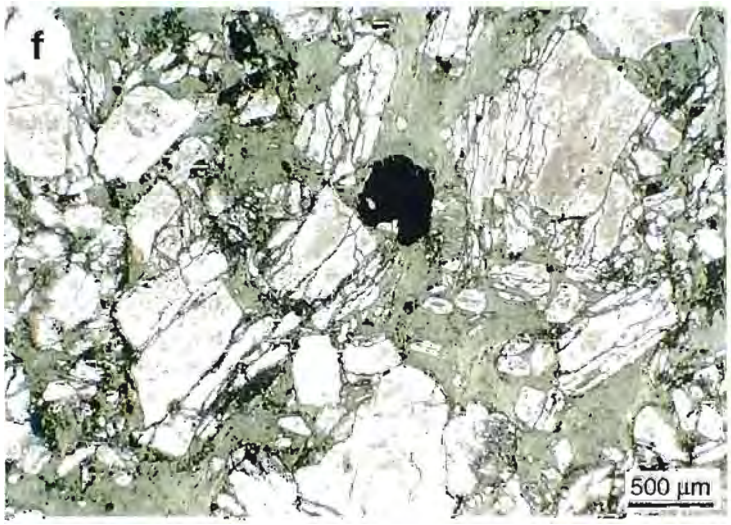

form a minor portion of the clastic component. Euhedral phenocrysts, now entirely replaced by chlorite, were observed in a small number of volcanic clasts. These possibly represent pseudomorphs after a ferromagnesian phase. Groundmasses of porphyritic clasts comprise devitrified former glass which in some cases are cross-cut by perlitic fractures. Some of the feldspar-porphyritic fragments show highly irregular, ragged margins and their crystal components are similar in both texture and composition to framework grains. These might represent juvenile lithic fragments. Rounded volcanic clasts and mudstone fragments are interpreted as accidental lithics incorporated during emplacement of the flow.

Feldspar crystals and crystal fragments comprise the bulk of the framework in the overlying sandstone (Fig. 3.8f). Individual crystal forms are anhedral to euhedral with maximum dimensions ranging from 0.2 - 3mm. Occasionally feldspar glomerocrysts occur that are up to 6mm in diameter. The corners of crystals are angular indicating the epiclastic reworking of these grains was minimal. Opaque mineral grains are an additionally conspicuous detrital component and include abundant euhedral to subhedral Fe-Ti oxides and very rare Cr-spinel. Highly corroded quartz crystals and chloritised vitriclasts with wispy habits, the latter interpreted as relict pumice fragments, are locally present in minor amounts. The matrix is entirely replaced by chlorite and/or a fine-grained mosaic of albite crystals and is considered to have been originally glassy. In places, alternating patches of chlorite and albite altered matrices produces a mesoscopic pseudoclastic texture.

Interpretation

The relatively homogenous composition of volcanic debris contained within the lower crystal-rich portion of the Ring Valley Mine unit, combined with crude normal grading and lack of internal bedding or amalgamation surfaces, is interpreted to indicate emplacement from a single depositional event. Cas and Wright (1987) argued that crystal-rich depositional units of this type, which are characterised by a paucity of vitric volcanic components and lack of evidence for hot emplacement (ie. welding, columnar jointing or gas segregation pipes), are formed from epiclastic redeposition of pyroclastic debris. The lack of abrasion of pyroclasts and the insignificant volume of non-volcanogenic material incorporated within the flow are interpreted to indicate that sedimentation occurred synchronously with eruption. Gross normal grading, sharp basal contact and low matrix content are features consistent with deposition from high density turbidites (cf. Lowe, 1982). The presence of large blocks of poorly consolidated mudstone at the base of the unit might also be considered as evidence for turbulent flow (ie. erosion at base of flow), however as pointed out earlier in this section, the origin of these fragments is uncertain.

The transition to thin interbeds of normally graded to massive or laminated ash layers and non-volcanogenic mudstone within the upper division is interpreted to indicate either i) settling from an unsteady low-density turbidity current formed after deposition of the basal concentrated load (cf. Lowe, 1982), or ii) deposition from episodic low density turbidity currents which are unrelated to the basal division. The latter hypothesis could possibly involve episodic deposition from a waning subaqueous eruption column (cf. Fiske and Matsuda, 1964; Stix, 1991; Cousineau, 1994) or episodic redeposition of pyroclastic material temporarily sorted in shallower portions of the basin.

Deposition from large volume turbulent flows and the lack of evidence for shoreline reworking are considered to indicate a subaqueous, below wave-base depositional environment.

3.6.2 Subfacies 5B: Felsic vitriclastic sandstone

Volcaniclastic units included in this subfacies consist of very thick (10-90m), crudely stratified beds of vitric tuff. Principal detrital components include formerly glassy juvenile volcanic particles including shards and pumice. Crystals and volcanic fragments are subordinate components.

The thickest and best exposed subfacies 5B unit recognised in this study is located in the western area on the southern slopes of Mt Razorback (Fig. 2.1). This particular unit has been mapped by several previous workers (Banks, 1956; Blissett, 1962; Brown, 1986) who described it as a 'keratophyric tuff' or 'crystal-vitric-lithic tuff'. Several small exposures were also identified from the central area between the re-entrant of the NE Dundas Tram at Great Northern Creek and Ringville. It is possible that these represent lateral equivalents of the same unit, or at least a succession of units which occupy a narrow stratigraphic interval. Also included in this facies is a deposit described and sampled by Rubenach (1967) from the northern slopes of Black Hill (Fig. 2.1). I was unable to re-locate this unit during mapping (due to significant vegetation regrowth since a fire in 1982) and inclusion of this unit is based solely on Rubenach's (op cit.) descriptions and re-examination of his hand and thin specimens. This unit is the oldest in the western domain and is situated approximately 35-55m above the Undillan RB1 fauna (Jago, 1979). The biostratigraphic level of the Mt Razorback unit is probably slightly younger than that of the Black Hill unit and is situated approximately 300m above the Undillan Razorback Mine fauna (Thomas and Henderson, 1945) and 440m below the upper Boomerangian to lower Mindyallan DB1 fauna in the Dundas River (Jago *in* Brown, 1986). A middle Middle Cambrian age is inferred for this unit. The biostratigraphic levels of units located in the central domain are poorly constrained but are probably of Middle Cambrian age.

Internal structure

Individual beds are generally massive, however local variations in grainsize and lithic or crystal content define crude internal organisation and stratification. They generally occur interbedded with dark laminated mudstone, however associations with clast-supported conglomerate (subfacies 1A), poorly organised sandstone (subfacies 2A) and sandstone-mudstone couplets (facies 3) were also observed. An idealised internal structure for this sub-facies is based largely on the reasonably well-exposed unit south of Mt Razorback (Fig. 3.9a). The base of this particular unit is unexposed and the upper portion is incised by an erosive channel within which massive to sparsely laminated sandstones (subfacies 2A) and interbedded mudstones were deposited. Poorly sorted, matrix-supported intervals comprising sedimentary intraclasts, juvenile crystals and rare dense (ie. non-vesiculated) volcanic fragments occur towards the base of the unit and again at 40m above the base (Fig. 3.9b). These intervals are normally graded, passing upward into fine-grained vitric sandstone and possibly define the lower portions of two amalgamated depositional units. Near the top of the inferred upper depositional unit, the overall normally graded structure is punctuated by another coarser-grained interval defined by the concentration of pumiceous vitriclasts (some up to 30mm in length).

Petrographic features

Recrystallised vitric particles form the matrix in lithic-rich intervals and the dominant component in fine-grained sandstones. Relict glass shard textures are patchily preserved in thin section and include cuspate, Y-shaped, blocky and platy morphologies. Glass shards are usually replaced by a mosaic of very fine-grained quartz crystals and show no evidence of compaction. Relict pumice occurs as elongate, tabular fragments with wispy terminations. Although they are completely replaced by cryptocrystalline aggregates of quartz and less commonly sericite, relict tube vesicle textures are preserved in many cases. The foliations defined by tube vesicles exhibit minor deformation around rigid crystals however are randomly oriented within individual samples. A streaky texture is developed in some fragments defined by dark, discontinuous lenses containing acicular to tabular microlites (Fig. 3.9 c, d).

Most pumice fragments are aphyric, however a few exhibit finely porphyritic textures with phenocrysts of quartz and subordinate plagioclase indicating rhyolitic to rhyo-dacitic compositions. Very small (0.01-0.1mm) opaque to translucent reddish-brown crystals were observed in one pumice fragment from the unit located south of Mt Razorback. These are tentatively interpreted as Cr-spinels, which if correct would indicate a basaltic composition. Other framework components include juvenile quartz and feldspar crystals which are locally up to 3mm in diameter, but are mostly less than 1mm. They exhibit euhedral to subhedral and less commonly anhedral habits, with

Figure 3.9 Textural and structural features of vitriclastic sandstone unit exposed in the Dundas River, south of Mt Razorback (subfacies 5B).

(**a**) Graphic log indicating two amalgamated, grossly normally graded depositional units. Concentration of pumice fragments near the top of the upper bed imparts a crude symmetrical grading. The upper surface of the unit is highly erosional, with deposition of massive sandstone and interbedded mudstone in a steeply-sided channel. X-axis of graphic logs is a schematic grainsize scale with grainsize increasing to right.

(**b**) Polished hand specimen from poorly sorted interval close to the base of the unit. Framework component is dominated by angular black mudstone fragments, with sub-ordinate quartz (q) and feldspar (f) crystals, porphyritic and holocrystalline volcanic lithic fragments (v) and rare wispy pumice (p). (Sample 828)

(**c**) Photomicrograph of 'streaky' pumice fragment contained in shard-rich interval. Uncompacted Y-shaped shards are denoted by black arrows heads. (Sample 95-002)

(**d**) Close up of (**c**) showing streaky patches in pumice as consisting of randomly oriented acicular to tabular microlites set in a 'dirty' grey groundmass. Dark micro-crystalline streaks possibly represent stretched inclusions of 'mafic' magma which were quenched on mixing with cooler 'felsic' host magma.

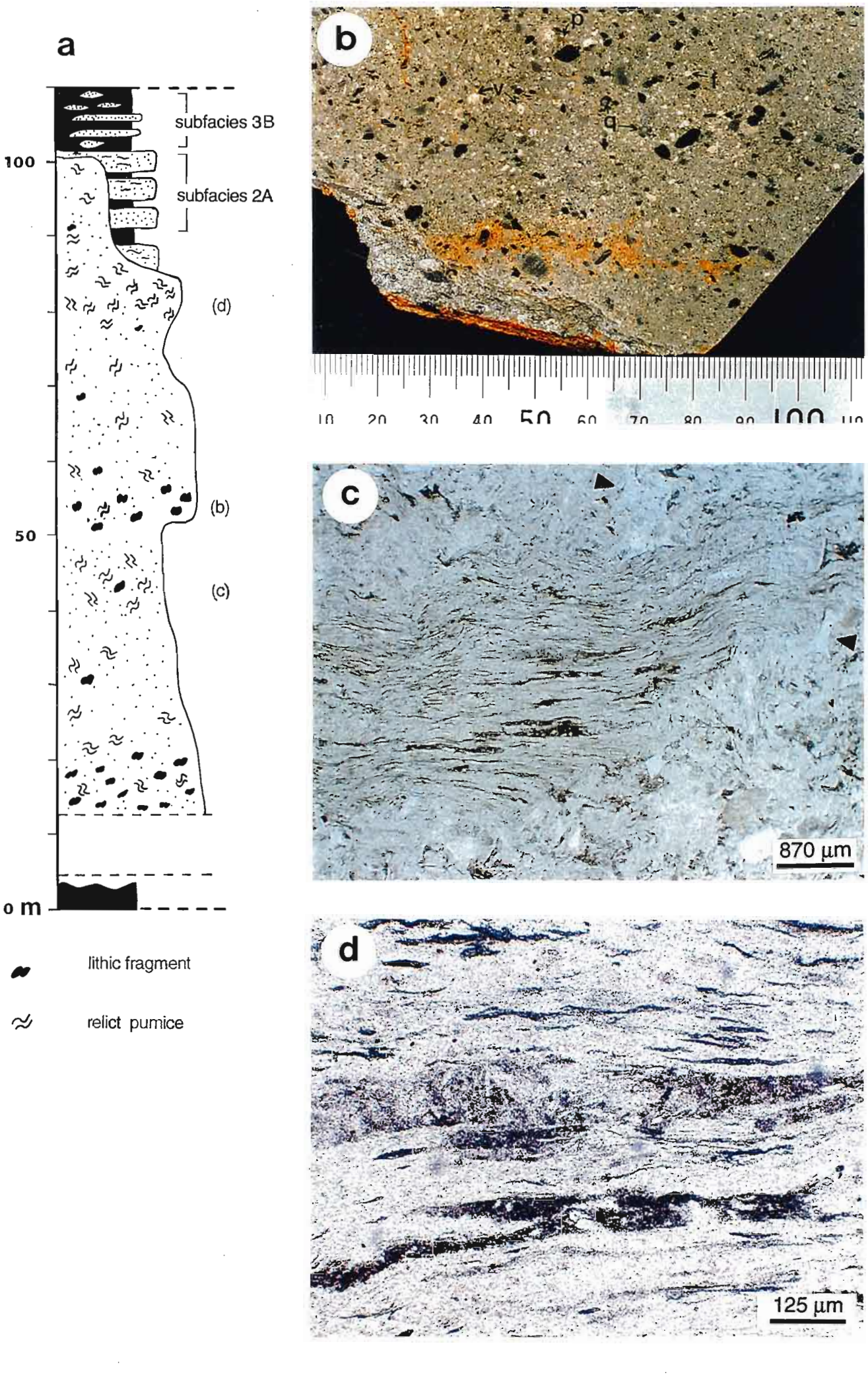
a
subfacies 3B
subfacies 2A
100
50
0 m
(d)
(b)
(c)
lithic fragment
relict pumice
b
p
v
f
g
q
c
870 µm
d
125 µm

rounded corners (interpreted to have resulted from resorption) and rare embayed crystal faces. The coarsest quartz grains are internally fractured and show mild undulose extinction and deformation lamellae. Feldspar grains show serrated albitised fringes, corroded margins and may be partially or completely replaced by sericite. Detrital heavy minerals include rutile, magnetite and very rare Cr-spinel. Lithic fragments are angular to subrounded and range in size from sand-sized particles to granules. They are almost entirely of sedimentary origin and include silty mudstone and poorly sorted muddy sandstone. The margins of these grains are highly irregular with delicate protrusions extending into the surrounding formerly glassy matrix. These are interpreted as accidental lithic fragments eroded from the unlithified substrate during emplacement.

Interpretation

Several factors are considered to provide strong evidence that subfacies 5B is a syn-eruptive product of large-scale explosive event(s). These include: i) the abundance of Y-shaped shards, which are typical of silicic explosive eruptions (Wohletz, 1983), ii) the very thick nature of the deposits; iii) minimal contribution from a non-volcanic source; iv) lack of evidence for significant epiclastic reworking and v) the monogenetic composition of the juvenile component. Well-preserved, uncompacted shard forms and the random orientation of pumiceous vitriclasts indicate that flows were non-welded and probably emplaced in a cold state. This suggests that they do not represent hot pyroclastic deposits, but rather rapidly emplaced mass flows comprising essentially unreworked, but redeposited pyroclastic debris. The association of this facies with other marine sequences (also marine fauna on the northern slopes of Black Hill) indicate a sub-aqueous environment of deposition. Deep channelling near the top of the Razorback unit and the association with inferred sandy debris flows may indicate deposition on a basin slope.

The presence of 'streaky pumice' fragments is an interesting feature in that it is normally associated with magmatic mixing of felsic and mafic liquids prior to eruption (cf. Sparks and Sigurdsson, 1977; Cas and Wright, 1987; Blake et al., 1992; Briggs et al., 1993). The significance of this observation is marked by the recognition of Cr-spinel grains as both 'free' crystals contained in the matrix and possible phenocrystal inclusions in pumice fragments. Before any wild conclusions can be made however, it is emphasised that crystals contained in the pumice are at best tentatively interpreted as Cr-spinels, and there no conclusive evidence that the 'free' crystals form part of the juvenile component. In other words, they could easily be detrital grains incorporated from an older and genetically unrelated source.

3.6.3 Subfacies 5C: Quartz-feldspathic crystal-rich sandstone

This facies consists of units of unstratified, poorly-sorted crystal-rich sandstone. It is distinguished from facies 5A crystal-rich sandstone primarily through the presence of abundant detrital quartz, but also by the fact that matrices are composed primarily of mud. All examples of this facies are very poorly exposed and true bedding thicknesses and the geometry of units are uncertain. Individual units were recognised in association with a number of different facies including black laminated mudstone (facies 4), chert-clast conglomerate (subfacies 1A), polymict mafic-clast conglomerate (subfacies 1A) and green to purple structureless mudstone (facies 4). Units associated with the first two facies associations are restricted to the central area wherein several small exposures occur between Godkin Ridge and Great Northern Creek and another in the Ring River 100m northwest of Ringville (Fig. 2.1). Although a direct stratigraphic relationship between these units and the sub-facies 5B unit(s) located within the central domain were never observed, projection of the latter along strike indicates that it is older (Fig. 2.1). There are no biostratigraphic constraints on the ages of subfacies 5C units in this region. The third facies association (ie. polymict mafic-clast conglomerate) is exposed on an exploration track at the southwestern foot of Mt Razorback (western area: Fig. 2.1). Intense weathering and patchy outcrop prevented detailed logging of the unit, and boundary relationships are poorly constrained. From the very limited outcrop, a minimum thickness of 45m is estimated. A likely correlate of this unit has been mapped by Brown (1986) from the Dundas River approximately 600m ESE. Brown (op cit.) estimated a thickness of 10m for the unit at this locality, which he described as 'acid to intermediate volcanic tuff'. It occurs interbedded with structureless fossiliferous mudstone (facies 4) which contains faunal assemblages of probable upper Boomerangian to lowermost Mindyallan age (*Lejopyge laevigata* III Zone: Jago *in* Brown op cit.). The subfacies 5B vitriclastic sandstone unit located south of Mt Razorback is situated approximately 400m below this biostratigraphic level.

Internal structure and petrographic features

Coarse fraction grading (*sensu* Cas, 1979) occurs towards the base of the very thick unit located at the southwestern foot of Mt Razorback. It is defined by the upward transition from basal very poorly sorted, open-framework pebble conglomerate to massive and disorganised crystal-rich sandstone. Lithic fragments contained within the basal conglomerate include rounded to sub-rounded plagioclase porphyritic andesite/basalt, quartzo-feldspathic greywacke and subrounded to angular mudstone. These clast-types comprise the bulk of the lithic fraction in the overlying subfacies 1A conglomerate units and are considered to represent accidental lithics entrained within the flow during transport. The overlying crystal-rich sandstone forms the dominant lithotype within all subfacies 5C units. Grain populations contained within this

lithotype are moderately to poorly sorted, ranging mainly from silt to coarse sand-sized and usually involve open framework organisation. Closed-framework sandstones are less common, patchily developed and probably occur as a result of post-depositional compaction. Outsize clasts are rare, with a notable exception involving the unit exposed near Curtin Davis Mine on Godkin Ridge (Fig. 2.1) which contains irregularly shaped porphyritic blocks up to 50cm in diameter. Matrices are dominantly composed of dark grey non-volcanogenic silty mud, however patchy albite alteration of the matrix in some deposits is interpreted to indicate that a formerly glassy component was locally significant.

The monocrystalline framework component of the sandstones involves unreworked, complete and fragmented crystals of quartz and plagioclase. Detrital rutile, magnetite, zircon and biotite occur as accessory mineral phases in some units. Quartz grains exhibit euhedral to anhedral forms with the latter resulting from extensive resorption and/or crystal fragmentation. The largest complete crystals (up to 8mm in diameter) commonly contain an internal network of curviplanar fracture surfaces (Fig. 3.10a). Smaller anhedral crystal fragments are bounded by both convex- and concave-outward surfaces consistent with having been derived from disaggregated fractured 'parent' crystals. This observation is considered to indicate that fracturing predated deposition of the sandstones and is therefore likely to have occurred either prior to fragmentation of the magma or during sediment transport. Furthermore, elongate embayments formed during grain dissolution were observed to follow fractures in some examples, suggesting that fracturing occurred whilst crystals were contained in a vesiculating groundmass.

Plagioclase crystals are extensively altered to sericite, chlorite and calcite. Unfragmented grains comprise individual lath-shaped crystals which are up to 3mm in length and glomerophyric aggregates exceeding 6mm in diameter. A few are compositionally zoned, with increased extinction angle and disseminated calcite towards the rims.

Lithic fragments are a minor fraction of the framework in the massive sandstones and include non-volcanogenic mudstone and rare volcanic material. Mudstone fragments show irregular margins which commonly merge with the surrounding matrix suggesting that they were unlithified at the time of incorporation within the flow. Volcanic fragments are of two types: a) granule-sized clasts of finely porphyritic felsic to intermediate volcanic rock with devitrified formerly glassy groundmass, and b) block-sized coarsely porphyritic volcanic rock with fine-grained sericitic groundmass and ragged margins (Fig. 3.10b). The first of these show sub-rounded to well-rounded forms and contain feldspar and quartz microphenocrysts set in a holocrystalline groundmass. These were probably reworked from rhyolitic to dacitic lavas or fine-grained intrusives. The second clast-type, as mentioned previously was

Figure 3.10 Subfacies 5C quartz-feldspar crystal-rich sandstones

(**a**) Photomicrograph of poorly sorted crystal-rich sandstone sampled from the unit located on at the south-western foot of Mt Razorback. The framework consists of large, internally fractured quartz crystals with sharp, rounded corners and fragmented, 'dirty' feldspar crystals (f) set in fine-grained recrystallised matrix. Quartz crystal fragments (qf) and opaque Fe-Ti oxides (o) are also abundant. Voids developed at the intersection fracture surfaces in the large quartz crystal are filled with glass (now extensively replaced by chlorite and/or albite), indicating that fragmentation occurred while crystals were enclosed by molten liquid. Plane polarised light. (Sample 95-004)

(**b**) Polished slab showing the edge of large (50cm diameter), coarsely-porphyritic juvenile volcanic clast (right) enclosed by dark, mud-matrix crystal-rich sandstone. Note the very ragged, wispy contact between the juvenile clast and the host sediment (arrow). Phenocrysts within the juvenile clast are dominated by large, dark grey, rounded quartz (q). Feldspar phenocrysts are less obvious in this figure and blend in with the sericitic groundmass. The host sediment is finer-grained, consisting mainly of crystal fragments. Subrounded white specks are small, dense volcanic lithic fragments, whereas dark, fine-grained patches represent mudstone intraclasts (m). Diameter of coin is 23mm. (Sample 88)

(**c**) Photomicrograph of juvenile volcanic fragment shown in (**b**). Note the coarsely porphyritic nature of the fragment and the textural similarities between the quartz phenocryst in the centre of the field of view and the large quartz crystal contained in the sandstone shown in (**a**). Although vesicular textures are not obvious in the extensively recrystallised groundmass, the former presence of bubbles is indicated from the small rounded embayments along the margins of phenocrysts (arrows). The dirty grey anhedral grains at the bottom of the figure are feldspar phenocrysts (f). Plane polarised light.

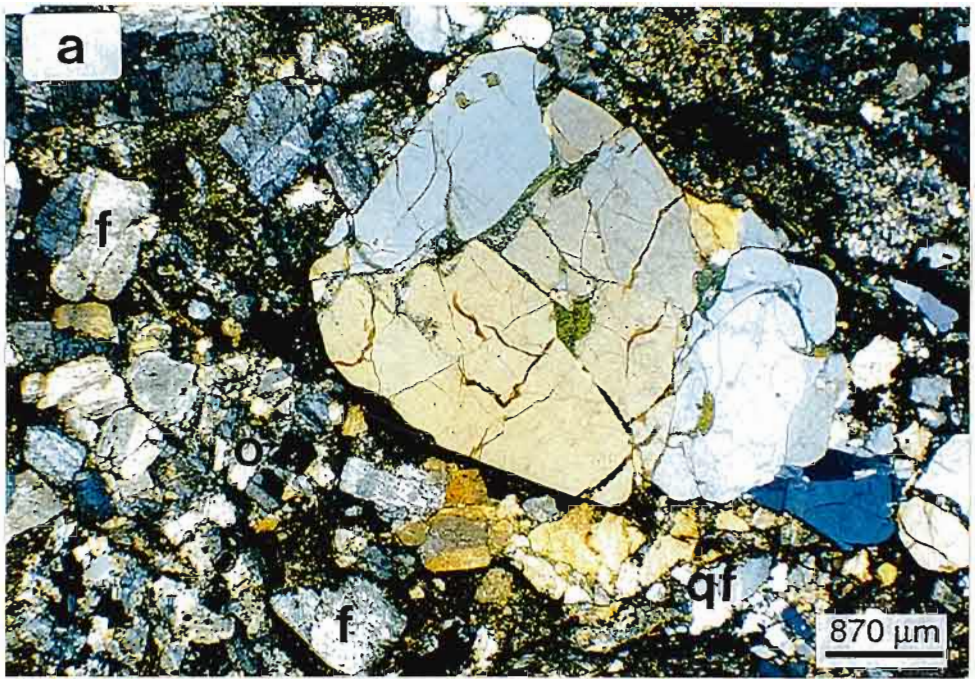
a
f
o
f
qf
870 µm

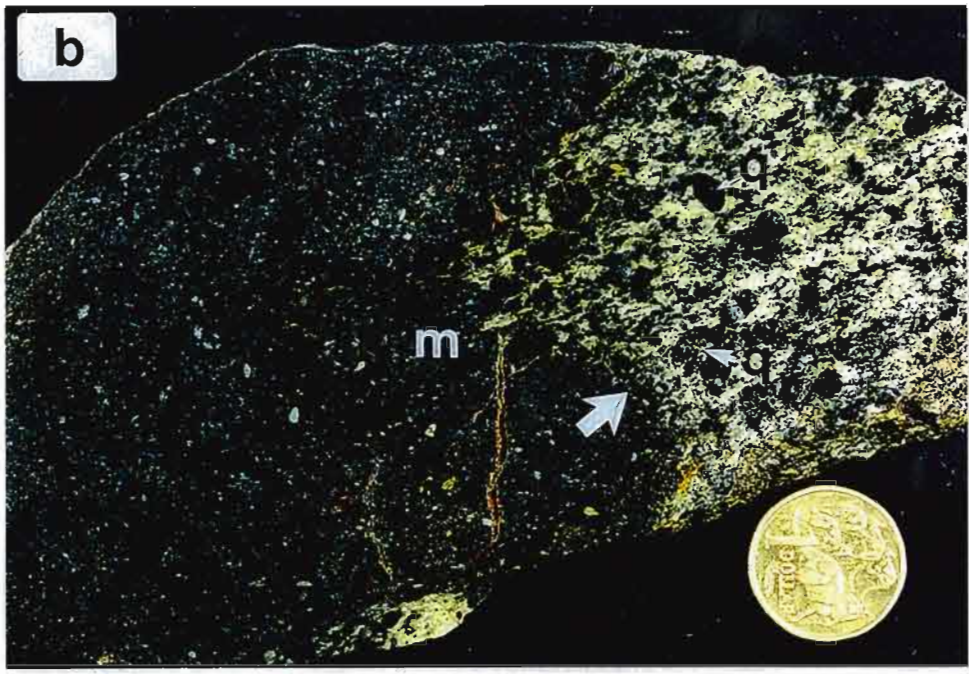
b
q
m
q

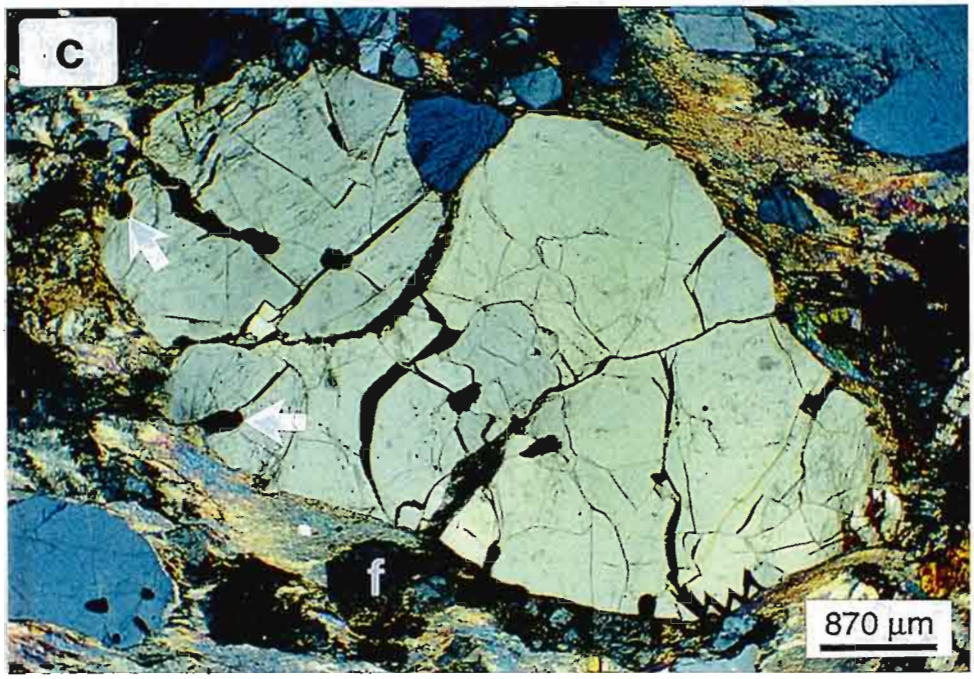
c
f
870 µm

only observed in the unit near Curtin Davis Mine. Clasts are very crystal-rich (crystals comprise >60% by volume) with phenocrysts ranging in size from 0.5 to 15mm. The phenocryst assemblage is identical to the medium to coarse-grained crystal framework in the enclosing sandstone and comprises large angular to rounded fractured and resorbed quartz, 'dirty' sericite-altered plagioclase and traces of euhedral zircon (Fig. 3.10c). The apparent high crystal content is possibly an artefact of post-depositional compaction during burial and/or tectonic flattening (ie. compaction of the groundmass). This is indicated by brittle-ductile strain features associated with phenocrysts such as deformation lamellae, undulose extinction, bent crystals and the development of sub-grains along grain-grain contacts. Some fracturing of quartz is interpreted to have preceded deposition however, as indicated by the abundant fracture-bound crystal fragments in the enclosing sandstone, cross-cutting of fractures by embayments formed during crystal resorption and filling of voids within internally fractured phenocrysts by formerly glassy mesostasis. Groundmasses are considered to have been originally glassy. They consist of homogenous felty mats of sericite and exhibit a crudely developed foliation which anastomoses about rigid phenocrysts. This foliation is interpreted to be of tectonic origin. No evidence of a primary vesicular texture was observed in these clasts, however in view of the extensive alteration of the groundmass and the inferred compaction this is perhaps not surprising. The features outlined above are considered to provide strong evidence for a juvenile origin for this clast-type.

Interpretation

The thick, unstratified character of subfacies 5C, coupled with the texturally immature nature of the framework component are considered to indicate that volcanic debris was rapidly resedimented after initial fragmentation of the parental magma, probably as cohesive debris flows or high-concentration turbidity currents. The overall paucity of vesicular juvenile fragments (pumice and bubble-wall shards) in these deposits and in particular, the crystal-rich texture of the inferred juvenile clasts from the Curtin Davis Mine unit may indicate that mode of eruption did not involve explosive fragmentation of a highly vesicular magma. Cas (1983) for example, argued that upward flow of magma at advanced stages of crystallisation would be inhibited due its high viscosity. He did note however, that if crystallisation occurred within a magma chamber positioned at high crustal levels, roof collapse could result in eruption of crystal-rich debris. As an alternative to this mode of fragmentation, crystal-rich debris may have been sourced during collapse of the margins of emergent domes. Gimeno (1994) described sub-aqueously deposited crystal-rich tuff units of Palaeozoic age from the Sarrabus region, Italy, which he interpreted as forming in this way. Of considerable interest is Gimeno's (op cit.) description of internally fractured quartz phenocrysts which closely resemble those observed in this study. He interpreted these fracture

surfaces to have developed in response to thermal shock during interaction of hot rhyolitic magma with sea water. Furthermore, he noted patches of interstitial mesostasis between the fracture surfaces (also observed in this study) and interpreted this to indicate that phenocrysts were enclosed within partial molten magma during the quenching process. It may be possible however, that similar 'quench' textures could be produced as hot pyroclastic flows produced from sub-aerial explosive eruptions came in to contact with cold (?sea) water. Continued vesiculation of the groundmass following 'quench' fragmentation of crystals would result in the late-stage development of resorption textures. In the case of this study at least, the presence of large fractured quartz grains may not require direct interaction of coherent magma and cold water.

In support of an eruptive mode of fragmentation is the widespread occurrence of thick volcaniclastic deposits throughout the Western volcano-sedimentary sequences (eg. Southwell Subgroup north of Hellyer, White Spur Formation south of Rosebery, in the hangingwall successions above the Rosebery and Hercules massive sulphide deposits and from the Huskisson River approximately 6km north of the Dundas region) which contain very similar juvenile components (ie. large, fractured and extensively resorbed quartz crystals, coarsely porphyritic juvenile (?pumice) fragments) and internal structure to subfacies 5C (Facies B of McPhie and Allen, 1992; Bull, 1995). McPhie and Allen (op cit.) argued on the bases of i) facies association, ii) the distinctive juvenile component common to each of these deposits, iii) the substantial thickness of the deposits (>50m) and iv) their wide distribution, that these deposits were potentially genetically related and products of a distinctive voluminous phase of explosive volcanic activity. Epiclastic sediments produced from the disaggregation of individual lava domes would be expected to show more restricted distribution and compositional contrast between deposits derived from different sources. If McPhie and Allen's (op cit.) inference of a genetic relationship between these deposits is correct, then the recognition subfacies 5C could be used a potential chrono-stratigraphic tool within the Dundas region.

3.6.4 Subfacies 5D: Basalt fragment-bearing mud-matrix breccia

The only mapped exposure of this subfacies is located in the Ring River at Bonnie Point (CP73706780: central area). The base of the bed is truncated by a small brittle fault and the top is unexposed: a minimum thickness of the bed is estimated at 6m. Underlying strata comprises interbedded laminated mudstone, turbiditic sandstone-mudstone couplets (subfacies 3A) and normally graded subfacies 1A conglomerate. This package is inferred to occupy an equivalent stratigraphic position to fossiliferous strata located approximately 200m to the south-west. The faunal assemblage at this locality is of Mindyallan age (latest Middle Cambrian) (Banks, 1956). If this

interpretation is correct, then subfacies 5D would be younger than any volcaniclastic facies mapped in the western area.

Internal structure and textural features

A graphic log of the breccia unit is shown in Figure 3.11a. The unit is disorganised, unstratified and very poorly sorted, with the framework grain component ranging from sand-size particles to large blocks . The matrix is fine-grained and consists of dark grey non-volcanogenic mudstone or silty mudstone. Monomineralic framework grains are dominantly of sedimentary origin and include sub-rounded to rounded quartz (0.01-0.2mm diameter), muscovite, biotite and rare rounded plagioclase. Lithic fragments include coherent volcanic (dacitic to basaltic in composition), vitriclastic and non-volcanogenic sedimentary lithotypes. The latter consist of irregularly shaped, plastically deformed intraclasts of laminated grey mudstone and laminated quartzwacke (Fig. 3.11b). The internal structure of the deposit is consistent with emplacement as a cohesive debris flow.

Vitriclastic fragments have a range in dimensions from millimetre-sized clasts to rafts up to 4m in length. They are invariably angular and have ragged margins which delicately interfinger with, or disaggregate within the enclosing matrix. These textures are considered to indicate that the vitriclastic clasts were at best only partially lithified when incorporated within the flow. Basalt fragments are also texturally immature and have variety of shapes ranging from angular, blocky forms, to more 'fluidal' forms with wispy or globular margins. They range in size from 2-120mm and occur both thoroughly mixed within vitriclastic clasts (Fig. 3.11a, c) and as discrete particles supported by the muddy matrix (Fig. 3.11d) . Furthermore, detailed examination of mesoscopic and microscopic textures associated with the basaltic fragments indicates that they were at least partially molten during mixing with host lithologies. Textures critical to this interpretation include: i) invariably fine-grained, aphanitic to sparsely porphyritic character of the basaltic clasts, ii) fluidal, globular shapes, iii) internal, non-explosive quench fragmentation of clasts, iv) delicate mingling at contacts with host material and v) high temperature devitrification textures developed in formerly glassy felsic vitriclastic host material. These textural relationships are described in detail below and are considered to be best explained in terms of resedimented peperite facies.

Description of volcanogenic clasts

The bulk composition of vitriclastic fragments varies according to the abundance of intermixed basaltic material. Fragments which lack basaltic material are characteristically felsic (rhyolitic to dacitic) in composition. Crystal assemblages contained in fragments of this type account for 5-35% of the clast volume and are

Figure 3.11. Mesoscopic textures of subfacies 5D.

(**a**) Graphic log showing poorly sorted, disorganised fabric within subfacies 5D, consistent with emplacement as cohesive debris flow. Clast-types include redeposited, plastically deformed mudstone blocks and rafts of volcaniclastic material exhibiting 'flamy' margins interfingering with enclosing silty mudstone matrix. Framework particles are texturally immature and clastic varieties were probably unlithified at the time of redeposition. X-axis of graphic logs is a schematic grainsize scale with grainsize increasing to right.

(**b**) Plastically deformed and partially disaggregated laminated mudstone clast. Diameter of coin is 20mm. (Sample 969)

(**c**) Polished slab of hand specimen extracted from raft comprising formerly glassy volcaniclastic debris. The sample is very poorly sorted and contains abundant pale grey, weakly vesicular blocky basalt clasts (bas) set in a vitriclastic groundmass of closely packed, swirled, aphyric and sparsely feldspar±quartz porphyritic pumice, crystal fragments, light coloured felsic volcanic fragments and minor mudstone. In detail, blocky basalt clasts have crenulate margins and a thin, pale chilled rind. (Sample 965)

(**d**) Polished slab from vitriclastic sandstone raft. Texture involves thoroughly mixed apple green pumice wisps (P), felsic and basaltic glass, and dense basaltic lithic fragments (bas). Width of view is 65mm. (Sample 883)

(**e**) Sample from mud-matrix rich interval containing texturally immature volcanogenic clasts, crystal fragments and minor dark grey mudstone. Volcanogenic clast-types include dense and vesicular basalt (bas(d) and bas(v) respectively), and quartz±feldspar bearing vitric tuff. At the left is a 'mingled' clast consisting of pale grey wispy to globular basalt fragments enclosed in dark grey mudstone and felsic vitriclastic material (V). Note that the globular basalt and tuff clasts in the top right hand corner were originally conjoined with sharp crenulate contact (arrow). Disaggregation along this contact and brittle fracture surfaces indicates that both materials were lithified during redeposition. Width of view is 80mm. (Sample 963)

(**f**) Quench-fragmented texture (hyaloclastite) developed in core of basalt clast. Fragments have blocky to splintery forms, curviplanar margins and display local 'jigsaw-fit' arrangements. They are enclosed in a very fine-grained formerly glassy basaltic matrix. Pale grey basaltic glass occurs towards the margin of the clast (to left) and has a crenulate contact with a dykelet of dark grey mud. Quench fragmentation is interpreted to have resulted from interaction of hot magma and wet, fine-grained sediment. 1mm divisions in scale. (Sample 971)

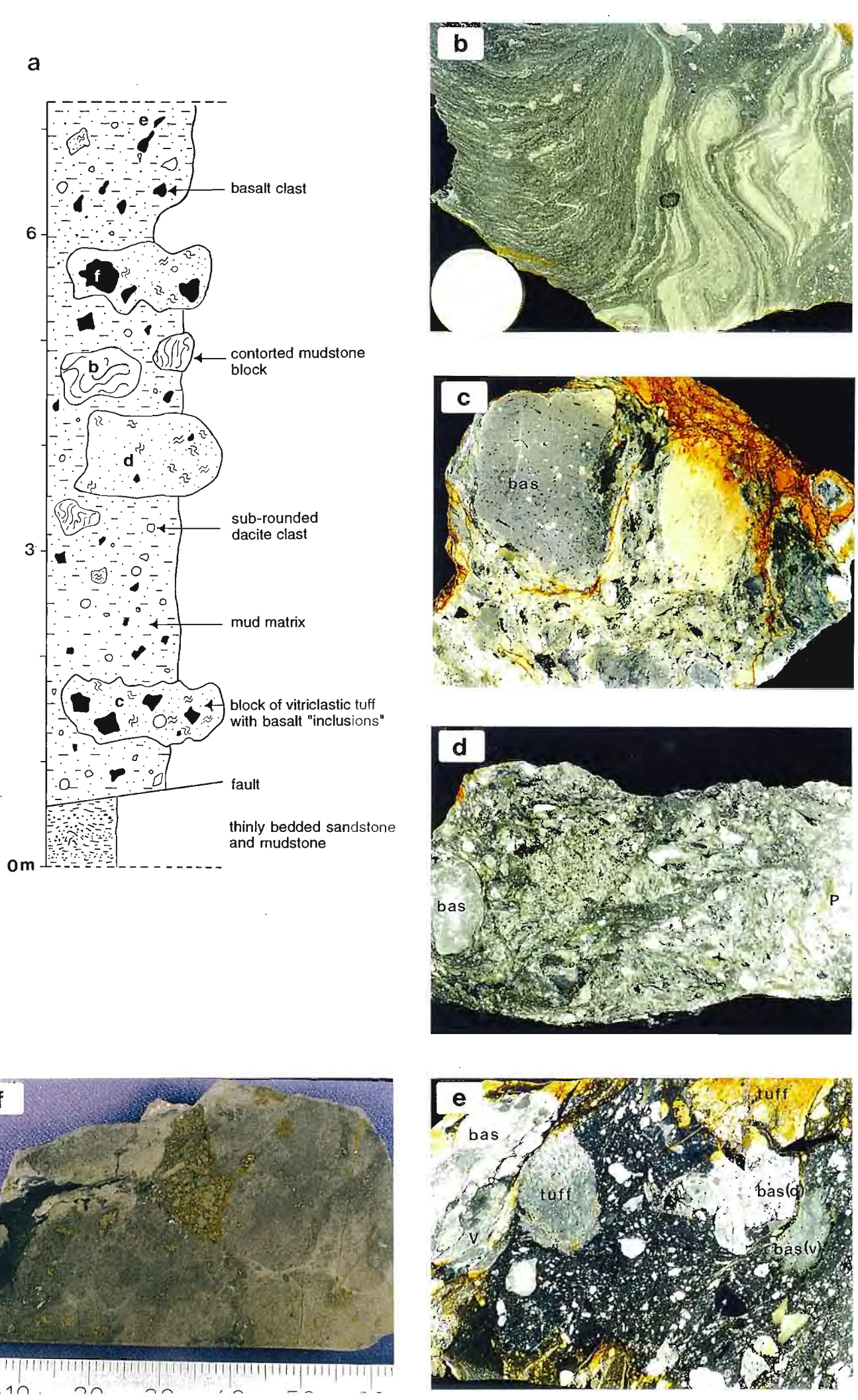
a
e
basalt clast
6
f
contorted mudstone block
b
d
sub-rounded dacite clast
3
mud matrix
c
block of vitriclastic tuff with basalt "inclusions"
fault
thinly bedded sandstone and mudstone
0m
b
c
bas
d
bas
P
f
e
tuff
bas
tuff
bas(d)
v
bas(v)

dominantly quartz, feldspar with traces of zircon, rare Fe-Ti oxide and apatite. Quartz and feldspar crystals have euhedral to anhedral forms, the latter resulting from crystal fragmentation and/or extensive dissolution. Skeletal quartz crystals with margins ornamented by elongate embayments are common, whereas feldspar crystals which have been affected by dissolution have cellular textures involving a box-work arrangement of thin, optically continuous feldspathic 'walls' which separate 'cells' of sericite-altered material. An outer mantle of globular quartz was observed around one cellular feldspar crystal. This crystal assemblage is essentially unchanged in vitriclastic tuff fragments which contain abundant basaltic material, however inclusion of the latter results in a bulk andesitic composition. Cr-spinels were also recognised in a small number of clasts, however these are interpreted as 'foreign' grains, released during disaggregation of basaltic inclusions.

The original vitriclastic texture is at best weakly preserved in many fragments and entirely absent in others, resulting in apparent coherent textures. Vitriclasts consist of patches of aphyric felty aggregates of chlorite or sericite which sometimes show blocky to wispy shapes and relict tube-pumice texture (Fig. 3.12a). Vesicles are strongly flattened within individual vitriclasts, however a coherent eutaxitic texture was not recognised in any clasts. In cases where a vitriclastic texture is no longer discernible, originally glassy 'groundmasses' appear as continuous felty mats of sericite or more commonly as mottled intergrowths of chlorite, sericite, feldspar and quartz. An excellent example of this mottled texture is shown in figure 3.12b, which involves a gradation from isolated chloritic spheroids with rarely preserved radiating fibres (0.05-0.2mm in diameter) $\rightarrow$ coalesced strings or masses of spheroids $\rightarrow$ dark grey amorphous patches consisting of microcrystalline quartz and phyllosilicate-altered feldspar. These textures are interpreted to represent progressive stages of spherulite growth and development of micropoikilitic texture which formed during high temperature devitrification of the originally glassy 'groundmass' (cf. Lofgren, 1971). Spherulite growth permeates the entire groundmass in some clasts, but is concentrated within poorly defined tabular domains in other cases. Although these tabular domains no longer contain a vesicular fabric, their shapes and dimensions are similar to pumice fragments observed in clasts with weakly preserved vitriclastic texture. Accordingly, they are tentatively interpreted to represent devitrified and recrystallised pumice fragments.

Basaltic particles can be broadly grouped into two types: a) aphyric, formerly glassy, highly vesicular wisps or blebs and b) weakly- to non-vesicular (dense), aphanitic to sparsely-porphyritic clasts with globular to blocky forms (Fig. 3.11c, e). In rare cases, a textural gradation was observed between these two types, with particles comprising dense cores and vesicular rinds. Both particle types occur as inclusions within vitriclastic clasts and as discrete fragments suspended in the muddy matrix.

Figure 3.12 Microscopic textures of clasts contained within subfacies 5D.

(**a**) Vitriclastic clast containing blocky pumice fragment with wispy terminations and crude relict tube pumice texture. Plane polarised light. (Sample 967)

(**b**) Vitriclastic fragment containing euhedral to anhedral quartz and subordinate feldspar crystals set in a mottled, formerly glassy 'groundmass'. The mottled texture is interpreted to have resulted from high temperature devitrification of glass and includes dark grey recrystallised chloritic spherulites (s) and irregular patches of micropoikilitic texture (m). To the left of the large quartz crystal positioned near the bottom of the figure, weakly flattened spherulites have coalesced to form 'trains'. In other areas of the 'groundmass', spherulites are enclosed by lighter grey patches of weakly-developed micropoikilitic texture (arrow). The ragged contact between the clast and the dark silty mudstone host is shown in the bottom left-hand corner of the figure. Photograph taken under crossed polars. (Sample 967)

(**c**) Vesicular 'bleb' of formerly basaltic glass enclosed by microlitic basalt. The 'glass' is considered to represent a residual liquid which segregated from the micro-crystalline mesh during rapid quenching (cf. Anderson et al., 1984). Plane polarised light. (Sample 970)

(**d**) Formerly glassy basaltic fragment (centre of field of view) enclosed by silty mudstone matrix. The fluidal shape of this clast is similar to microglobular peperite (Busby-Spera and White, 1987). The small dark inclusion (arrow) at top right of clast is a Cr-spinel crystal. A small felsic vitriclastic fragment (v) impinges on the basalt fragment. The ductile response of the latter may be due to post-depositional compaction or plastic flow whilst hot. Plane polarised light. (Sample 867)

(**e**) Photomicrograph (left) and line drawing (right) showing edge of 'mingled' clast containing highly altered perlitic basaltic glass (bas) and crystal-bearing vitriclastic tuff. Note the very delicate crenulate contact between the two lithologies and the finger-like re-entrant of tuff within the basaltic material. Fragmentation and incorporation of the parent unit within silty mudstone matrix (mat) clearly post-dated commingling of basaltic and felsic material. Plane polarised light. (Sample 867)

(**f**) Lensoidal 'pods' and veinlets of grey silty mud (s) enclosed by highly altered Cr-spinel bearing basalt clast. Plane polarised light. (Sample 867)

(**g**) Highly vesicular inclusions of basalt containing abundant Cr-spinel crystals (short arrows). The margins of inclusions are usually indistinct and transitional into enclosing mottled glass. Note however sporadic preservation of sharp scalloped margins defined by broken bubble walls (long arrows). Vesicles show slight flattening and crude flow alignment in right hand inclusion. Plane polarised light. (Sample 967)

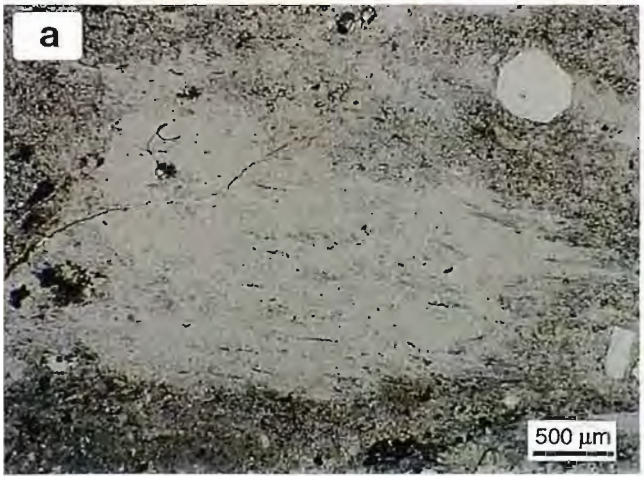
a
500 µm

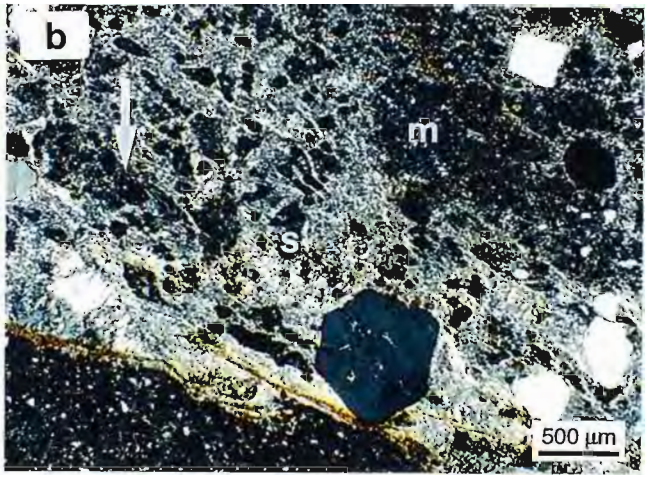
b
m
s
500 µm


c
500 µm


d
v
500 µm

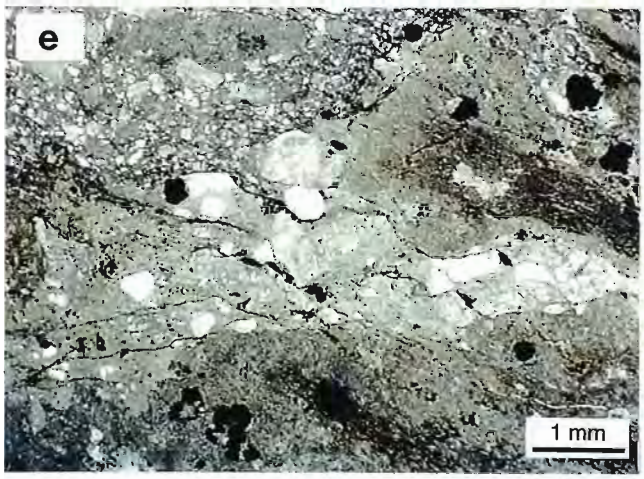
e
1 mm

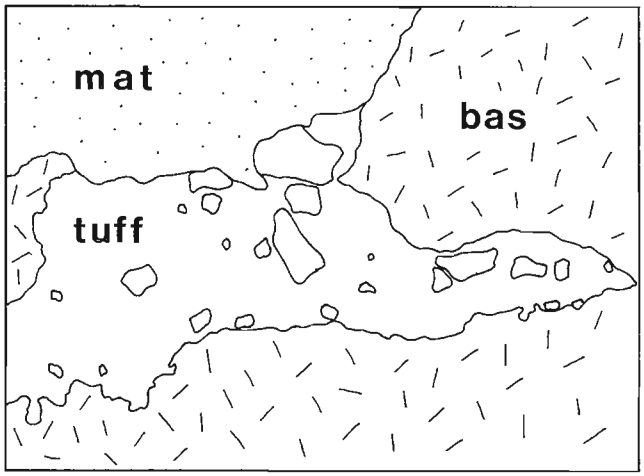
mat
bas
tuff


f
s
s
s
500 µm

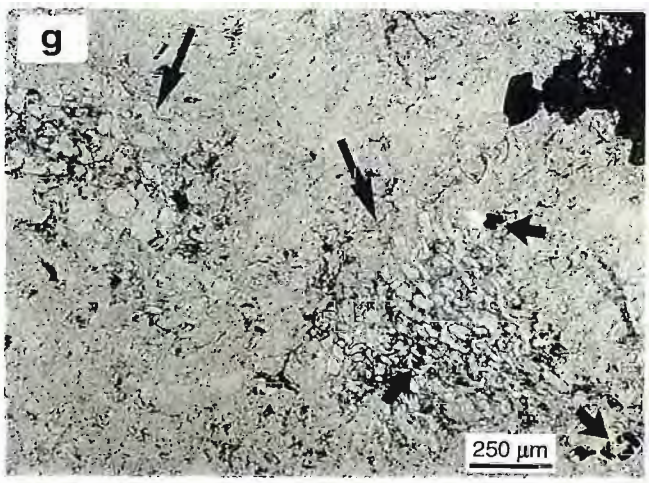
g
250 µm

Dense basaltic fragments range in diameter from 2-120mm and include microlitic to entirely 'glassy' varieties. In thin section, microlitic fragments exhibit well-developed quench textures involving closely packed bow-tie and fan shaped spherulitic aggregates of tabular to acicular feldspar microlites. Translucent reddish-brown Cr-spinels grains (0.01-0.1mm in diameter) occur as an accessory phase. Extremely fine-grained formerly glassy material occupies spaces between microlites, but is more commonly segregated from microcrystalline framework to form vesicular, sub-circular or elongate blebs 0.4-3.5mm in diameter (Fig. 3.12c). These textures are interpreted to be analogous to segregation veins described from lavas and shallow intrusive rocks. They form as a result of separation of a volatile-rich residual liquid phase from the rapidly quenching crystal mesh and migration to zones of relatively low pressure (cf. Anderson et al., 1984). 'Glassy' fragments are extensively altered to chlorite and/or epidote and with the exception of sparse Cr-spinels, are aphanitic. Altered perlitic fracturing is well-developed in some 'glassy' fragments.

The shapes of many dense basalt fragments are highly irregular, with fluidal forms and crenulate or globular margins (Fig. 3.12d). Locally, complex commingling of host sediment (either mud or vitriclastic material) and the basalt was observed, with the former filling delicate re-entrants along the margins of clasts, or occurring as blebs and veinlets wholly enclosed within the basalt fragment (Figs. 3.12e, f). Such textures are difficult to explain by epiclastic reworking of solidified lava, but are strongly reminiscent of globular particles formed as the result of fragmentation of hot magma during interaction with a cooler fluidal medium (cf. Kokelaar, 1986). Many natural examples of this process can be found in recent literature and include mingling of hot inclusions of mafic magma with cooler felsic host magmas (Eichelberger, 1980; Blake, 1981; Bacon and Metz, 1984; Bacon, 1986) and globular or microglobular peperite formed during the interaction of hot magma and wet sediment (Kokelaar, 1983; Busby-Spera and White, 1987).

In contrast to the fluidal character of clast margins, the interiors of some clasts are extensively brecciated. An example of this texture is shown in Figure 3.11f wherein angular to sub-rounded polygonal fragments occur enclosed by a groundmass of formerly continuous glassy basalt. Fragments have a 'jigsaw-fit' texture, indicating that brecciation occurred with minimal rotation or redistribution of framework particles (at a mesoscopic scale at least). This texture is consistent with fragmentation due to thermal shock ('cooling contraction granulation' of Kokelaar (1986)) which results from hot basalt coming into contact with a cooler medium. The presence of basaltic glass as an interstitial groundmass however (presumably crystallised from chilled magmatic liquid), is interpreted to indicate that solidification was neither instantaneous nor pervasive and that portions of the basalt were still at least partially molten during the quenching process. That fluidal intermingling of glassy basalt and host sediment occurs along the

margins of these internally brecciated clasts (Fig. 3.11f) suggests that the sediment acted as the coolant responsible for fragmentation.

Vesicular basaltic material occurs as irregular inclusions within vitriclastic clasts and as wispy fragments with ragged margins contained in the muddy matrix. Their interiors resemble some of the more highly vesiculated blebs of segregated glassy 'melt' recognised in the dense clasts and basaltic composition is indicated by numerous micro-phenocrystal Cr-spinels. Examples of inclusions contained within vitriclastic clasts are generally less than 10mm in their longest dimension and have sub-spherical to ductilely swirled stringer-like shapes. Their margins are usually indistinct and transitional with the surrounding host, however sharp, scalloped contacts defined by broken bubble walls are preserved in rare cases (Fig. 3.12g). Vesicles are generally undeformed with exceptions observed when inclusions are positioned along the edges of mingled clasts. In such cases vesicles are stretched and aligned parallel to the clast margins, with the degree of vesicle sphericity decreasing towards the contact with the muddy matrix. This ductile flattening of vesicles cannot be attributed to post-depositional compaction (either as the result of burial or tectonic flattening) as the orientations of long axes of flattened vesicles are variable throughout a given clast, and hence do not define a pervasive foliation. The concentration of strain towards the margins of clasts is instead interpreted to indicate that basaltic inclusions were plastically deformed during fragmentation of mingled clasts and resedimentation within the debris flow.

Interpretation

Subfacies 5D can be distinguished from the previously discussed volcaniclastic facies (subfacies 5A-5C) mainly by the presence of juvenile basaltic material. Furthermore, that there is good evidence to indicate reworking of pre-existing volcaniclastic deposits (ie. blocks of vitriclastic material). Redeposition of material probably initiated through slumping of a poorly lithified package of interbedded volcaniclastic and non-volcanogenic sedimentary units, with progressive dismemberment of sedimentary layers during transformation of the slump to a cohesive debris flow. The presence of large rafts of volcaniclastic material suggests that transport distances where not sufficiently great to allow thorough fragmentation and mixing of the constituent lithotypes. In addition, clasts that contain delicately commingled basalt with felsic vitriclastic debris and/or mudstone indicate that incorporation of basaltic material occurred prior to redeposition of the sediment mass.

Most examples of peperitic textures in ancient successions are attributed to interaction of high-level sills or lavas with wet sediment (ie. lavas or shallow intrusives) (eg. Brooks et al., 1982; Kokelaar, 1982; Busby-Spera and White, 1987; Branney and Suthren, 1988; Krynauw et al., 1988). Although the shapes of basaltic inclusions in this study show striking similarities to peperitic fragments described by these workers, it is

difficult to draw a direct analogy with this process due to the remobilisation of sediment and hence the lack of a clear spatial and/or genetic relationship with a parental coherent volcanic body. Providing possible support for an origin of basalt fragments from the dismemberment of intrusions of lava flows are the presence of high temperature devitrification textures in the felsic vitriclastic host material and the development of apparently coherent volcanic textures. In their study of secondary welding textures developed in pumice breccias intruded by hot magma, McPhie and Hunns (1995) argued that the development of spherulitic and micropoikilitic textures in the host volcaniclastics could only have resulted from superheating of the glass adjacent to the hot intrusion. The presence of these textures in vitriclastic clasts from subfacies 5D could therefore record an originally close spatial relationship between the host sediment and a hot magmatic body.

An alternative, but less likely origin for the clasts could involve basaltic ejecta (ie. spatter or bombs) erupted from a nearby volcano. Jones (1969) has argued for this mode of peperite formation in Oligocene lacustrine sediments from Gregovia, France, where ejecta was inferred to have become incorporated within steadily accumulating lime-mud. Although episodic eruption of a basaltic volcano could conceivably account for the inclusion of basaltic fragments within mudstone documented in the present study, it is difficult to envisage how thorough mixing could be achieved in vitriclastic deposits. Other examples of vitriclastic deposits in the Dundas region (eg. subfacies 5B) have been interpreted to have been deposited almost instantaneously from large turbidity flows. For mixing of basaltic and felsic pyroclastic material to have occurred therefore, hot basaltic ejecta must have been introduced directly into a genetically unrelated, high velocity flow. Although such a scenario cannot be ruled out entirely, it is considered to be geologically unlikely.

Regardless of which of these two mechanisms of peperite formation is applicable in this case, a requirement of both is that basaltic debris was proximally derived. Peperitic facies therefore indicates the presence of a basaltic volcanic centre nearby. If the interpretation that resedimentation distances were small and that emplacement of the debris flow was essentially coeval with the initial inclusion of basaltic debris are correct, then an intrabasinal, latest Middle Cambrian phase of basaltic magmatism can be inferred. The only documented coherent mafic volcanic facies of Cambrian age in the Dundas region occurs 1km SSW of the subfacies 5D unit at Montezuma Falls (Curtin Davis Volcanics: Elliston, 1954; Corbett and Solomon, 1989). Although structural complexity and lack of good, continuous exposure between these two areas prevents a direct chrono-stratigraphic correlation from mapping, both subfacies 5D volcaniclastics and the coherent volcanics have similar geochemical affinities, indicating that they were likely to have been comagmatic (see next section).

3.7 Geochemical affinities of volcaniclastic deposits

Six samples of volcaniclastic sedimentary rock and one 'pumice' fragment (from subfacies 5C) were selected from sub-facies 5A-D units for whole rock geochemical analysis. A description of the geochemical techniques used in this study are outlined in section 4.3. Due to the significant component of rapidly (?re)deposited juvenile volcanic debris contained within these units, their chemical compositions are likely to provide useful *estimates* of the chemistries of their parental magmas (cf. Hiscott and Gill, 1992; Skilbeck and Cawood, 1994). As such, it may be possible to track the compositional evolution of Middle to Late Cambrian magmatism in the Dundas region and neighbouring areas. It is important to note however, that during primary fragmental and sedimentological processes, the potential exists for significant deviation of sediment chemistries from that of their source. In addition to the likelihood of contamination from 'exotic' material (ie. that not produced directly during the volcanic event), the effects of turbulence during both eruption and transport of juvenile debris may be considerable. Turbulent flow causes segregation of particles according to their relative densities (Cas, 1979) and as such can result in separation of the crystal component from the less dense vitric component. Flood et al. (1980) for instance, estimated that a 36% loss of the vitric component during emplacement of the Dundee Rhyodacite ash flows (eastern Australia) resulted in rhyodacitic compositions, in contrast to the rhyolitic composition of their inferred magmatic source rocks. Trace element compositions are likely to be similarly effected, with the concentration of highly incompatible elements originally partitioned within the melt phase of the parent magma, becoming progressively diminished as the vitric fraction is 'driven-off' during turbulent flow. Conversely, compatible elements partitioned within crystal phases of the melt might be expected to show anomalously high concentrations in crystal-rich volcaniclastic units. The processes outlined above must be considered when interpreting geochemical data. In order to minimise the effects of 'density segregation', samples of similar crystal content are compared. Samples rich in pumice are considered to most accurately reflect initial compositions as the relative proportions of crystal and melt within the parental magma should be represented.

Whole rock analyses are shown in Table 3.2, with major elements recalculated as volatile-free percentages. SiO_2 contents range from 56-80%, with the majority of samples containing more than 70% SiO_2, indicating dominantly rhyodacitic to rhyolitic compositions. A basaltic andesite composition is indicated for subfacies 5A (56 wt% SiO_2), whereas SiO_2 contents in the subfacies 5D sample and the 'pumice' sample from subfacies 5C (sample 88) are suggestive of andesitic compositions. Thin section examination has revealed that silica alteration is negligible in most samples, however some vitriclastic (pumiceous) sandstones are probable exceptions to this rule. SiO_2 contents of 79% and 80% of sub-facies 5B samples D86 and 828 respectively may have

Table 3.2. Wholerock geochemical data for subfacies 5 volcaniclastic rocks

	Subfacies 5A	Subfacies 5B		Subfacies 5C			Subfacies 5D
Sample	**982**	**828**	**D86**	**D158**	**88***	**95004**	**883**
SiO2	56.16	79.74	78.92	75.76	61.59	70.46	60.49
TiO2	1.07	0.33	0.32	0.48	0.63	0.55	0.89
Al2O3	19.54	12.09	12.52	13.54	24.97	15.96	23.75
Fe2O3(tot)	9.84	2.95	2.49	3.57	2.61	4.18	5.61
MnO	0.08	0.01	0.25	0.04	0.01	0.04	0
MgO	4.62	1.5	1.4	1.31	1.27	1.63	1.27
CaO	0.72	0.03	0.32	0.28	0.11	0.09	0.26
Na2O	7.34	0.45	0.61	3.03	3.65	6.53	0.53
K2O	0.36	2.86	3.08	1.89	5.05	0.47	6.95
P2O5	0.26	0.03	0.09	0.09	0.1	0.09	0.26
La	52	65	61	20	20	36	107
Ce	103	128	122	46	43	75	196
Nd	45	57	51	22	22	37	83
Nb	11	14	13	9	14	14	25
Zr	149	208	197	154	335	230	368
Sr	305	17	40	115	139	200	26
Cr	51	29	109	26	7	28	329
Ba	227	300	447	282	632	244	731
Sc	27	6	10	10	9	11	15
V	309	23	50	53	42	76	94
Y	29	38	36	22	30	38	50
Rb	13	106	112	84	180	19	228
Th	11	24	25	7	31	15	44
Ni	21	12	20	13	9	10	105
Pb	8	7	10	8	3	4	73
Ti/Zr	43.22	9.49	9.73	18.79	11.36	14.31	14.45
Ti/Y	222.06	51.92	53.25	131.54	126.82	86.61	106.36
Zr/Sc	5.52	34.67	19.70	15.40	37.22	20.91	24.53
Nb/Sc	0.41	2.33	1.30	0.90	1.56	1.27	1.67

* denotes pumice clast

been enriched by the addition of silica. Extensive sericite alteration in samples 883 (sub-facies 5D) and 88 (sub-facies 5C) indicated both petrographically and by anomalously high abundances of Al_2O_3 and K_2O ,is inferred to have resulted in depleted SiO_2 content (60% and 62% respectively). In view of the apparent mobility of silica, examination of relatively immobile incompatible element abundances is considered to be more reliable as a means of determining geochemical affinities .

On the Zr/TiO_2 vs Nb/Y plot of Winchester and Floyd (1977) (Fig. 3.13), all samples plot within the field of rhyodacite-dacite with the exception of subfacies 5A which plots on the andesite-subalkaline basalt boundary. It should be noted however, that Zr/TiO_2 values in volcaniclastic rocks are likely to be particularly sensitive to mechanical concentration of zircon, magnetite or rutile during the sedimentation process. Concentration of zircon, for instance, will result in an upward displacement of points on the Zr/TiO_2 vs Nb/Y plot, whereas magnetite or rutile concentration will cause a downward displacement of data. The abundance of detrital magnetite contained with sample 982 (indicated both petrographically and by high magnetic susceptibility) is therefore likely to result in a more 'mafic' position in Figure 3.13 compared to its parental magma.

MORB-normalised multi-element patterns for vitric-rich and crystal-rich samples are shown in Figs 3.14a and b respectively. Also included in these diagrams are the average compositions of lava suites which represent the later stages of magmatism in the Mt Read volcanic 'arc' (Crawford et al., 1992) and occur in association with biostratigraphic equivalents of the Dundas Group in areas to the east and northeast of the Dundas region: i) basaltic to andesitic shoshonitic lavas and shallow intrusives from the Hellyer and Howards Plains areas, ii) rhyolitic lavas from the Tyndall Group and iii) tholeiitic lavas of the Henty fault wedge (Suites III, I and IV respectively of Crawford et al., op cit.). Whole rock geochemical data is also shown from a suite of highly altered ?andesitic lavas which crop out in the central area of the Dundas region near Montezuma Falls (Curtin Davis Volcanics: Elliston, 1954). Vitriclastic sandstone samples exhibit a marked compositional range with progressive enrichment of P, Ti and ferromagnesian elements from the more 'felsic' subfacies 5B units to subfacies 5D, the latter having been interpreted to consist of mingled felsic and basaltic volcanic debris (see previous section). The very high concentrations of Cr (329ppm) and Ni (105ppm) in subfacies 5D are consistent with the inferred input of basaltic material, however incompatible elements including Th, light rare earth elements (LREE), Nb and Zr are also significantly enriched relative to both subfacies 5B and 5C samples.

The shape of the multi-element patterns and the absolute abundances of elements for subfacies 5B and 5C samples compare well with the available data for the Tyndall Group lava suite (Fig. 3.14a). Slight enrichment of ferromagnesian elements in

Figure 3.13. Zr/TiO_2 vs Nb/Y plot of subfacies 5 volcaniclastic rocks.

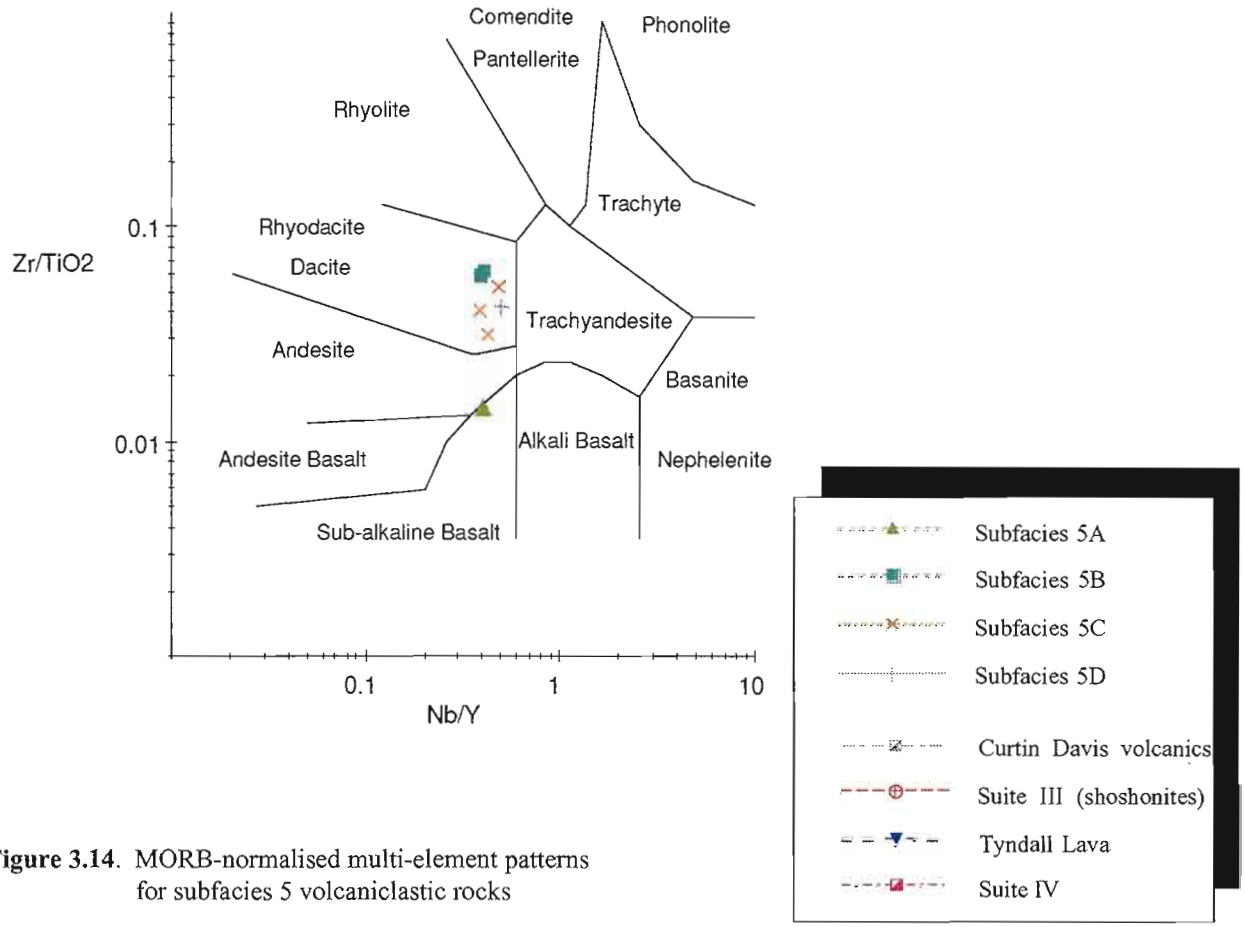

Figure 3.14. MORB-normalised multi-element patterns for subfacies 5 volcaniclastic rocks

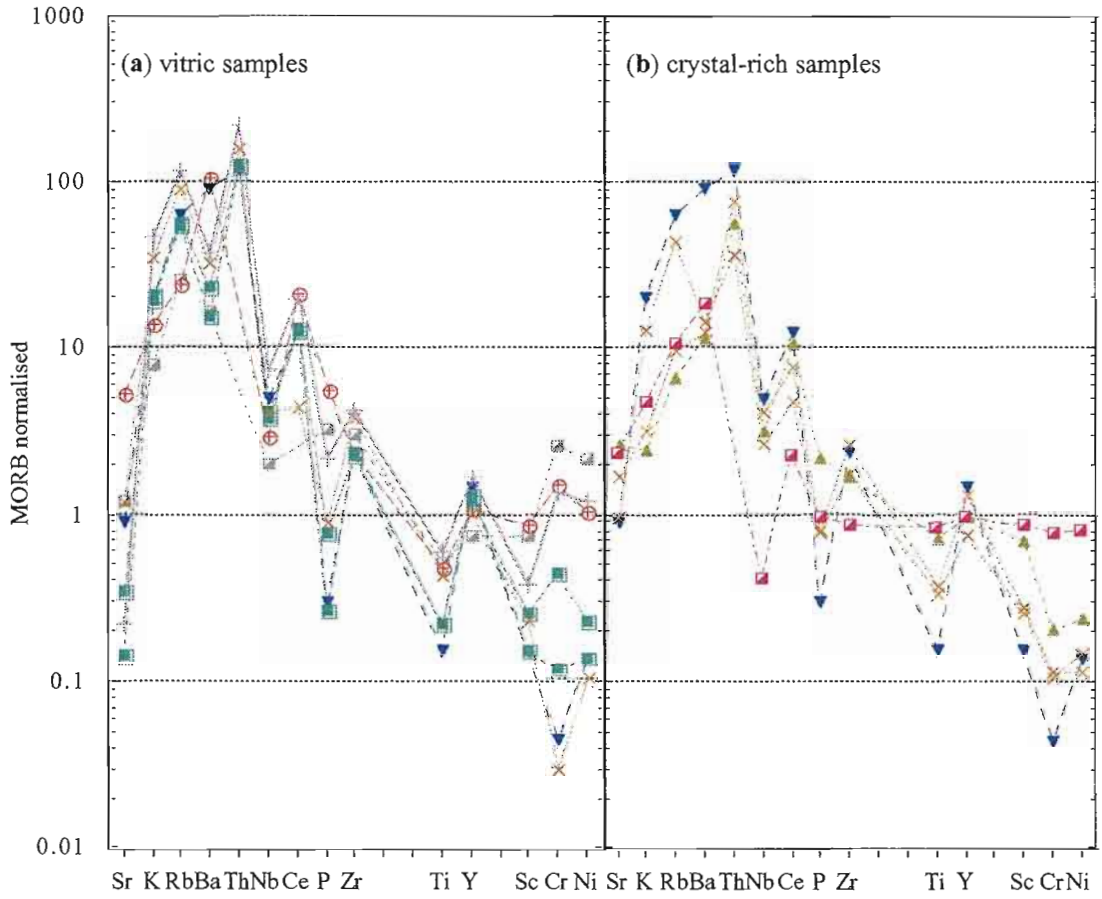

Data sources: i) average MORB (Pearce, 1983)
ii) Suite III and suite IV (Crawford et al., 1992)
iii) Tyndall Group lavas (White, in prep.)
iv) Curtin Davis Volcanics (Corbett and Solomon, 1989)

subfacies 5B relative to Tyndall Group lava indicates minor contamination from a more mafic source. This trend is consistent with the petrographic observation of detrital chromite grains and possible mixed rhyolitic and basaltic pumice fragments within this subfacies (see section 3.6.2). The marked enrichment in both incompatible and ferromagnesian elements in subfacies 5D results in a pattern comparable with that of Suite III (shoshonitic) basaltic to andesitic lavas of the Mt Read volcanic arc and the Curtin Davis Volcanics. Although extreme incompatible element enrichment is characterised by suite III (Crawford et al., 1992), Nb and Zr values of subfacies 5D are also considerably higher than typical compositions shown by this magmatic suite. This problem may be explained by concentration of zircons during the sedimentation process (possibly sourced from felsic volcanic or sedimentary sources) or it may indicate that the basaltic glass was derived from a more evolved liquid compared to typical western Tasmanian shoshonitic magmas. In view of the petrographic evidence for mixing of felsic and basaltic debris in subfacies 5D however (section 3.6.4), contamination of the dominant shoshonitic signature via sedimentary or intrusive processes is the preferred interpretation.

The multi-element patterns of quartz-bearing crystal-rich sandstones (subfacies 5C) are comparable with those of subfacies 5B and 5C vitriclastic samples (Fig. 3.14b). Th and LREE values are somewhat depleted relative to subfacies 5B vitriclastic units however, which may have resulted from elutriation of incompatible element-enriched fines during eruption and transport or derivation from a more incompatible element-depleted magma. The very low values of LREE (La: 20ppm) contained in the 'pumice' fragment extracted from the subfacies 5C unit near Curtin Davis Mine is considered to support the latter interpretation.

The progressive enrichment of P, Ti, Sc and Cr in the feldspathic subfacies 5A unit relative to quartz-bearing varieties is indicative of a trend towards a mafic composition (Fig. 3.14b). This is consistent with the low SiO_2 abundance of subfacies 5A as well as its more 'mafic' position on the Zr/TiO_2 vs Nb/Y plot. Shoshonitic affinities are not indicated however, with LREE, Th, Nb, Ni and Cr abundances well below those of subfacies 5D and suite III lavas. These elevated abundances of Ti and V (309ppm) coupled with high Ti/Zr, Ti/Y and low Zr/Sc in subfacies 5A (Table 3.2) are considered to indicate a parental magma with tholeiitic composition. A reasonable correlation is shown between subfacies 5A and tholeiitic suite IV lavas, particularly in terms of high Ti and Sc abundances (Fig. 3.14b). However, more incompatible elements (positioned towards the left of Figure 3.14b) are noticeably enriched in subfacies 5A compared to suite IV data , possibly indicating mixing of material derived from a mafic tholeiitic source and more felsic material.

Summary

Discrimination between the various volcaniclastic units on the bases of petrographic and textural features compares well with geochemical discrimination techniques. Three distinct geochemical signatures are identified: i) a felsic magmatic source comparable with that of the Tyndall Group rhyolitic lavas (subfacies 5B and 5C); ii) a mafic tholeiitic source possessing subtle affinities with suite IV (subfacies 5A), and iii) a shoshonitic source component within subfacies 5D that compares well with both suite III lavas and the local Curtin Davis Volcanics. In both ii) and iii) dilution of the mafic source component by more felsic is indicated both petrographically and geochemically. In subfacies 5D, mixing of basaltic and felsic volcanogenic debris was achieved mechanically during inferred peperitic intrusion of basalt into a mixed felsic volcaniclastic and non-volcanogenic sedimentary package (see section 3.6.4). The essentially monogenetic juvenile component of subfacies 5A however (section 3.6.1), may indicate that inferred mixing of mafic and felsic material occurred prior to eruption (ie. within the magma chamber).

As most volcaniclastic deposits are voluminous, widely distributed (with the exception of subfacies 5D) and both petrographically and geochemically distinct, they are potentially useful tools for litho- and chemo-stratigraphic correlation (cf. McPhie and Allen, 1992). Further work in the Dundas Group should attempt to utilise these deposits for stratigraphic analysis, particularly in view of the characteristically restricted distribution of many non-volcanogenic lithotypes (eg. conglomerate facies).

Chapter 4
Provenance of siliciclastics

4.1 Introduction

The composition of clastic material, determined from geochemical and/or petrological techniques, has long been recognised as providing a good approximation of the composition of parental lithologies. This fundamental link between the composition of sediments and their respective sources forms the basis for all provenance studies and has been shown to provide a powerful tool in determining: i) tectonic settings of sedimentary successions (eg. Crook, 1974; Dickinson and Suczek, 1979; Condie and Martell, 1983; Bhatia and Crook, 1986; Roser and Korsch, 1988; Floyd et al., 1989; McLennan et al., 1990), ii) compositional evolution of contemporaneous magmatic systems (Hiscott and Gill, 1992; Cawood, 1991; Skilbeck and Cawood, 1994), and iii) tectonic evolution and sediment dispersal patterns in sedimentary basins (eg. Chiocchini and Cipriani, 1992; Ahmad et al., 1994).

In this chapter, I present data from a study of the composition of siliciclastics located mainly in the Dundas region. Additional samples were collected from the Que River and Farrell Rivulet (situated approximately 25 km NNE and 10 km S of the Dundas region respectively: Fig. 1.1). This study aims principally to identify the nature and location of source regions which were actively supplying clastic material during the Middle and Late Cambrian. Furthermore, it was envisaged that any temporal and/or spatial variation in sediment provenance would allow constraints to be placed on the palaeogeography and structural evolution of the basin. Accordingly, samples were selected from a range of stratigraphic levels and geographic locations.

Detailed petrographic study of the sediments is hampered in many instances as the combined effects of diagenesis, low-grade metamorphism, as well as weathering of the source lithologies prior to erosion and transport, has resulted in recrystallisation of labile framework grains (ie. ferromagnesians, plagioclase and vitric volcanic rock particles). Unaltered ferromagnesian grains were not identified in any of the thin sections examined in this study. As a result, petrological descriptions presented below are mainly qualitative and aim to highlight distinctive clast or mineral assemblages which aid in constraining provenance characteristics. Modal analyses of detrital grains were carried out on a few granule conglomerate and coarse sandstone samples.

Whole rock geochemical techniques were considered to be effective in provenance determination as certain trace elements (in particular the high field strength elements (HFSE) as well as Cr, P and possibly Ni) have been shown to be largely insensitive to weathering, transport and post-depositional processes (Taylor and McLennan, 1985), but

also in that the composition of fine-grained lithotypes can be determined. Moreover, the potential source lithologies (ie. Proterozoic basement, MUC and the Mt Read Volcanic 'arc') have distinct and well-constrained geochemical characteristics (Brown, 1986; Crawford and Berry, 1992; Crawford et al., 1992). It was found that despite mixing of clastic material derived from two or more of these sources, the geochemical signature of the dominant source was retained in daughter sediments, in most cases regardless of grainsize.

Another useful tool in provenance study is the chemistry of individual detrital phases. Of particular interest are detrital grains derived from volcanic successions as they may indicate the chemical affinities of parental magmatic suites. This technique has the advantage over bulk composition methods (ie. modal and whole rock geochemical analysis) in that the 'averaging' effects of source mixing can be minimised and individual source components identified (cf. Cawood, 1991). Although the contribution from some sources may be very minor in a given sample, their identification nevertheless has the potential of more exactly constraining source areas and discriminating between packages of strata, which in terms of their bulk composition alone, may be indistinguishable. The chemistry of detrital Cr-spinels, although used in a very preliminary manner in this study, were considered to be potentially effective in discriminating between mafic and ultramafic sources. This approach follows recent work by Greenhill (1995) which suggested that input of clastic material derived from various mafic and ultramafic magmatic suites contained within pre-Dundas Group successions (ie. Crimson Creek Formation and MUC) can be distinguished on the Ti content of detrital Cr-spinels.

4.2 Chemical data sources

In addition to the 69 samples selected for whole rock chemical analysis from the Dundas region and the two smaller satellite areas, this study incorporates a wealth of published geochemical data (major and trace elements, including rare earth elements) from pre-Dundas Group successions (Brown, 1986; Crawford and Berry, 1992) and the Mt Read volcanics (Crawford et al., 1992). The studies from which the published data are sourced were concerned primarily with the discrimination and evolution of magmatic systems and hence mainly involve chemical analyses of coherent volcanic units. On the other hand, analyses of sedimentary lithologies associated with potential source areas are not so readily available. To supplement existing chemical data for sediments contained in the Crimson Creek Formation (eg. Brown, 1986; Haines, 1991), I selected an additional 5 samples of mudstone and volcanogenic greywacke from the Ring River between 714702 and 712711 (NW of the Serpentine Hill MUC). In addition, 8 samples of mudstone and micaceous quartz sandstone were collected from the upper portion of the Oonah Formation in the Stanley River area.

Chemical composition of Cr-spinels contained within plutonic and boninitic lava successions from the MUC are sourced from Brown (1986). Cr-spinel data from Middle Cambrian shoshonitic lavas located outside the Dundas region are from Jones (in prep.) and include samples from the Hellyer basalt (Mount Charter Group) as well as a basaltic unit contained in the Anthony Road andesite. Available data from the Crimson Creek Formation is small and involves chemical analyses of 27 detrital Cr-spinels contained in a volcanogenic sandstone located on the Pieman Dam Road (Berry and Fulton, 1994).

4.3 Sample preparation and analytical techniques

Samples included for whole rock analysis were trimmed to remove oxidised and vein material using a diamond saw and then broken into pea-sized chips in a jaw crusher. The minimum sample size for lutites was 250 gm, whereas 1000 gm of rock was crushed and split in cases where coarse-grained sandstone or conglomerate were analysed. Any remaining weathered, veined or saw-marked particles were hand picked from the coarse crush. Between 100-250 gm of chips were then pulverised to a fine powder in a tungsten-carbide ring mill from which powder pellets and glass disks were prepared. Major and trace elements were determined by X-ray fluorescence (XRF) using a Phillips P1410 X-ray spectrometer at the Department of Geology, University of Tasmania. Only those rare earth elements sufficiently abundant to be measured directly on pressed powder pellets were analysed. These included three light rare earth elements (LREE): La, Ce and Nd. Major element values were recalculated to 100% ignoring loss on ignition values (LOI) and are presented as volatile-free percentages. Raw geochemical data is presented in Appendix A.

The chemistry of detrital Cr-spinel grains were analysed from polished thin sections using a Cameca SX-50 electron microprobe at the Central Science Laboratory, University of Tasmania (Appendix B).

4.4 Compositional variation and classification

The analysed samples exhibit a relatively continuous spectrum of compositions. Although the bulk of this variability is likely to be controlled by differences in the relative contributions from compositionally distinct sources, several other important factors should be considered, especially when interpreting chemical data. For example, sedimentological processes such as grainsize sorting (ie. hydraulic fractionation) during transport or intrabasinal reworking (eg. via bottom current activity), source area weathering and post-depositional diagenesis, can all result in substantial modification of the source signature (eg. Wronkiewicz and Condie, 1987; McLennan et al., 1990). In classifying samples in terms of their source signature, it important therefore to establish whether these processes have had a significant effect. The effects of these processes have been minimised to some extent by initially comparing samples of similar grainsize and by

establishing provenance characteristics in terms of relatively immobile element concentrations such as LREE, Ti, Nb, Sc, Zr, Th, P and Cr (cf. Taylor and McLennan, 1985). It was found however, that in packages of strata involving compositionally and texturally immature sediments of similar provenance, absolute abundances of many immobile elements were broadly comparable regardless of grainsize. With higher degrees of sediment maturation, discrepancies between element abundances in sandstones and mudstones increase (primarily due to the dilution effect of quartz in sandstones and the concentration of trace elements in clay minerals), however correlation can still be made using certain element ratios.

Fundamental differences in carefully selected chemical and petrological criteria of the analysed sedimentary rocks and in particular, the recognition of distinctive source signatures provide the bases for a first-order classification. Four broad compositional suites have been identified. Suites 1, 2 and 4 are considered to represent compositional "end-members" and show clearly identifiable affinities with distinct pre-Dundas Group sequences. Although mixing of detritus derived from two or more source terrains is important in some samples a major contribution from a single source is apparent within each suite. Suite 3 lacks the distinctive signatures shown by the other suites and involves a broad range of compositions consistent with thorough mixing of detritus derived from two or more sources. The geographic distribution of samples and suites are shown in Figure 4.1.

4.5 Suite 1

Samples were classified as suite 1 if they had a significant component of mafic detritus which showed compositional affinities with the Crimson Creek Formation. This provenance signature was identified in most samples by chemical means, specifically through high abundances of Ti (> 2.1 wt% in sandstones and > 1.8 wt% in mudstones) and Nb (> 22 ppm in sandstones and > 21 ppm in mudstones: Fig. 4.2), however conglomeratic samples containing clast assemblages that can be related specifically to parent lithologies of the Crimson Creek Formation were included on petrological criteria alone.

Further separation of suite 1 (suite 1A-1C) was achieved on the bases of i) geographic distribution of samples, ii) differences in the relative abundances of key elements (in particular trace element abundances) and iii) petrological characteristics of coarse-grained samples (Table. 4.1: Fig. 4.3). The distribution and provenance characteristics of each sub-suite are discussed in detail below.

4.5.1 Suite IA

Suite 1 samples which are located in the western area of the Dundas region and the Que River region are defined as suite 1A (Fig. 4.1). Coarse-grained suite 1A samples

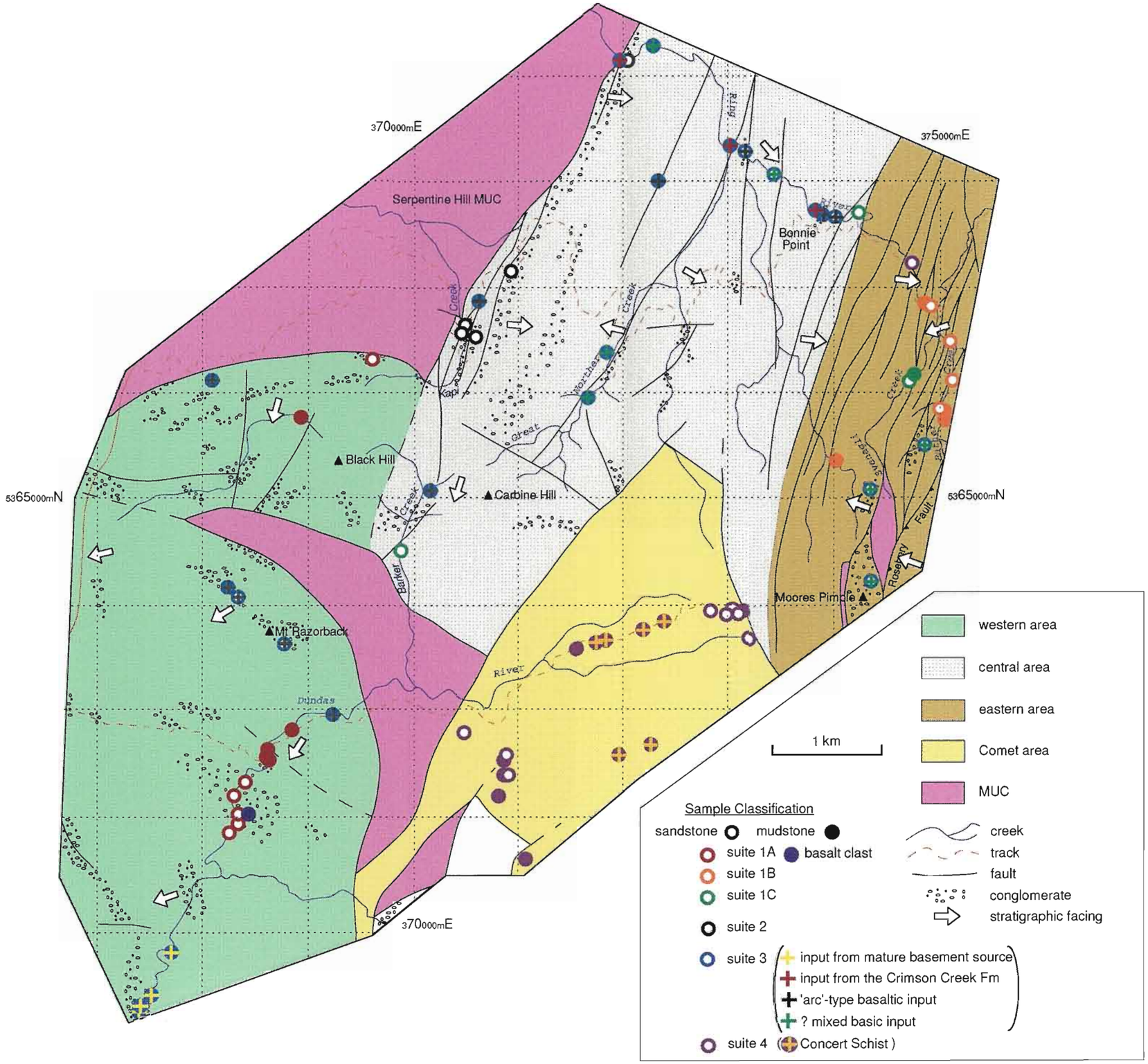

Figure 4.1. Simplified geological map of the Dundas region showing area boundaries and distribution of samples.

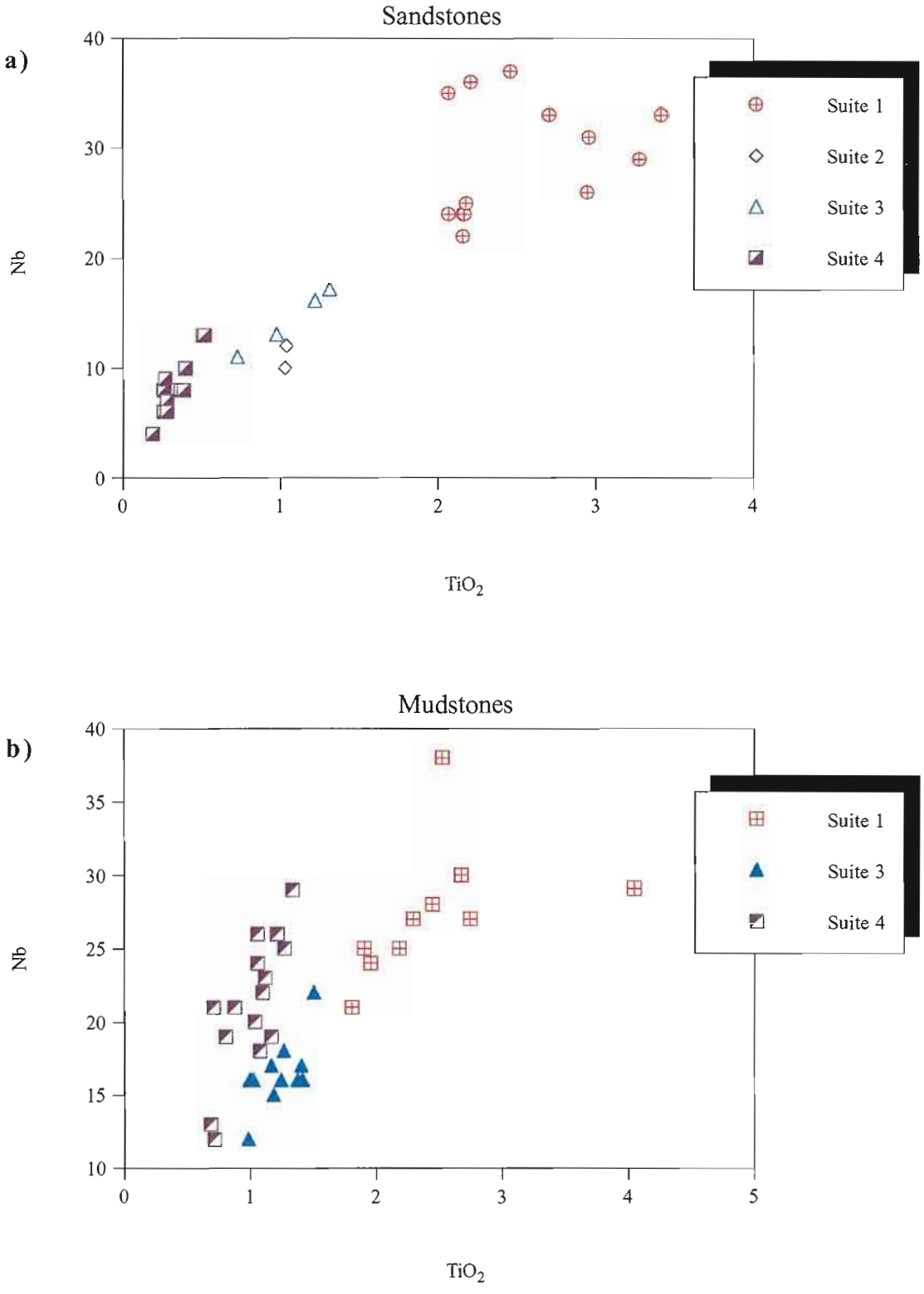

Figure 4.2. TiO_2 vs Nb plot for sandstones and mudstones showing chemical discrimination of suite 1.

Table 4.1. Features used to sub-divide suite 1. Those features highlighted in italics are diagnostic of particular sub-suites.

	Geographic Distribution	Stratigraphic Distribution	Chemical Characteristics		Petrological Characteristics	Cr-spinel chemistry
			Sandstone	Mudstone		
Suite 1A	•*western area of Dundas region and Que River region* • located close to the western limits of Middle-Late Cambrian strata	• lower to upper portions of Dundas Group • broad biostratigraphic range from ?Undillan to ?Iverian	• moderate abundances of LREE, ferromagnesian elements with very high Cr and Cr/Nb in some samples	• high TiO_2, Mg, Sc, Nb, low to moderate Th •*moderate to high Ti/Th*	• *very high lithic content, with sedimentary clasts most abundant* • volcanic quartz is a significant component in some samples	• high-Ti Cr-spinels contained Fernfields Conglomerate • low-Ti Cr-spinels contained in Que River and Black Hill members
Suite 1B	•*eastern area of Dundas region*	• ?correlates of Crimson Creek Formation	•*very high TiO_2, Nb, ferromagnesian elements, low LREE, Th* •*very high Ti/Th, Nb/La, Ti/Zr*	•*very high TiO_2,* Sr, Nb, P_2O_5, moderate to very high Sc, low Th •*high to very high Ti/Th,* low to moderate Th/Sc	• intensely recrystallised lithic-rich framework • resolvable lithic fraction dominated by formerly glassy basalt clasts	• high-Ti Cr-spinels
Suite 1C	• broad geographical distribution with samples coming from eastern and central areas of the Dundas region	• Dundas Group, but poorly constrained bio-stratigraphically	•*high SiO_2,* moderate Mg, low Ca and Sr, moderate to high Th and LREE • high Zr abundances resulting in *low P/Zr and high Zr/Sc, Zr/Nb*	• low Cr, high Sc and Th •*moderate Ti/Th*	• quartz comprises > 30% of the framework • the remainder is intensely recrystallised, with low lithic content	• no Cr-spinels analysed from this suite

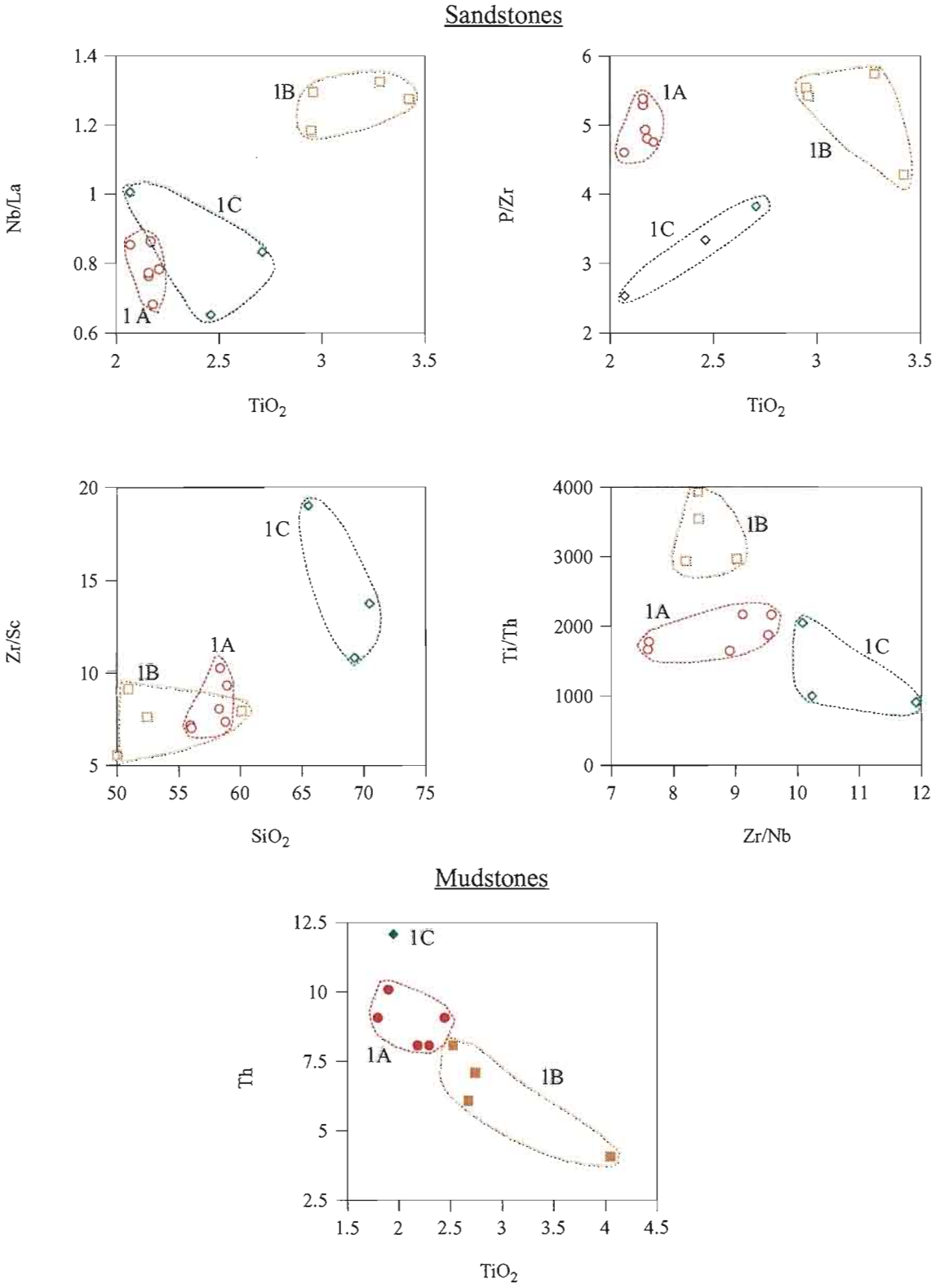

Figure 4.3. Plots showing discrimination of suites 1A-1C via chemical characteristics. Depletion of TiO_2 in suites 1A and 1C sandstones relative to suite 1B, with correspondingly lower values of Nb/La and Ti/Th in the former indicate dilution of the high-Ti and Nb basaltic signature, probably due to greater input from 'felsic' source material. Similarly, progressive enrichment of Th with decreasing TiO_2 from suite 1B⟶1A⟶1C mudstones is consistent with a trend towards more 'felsic' compositions.

differ from the remaining coarse-grained suite 1 samples. They have very high lithic component (>75% of the framework component) and in particular an abundance of sedimentary lithic fragments (between 64-88% of the lithic fraction). They differ from suite 1B sandstones in many element ratios including Ti/Th, Nb/La, Ti/Zr and Ti/Y (Table 4.2), all of which are lower in coarse-grained suite 1A samples, and are interpreted to indicate dilution of the high Ti-Nb Crimson Creek tholeiite signature through input of either 'felsic' material and/or MUC-derived detritus in suite 1B sandstones. Suite 1C sandstones have an even higher component of 'felsic' source material as shown by moderate to high SiO_2 abundances (65-71 wt%) compared to 56-59 wt% for suite 1A coarse-grained samples (Fig. 4.3).

Ti/Th values provide the best means of chemical discrimination within suite 1 (suite 1A: 1150-1725, suite 1B: 1900-6069, suite 1C: 980) (see also Fig. 4.3), however the ranges are close and more data would be required to validate separation using this parameter. The range in Ti/Th is considered to indicate a progressively increasing component of 'felsic' detritus from suite 1B→1A→1C. The geographic distribution of samples remains as a principal factor in discriminating between suite 1 mudstones.

A total of five mudstone samples (all from the Dundas region) and thirteen coarse-grained sandstone or granule conglomerate samples (seven from the Dundas region and six from the Que River region) are included within suite 1A (Fig. 4.1). Of the latter, six were analysed for whole-rock geochemistry whereas the remainder are classified solely on petrographic characteristics.

Coarse-grained samples from the Dundas region were collected from two chrono-stratigraphically and spatially distinct conglomerate-dominated packages. The oldest of these two packages is located on the northern slopes of Black Hill and lies with erosional contact on low-Ti pillowed lavas of the Serpentine Hill MUC (Fig. 4.4b). It is of probable Undillan age and is referred to herein as the Black Hill member. The younger package occurs within the type section of the Dundas group exposed in the Dundas River (Fig. 4.4a: Fernfields Conglomerate) and totals 500m in thickness. A lower age limit for the package is provided by fossiliferous mudstones containing an uppermost Mindyallan faunal assemblage (Jago, 1979), which occur approximately 50m below the base (Brown, 1986). The bio-stratigraphic position of the upper part of the package is poorly constrained however, with Iverian fauna positioned approximately 800m above the top (Jago, 1978; Laurie et al., 1995). Assuming a high rate of sedimentation for the conglomerates, an uppermost Mindyallan or Idamean age is inferred.

Mudstone samples are reasonably well constrained bio-stratigraphically, ranging in age from Boomerangian to Mindyallan. The two oldest samples are probable chrono-stratigraphic equivalents and come from the Black Hill area (sample 446) and type section of the Dundas Group (sample 823) respectively (Figs. 4.4a and b). The former is positioned stratigraphically 400m above the top of the Black Hill member and

Table 4.2. Whole rock geochemical data for Suites 1 and 2.

	Suite 1A												Suite 1B								Suite 1C				Suite 2	
Lithology	Sandstone						Mudstone					basalt clast	Sandstone				Mudstone				Sandstone			Mudstone	Sandstone	
	FM			BHM	QRM																					
Sample #	336	340	341	958	917	919	320	324	817	823	446	339	196	211	192S	868	167	210	214	192M	218	386	890	216	D94	RL1
SiO2	58.78	55.97	58.27	56.06	58.36	58.91	56.70	55.87	57.38	60.49	61.13	45.43	60.06	50.96	52.49	50.06	63.69	52.16	47.34	54.79	70.48	69.29	65.55	59.76	62.13	65.79
TiO2	2.16	2.16	2.18	2.17	2.21	2.07	2.45	2.30	1.91	2.19	1.81	2.84	3.28	2.96	3.42	2.95	2.53	2.75	4.05	2.68	2.07	2.71	2.46	1.96	1.03	1.04
Al2O3	12.84	12.99	12.40	13.92	13.24	12.12	16.46	16.60	16.30	14.62	15.62	15.97	13.87	16.34	13.73	14.22	15.65	17.95	12.84	15.24	12.28	13.53	11.69	17.84	12.15	13.00
Fe2O3(tot)	13.08	13.36	13.17	13.07	15.55	13.45	14.04	14.80	12.14	12.97	11.98	10.40	10.50	17.07	16.40	15.46	12.67	15.92	18.96	14.17	8.47	8.80	12.45	11.57	8.68	8.72
MnO	0.15	0.18	0.15	0.12	0.07	0.13	0.05	0.32	0.13	0.40	0.13	0.24	0.16	0.11	0.18	0.20	0.02	0.16	0.35	0.17	0.09	0.03	0.13	0.03	0.21	0.13
MgO	5.03	5.01	5.15	5.71	6.23	6.23	5.13	5.09	4.83	4.52	4.55	3.88	4.59	6.70	5.40	5.05	1.46	3.93	6.59	4.36	2.36	2.28	3.44	3.48	4.92	4.26
CaO	4.02	6.22	5.09	5.04	0.58	3.54	0.34	0.70	2.63	1.20	0.33	14.30	4.74	3.28	4.49	5.82	0.25	3.31	6.84	2.48	0.43	0.37	1.97	0.39	8.54	2.98
Na2O	2.10	2.32	1.90	2.02	1.90	2.14	1.68	1.38	1.46	2.07	1.93	6.26	0.25	1.16	3.48	5.94	0.58	0.72	0.71	5.48	2.63	0.04	0.14	2.55	0.21	2.50
K2O	1.58	1.52	1.44	1.64	1.56	1.14	2.86	2.67	3.00	1.31	2.32	0.38	2.24	1.07	0.14	0.01	2.83	2.79	2.06	0.31	1.03	2.66	1.88	2.14	1.99	1.41
P2O5	0.25	0.27	0.24	0.26	0.30	0.28	0.27	0.27	0.23	0.22	0.20	0.30	0.32	0.35	0.26	0.28	0.31	0.31	0.25	0.30	0.17	0.29	0.29	0.27	0.14	0.15
La	29	31	37	28	46	41	41	39	35	26	30	14	22	24	26	22	49	36	28	27	24	40	57	30	22	25
Ce	56	61	60	62	86	72	85	83	73	59	64	36	57	56	55	52	104	75	59	59	60	84	126	60	43	48
Nd	30	32	31	32	48	41	43	40	35	30	30	24	26	29	27	27	51	38	30	29	28	46	61	32	21	23
Nb	22	24	25	24	36	35	28	27	25	25	21	12	29	31	33	26	38	27	29	30	24	33	37	24	10	12
Zr	211	219	223	229	274	267	258	245	227	236	200	177	244	280	271	219	304	251	236	254	286	333	379	219	125	163
Sr	88	102	92	92	91	112	37	38	80	80	46	474	77	95	159	237	153	210	317	139	59	16	53	56	120	148
Cr	188	187	207	362	876	1255	235	229	195	194	159	135	224	199	369	265	262	202	246	152	132	306	231	132	254	284
Ba	213	174	200	247	195	148	183	311	263	179	367	188	93	102	216	49	408	487	505	226	178	614	169	402	705	198
Sc	29	31	28	33	27	29	35	35	30	28	29	42	31	31	36	40	30	41	42	39	21	31	20	36	35	27
V	276	258	261	228	234	223	277	265	234	209	223	300	312	289	402	347	212	305	474	302	187	290	172	211	198	142
Y	40	42	41	36	50	46	44	48	40	43	39	38	33	36	45	38	47	46	43	41	36	40	49	45	32	32
Rb	71	56	53	64	59	45	110	110	126	57	91	9	100	40	7	1	109	107	105	14	39	110	79	86	115	126
Th	6	6	8	7	8	7	9	8	10	8	9	2	5	6	7	5	8	7	4	6	14	8	15	12	4	8
Ni	105	128	101	187	250	290	122	239	110	102	95	82	119	120	112	141	121	142	87	85	49	113	77	80	71	93
Pb	17	18	25	6	37	26	12	13	12	11	23	9	8	7	6	9	8	10	17	2	19	7	9	6	4	7
Ti/Zr	61.24	59.20	58.65	56.93	48.35	46.37	57.00	56.32	50.53	55.58	54.18	96.08	80.50	63.45	75.70	80.72	49.90	65.58	102.87	63.37	43.31	48.85	38.95	53.56	49.32	38.33
Ti/Y	323.06	308.67	319.00	362.15	264.95	269.14	334.22	287.49	286.73	305.04	277.83	447.52	595.21	493.47	455.90	465.21	322.76	357.86	564.60	392.59	344.06	406.68	301.24	260.65	192.67	195.24
Zr/Sc	7.28	7.07	7.96	6.94	10.15	9.21	7.37	7.00	7.57	8.43	6.90	4.21	7.87	9.03	7.53	5.48	10.13	6.12	5.62	6.51	13.62	10.74	18.95	6.08	3.57	6.04
Ti/Sc	445.60	418.20	467.10	395.07	490.65	426.92	420.16	394.27	382.31	468.45	373.64	404.90	633.61	573.07	569.88	441.95	505.66	401.51	578.04	412.72	589.82	524.75	738.04	325.82	176.16	231.39
Cr/Nb	8.55	7.79	8.28	15.08	24.33	35.86	8.39	8.48	7.80	7.76	7.57	11.25	7.72	6.42	11.18	10.19	6.89	7.48	8.48	5.07	5.50	9.27	6.24	5.50	25.40	23.67
Ni/Nb	4.77	5.33	4.04	7.79	6.94	8.29	4.36	8.85	4.40	4.08	4.52	6.83	4.10	3.87	3.39	5.42	3.18	5.26	3.00	2.83	2.04	3.42	2.08	3.33	7.10	7.75
La/Sc	1.00	1.00	1.32	0.85	1.70	1.41	1.17	1.11	1.17	0.93	1.03	0.33	0.71	0.77	0.72	0.55	1.63	0.88	0.67	0.69	1.14	1.29	2.85	0.83	0.63	0.93
Th/Sc	0.21	0.19	0.29	0.21	0.30	0.24	0.26	0.23	0.33	0.29	0.31	0.04	0.16	0.19	0.19	0.13	0.27	0.17	0.10	0.15	0.67	0.26	0.75	0.33	0.11	0.30
P/Zr	5.27	5.36	4.79	4.92	4.74	4.59	4.63	4.89	4.50	4.08	4.33	7.49	5.72	5.40	4.27	5.52	4.47	5.47	4.71	5.21	2.53	3.82	3.34	5.42	5.02	4.10
Ti/V	46.82	50.25	50.11	57.18	56.61	55.52	53.09	52.07	49.01	62.76	48.59	56.69	62.95	61.47	51.03	50.94	71.56	53.97	51.22	53.30	66.24	56.09	85.82	55.59	31.14	44.00
Ti/Th	2153.72	2160.72	1634.85	1862.47	1655.96	1768.66	1633.95	1724.94	1146.92	1639.58	1203.94	11337.17	3928.36	2960.84	2930.81	3535.58	1896.23	2351.68	6069.42	2682.71	884.73	2033.41	984.05	977.46	1541.40	780.94
Cr/Zr	0.89	0.85	0.93	1.58	3.20	4.70	0.91	0.93	0.86	0.82	0.80	0.76	0.92	0.71	1.36	1.21	0.86	0.80	1.04	0.60	0.46	0.92	0.61	0.60	2.03	1.74
Nb/La	0.76	0.77	0.68	0.86	0.78	0.85	0.68	0.69	0.71	0.96	0.70	0.86	1.32	1.29	1.27	1.18	0.78	0.75	1.04	1.11	1.00	0.83	0.65	0.80	0.45	0.48
P2O5/TiO2	0.12	0.12	0.11	0.12	0.13	0.14	0.11	0.12	0.12	0.10	0.11	0.11	0.10	0.12	0.08	0.09	0.12	0.11	0.06	0.11	0.08	0.11	0.12	0.14	0.14	0.15
Zr/Nb	9.59	9.13	8.92	9.54	7.61	7.63	9.21	9.07	9.08	9.44	9.52	14.75	8.41	9.03	8.21	8.42	8.00	9.30	8.14	8.47	11.92	10.09	10.24	9.13	12.50	13.58

FM = Fernfields member
BHM = Black Hill member
QRM = Que River member

* major elements presented as volatile-free percentages

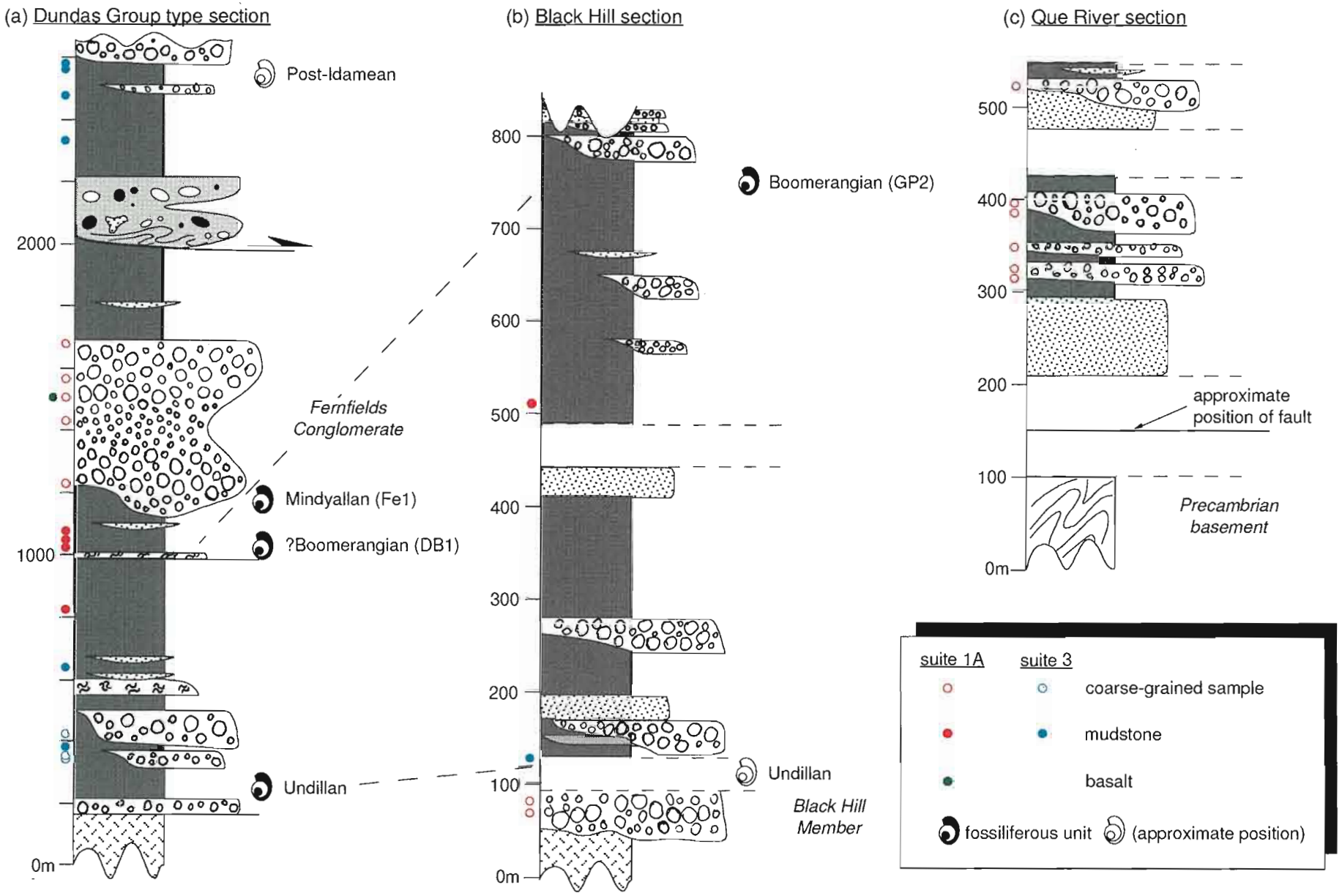

Figure 4.4. Stratigraphic positions of suites 1 and 3 samples from the western domain of the Dundas region and Que river region.

approximately 250m below the uppermost Boomerangian 'GP2' fauna of Jago (1979). The latter occurs 290m below the 'DB1' fauna, which was considered by Jago (*in* Brown, 1986) to be equivalent to the 'GP2' fauna. The remaining samples (817, 320 and 324) come from a 45m thick interval in the Dundas Group type section which directly overlies the 'DB1' fauna (Fig. 4.4a). The stratigraphically highest of these occurs 150m below the base of the Fernfields Conglomerate.

Coarse-grained samples from the Que River region were collected from the lower portions of 1100m thick turbidite-dominated package which comprises lithic-rich sandstone, conglomerate and mudstone (referred to herein as the Que River member) (Fig. 4.4c). The package represents the western-most exposure of Middle and Late Cambrian strata in the northern region and its base is faulted against an inlier of highly deformed mudstones and mature quartzose sandstone which Brown (1986) correlated with Precambrian Oonah Formation. Although no fossils have been discovered from the Que River region, Corbett and McNeill (1986) showed the package as being structurally continuous southward towards the Higgins Creek area, where a lithologically similar succession has been reported to contain Post-Idamean faunal assemblages (Jell et al., 1991). Further mapping is required to clarify the stratigraphic relationship between the units in these two areas, but on the basis of the presently available data those exposed in the Que River section are tentatively placed within the Upper Cambrian. If this age limit is valid, possible chrono-stratigraphic equivalents of the Que River member in the Dundas region would involve the upper portions of the Dundas Group (including the Fernfields Conglomerate: Fig. 4.4).

4.5.1.1 Sandstone petrography

The framework component of suite 1A sandstones is characterised by high abundances of lithic fragments and correspondingly low abundances of monocrystalline grains. Matrix contents are generally low, with clearly defined individual lithic fragments in grain contact. Quartz and feldspar are present in roughly similar amounts, and comprise less than 17% of the rock volume. Quartz occurs most commonly as angular to subrounded monocrystalline grains with mild to intense undulose extinction. Conspicuous in thin section, but forming only a minor proportion of the framework (<1%) are quartz grains with straight extinction and crude hexagonal habits with sharp, planar or embayed margins (Fig. 4.5a). These are interpreted as volcanic in origin.

The heavy mineral fraction is dominated by opaque Fe-Ti oxides (commonly in the form of leucoxene and limonite), with accessory abundances of zircon and tourmaline. Deep red Cr-spinels were recognised as traces in the Black Hill member and are locally abundant in Que River samples. In some cases, they were found as phenocrystal phases in mafic igneous rock fragments. Cr-spinels were not identified in thin sections prepared from slabbed specimens of the Fernfields Conglomerate, but were

Figure 4.5. Photomicrographs showing detritus in coarse-grained suite 1A and suite 1B samples.

(**a**) Volcanic quartz grain with prismatic bi-pyramidal habit. Note the lack of evidence for abrasion during transport (sharp, unrounded corners) and the low degree of intracrystalline strain as indicated by straight extinction. (crossed polars: sample 924)

Detritus derived from the Crimson Creek Formation

(**b**) Well-rounded clast of feldspathic greywacke with thin remnant of a mudstone interbed at base (centre of field of view). The framework component of this clast consists mainly of texturally immature broken feldspar grains. Note the textural and compositional immaturity of the sample. (plane polarised light: sample 920)

(**c**) Aphyric basalt clast with localised crude ?flow alignment of feldspar crystals. (plane polarised light: sample 926)

Detritus derived from mature PMS or basement sequences

(**d**) Margin of well-rounded clast consisting of texturally and compositionally mature quartz sandstone. (crossed polars: sample 358)

(**e**) Well preserved oolitic texture in a clast now entirely replaced by chlorite and silica. (plane polarised light: sample 924)

MUC-derived basalt

(**f**) Aphyric quench-textured basalt clast with well-developed "bow-tie" spherulitic textures. (crossed polars: sample 926)

(**g**) Fragment of serpentinised pyroxenite contained within a conglomerate unit from the Que River member (crossed polars: sample 920)

Suite 1B

(**h**) Basaltic volcanogenic sandstone of suite 1B. The framework consists of altered lathwork basaltic grains, feldspar, abundant Fe-Ti oxides and plutonic quartz grains. The texture and composition of these sandstones are similar to the rounded greywacke clasts contained in suite 1A conglomerates (**b**). (plane polarised light: sample 192)

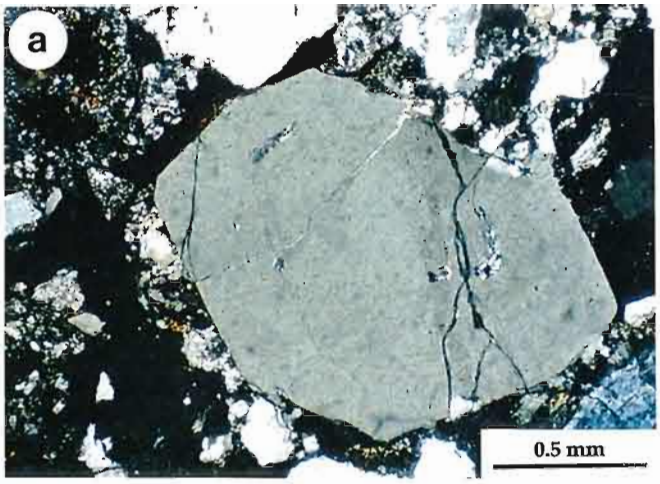
a
0.5 mm

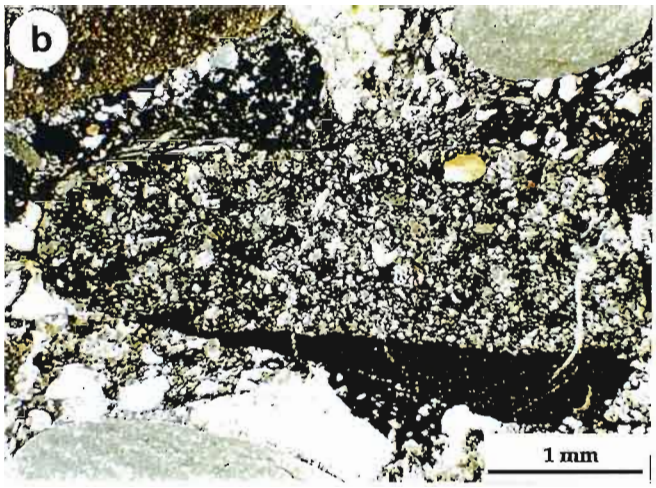
b
1 mm

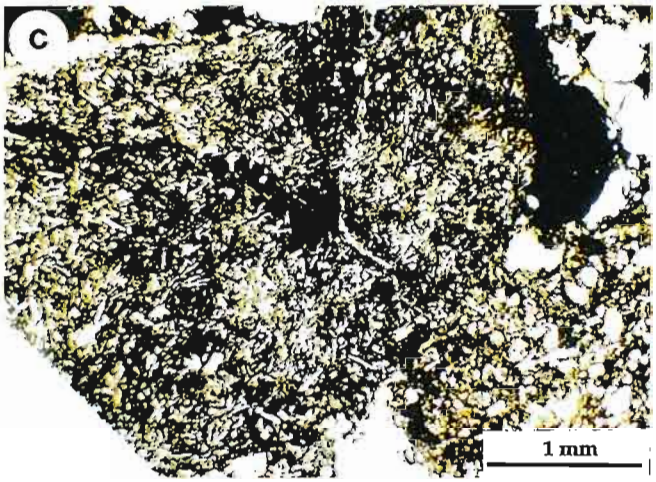
c
1 mm

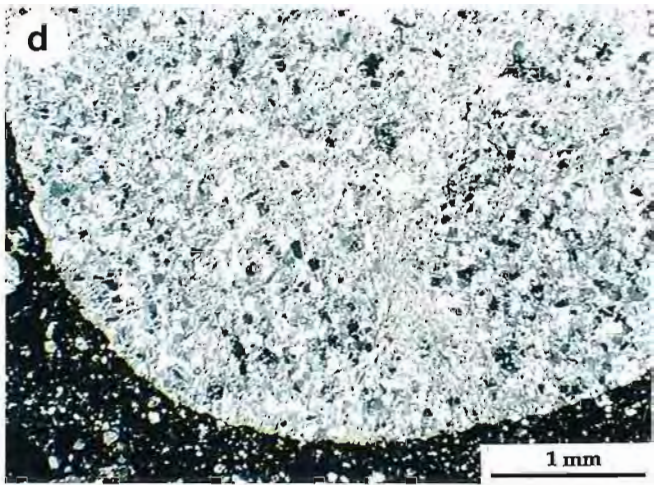
d
1 mm

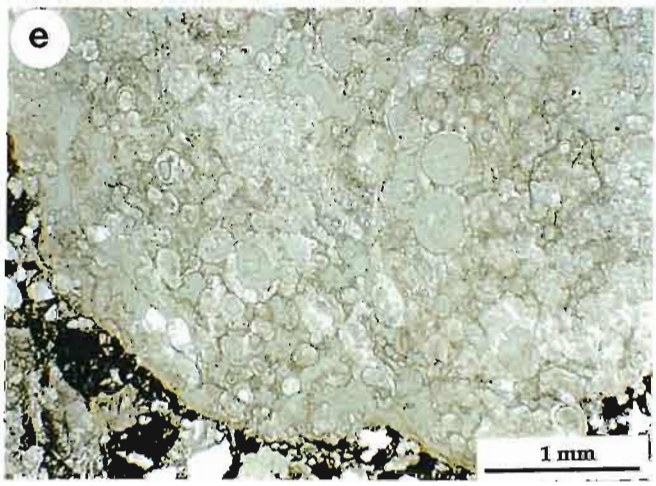
e
1 mm

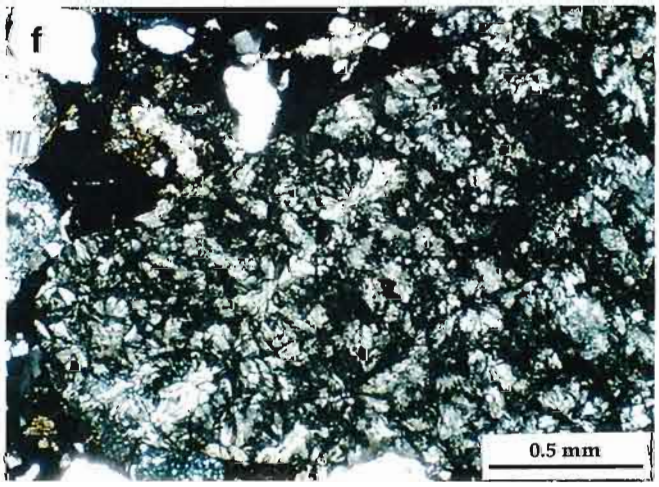
f
0.5 mm

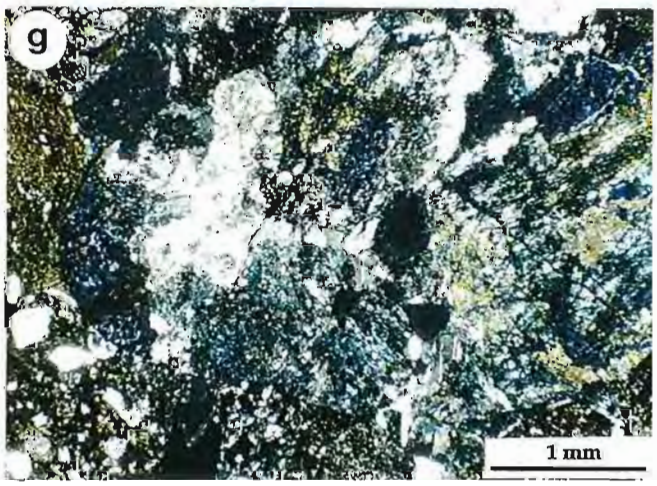
g
1 mm

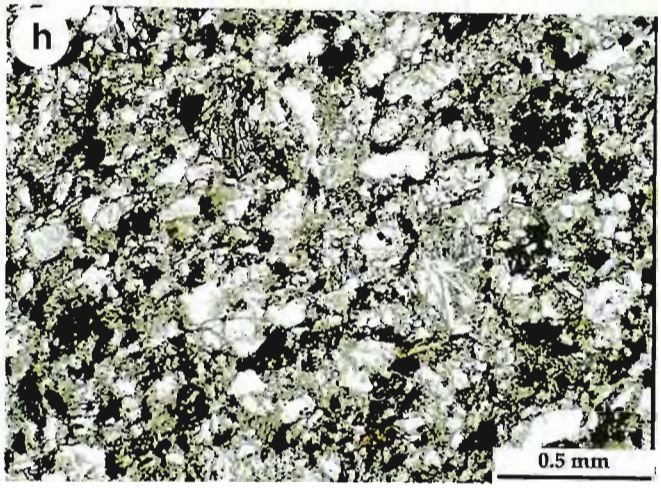
h
0.5 mm

found in heavy mineral concentrates. Other accessory mineral phases include calcite, muscovite and epidote. No fresh ferromagnesian grains were recognised, however chloritised grains are common.

Lithic fragments involve a diversity of rock-types and compositions. In general they are well-rounded. Igneous clast-types are proportionally subordinate to clasts of sedimentary origin, with each variety comprising between 5-20% and 64-88% of the lithic fraction respectively. Comparison of clast assemblages to potential source lithologies shows that coarse-grained detritus was derived principally from the passive margin sequence (PMS) and basement terrains, with dominant contribution from the Crimson Creek Formation. Additional input from compositionally and texturally mature sequences (eg. Oonah Formation and/or Success Creek Group) is manifested in all samples and minor input from the MUC was recognised in the Black Hill and Que River members. Clast types representative of each source terrain are described below.

Clasts derived from Crimson Creek Formation

Greywacke clasts interpreted to have been sourced from the Crimson Creek Formation form between 50% and 72% of sedimentary clast-types. They range from feldspar- to quartz-dominated. The more feldspathic end members consist almost entirely of mafic to intermediate volcanic detritus and are characterised by angular crystals of plagioclase, basalt fragments, chloritised fragments of uncertain origin and opaques, set within a groundmass of broken feldspar microphenocrysts (Fig. 4.5b). Basaltic fragments are angular to subrounded. They are characteristically aphyric, with acicular to tabular plagioclase microlites forming pilotaxitic, trachytic or random arrangements. They contain abundant matrix which occurs as fine opaque Fe-oxide, chlorite, carbonate and less commonly sericite. Much of the matrix may be altered labile rock fragments or grains, and may in part explain the apparent lack of ferromagnesian grains within these clasts. Greywacke clasts with higher quartz contents contain more chert fragments, detrital white mica, pink calcite and non-opaque heavy minerals (eg. tourmaline and zircon). None of the quartz grains contained within these fragments show features indicative of a volcanic origin (ie. prismatic form or embayed crystal faces). The transition from feldspathic greywackes to quartz-rich compositions is interpreted to reflect a change from a dominantly volcanic provenance to a mixed or sedimentary provenance. The angular form of crystal fragments and the predominance of basaltic detrital components in these greywacke clasts is considered to indicate they were derived from a sedimentary precursor rich in first-cycle volcanogenic detritus.

Igneous rock fragments are mafic in their composition and have textures typical of basaltic lava. Most basaltic fragments are aphanitic, with microphenocrysts of feldspar and relict pyroxene set in a very fine-grained, near opaque groundmass which is now composed of chlorite, feldspar, quartz and Fe-oxides (Fig. 4.5c). In some instances, a

texture approaching that of trachyte is preserved in which feldspar microphenocrysts show a relict flow alignment. These clast types are texturally akin to the small volcanic fragments contained in feldspathic greywacke clasts.

Coarser grained basaltic clasts have an interlocking arrangement of feldspar crystals which are up to 2 mm in length. No pristine ferromagnesian grains were observed in these clasts, however subhedral crystals, now pseudomorphed by chlorite or actinolite and sub-ophitically enclosing feldspar laths are likely to represent original ferromagnesians. Fe-Ti oxides are ubiquitous. They are commonly replaced by skeletal leucoxene. Primary volcanic textures are obscured in many fragments by intense chlorite, carbonate and silica alteration.

That coarse grained basaltic detritus appears absent from the greywacke clasts may be due to mechanical instability of these fragments compared to finer, more glassy fragments. The coarser-grained material may breakdown to release phenocrysts. Finer grained fragments may on the other hand disintegrate along microfractures formed during rapid cooling, and thus preserve clast-shapes (eg. Macaire et al., 1994).

Clasts derived from mature PMS or basement sequences

Compositionally mature sandstone fragments are rare in comparison to the greywackes, and comprise less than 3% of the sedimentary clast fraction in each area, with the exception of the Black Hill member where it approaches 25%. The sandstone clasts are lithic-poor (cryptocrystalline chert grains are present in some clasts) and their detrital fraction is dominated by moderately sorted, sub-angular to rounded and mildly strained quartz (Fig 4.5d). In most clasts, detrital quartz grains are isolated and set in a fine-grained recrystallised groundmass of quartz and sericite. Rare, matrix-poor varieties have been observed, in which quartz grains are bound by a silica cement and have sutured margins. Rounded detrital cores were identified in only a few grains. Accessory minerals include muscovite (which is particularly abundant in finer-grained clasts), zircon, rutile and blue to green tourmaline. A pre-existing tectonic fabric defined by the preferred alignment of muscovite flakes was observed in a few clasts and highly strained fragments such as quartz-mica schist or ribbon quartz are very rare.

Chert, dolomite and dolomitic mudstone clasts occur as minor constituents in most sandstones (< 5% of the framework) but form a conspicuous component (17-20%) in higher stratigraphic levels of the Que River section (ie. samples 924 and 926). Chert clasts usually consist entirely of massive cryptocrystalline quartz however clasts containing relict lamination and crudely granular (with ?dolomite pseudomorphs) to well-developed oolitic textures (Fig. 4.5e) are also present. Lithologies are comparable to dolomitic horizons contained in the Success Creek Group (cf. Patterson, 1979; Newnham, 1975).

MUC-derived clast assemblage

Quench-textured fragments interpreted to have been derived from the MUC are particularly common in Que River Member sandstones. They consist of felty masses of fine feldspar laths (partially altered to chlorite), which characteristically form radiating bow-tie or fan-shaped spherulites (Fig. 4.5f). Some of these also appear vesicular, with zoned amygdales of very fine radiating quartz and chlorite. Rare serpentinised pyroxenite fragments from the Que River Member (Fig. 4.5g) represent the only igneous clasts of plutonic origin detected.

4.5.1.2 Chemical composition and source characteristics

Shown in Figure 4.6 are average post-Archaean shale (PAAS: Taylor and McLennan, 1985) normalised multi-element patterns for suite 1A siliciclastics. The patterns for all samples, regardless of grainsize, are grossly similar with enrichment of P, Ti, Sc, V, Ni and Cr relative to PAAS reflecting the significant input of basaltic material. Considering the diversity of clast-types shown by coarse-grained samples and the well-documented effects of grain size on element abundances in sediments (eg. McLennan et al., 1990) this consistency in chemical composition is rather surprising. Several factors are likely to have contributed to this feature. Firstly, the framework of coarse-grained samples is mineralogically immature, with the large lithic fraction involving a significant contribution from sedimentary precursors (in particular greywacke and mudstone). Not only is the dilution effect from quartz minimal, but also high trace elements abundances contained in clay-rich sediments in the source region(s) are likely to have been faithfully transferred into lithic-rich daughter sediments. With the exception perhaps of samples from the Que River member, concentration of heavy minerals into the coarse-grained fraction either in the source region or during sediment transport also appears to have had little effect on absolute element abundances, with Zr, Y, LREE (partitioned in zircon) and Ti and Nb (partitioned in Fe-Ti oxides) showing similar concentrations in both mudstones and sandstones. This suggests that either concentration of trace elements in heavy mineral phases is matched by absorption of elements onto clay minerals in mudstones, or fine heavy mineral grains have been incorporated in the mudstones. Cr is an exception, with anomalously high values shown by the Black Hill Member (958) and samples from the Que River section (917, 919). Elevated Cr values in these units are consistent with the identification of detrital Cr-spinels in thin section and are interpreted to record input from an MUC source. The effects of grain size on the chemical composition of suite 1A siliciclastics are therefore considered to be insignificant in terms of most trace element abundances. Similarly, the polymict character of the clast assemblages contained in coarse-grained samples, which would intuitively result in some variation in bulk

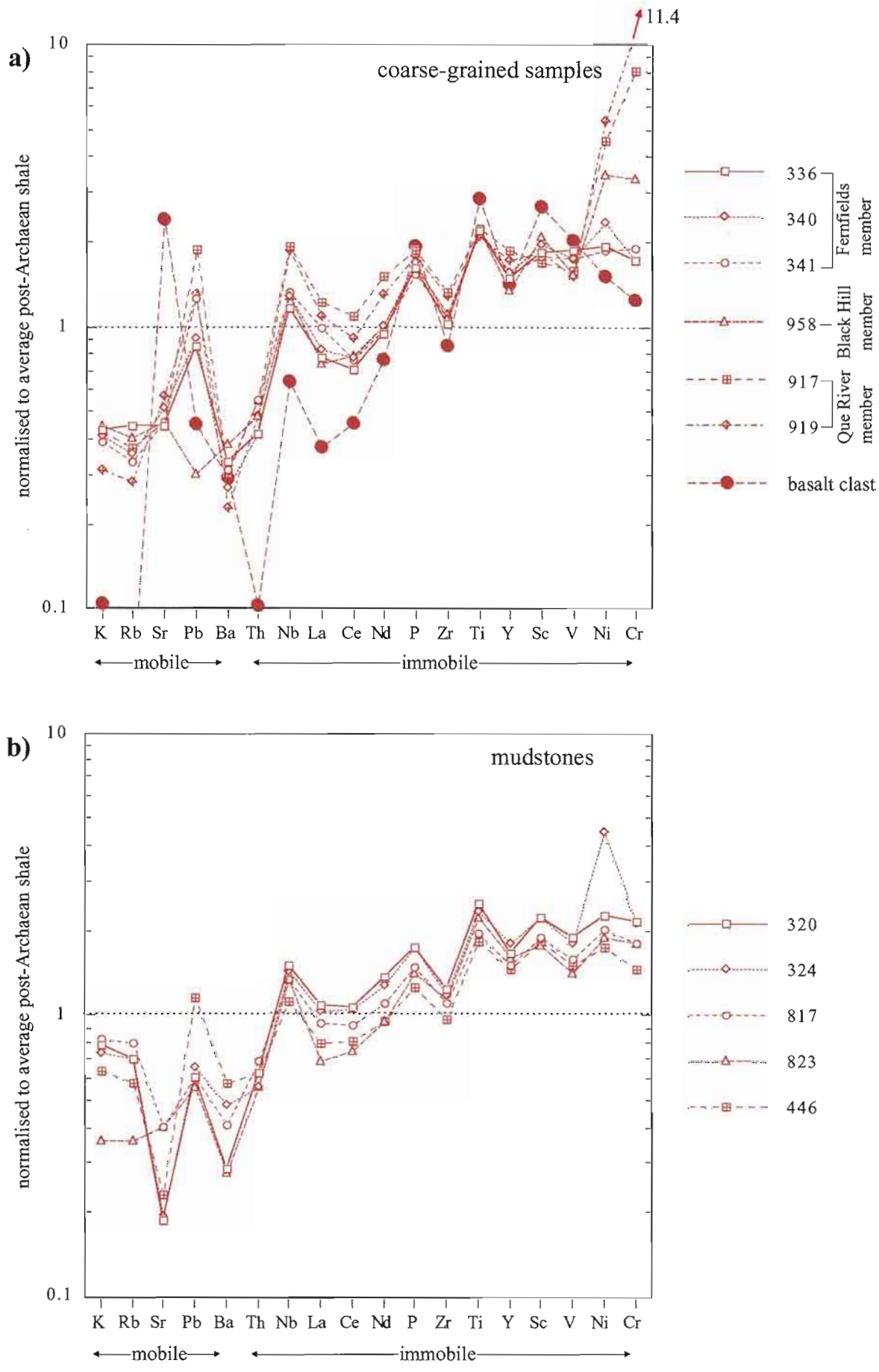

Figure 4.6. Average post-Archaean shale normalised extended trace element and LREE plot for suite 1A sandstones and mudstones. The multi-element pattern of a basalt clast sampled from a suite 1A conglomerate (340) is also shown in (**a**).

composition, does not appear to affect chemistries to any significant degree. Although this may be partly explained by grossly similar proportions of the various clast-types in each unit, it is probably best explained by comparable compositions of the detrital components. In other words, although the principal source for coarse-grained sediments was lithologically heterogeneous (ie. comprising a variety of both sedimentary and volcanic rock-types), it was chemically homogenous. Gross chemical homogeneity would be expected in a succession involving genetically and temporally related volcanogenic sediments and magmatic rocks (cf. Hiscott and Gill, 1992; Skilbeck and Cawood, 1994).

In order to test this hypothesis, the whole rock chemistry of a cobble-sized basalt clast (sample 339) from a sandstone-conglomerate unit in the Fernfields Conglomerate was analysed. A comparison of the chemical signatures of the basalt clast and its host sediment (340) is shown in Figure 4.6a. Although the absolute values for some element abundances vary between the basalt clast and its host sediment (in particular, Th, Nb and LREE), the overall pattern is very similar for both samples. Moreover, despite these variations in element concentration, element ratios such as Nb/La, P_2O_5/TiO_2 and Ti/V are remarkably similar (Table 4.2). These relationships are very significant considering that igneous fragments average less than 10% of the framework component of Fernfields Conglomerate, whereas sedimentary lithics comprise almost 70%. The marked increase in absolute abundances of Nb, LREE and perhaps Th in the sandstone relative to the basalt clast can be explained by concentration of these elements in clay minerals. Contamination of the basaltic signature from a more felsic source however, must also be considered as an explanation for the increased abundances of these elements in view of the presence of siliciclastic lithic fragments and detrital quartz grains.

4.5.2 Suite 1B

Samples were classified as suite 1B if they were located in the eastern area of the Dundas region (Fig. 4.1) and contained particularly high abundances of TiO_2 (3.0-3.4 wt% in sandstones; 2.5-4.1 wt% in mudstones: Table 4.2). Intercorrelations of very high TiO_2, Nb, P_2O_5, V and low Th in all samples regardless of grainsize, indicates a significant input of basaltic detritus and only very slight dilution from 'felsic' source material. Correspondingly high Ti/Th values (2930-3930 in sandstones; 1900-6070 in mudstones) effectively distinguish suite 1B from other suite 1 samples located in the eastern area (ie. suite 1C samples 218 and 216: Table 4.1: Fig. 4.3).

Samples (four sandstones and four mudstones) were collected from a number of fault bounded, turbidite-dominated packages comprising basaltic greywacke and purple mudstone with minor calcareous siltstone (Fig. 4.1). Although suite 1B samples can be correlated on the basis of their chemical similarity and geographic distribution, their stratigraphic position, both relative to one another and to neighbouring units is difficult to

constrain. This problem is inherent throughout the eastern area of the Dundas region and occurs as a result of intense faulting and folding coupled with a lack of good, continuous exposure or biostratigraphic constraints (cf. Corbett, 1984a; Corbett and Lees, 1987).

4.5.2.1 Sandstone petrography

As with suite 1A coarse-grained samples, those included within suite 1B are quartz-poor and compositionally immature. They are distinguished from suite 1A by a paucity of sedimentary lithic fragments and a lower degree of textural maturity (ie. poor sorting coupled with lack of abrasion or rounding of much of the framework component). A fine-grained matrix, probably consisting of both fine-grained detritus and recrystallised labile constituents (eg. feldspar, ferromagnesian grains and glassy lithic fragments), comprises a significant volume of these sandstones (≈30% in 192S and 868). It is largely textureless, comprising chlorite, calcite and Fe-oxides.

Intense recrystallisation of the framework component has prevented a thorough quantitative analysis of detrital constituents in suite 1B sandstones. Approximately 200 grains were counted in samples 192S and 868, wherein less than 67% of the framework was resolvable, however in 196 and 211, quartz and resistant heavy mineral grains are commonly the only identifiable detrital minerals. Of the resolvable framework component, the main constituents are volcanic rock fragments, feldspar, quartz and opaque heavy minerals. Monocrystalline grains are dominantly plagioclase, which are angular, commonly fragmented and at least partially replaced by calcite ± chlorite ± quartz. Plagioclase accounts for 19% of the framework, however assuming that a large proportion of the recrystallised monocrystalline grains were originally feldspar, this percentage is probably an under-estimate. Quartz grains form less than 19% and have angular habits and straight to mildly undulose extinction. No grains of definite volcanic origin were observed and most are interpreted to have been reworked from pre-existing sandstones. The heavy mineral fraction is dominated by opaque grains (Fe-Ti oxides and minor Cr-spinel), with subordinate rounded zircons and blue to green tourmalines. No ferromagnesian grains were recognised and if originally present, are now likely to form part of the recrystallised matrix.

Of the lithic component whose original composition and texture is not entirely obscured by alteration, the most common lithotype is basalt (31-36% of the framework). These basaltic fragments exhibit pilotaxitic, trachytic and vitric textures and contain microlitic plagioclase, chloritised crystals (probably pseudomorphs after ferromagnesian crystals) and Fe-Ti oxides. Although less well-rounded and generally small in diameter (< 1.5 mm), in terms of their primary volcanic textures and composition, they closely resemble finer-grained Crimson Creek Formation-derived basalt clasts contained within suite 1A sandstones (Fig. 4.5h). A minor proportion of the resolvable lithic fraction are 'cherty' fragments of probable volcanic origin and argillite. The 'cherty' clasts are

generally aphyric and consist predominantly of very fine-grained secondary quartz and feldspar. Many have a 'dirty' appearance in plane polarised light due to disseminated calcite. They may represent devitrified or silicified formerly glassy material, the original composition of which is indeterminable.

The large component of chemically unstable volcanogenic debris contained in these sandstones suggests that the source was mineralogically immature and essentially unaffected by weathering and/or diagenesis prior to reworking. This feature, coupled with the abundance of texturally immature, monogenetic basaltic detritus (broken feldspar grains and basalt clasts), none of which is contained within reworked sedimentary clasts (cf. suite 1A) is interpreted to indicate a first-cycle origin for the volcanic component. That is, volcanogenic debris was either eroded directly from an older, uplifted volcanic massif, with negligible contamination from sedimentary sources, or derived from a genetically and temporally related phase of basaltic magmatism.

4.5.2.2 Chemical composition and source characteristics

The overall shape of PAAS-normalised multi-element variation patterns (Fig. 4.7) is similar to corresponding lithotypes of suite 1A. Absolute abundances of some elements differ between the two suites however, especially in the sandstones. In particular, Ti, V, Sc and Nb are noticeably enriched in suite 1B sandstones, whereas LREE concentrations are consistently low. Are these relationships merely a result of sedimentary fractionation processes, or do they reflect subtle differences in source characteristics? In order to evaluate the effects of sedimentary fractionation on the composition of these sediments, in particular those of hydraulic sorting (ie. fractionation of detritus of differing densities), both the lower sand-rich and upper mud-rich divisions of a single turbiditic sedimentation unit were analysed: samples 192S and 192M represent Bouma Ta and Td-e divisions respectively. McLennan et al., (1990) argued that sediments of different grain size deposited from a single turbiditic pulse are useful for examining the effects of sedimentary sorting on chemical composition. The rationale behind this argument stems from the fact that detritus suspended in turbidity currents are derived from a point source and that contamination of this source material by exotic material entrained during flow is negligible. Thus any chemical variation throughout a turbiditic sedimentation unit is likely to have resulted from sedimentary fractionation processes during transport. Figure 4.8a shows major and trace element abundances of both 192S and average suite 1A sandstone normalised to 192M. Differences in element abundances between 192M and 192S are generally very subtle, with the spiky pattern shown by elements positioned towards the left of the diagram reflecting fundamental mineralogical differences between the two lithologies. Concentration of clay minerals (now sericite) in the mudstone is indicated by relative enrichment of K and Rb, whereas the small peaks at Mg and Ca in the sandstone are interpreted to correspond to mechanical

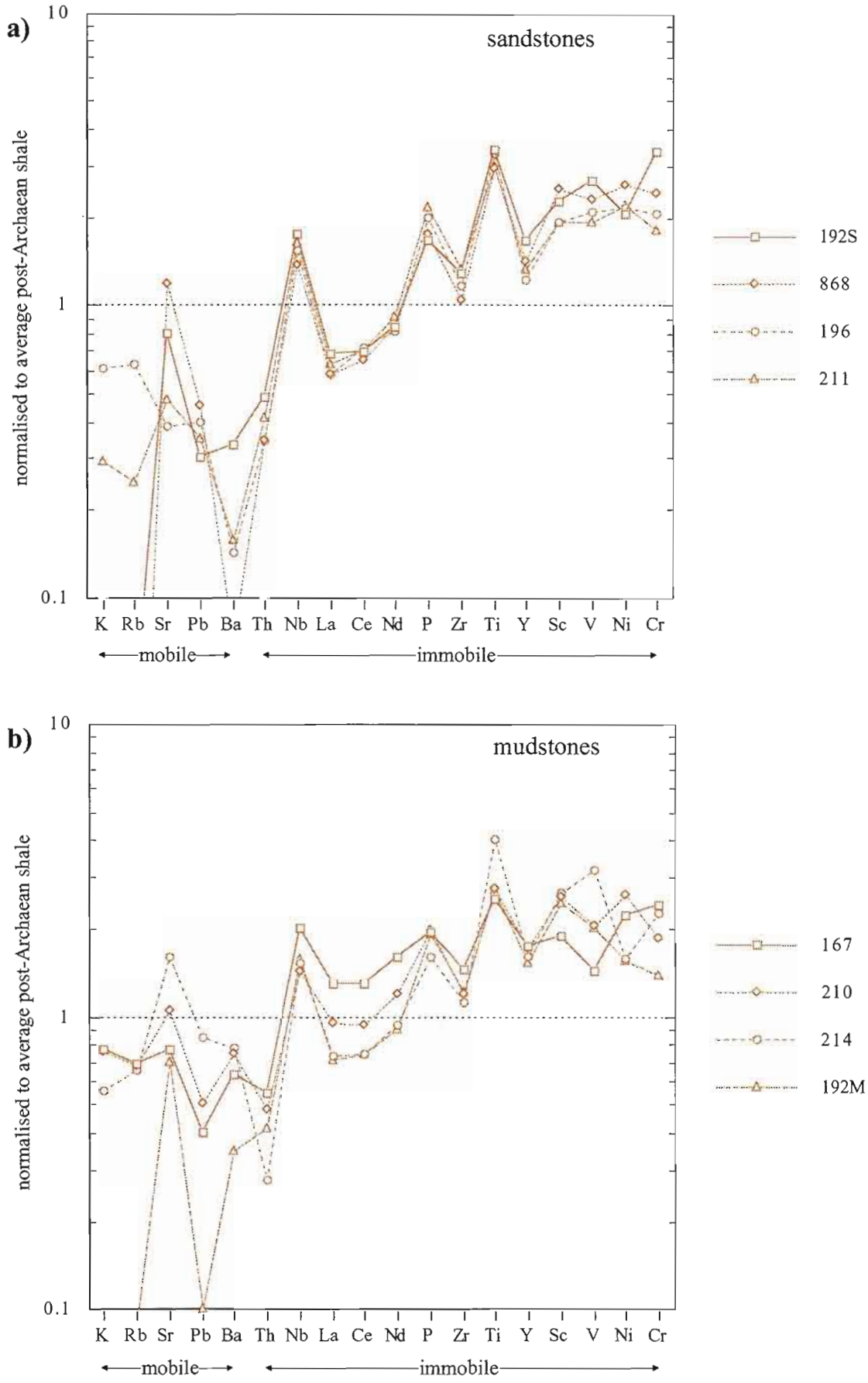

Figure 4.7. Average post-Archaean shale normalised extended trace element and LREE plot of suite 1B sandstones and mudstones.

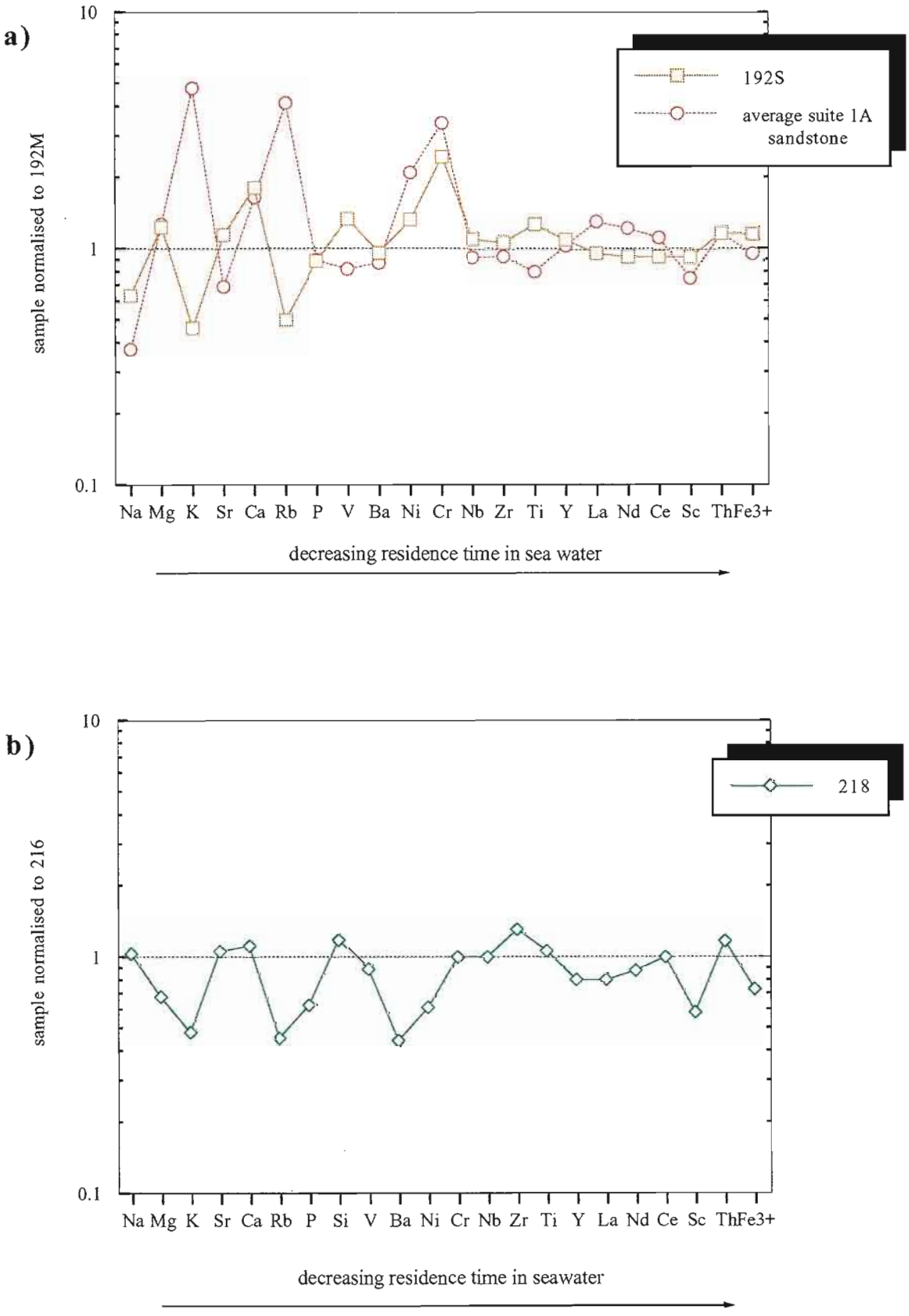

Figure 4.8. Multi-element plots of mudstone-normalised sandstone / mudstone couples. (**a**) Suite 1B sandstone (192S) and average suite 1A sandstone normalised to suite 1B mudstone (192M). Patterns are relatively flat, with notable exceptions including Cr, Ni and V enrichment in sandstone, possibly resulting from heavy mineral concentration. (**b**) Suite 1C sandstone-mudstone couple, with marked 'depletion' of Sc, Ni and alkaline earth elements in the sandstone.

concentration of dense ferromagnesian minerals, plagioclase and basaltic rock fragments (presently at least partially altered to chlorite and/or calcite). The relatively flat pattern towards the right of the diagram suggests that separation of these mineral phases has had little effect on the absolute abundances of less mobile elements. Sample 192S has slight relative enrichment in some elements however, including Cr, Ti, V, Ni and Th. The concentration of Th is so low in both 192S and 192M (7 and 6 ppm respectively) that any variation falls well within the limits of analytical error. Enrichment of ferromagnesian elements in 192S may be controlled in part by concentration of basaltic rock fragments of ferromagnesian minerals however partitioning of heavy mineral phases (in particular spinels) within the sandstone is probably the main contributing factor to these peaks: ie. Cr in chromium-spinel and Ti, V and possibly Ni in magnetite.

The significant enrichment of K and Rb in suite 1A sandstones relative to 192S in part reflects the large component of sedimentary lithic fragments in the former. Markedly lower Na_2O/K_2O ratios of both 192S and 192M relative to suite 1A sandstones however indicates that the clay mineralogy is different to that of suite 1B. It is reasonable to assume that contribution from either a more weathered source or additional input from a mineralogically mature source could account for these differences. Lower abundances of Nb, Sc in suite 1A sandstones relative to those of suite 1B cannot be attributed to heavy mineral fractionation in the latter. They are therefore interpreted to reflect a felsic or siliciclastic contamination of the dominant basaltic signature in suite 1A sandstones. The significant enrichment of K and Rb in these sandstones, coupled with low values of Na_2O/K_2O is interpreted to indicate a more mature source for suite 1A.

Mudstone chemistries are more diverse than those of the sandstones, with significant fluctuations of LREE and ferromagnesian elements. Sample 167 in particular, shows depletion of Ti, but relative increases in SiO_2, Nb, Th, LREE, Zr and LILE (see also Table 4.2). Mixing from a non-volcanic source appears most probable in this case. It shows a LREE enrichment of a factor of 3.5 compared to that of the basalt clasts extracted from the Fernfields Member.

4.5.3 Suite 1C

Suite 1C sandstones (218, 890 and 386) are classified on the basis of provenance characteristics rather than geographic distribution. Relative to other suite 1 samples, they show a smaller component of basaltic detritus and a higher degree of mineralogical maturity. These features are best demonstrated by their chemical composition. They are defined principally on the basis of high SiO_2 content (65-71 wt% compared to 50-60 wt% for other suite 1 sandstones), however high concentration of Zr relative to most ferromagnesian elements and Nb is also diagnostic: Zr/Sc and Zr/Nb are higher than, or within the upper limits of the ranges shown by other suite 1 sandstones, whereas Cr/Zr and Ti/Zr values are towards the lower range limits (Fig. 4.3: Table 4.2).

One silty mudstone sample (216) is included within suite 1C. It was collected from a bed immediately adjacent to a suite 1C sandstone (218) and its classification is based simply on a spatial relationship with the latter. The mudstone does not share the chemical characteristics of suite 1C sandstones however, with SiO_2 content (60 wt%) occurring within the ranges of other suite 1 mudstones (47-64 wt%) and is Zr is not noticeably enriched relative to other trace elements. Its slightly higher concentration of Th (and correspondingly low Ti/Th and high Th/Sc) is the only chemical feature which allows discrimination from other suite 1 mudstones (Fig. 4.3) and is considered to reflect a greater component of 'felsic' detritus.

Suite 1C samples are located within the central and eastern areas of the Dundas region (Fig. 4.1). Units from which samples were collected are unfossiliferous, fault bounded and their stratigraphic positions are poorly constrained. Samples 386 and 890, located in Barker Creek (800m SW of Carbine Hill) and the Ring River respectively (Fig. 4.1), have a close spatial relationship with latest Middle Cambrian or early Late Cambrian suite 3 strata. Although the relative stratigraphic positions of these units are obscured by folding and faulting, a tentative latest Middle Cambrian to early Late Cambrian age is inferred for samples 386 and 890.

Suite 1C sandstone units have massive and disorganised to chaotic internal structures and were probably deposited from sandy debris flows or slumps. The potential exists therefore that sandstone units were intrabasinally derived.

4.5.3.1 Sandstone Petrography

Samples included in this petrographic study (890 and 386) are poorly sorted, fine- to medium-grained, lithic-poor quartzo-feldspathic greywackes. As with suite 1B, intense recrystallisation of suite 1C sandstones and the resultant high proportion of unresolvable grains hampers accurate determination of detrital modes. Matrix forms 39% and 46% of the whole rock in 890 and 386 respectively and consists mainly of chlorite, with minor epidote, calcite and white mica. Although it may include some original fine-grained detritus, the bulk of the matrix probably consists of either relatively soft grain types which have merged during compaction or recrystallised labile constituents. Quartz is the dominant resolvable monomineralic grain and comprises between 32% and 57% of the framework. Individual grains are angular to rounded and undulose extinction is ubiquitous. Round detrital cores with silica overgrowths were observed in a few instances, indicating that some grains at least, were reworked from pre-existing, silicified sandstones. Vein-quartz fragments comprise a minor proportion of the quartz population.

Feldspar grains have a 'dirty' appearance and show extensive alteration to sericite and less commonly chlorite or carbonate. Relict multiple twinning was observed rarely. In many instances, recrystallisation is so intense, that grains are only identifiable by their euhedral, tabular forms. Where rounding of grains has occurred, it is almost impossible

to distinguish them from fine-grained sericitic lithic fragments. Dirty polycrystalline aggregates of quartz with tabular habits are also considered to be altered feldspar grains.

Accessory grains include coarse-grained muscovite, abundant Fe-Ti oxides, goethite, rounded zircon, tourmaline, rutile and rare biotite. Rare epidote and chlorite grains were also observed, however these are considered to have replaced labile mafic phases.

The resolvable lithic component is small in comparison to other suite 1 sandstones (0-17%) and consists of siliciclastic, 'chert' and volcanic rock fragments. Siliciclastic rock fragments include greywacke, mudstone and quartzose sandstone. 'Chert' clasts consist of textureless, cryptocrystalline quartz, commonly with fine intergrowths of sericite. Their origin is uncertain and may include formerly glassy material, silicified mudstone or a primary chert deposit. Both mafic and felsic volcanic rock fragments were observed, the former showing microlitic textures similar to the Crimson Creek Formation-derived basaltic clasts found in other suite 1 rocks. Felsic volcanic fragments contain sparse microphenocrysts of quartz and/or feldspar set in a groundmass which is extensively altered to fine-grained silica.

4.5.3.2 Chemical composition and source characteristics

In addition to their characteristically high concentrations of SiO_2, suite 1C sandstones show variable degrees of 'depletion' of ferromagnesian elements (Mg, Fe, Sc, V, Ni and Cr) and 'enrichment' of incompatible elements (Th, LREE and Zr) relative to other suite 1 sandstones (Fig. 4.9: Table 4.2). CaO, Sr and Na_2O are also 'depleted' in most samples with corresponding increases of both K_2O and Rb reflecting breakdown of feldspar to clay. Sample 218 is an exception and shows a relatively high Na_2O content suggesting that a significant proportion of feldspar is present in the form of albite. In contrast, the mudstone sample (216) is largely indistinguishable in terms of its chemistry from other suite 1 mudstones (the slightly higher Th value providing the only means of chemical discrimination).

In order to constrain the provenance of suite 1C siliciclastics, it is important to establish whether the departure of their geochemical signatures from other suite 1 rocks is principally a function of source mixing (ie. dilution of the suite 1 'basaltic' component) or sedimentological processes such as source area weathering, sedimentary recycling or depositional processes (eg. hydraulic sorting). In an attempt to distinguish between these effects on sediment chemistry, element abundances were compared between the coarse- and fine-grained components of a sandstone-mudstone couple (Fig. 4.8b). Unlike the sandstone-mudstone couple analysed from suite 1B however (see section 4.5.2.2), it is unclear as to whether both lithotypes were derived from a single depositional pulse as sandstones are generally massive and exhibit sharp contacts with neighbouring mudstone horizons. Thus the possibility exists that the mudstone records the composition of

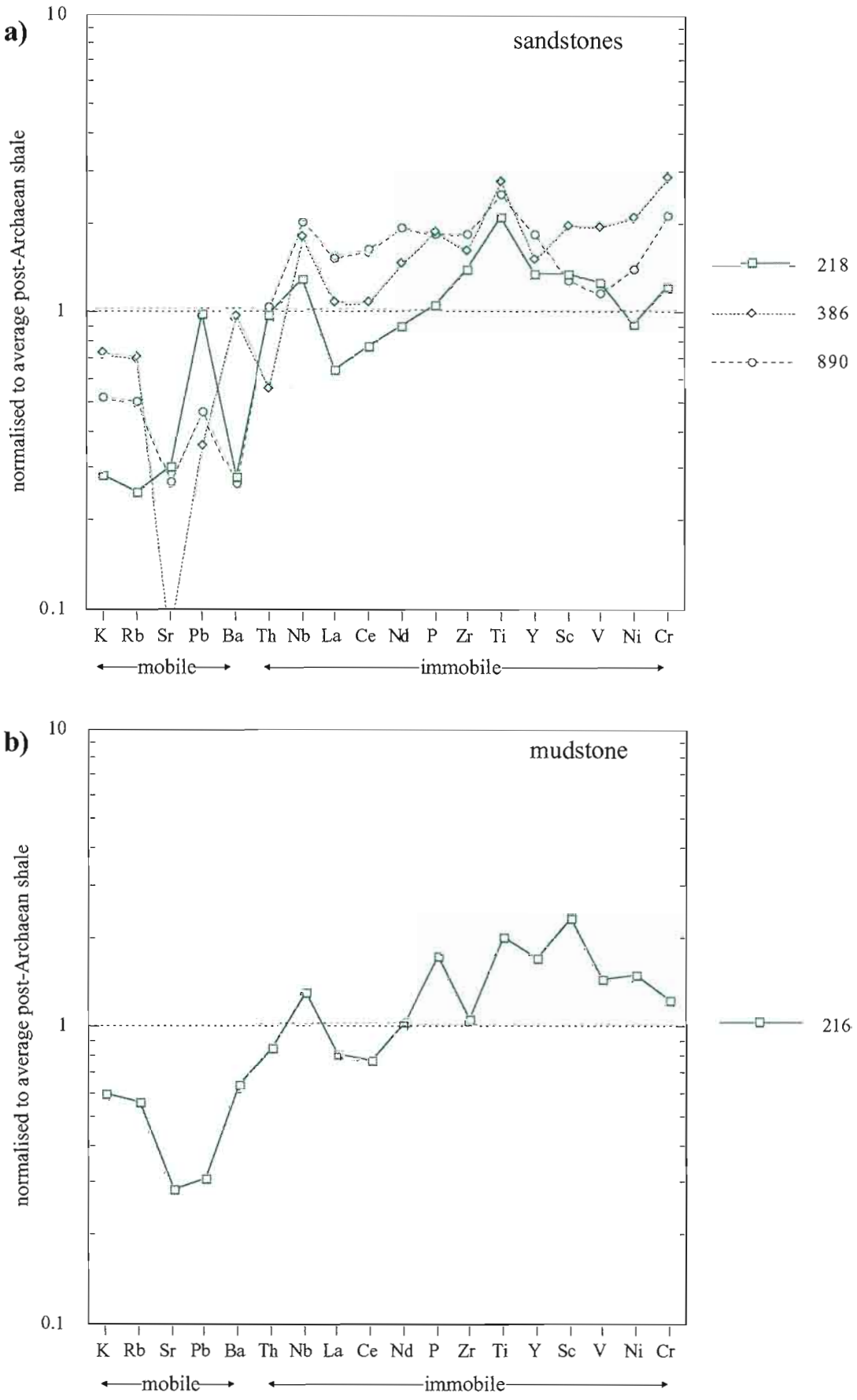

Figure 4.9. Average post-Archaean shale normalised extended trace element and LREE plot of suite 1C sandstones and mudstone.

pelagic sedimentation and hence the source characteristics may be different from those of the associated sandstone. An assumption that the sandstone and the mudstone involve similar provenances is therefore perhaps tenuous. This factor should be kept in mind when comparing compositions of these two lithologies.

In reference to Figure 4.8b, there are subtle, but noteworthy differences between the sandstone and the mudstone in terms of the absolute abundances of many elements. The mudstone shows similar abundances or slight to moderate enrichment in most elements compared to the sandstone. Exceptions to this pattern include Si, Zr and Th, which are enriched by 17%, 30% and 15% respectively in the sandstone. The most significant increases of element concentrations in the mudstone involve K, Rb and Ba (each by a factor of 2), which are readily adsorbed onto clay minerals in weathering profiles (Nesbitt et al., 1980). Other elements which show enrichment in the mudstone include those usually associated with an input of mafic detritus: ie. Sc, Ni, Fe and Mg. As a result, ratios of elements with markedly different compatibilities such as Th/Sc, La/Sc, Zr/Sc, Nb/Ni and Zr/Cr are all considerably higher in the sandstone relative to the mudstone (Table 4.2). Note, however, that the values of these ratios and the absolute abundances of ferromagnesian elements in the mudstone occur within the ranges, or are slightly lower than those shown by other fine-grained sediments of suite 1.

Differences in sandstone and mudstone chemistries could be explained in number of ways: 1) adsorption of trace elements onto clay minerals, resulting in overall enrichment in mudstone; 2) the dilution effect of quartz in sandstone, such that SiO_2 is enriched at the expense of all other elements; or 3) differences in provenance characteristics. The effects of these first two processes are likely to be enhanced in environments where source area weathering is important. Consider a source region which contains a dominant basaltic component, but which also involves a component of mature siliciclastic material. A deeply incised weathered profile through such a terrain would be expected to consist of a highly fractionated "residue" comprising a coarse-grained fraction involving resistant mineral phases such as quartz, stable heavy minerals (eg. zircon, rutile, tourmaline, Fe-Ti oxides, chromite and perhaps apatite) and possibly partially degraded labile constituents such as feldspar and formerly glassy rock fragments. The fine-grained fraction would be expected to be rich in clays produced from the breakdown of unstable phases such as plagioclase, volcanic glass and ferromagnesian minerals. In such a scenario, trace elements would be partitioned between the fine-grained fraction due to adsorption on clays, and heavy mineral phases concentrated within the coarse-grained fraction. For instance, heavy minerals could fractionate Ti, Nb, Ni and V in Fe-Ti oxides or rutile, and Zr, Y, LREE and perhaps Th in zircons or apatites. On the other hand, Sc, FeO, MgO and Ni may show elevated abundances in the fine-grained fraction during alteration of basaltic glass to smectites. Ca, Na_2O and Sr would be either be leached during weathering or contained in smectites. During the breakdown

of feldspar or degradation of smectite to illite, released SiO_2 may lead to the silicification of partially altered lithic fragments and perhaps altered feldspar.

On erosion and transport of detritus derived from a weathered "residue" of this type, quartz, heavy minerals and silicified lithic fragments would be partitioned into coarse-grained sandstones, whereas clay minerals would be suspended in the water column and deposited to form mudstones. Thus element fractionation may result not only from hydraulic sorting during transport and deposition, but also from weathering of the source area.

An major inconsistency with this model of derivation from a weathered parent rock is the relatively low values of Ti/Zr in the sandstone sample (Table. 4.2). If the inference that the composition of the sandstone is strongly influenced by heavy minerals is correct, concentrations of Zr and Ti, Nb would be expected to controlled largely by the abundances of zircons and Fe-Ti oxides respectively. Ratios of these elements may therefore be used to monitor the relative contributions from 'felsic' and 'basaltic' sources. The decrease of both Ti/Zr (39-49) and 100*Nb/Zr (8.3-9.9) in suite 1C sandstones relative to most other suite 1 sandstones (Ti/Zr ranges 46-81; 100*Nb/Zr ranges 10.4-13.1) indicates that an additional 'felsic' component was included in the sandstone. Thus although weathering of the source region may play a part in determining the composition of suite 1C rocks, the poor correlation between sandstone sample 218 and the neighbouring mudstone sample 216 is most probably due to differences in provenance characteristics.

4.5.4 Origin of the basaltic signature

The various basaltic successions which could have provided the basaltic detritus in suite 1 sediments include:

1) Late Proterozoic rift tholeiites of the Crimson Creek Formation and Smithton Trough correlates

2) ?Middle Cambrian low-Ti tholeiitic and boninitic lava successions of the allochthon (MUC)

3) Middle Cambrian medium- to high-K calc-alkaline basalts and andesites and shoshonitic basalts of the Mt Read volcanic arc (Suite III of Crawford et al., 1992)

4) Middle Cambrian tholeiitic lavas and shallow intrusives of the Mt Read volcanic arc (Suite IV of Crawford et al., op cit.).

Hiscott and Gill (1992) and Skilbeck and Cawood (1994) have shown that first-cycle volcaniclastic sediments provide a valid estimation of their parental magmatic compositions. Although some of the units included within suite 1 contain reworked sedimentary detritus, and are therefore clearly second-cycle (eg suite 1A), they are considered to reflect the composition of their basaltic source. The similarity of chemical

signatures of sediments to that of the basaltic fragment extracted from the Fernfields Member supports this interpretation. Indeed, it can be argued that second-cycle mixing of volcaniclastic sediments in which detritus is re-deposited largely as lithic fragments, may help to homogenise the bulk composition of the sediments and reduce the effects of hydraulic fractionation.

4.5.4.1 Discrimination using MORB-normalised multi-element patterns

Multi-element diagrams for suite 1 sediments and possible source terrains are shown in Figure 4.10. Only those sediments which showed a basaltic or basaltic andesite composition (ie SiO_2 ranging 45-56%) were considered in these plots in an attempt to reduce the effects of contamination from more 'felsic' sources. As expected, strongly incompatible elements (ie Sr, K, Rb and Ba), with their tendencies for mobility during seawater alteration, diagenesis and metamorphism, show erratic distributions, with suite 1B sandstones displaying greatest variation (Fig. 4.10a). Consequently, little attention is placed on these elements in terms of basalt-type discrimination. Relative to average MORB compositions (Pearce, 1983), both suite 1 sediments and the extracted basalt clast show smoothly increasing abundances with decreasing element compatibility (ie. Sc through to Th at the left hand side of the diagram), indicating a fairly enriched composition. The high Nb contents, coupled with moderate enrichment of Ti and Zr are inconsistent with typical magma compositions generated in arc settings. In consideration of this signature and the tholeiitic affinities shown by both suite 1 siliciclastics and the extracted basalt clast, derivation from the oceanic forearc lavas of the MUC (Fig. 4.10c) or the Mt Read volcanic arc basalts (Fig. 4.10d) would seem unlikely. Other chemical characteristics of the most 'mafic' suite 1 sediments which differ from these arc-related basalts include:

1) TiO_2 abundances of suite 1 (2.2-4.1%) are a factor of two greater than average Mt Read volcanics and a factor of ten greater than average MUC abundances;

2) Ti/Sc (418-578) and Ti/V (50-62) values are considerably higher than the ranges shown by any of the arc-related basalt sequences (Mt Read Volcanics: Ti/Sc 39-323, Ti/V 8-30; MUC: Ti/Sc 8-71, Ti/V 2-12)

3) enriched incompatible element concentrations (relative to average MORB) in suite 1 siliciclastics are in stark contrast to the strongly incompatible element depleted signature of the MUC lavas (compare figs 4.10a and c);

4) LREE abundances are considerably lower than the high-K and shoshonitic lavas of the Mt Read Volcanic arc (Suite III), as too is the range of P_2O_5/TiO_2 (0.08-0.12 compared to 0.4-1.2 for Suite III);

5) Nb/La (0.8-1.3) values are higher than Mt Read volcanic arc basalts (0.02-0.28), but considerably lower than low-Ti tholeiitic basalts of the MUC (2-9);

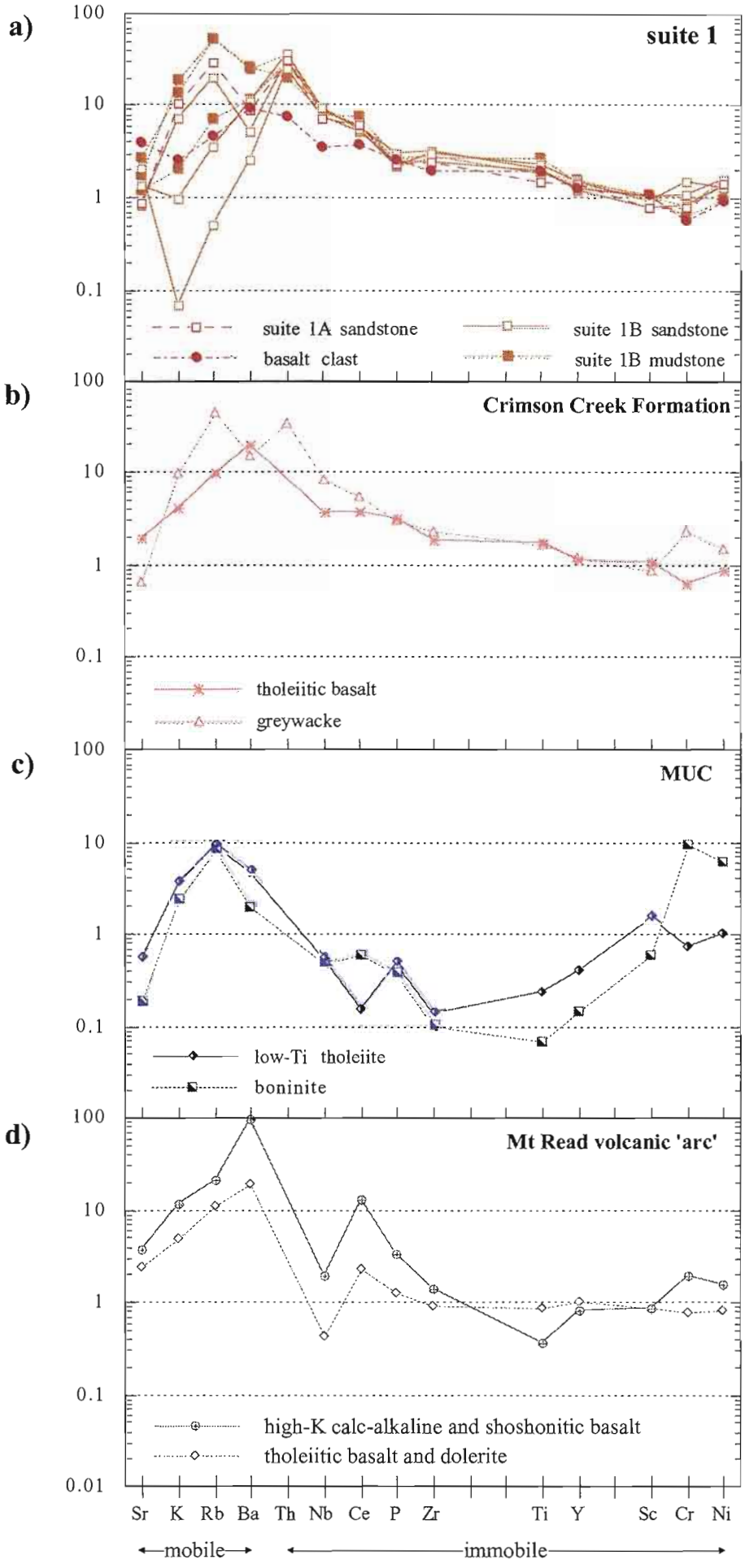

Figure 4.10. Average MORB (Pearce, 1983) normalised trace element plots of "basaltic" suite 1 samples (SiO_2<56%) and potential mafic source terrains.

6) Zr/Nb ratios (8-9) are lower than Mt Read volcanic 'arc' basalts (11-70); they fall within the ranges of MUC lavas (2-12), however the have latter extreme depletion of Zr.

The enriched MORB-type signature of suite 1 compares best with the patterns shown by tholeiitic basalts and related volcanogenic sediments of the Crimson Creek Formation (Fig. 4.10b). Not only are the overall shapes of the patterns remarkably similar, but the sediment compositions deviate from their respective basalt compositions in an identical fashion. Nb, Ce and to a lesser extent Zr show slightly higher abundances in the sediments compared to the basalts (Th is also enriched in suite 1 sediments, however Th data is unavailable for the Crimson Creek Formation basalts, so a comparison cannot be made). Both suite 1 sandstones and mudstones show this relationship, hence enrichment of these elements is unlikely to have resulted from hydraulic fractionation as it occurs independently of grainsize. The most likely explanation therefore, is contamination from an exotic source. The fact that similar enrichment patterns are shown in the Crimson Creek greywackes strongly suggests that the contaminant is derived from basement (ie. Precambrian) sequences.

4.5.4.2 Composition and significance of detrital Cr-spinels in suite 1 sandstones

As previously mentioned in section 4.1, potential basaltic-andesitic source terrains for Dundas Group siliciclastics can be distinguished in terms of their respective Cr-spinel chemistries. Arai (1992) showed that the composition of Cr-spinels faithfully reflects that of their parent magmas. Moreover, the geochemical signature of the parent magma may be retained by Cr-spinels even after alteration, metamorphism and sedimentary reworking of the igneous host. The resistance of Cr-spinels to significant chemical modification is of particular significance to sediment provenance studies as the composition of detrital grains can be therefore be employed as a powerful tool for discriminating between source areas.

A plot of TiO_2 vs Cr# (ie. Cr/(Cr+Al)) for available Cr-spinel data from potential ultramafic to intermediate sources is presented in Figure 4.11a. A similar plot was shown by Greenhill (1995) to effectively discriminate between Cr-spinels derived from the Crimson Creek Formation (CCF) and the MUC. The relative TiO_2 abundances of Cr-spinels from each of these successions closely reflect the concentration of Ti in their respective igneous hosts, with >80% of MUC data having TiO_2 abundances below the detection limit (≈0.15wt%) and CCF TiO_2 data ranging from 0.27 to 5.00 wt% with an average of 2.03 wt% (compare Fig, 4.11a and Fig. 4.10 b, c). Although there is minor overlap between the CCF and MUC in terms of TiO_2 content, the bulk of the data from each succession are distinguishable. Also shown in Figure 4.11a, are the chemistries of Cr-spinel grains from shoshonitic basalts and andesites of the Mt Read volcanic 'arc' (MRV: suite III of Crawford et al., 1992) as well as grains analysed from inferred late Middle Cambrian basaltic material contained within a volcaniclastic debris flow from the

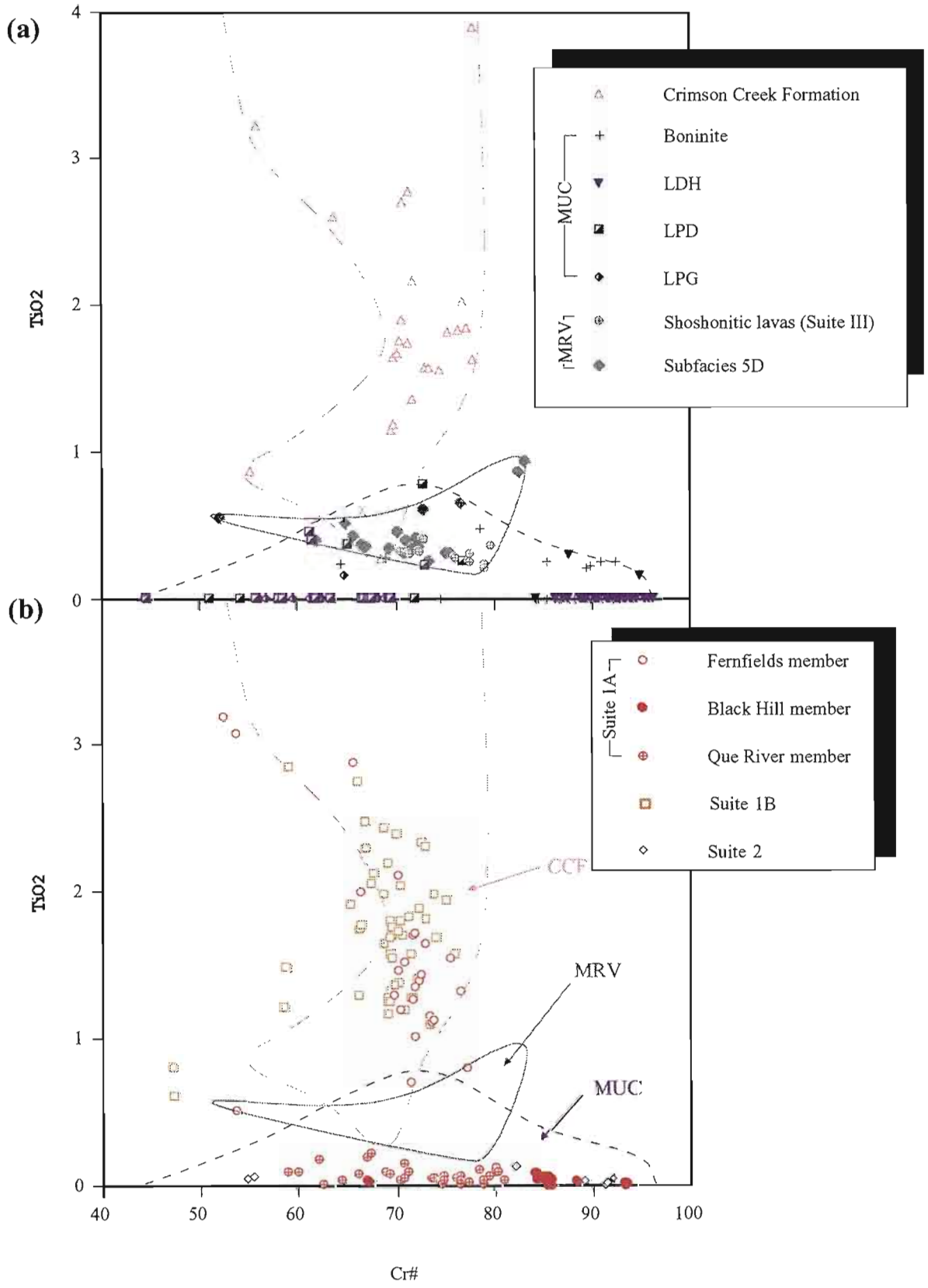

Figure 4.11. (**a**) TiO_2 vs Cr# plot for Cr-spinels contained in potential source lithologies: (i) Crimson Creek Formation (CCF), (ii) Mt Read volcanics/Dundas Group (MRV), (iii) Mafic-ultramafic complexes (MUC*).
* MUC data plotting at zero TiO_2 are below detection limit of electron micro-probe (~0.15 wt%)

(**b**) TiO_2 vs Cr# plot for detrital Cr-spinels from suites 1 and 2.

Data sources: CCF (Berry and Fulton, 1995); MRV (Jones, in prep.); MUC (Brown, 1986)

Dundas region (subfacies 5D: see section 3.6.4). The basaltic debris which hosts the latter data set was interpreted in section 3.7 to possess shoshonitic affinities and a genetic relationship with other Cambrian suite III volcanic rocks. The distribution of MRV data on the TiO_2 vs Cr# plot occupies an intermediate position between the bulk of the MUC and CCF data, with TiO_2 ranging from 0.21 to 1.05 wt%. Anomalously high-TiO2 MUC spinels and low-TiO_2 CCF spinels plot within the MRV field.

Cr-spinel data collected as part of this provenance study were derived from four coarse-grained suite 1A samples and two suite 1B sandstones. On the basis of their TiO_2 content, the population is effectively divided into two groups: low-Ti (<0.01-0.22 wt%) and high-Ti (0.51-4.04 wt%) groups (Fig. 4.11b). Of the suite 1 samples, the low-TiO_2 group only involves suite 1A and plots neatly within the MUC field. It encompasses all data from the Black Hill and Que River members, however no spinels from the Fernfields member plot within this group. The larger proportion of Cr-spinels from the Black Hill member are highly refractory, with Cr# in excess of 84. This would tend to suggest principal contribution from the boninitic lava suite or its cumulate equivalent (layered dunite-harzburgite succession or LDH: Brown, 1986) (cf. Fig 4.11a). Lower Cr# shown by spinels contained in the Que River member are interpreted to indicate sourcing from pyroxenite-bearing MUC successions (layered pyroxenite-dunite or LPD; layered pyroxenite gabbro LPG successions: Brown, op cit.). This interpretation is consistent with the petrographic observation of serpentinised pyroxenite clasts within this unit.

The high-Ti group includes all suite 1B and Fernfields member data. The scatter of data in this group coincides roughly with that of CCF spinels and defines a crude arcuate field which probably reflects a fractionation trend formed during crystallisation of the parental magma(s) (ie. Al and Ti abundances controlled by the crystallisation of plagioclase, and ferromagnesians respectively). Although a few high-TiO_2 data points plot away from this trend (and the CCF field), the overwhelming proportion of the data indicates principal contribution from the CCF.

The contribution from the MUC in the Black Hill and Que River members (suite 1A) indicated by the low-TiO_2 spinel population corresponds with the enrichment of Cr and Ni relative to both the Fernfields member and suite 1B sandstones indicated from whole rock geochemical analyses (Figs. 4.6, 4.7). Considering the strong input from the CCF inferred from whole geochemical data however, the lack of high-TiO_2 Cr-spinels is surprising. For example, apart from the high Cr and Ni abundances in the Black Hill member (sample 958), the multi-element pattern shown in Figure 4.6 is almost identical to that of the Fernfields member sample analysed for Cr-spinel compositions (sample 336). Despite the apparent correlation between these two units indicated by whole rock geochemical data, the composition of Cr-spinel suggest two distinct volcanic sources. The cause of this inconsistency does not appear to be explainable with the present data set and more thorough sampling is required.

4.6 Suite 2

Suite 2 involves sandstones which are characterised by a mixed sedimentary - basaltic input, low abundances of incompatible elements but elevated Sc and Cr contents. Low values of La/Sc (0.6-0.9) and Th/Sc (0.11-0.13) are thus characteristic but these show some overlap with the most 'basic' suite 1 samples (Table 4.2). The definitive features of suite 2 are coarse-grained sedimentary textures and Ti/Sc values ≤ 231.

4.6.1 Distribution of samples

Suite 2 comprises polymict conglomerate and lithic sandstone which form part of an easterly facing package in the Kapi Creek-Ring River area (central area: Fig. 4.1). This package is bound to the west by the Serpentine Hill MUC. To the east, the package is overlain by a mudstone-dominated sequence with suite 3 affinities. Lenses of gabbroic breccia (subfacies 1C: see section 3.2.3) directly underlie the package in the Ring River and are intercalated with the lowermost units. No fossils have been discovered within these units, however Brown (1986) correlated the package with the basal portion (?Undillan) of the Dundas Group type area on lithostratigraphic grounds.

In the Ring River region, proximity of the siliciclastic package to the Devonian Pine Hill Granite has resulted in extensive actinolite $\pm$ epidote $\pm$ prehnite alteration. This pervasive alteration has obliterated many of the primary igneous textures and hence identification of clast-types is particularly difficult in samples from this region. Most of the sandstone and conglomerate samples investigated in the petrographic study come from the Kapi Creek area, approximately 3 km south of the Ring River, however a few less altered samples from the latter region were included.

4.6.2 Sandstone Petrography

Sandstones are poorly sorted and rich in lithic fragments. Quartz is common, comprising up to 30% of the framework component of better-sorted sandstones. Grains are typically poorly-sorted, angular and anhedral, with straight to mildly undulose extinction. Rare euhedral quartz grains ranging up to 1.5 mm in diameter and containing melt inclusions were observed. These are interpreted to be of volcanic origin. No porphyritic fragments of felsic composition were observed in association with these grains, hence they are most likely to be reworked from volcaniclastic deposits comprising 'free' crystals. Feldspar grains include dominant albitised plagioclase and minor potassium feldspar. They have moderately coarse grainsizes (up to 1 mm in length) and show subhedral to euhedral stubby or lath-shaped habits. Dusting of grains with sericite was observed in many cases. There is little textural similarity between these framework feldspars and those contained within mafic volcanogenic lithic fragments. A felsic volcanic origin for these grains would also seem likely.

Accessories include opaques, chromite, coarse-grained rutile, pyroxene and minor zircon. Pyroxene grains are always altered to actinolite.

Sedimentary fragments

Sedimentary clast-types comprise the bulk of the lithic component in suite 2 sandstones and conglomerates. Feldspathic greywacke clasts, closely resembling lithotypes contained in suite 1 are locally abundant, especially towards the base of the package. Well-rounded cobbles and boulders of quartzo-feldspathic sandstone and chert are present in all samples and become the dominant clast-types in the uppermost conglomerate units from the Kapi Creek area. The former contain large, angular quartz grains, some of which show features indicative of a volcanic origin, relatively unaltered plagioclase grains, biotite and coarse muscovite. Euhedral and rounded zircons, blue-green tourmaline, and rutile are accessory phases in these clasts. Mudstone, metaquartzite, quartz-mica schist, unmetamorphosed quartz arenite and dolomite fragments are present in variable amounts throughout the package.

Igneous fragments

Igneous fragments comprise between 20-30% of the lithic component of sandstones and conglomerates analysed for detrital modes. They are with few exceptions, mafic in composition and fine- to medium-grained. They appear to be derived almost entirely from lavas or fine-grained intrusives, and only the lowermost units contain clasts with plutonic textures. Even in these lower units however, plutonic fragments are scarce and generally more angular than neighbouring lava fragments. The paucity of plutonic debris is perhaps surprising considering the close spatial and temporal relationship of these rocks to gabbroic breccias. The diversity of textures and compositions shown by fine-grained fragments are matched only by those contained in the stratigraphically highest portions of the Que River member (suite 1A). Four clast-types are distinguished on the bases of their composition and texture, however not all are present throughout the stratigraphy.

Type-2*a* basalt fragments (Fig. 4.12a) were recognised in most samples, but become scarce in the uppermost conglomerates from the Kapi Creek area. Although generally aphyric and quench-textured, phenocrysts and glomerocrysts of a ferromagnesian phase (olivine or pyroxene) now replaced by chlorite, actinolite or serpentinite, were observed in a few clasts. Textures shown by aphyric varieties range from lathwork arrangements of microlites set in a silica ± chlorite ± epidote altered groundmass, to vitric textures consisting of felty masses of spherulitic sheaves. Curved microlites are common and are locally confined to the margins of rigid phenocrysts or may pervade the entire clast, resulting in swirled foliation. Similar fragments have been observed from the Black Hill and Que River members (compare with Fig. 4.5f).

Figure 4.12. Photomicrographs of basaltic detritus in suite 2.

(a) Type- 2a vitric textured basalt clast with felty masses of spherulitic sheaves. This clast type closely resembles MUC derived material contained in suite 1A (cf. Fig. 4.5f). (crossed polars: sample 150A)

(b) Type-2b basalt clast showing relict subhedral to euhedral crystals (probably originally olivine) set in a groundmass of altered ?pyroxene needles (plane polarised light: sample 150A)

(c) Type-2c basalt or andesitic fragment containing blocky feldspar phenocrysts set in a formerly glass-charged groundmass of feldspar microlites. (plane polarised light: sample 380)

(d) Type-2d basaltic fragments consisting predominantly of feldspar laths, Fe-Ti oxide grains and minor altered clinopyroxene grains. (crossed polars: sample 845)

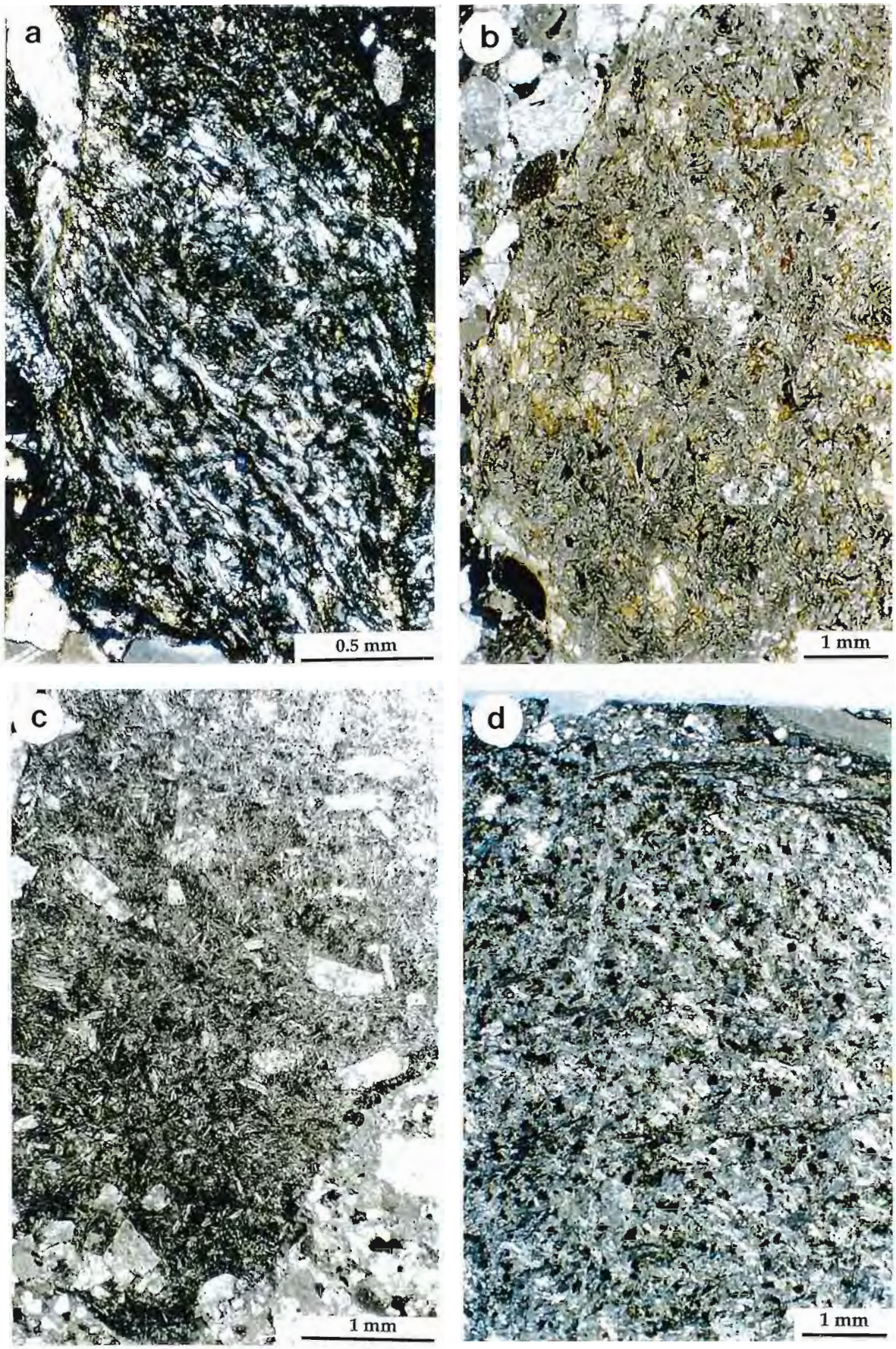
a
0.5 mm
b
1 mm
c
1 mm
d
1 mm

Type-2*b* igneous fragments (Fig. 4.12b) are always fine grained, quench-textured and range from non-vesicular to highly vesicular. In thin section, they are generally dark green in colour due to extensive alteration to chlorite ± actinolite, however pervasive quartz or carbonate replacement of the groundmass is shown by some clasts. Vitrophyric textures are rare, with chlorite and serpentinite pseudomorphs after a ferromagnesian phase (probably olivine) occurring up to 0.5 mm long. The most commonly preserved phenocrysts however, are pale to deep red, anhedral to subhedral chromites. This mineral is diagnostic of type-2*b* fragments and provides an easy method of identification regardless of the degree of alteration. Formerly glassy groundmasses show chlorite and actinolite pseudomorphing fan-shaped aggregates of ?pyroxene microlites. Fracture textures, resembling classical perlite were also recognised. No parent rock to these fragments have been observed in the Dundas region, however the abundance of large phenocrystal chromites restricts them to two likely volcanic sources: boninitic lavas of the MUC and shoshonitic lavas of the Mt Read volcanic arc (MRV).

Type-2*c* feldspar phyric basaltic or andesitic fragments (Fig. 4.12c) form a minor component of the upper-most units from the Kapi Creek area . They are commonly porphyritic, with fractured feldspar phenocrysts and glomerocrysts occurring up to 3 mm in length. Spherulitic textures are comparatively rare, and the silica ± chlorite ± epidote alteration which is so pervasive throughout type-*a* basalts is largely absent. Feldspar crystals are instead altered to albite ± sericite ± carbonate, and are enclosed either by a very dark, holocrystalline Fe-rich groundmass or randomly arranged acicular feldspar microlites. Clast shapes are commonly irregular, formed in part by impingement from neighbouring rigid clast-types. In these cases, microlites exhibit either a distinct alignment which appears as a pseudo-flow foliation (ie. pseudo-trachytic texture), or are crenulated in a ductile fashion. This compactional foliation is probably the result of tectonic flattening rather than burial as the long axes of clasts are generally re-oriented into the tectonic foliation. This apparent mechanical weakness is characteristic of this clast-type. Clasts with similar compositions and textures form a large proportion of the volcanic lithic fraction of suite 3 sandstones and conglomerates.

The final igneous lithic-type, type-2*d*, are medium-grained plagioclase and clinopyroxene phyric lava or fine-grained intrusive fragments (Fig. 4.12d). They are most commonly observed in the lower portions of the Ring Conglomerate and usually occur in association with feldspathic greywacke fragments. Actinolite and chlorite are the dominant alteration products. They are distinguished from all other fragment-types by their abundance of Fe-Ti oxides, which occur as intersertal grains. In this respect they are similar to many mafic fragments contained in suite 1A sandstones and are considered to be derived from the Crimson Creek tholeiites.

4.6.3 Chemical composition and source characteristics

In terms of major element abundances, a less 'basic' signature is shown for suite 2 sandstones compared to those of suite 1. SiO_2 values indicate intermediate to felsic compositions (62 and 66 wt%) and exceed most suite 1 sandstones (the exceptions being suite 1C), whereas $Fe_2O_{3(tot)}$, MgO and P_2O_5 abundances are generally lower (Table 4.2). Of particular significance are the low TiO_2 abundances, which are less than half those of suite 1. As Th and Zr increase correspondingly with SiO_2, whereas Sc is reduced, it would seem reasonable to suggest that higher SiO_2 levels reflect contamination of a basic component with more 'felsic' material.

The PAAS normalised spider-diagram shows a progressive enrichment of compatible elements relative to the least mobile incompatible elements (Fig. 4.13a). The overall smooth increase in immobile element concentrations relative to PAAS from left to right is punctuated by troughs at Th, Zr and V, and a sharp peak at Sc. Although low values of La/Sc and Th/Sc compare with the most 'basic' samples of suite 1, the 'depleted' concentrations of Ti, Nb and Zr provide a means of discriminating between sandstones of the two suites. Ratios of Ti/Sc, Ti/Y, Nb/La and Zr/Sc for suite 2 sandstone fall below, or at the bottom of the ranges shown by coarse-grained samples from suite 1 (Table 4.2) . Moreover, despite the relatively low concentration of Zr in suite 2 sandstones, Zr/Nb is considerably higher than suite 1 ranges, reflecting the strong depletion of highly incompatible elements. Cr/Zr and Cr/Nb values occur well above the ranges shown for suite 1, with the exception of samples from the Que River Member and the Black Hill unit, whose elevated Cr values have been interpreted to indicate a contamination of the Crimson Creek tholeiitic signature by detritus derived from the MUC.

4.6.4 Discussion of likely sources

Concentrations of Ti, Y and Zr are either comparable to, or slightly depleted with respect to average MORB, whereas Nb is somewhat enriched (Fig. 4.13b). Abundances of these elements immediately rule out an enriched MORB-type composition (ie. Crimson Creek tholeiites) for the volcanic component and are indicative of mafic to intermediate sources generated in supra-subduction zone settings (Pearce, 1983). Possible source terrains can therefore be constrained to either lava successions of the Mt Read Volcanic arc or the MUC. Although the overall shape of the suite 2 sandstone MORB-normalised spider-diagram shown in Figure. 4.13b is similar to that of the high-K and shoshonitic lavas of the Mt Read Volcanic arc (Suite III), the absolute abundances of LREE and P are well below the ranges characterised by the latter. 'Depletion' of these elements by source mixing is considered to be unlikely as dilution of the basaltic component by material of more 'felsic' composition would be expected to result in an increase, rather than a decrease in incompatible element concentrations. In addition, Zr/Nb values for suite 2

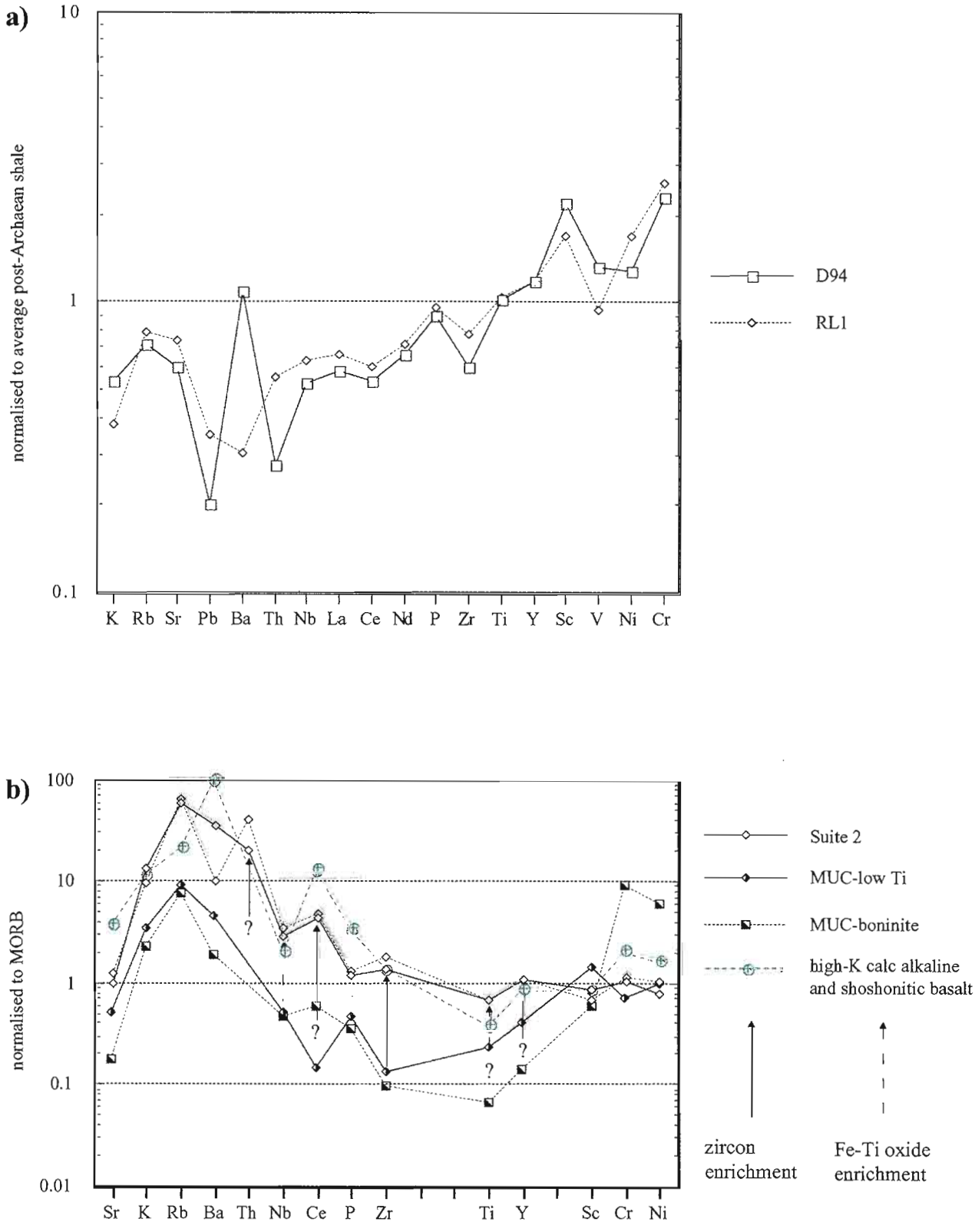

Figure 4.13. Multi-element patterns for suite 2. (**a**) PAAS-normalised plot showing strong depletion of incompatible elements and 'enrichment' of Sc and Cr. (**b**) MORB-normalised plot of suite 2 sandstones and potential mafic source terrains. Arrows indicate possible enrichment of HFSE relative to MUC lavas due to heavy mineral concentration in sandstones. Data sources: i) boninities (Brown, 1986), ii) low-Ti lavas of the MUC (Brown, op cit.; Crawford and Berry, 1992; "shoshonitic" lavas (Crawford et al., 1992).

sandstones (12 and 13), which would also be expected to increase due to concentration of zircons derived from a 'felsic' source, occur at the lowermost end of the spectrum shown by high-K and shoshonitic lavas (11-51). Similarly, Nb/La ratios for suite 2 sandstones (0.45-0.48) are well above the range shown by the LREE-enriched shoshonites (0.02-0.3). Considering the low absolute concentration of Nb in suite 2 sandstones and the likelihood of LREE enrichment due to 'felsic' contamination, high Nb/La values would imply a strongly LREE-depleted source.

The chemical signature of lava successions of the MUC are characterised by highly depleted Ti, Zr, LREE, Nb, P and Y (Fig. 4.13b) relative to average MORB, and would therefore seem the most likely source of mafic detritus. Moreover, deviation of suite 2 sandstone trace-element ratios and absolute element abundances from those shown by lavas of the MUC are consistent with contamination by a 'felsic' component. For instance, concentration of Zr and LREE in zircons results in Ti/Zr (38-49) values occurring at the bottom of the MUC ranges (16-234) , whereas Zr/Sc and La/Sc are much higher. Likewise, housing of Ti and Nb in rutile or Fe-Ti oxide (the latter possibly indicating a minor Crimson Creek tholeiite component) may result in Ti/Sc values (176-231) well below the range shown by suite 1 rocks, but considerably higher than MUC ranges (8-71). That Zr/Nb ratios for suite 2 sandstones are slightly higher than MUC (2-12) is interpreted to indicate that the contribution of zircons from a compositionally mature siliciclastic source or a felsic volcanic source is more significant than dilution from a Ti-Nb-rich basaltic source.

The composition of Cr-spinels involve consistently low TiO_2 abundances (commonly below detection limit-0.13 wt%) and support the interpretation of an MUC source component (Fig. 4.11b). Data overlaps with that of the Black Hill member (suite 1A), with the extremely high Cr# (>90) shown by most spinels considered to indicate a significant contribution from either boninitic lavas or their associated cumulate succession (layered dunite-harzburgite: Brown, 1986). The SiO_2 abundances of this suite of rocks are higher than those of the Crimson Creek Formation tholeiites (Crawford and Berry, 1992) and may in part account for the relatively high SiO_2 contents in suite 2 compared to suite 1.

4.7 Suite 3

Suite 3 rocks involve a broad range of compositions which do not correspond directly with any single source terrain. Significant overlap is shown with other suites (suite 1, 3 and 4) in terms of many absolute element concentrations and discrimination is based principally on definitive ranges of element-element ratio values. Compatible/incompatible element ratios have values which are generally lower than those of the basalt-derived suites 1 and 2, but are higher than those shown by the mature siliciclastics contained within suite 4. As shown in Figure 4.14a, suite 3 sandstones can

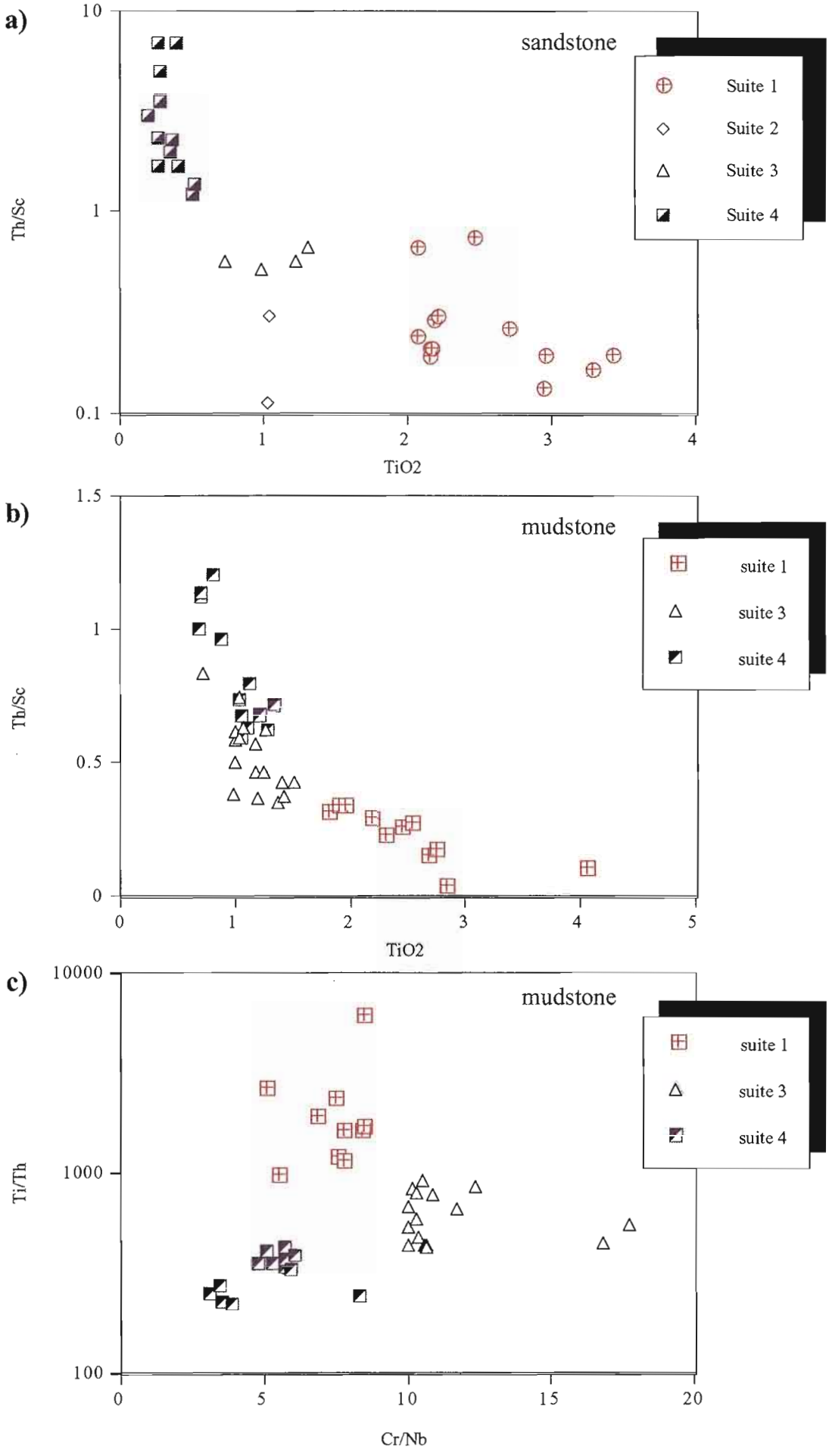

Figure 4.14. Discrimination plots for suite 3 sandstone and mudstone.

be distinguished from suites 1, 2 and 4 samples of similar grain-size through the moderate values of Th/Sc (0.5-0.7). Two suite 1 samples show anomalously high Th/Sc values (probably due to concentration of Th in zircons), but are nevertheless clearly distinct from suite 3 with considerably higher TiO_2 abundances. Moderate values of Ti/Th (435-652) and Ti/Zr (26-34) are also diagnostic of suite 3 sandstones (Table 4.3). The TiO_2 vs Th/Sc plot for mudstones (Fig. 4.14b) is less effective in distinguishing between suites, with considerable overlap between suites 3 and 4 (note also that the Y-axis is now shown as a linear scale). The most diagnostic feature of suite 3 mudstones is the high abundance of Cr relative to less compatible elements (in particular, Nb). As shown in Figure 4.14c, Cr/Nb values exceed all other suites and is a useful parameter for discrimination from Nb-rich suite 1 mudstones. Cr, although useful for indicating input from mafic rocks of primitive composition, is a less reliable discriminator in sandstones due to the potential for anomalously high values resulting from concentration of Cr-spinels (eg. suite 1 sandstones).

4.7.1 Sample distribution

Suite 3 samples are the most widespread in the Dundas region, with data collected from western, central and eastern areas. The sample set is dominated by fine-grained lithotypes (17 mudstones and 4 sandstones), with all the mudstone samples collected from the central area included within suite 3. In the western area, suite 1 rocks occupy both the lower and upper portions of the Dundas Group stratigraphy (Figs. 4.1 and 4.4). In the type area of the Dundas Group, packages of strata yielding suite 3 samples are separated by a substantial thickness of suite 1A strata which contains late Middle Cambrian to early late Cambrian fauna towards the base (Fig. 4.4a). These fossil localities occur between 200m and 400m above the stratigraphically lowest suite 1A sample and provide an upper age constraint on the underlying, suite 3 strata. The oldest suite 3 unit in this area (Hodge Slate) contains fossils of Undillan age (middle Middle Cambrian) and is a biostratigraphic correlate of the suite 3 sample collected from the Black Hill area (Fig. 4.4b). In the latter area, the suite 1A provenance signature re-appears approximately 430m above the position of the Undillan fauna, a thickness roughly comparable with the minimum thickness of lower suite 3 strata in the Dundas Group type area. Furthermore, the stratigraphic position of the higher suite 1A sample in the Black Hill area occurs at a similar distance below the Boomerangian fauna to that of the lowermost suite 1A sample in the type area. Although provenance data is thin in the Black Hill region, this apparent consistency between chemical and palaeontological data indicates that chemo-stratigraphic techniques may provide an accurate means of correlation between packages of strata in the western area (within the lower part of the Dundas Group stratigraphy at least).

Table 4.3 Whole rock geochemical data for Suite 3.

Lithology	**Sandstone**				**Mudstone**															
	'arc-type' magmatic affinities		*?*	*?*	*'arc-type' magmatic affinities*							*Crimson Creek tholeiitic affinities*			*dominant mature basement input*				*?mixed basic input*		
Sample #	**835**	**839**	**858**	**222**	**367**	**811**	**824**	**238**	**308**	**390**	**22**	**808**	**135**	**884**	**456**	**452**	**453**	**458**	**813**	**899**	**D90**
SiO2	60.13	72.45	72.29	72.14	73.80	63.79	61.79	69.62	74.79	63.56	46.70	64.10	61.57	57.46	66.43	65.75	78.00	66.31	60.76	63.51	64.57
TiO2	0.98	0.73	1.22	1.31	0.99	1.19	1.17	1.03	1.01	1.00	1.01	1.41	1.27	1.03	1.51	1.17	0.72	1.08	1.42	1.25	1.38
Al2O3	13.75	11.78	16.36	11.99	11.36	14.34	15.51	15.22	13.70	16.22	11.62	16.39	15.64	11.94	14.34	15.43	9.60	16.59	15.53	16.48	16.74
Fe2O3(tot)	8.97	6.05	3.41	7.06	6.56	8.88	9.47	6.95	4.24	6.30	7.49	8.92	8.68	5.62	9.86	9.94	6.86	8.45	9.90	8.44	8.57
MnO	0.38	0.11	0.01	0.05	0.03	0.09	0.16	0.03	0.01	0.12	0.30	0.09	0.10	0.21	0.06	0.05	0.05	0.05	0.12	0.07	0.04
MgO	5.55	2.39	1.38	3.15	4.56	4.48	3.78	3.66	2.12	3.51	10.01	4.34	5.39	6.46	4.14	3.62	2.83	3.63	5.18	4.12	3.82
CaO	6.32	2.84	0.22	1.99	0.07	3.11	3.47	0.14	0.04	4.68	18.71	0.23	3.31	13.05	0.25	0.18	0.07	0.09	2.79	1.72	0.35
Na2O	0.82	0.95	1.06	0.19	0.04	1.92	1.60	0.09	0.77	0.10	0.88	0.15	3.65	0.85	0.06	0.04	0.08	0.31	2.00	1.22	0.75
K2O	2.92	2.54	3.89	1.94	2.41	2.01	2.81	3.11	3.17	4.36	3.12	4.20	0.15	3.19	3.15	3.64	1.68	3.34	2.11	2.98	3.53
P2O5	0.18	0.16	0.16	0.17	0.17	0.17	0.23	0.16	0.14	0.15	0.16	0.18	0.23	0.19	0.19	0.17	0.09	0.14	0.20	0.20	0.25
La	28	28	36	39	25	23	38	30	28	31	30	27	30	28	27	37	24	43	31	33	37
Ce	63	57	81	82	53	50	80	64	63	68	62	59	65	60	62	74	55	87	55	71	63
Nd	28	25	36	35	26	23	36	26	29	29	31	28	34	27	26	33	28	45	28	32	34
Nb	13	11	16	17	12	15	17	16	16	16	16	17	18	16	22	19	12	18	16	16	16
Zr	171	166	258	275	147	161	182	164	160	205	174	193	226	245	261	242	200	230	200	177	172
Sr	105	56	36	39	15	169	123	12	26	76	256	27	370	196	18	25	32	23	133	104	73
Cr	171	201	530	327	141	155	175	166	169	171	284	185	185	269	223	190	128	180	198	161	168
Ba	341	209	453	215	261	254	364	502	373	515	519	542	44	544	246	295	206	290	312	503	382
Sc	21	18	23	18	24	25	26	22	23	24	22	26	21	19	26	23	12	24	27	24	26
V	148	126	173	153	186	228	176	164	215	144	111	206	157	108	186	166	95	155	217	242	186
Y	36	24	33	31	35	29	37	30	28	31	28	35	39	33	35	40	30	44	34	33	33
Rb	144	124	144	75	104	85	121	137	133	164	111	154	24	119	115	137	65	135	90	134	181
Th	11	10	13	12	9	9	12	13	14	14	11	11	13	14	11	13	10	15	10	11	9
Ni	66	60	160	91	45	74	82	62	72	81	179	99	85	49	107	100	56	77	87	98	94
Pb	20	5	129	1	17	4	13	16	34	10	17	1	6	3	32	18	23	14	7	30	16
Ti/Zr	34.22	26.24	28.36	28.48	40.55	44.32	38.69	37.65	37.98	29.25	34.89	43.74	33.69	25.21	34.66	29.07	21.67	28.19	42.69	42.30	48.11
Ti/Y	162.54	181.46	221.72	252.63	170.31	246.03	190.30	205.80	217.03	193.41	216.84	241.21	195.25	187.16	258.44	175.87	144.45	147.34	251.09	226.90	250.74
Zr/Sc	8.14	9.22	11.22	15.28	6.13	6.44	7.00	7.46	6.96	8.54	7.91	7.42	10.76	12.89	10.04	10.52	16.67	9.58	7.41	7.38	6.62
Ti/Sc	278.63	241.95	318.11	435.08	248.36	285.40	270.81	280.64	264.21	249.83	275.98	324.70	362.61	325.06	347.91	305.86	361.13	270.13	316.19	311.98	318.25
Cr/Nb	13.15	18.27	33.13	19.24	11.75	10.33	10.29	10.38	10.56	10.69	17.75	10.88	10.28	16.81	10.14	10.00	10.67	10.00	12.38	10.06	10.50
Ni/Nb	5.08	5.45	10.00	5.35	3.75	4.93	4.82	3.88	4.50	5.06	11.19	5.82	4.72	3.06	4.86	5.26	4.67	4.28	5.44	6.13	5.88
La/Sc	1.33	1.56	1.57	2.17	1.04	0.92	1.46	1.36	1.22	1.29	1.36	1.04	1.43	1.47	1.04	1.61	2.00	1.79	1.15	1.38	1.42
Th/Sc	0.52	0.56	0.57	0.67	0.38	0.36	0.46	0.59	0.61	0.58	0.50	0.42	0.62	0.74	0.42	0.57	0.83	0.63	0.37	0.46	0.35
P/Zr	4.58	4.21	2.67	2.70	4.97	4.73	5.63	4.19	3.74	3.28	3.91	4.01	4.39	3.45	3.15	3.02	2.03	2.59	4.28	5.00	6.37
Ti/V	39.54	34.56	42.29	51.19	32.05	31.29	40.01	37.65	28.26	41.64	54.70	40.98	48.50	57.19	48.63	42.38	45.62	41.83	39.34	30.94	44.49
Ti/Th	531.93	435.50	562.82	652.62	662.30	792.77	586.76	474.93	434.06	428.28	551.95	767.47	585.75	441.15	822.32	541.13	433.36	432.20	853.72	680.69	919.38
Cr/Zr	1.00	1.21	2.05	1.19	0.96	0.96	0.96	1.01	1.06	0.83	1.63	0.96	0.82	1.10	0.85	0.79	0.64	0.78	0.99	0.91	0.98
Nb/La	0.46	0.39	0.44	0.44	0.48	0.65	0.45	0.53	0.57	0.52	0.53	0.63	0.60	0.57	0.81	0.51	0.50	0.42	0.52	0.48	0.43
P2O5/TiO2	0.18	0.22	0.13	0.13	0.17	0.15	0.20	0.15	0.14	0.15	0.15	0.13	0.18	0.19	0.13	0.14	0.13	0.13	0.14	0.16	0.18
Zr/Nb	13.15	15.09	16.13	16.18	12.25	10.73	10.71	10.25	10.00	12.81	10.88	11.35	12.56	15.31	11.86	12.74	16.67	12.78	12.50	11.06	10.75

* major elements presented as volatile-free percentages

The stratigraphically youngest samples from the Dundas Group type area are mudstones collected from exposures of the Climie Slate in the Dundas River (Figs 4.1 and 4.4a). Fossils contained within the uppermost part of this sequence indicate a middle Late Cambrian age (Iverian). These are the youngest rocks sampled in this study.

Sediments from the central and eastern domains are more difficult to constrain stratigraphically due to the paucity of age diagnostic fossils. Strata in the central area, although locally closely folded, are dominantly E-facing. Brown (1986) made a litho-stratigraphic correlation between the lowermost units positioned along the western margin of the Serpentine Hill MUC (Fig. 4.1) with the oldest (?Undillan) strata from the Dundas River section. The minimum youngest age of rocks contained in the central area is constrained by fossiliferous suite 3 strata of latest Middle Cambrian to earliest Late Cambrian age (Mindyallan: Banks, 1956 and 1982) located near Bonnie Point in the eastern portion of the area. Faunal assemblages of similar age have been recorded from suite 3 mudstones located in the SW corner of the central area at Barker Creek (Fig. 4.1: Jago, 1979; Banks, 1982). Rocks at both fossil localities are biostratigraphic equivalents of suite 1A strata of the western area.

A single sandstone sample from the structurally complex eastern area possesses a suite 3 geochemical signature. However, conglomerate units located north of Moores Pimple are also included in suite 3 on the basis of petrographic features. No age diagnostic fossils have been recorded from the eastern area and the stratigraphic position of these units relative to rocks in the central and western areas is uncertain. A very tenuous late Middle Cambrian-early Late Cambrian age is suggested on the basis of litho-stratigraphic correlation of conglomerate units at Moores Pimple with compositionally and texturally similar units contained within fossiliferous mudstone-dominated strata located near Bonnie Point (central area).

4.7.2 Petrography of coarse-grained lithotypes

Samples which were included in this petrographic study were fine- to medium-grained lithic arenites, greywackes and pebble conglomerate. Sandstones contain low to high abundances of lithic fragments and a monomineralic grain component dominated by quartz. The margins of individual lithic fragments are poorly defined in many sandstones however, and probably results from a combination of distortion and 'mergence' of relatively soft clast-types during sediment compaction, recrystallisation of labile constituents and extensive carbonate or silica cementation. This problem is alleviated in some of the more highly strained rocks, in which an anastomosing spaced cleavage wraps around individual lithic fragments, enhancing their clastic texture.

As mentioned in the preceding paragraph, quartz is the dominant monomineralic grain type in sandstones, comprising between 7% and 35% of the total rock volume. Most of these grains are angular to subrounded and exhibit mild undulose extinction. In a

few cases, polycrystalline grains of probable metamorphic origin were observed. Both of these grain-types are likely to have been reworked from pre-existing sandstones. Less commonly observed, were angular quartz grains, with sharp curviplanar boundaries and straight extinction. These resemble portions of large fractured quartz phenocrysts contained in felsic volcanic lithic fragments and a volcanic origin is tentatively interpreted for these grains. The certainty of a volcanic origin for this type of quartz grain is diminished somewhat, as despite thorough examination, no quartz grains with prismatic habits or resorbed crystal faces were identified.

Feldspar comprises between 2% and 12% of the lithic arenites and its abundance relative to quartz is roughly 1:3. In general, it appears less altered and coarser-grained than the feldspar grains contained in sandstones of suites 1 and 2 and multiple twinning is well preserved in many examples. Partial alteration to sericite, chlorite and calcite has occurred in a few grains however, and others show a fine brown 'dusting'. Untwinned grains with biaxial optic figures are likely to represent albite after Ca-rich feldspar. Grain shapes are angular to subrounded, the most angular showing subhedral prismatic forms. Rare examples of the latter are fractured internally. The immature form and relatively unaltered character of the grains imply that they have not seen a prolonged history of sedimentary reworking. Possible origins include first-cycle grains released from feldspar-porphyritic volcanic parents or perhaps minor epiclastic reworking of feldspathic crystal tuffs.

Minor monomineralic constituents include biotite (partially altered to chlorite), muscovite, very rare clinopyroxene (in most cases altered to epidote or chlorite), non-opaque and opaque heavy minerals. In descending order of abundance, non-opaque heavy minerals include rutile, rounded and euhedral zircon, yellow-green tourmaline, chromite and goethite. The proportions of euhedral zircons relative to rounded varieties is greatest in sandstones and conglomerates situated in the eastern portions of the Dundas region. Chromite grains are generally less than 0.1 mm in diameter and although present in most units, show variable abundances in individual samples and range from 0 to 15 grains per thin section. Opaque Fe-Ti oxides are rare in most samples, however they become a conspicuous constituent of some beds contained in the conglomerate package on Moores Pimple.

Rock fragments derived from sedimentary precursors comprise the bulk of the lithic fraction in sandstones and conglomerates. They include 'cherty' material, mudstone, protoquartzite, carbonate, quartzose- and less commonly feldspathic-greywacke fragments. 'Cherty' fragments (Fig. 4.15a) are by far the most common, constituting more than 55% of the total lithic fraction in sandstones and conglomerates from the western area (eg. Razorback Conglomerate). Included in this category are a spectrum of lithotypes which range from silicified mudstone, in which relict detrital grains of mica and quartz are observed, to microcrystalline and cryptocrystalline

Figure 4.15. Photomicrographs showing detrital components of lithic-rich suite 3 sandstones and conglomerates.

(a) Conglomerate consisting primarily of subrounded 'cherty' fragments. 'Chert' fragments in this example are interpreted to comprise silicified mudstone. A quartzite clast is also shown in the upper portion of the photograph. (crossed polars: sample 837)

(b) Aphyric, formerly glassy basalt clast with crenulated feldspar microlites set in a dark groundmass. Note how the neighbouring rigid chert clasts impinge upon and plastically deform the the basalt fragment (plane polarised light: sample 302)

(c) Highly altered, texturally immature volcanic clast. The complex network of curviplanar seams delineated by sericite are interpreted as relict perlitic fractures. (plane polarised light: sample 180)

(d) Carbonate altered basalt clast with mottled texture interpreted as relict spherical spherulites. Small brown chromite grains (eg. arrow) are dispersed throughout the fragment. (plane polarised light: sample 180)


a
1 mm

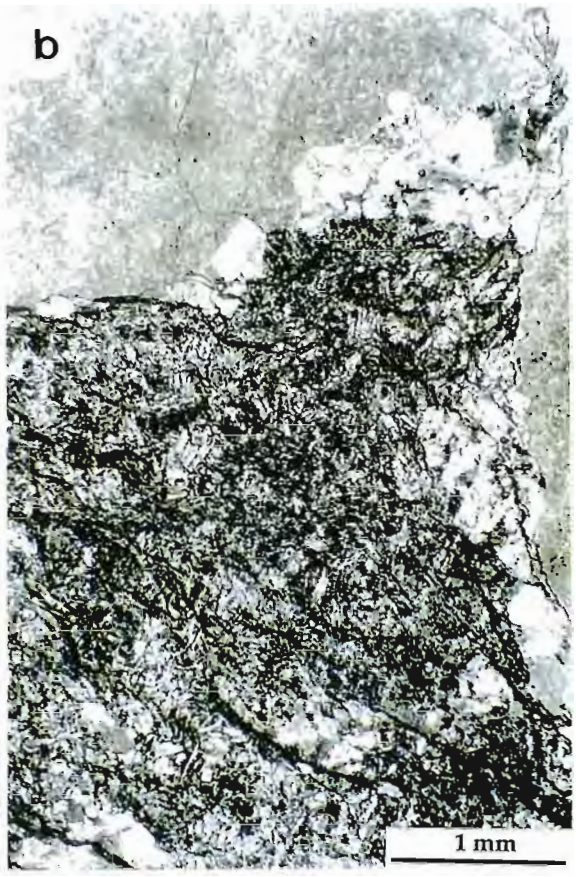
b
1 mm


c
1 mm


d
1 mm

aggregates of quartz. Banding defined by abrupt changes in crystal size was observed in some grains. Others show features which resemble devitrification textures in glassy volcanic rocks such as micropoikilitic textures and possible relict spherulites now seen as circular 'ghosts' or chalcedonic rosettes. Similar textures could also be developed in silicified oolitic limestone, so only in cases where clear phenocrystal textures were observed, were clasts included in the volcanic category. Feldspathic greywacke clasts of probable Crimson Creek Formation origin were recognised only in a few beds from the conglomerate package at Moores Pimple, where they occur in association with purple mudstone fragments containing scattered dolomite rhombs and significant quantities of opaque oxides.

Metamorphic lithic fragments form a minor constituent of all coarse-grained lithologies and include metaquartzite, phyllite and 'ribbon quartz' lithotypes.

The diversity and abundance of volcanic fragment-types increases towards the east. Due to the extensive alteration shown by most of these fragments and their small dimensions in the finer sandstones, the descriptions given below are largely of those identified in conglomerates and coarse-grained sandstones. In general, clast shapes are highly irregular, partly as a result of limited epiclastic reworking, but also due to their relative weakness compared to neighbouring 'rigid' fragments, which have impinged upon and distorted the volcanic clasts during sedimentary compaction and deformation. The most common fragments are mafic to intermediate in composition and exhibit vitric and vitrophyric textures in which fractured plagioclase phenocrysts up to 3mm occur set in a glass-charged groundmass of feldspar microlites, fine-grained chlorite and opaque oxides (Fig. 4.15b). Feldspar microlites and phenocrysts are commonly extensive altered to chlorite, calcite or sericite. Rarely they contain anhedral to euhedral intersertal grains of chlorite, epidote or calcite which may have replaced ferromagnesian crystals. These closely resemble the type *2c* basaltic/andesitic fragments contained in suite 2 rocks and may involve a similar parent lava type.

Found only in conglomerates from the eastern area is a highly altered, Cr-spinel bearing mafic volcanic clast type. Fragments are almost completely altered to carbonate, however a network of planar to curvaceous seams, defined by sericite and resembling relict perlitic texture is developed in many examples (Fig. 4.15c). Small circular clots of fine-grained carbonate, interpreted as relict spherulitic texture, are also shown in a few clasts (Fig. 4.15d). The association of inferred relict spherulitic and perlitic textures is considered to indicate that the volcanic parent of this clast-type was originally glassy. With the exception of very small (0.04-0.2mm), euhedral to anhedral brownish-red chromites, no phenocrysts are preserved. As with the feldspathic clast-type described in the previous paragraph, these clasts show highly irregular shapes and are likely to be proximally derived.

Volcanogenic fragments interpreted to have intermediate to felsic compositions are rare. They include feldspar/?pyroxene, quartz/feldspar, and quartz-porphyritic varieties. The originally glassy groundmass in these fragments is entirely recrystallised to fine quartz and albite. A banded texture is developed in a few quartz-phyric clasts which may represent flow banding in a rhyolitic lava precursor. This clast-type may have been reworked from coherent lavas, intrusive rocks or perhaps felsic tuffs.

4.7.3 Chemical composition and source characteristics

Whole rock geochemical data for suite 3 is shown in Table 4.3. Both sandstones and mudstones are broadly intermediate to acidic in composition and have SiO_2 contents ranging from 60 to 78wt% (average: 65wt%), with the exception of two dolomitic mudstone samples from Bonnie Point (samples 884 and 22: 58 and 46wt% SiO_2 respectively). TiO_2, Fe_2O_3, MgO and P_2O_5 abundances are on average lower than those of suite 1 and indicate a lesser contribution from a basaltic source. This feature is also shown in PAAS-normalised spider diagrams (Fig. 4.16) which involve relatively flat patterns with absolute abundances of immobile elements comparable with average upper crustal compositions (ie. granodioritic: Taylor and McLennan, 1985). These patterns are in marked contrast to the 'spiked' form of suite 1 patterns (in particular the sharp peaks at Nb and Ti are absent) and lack the steeply increasing gradient from incompatible to compatible elements characterised by suite 2. Apart from subtle peaks, or in a few cases troughs, at P and Sc and a slight trough at V, there is an overall enrichment of progressively more compatible elements relative to PAAS (ie. positive increase from left to right in the diagrams). This relatively smooth positive trend of the patterns is interpreted to indicate a minor basic component. The sharp jump in Cr and to a lesser extent Ni shown by some samples supports this interpretation, however the large range in values relative to other elements suggests that anomalously high values are enhanced by heavy mineral concentration. Heavy mineral fractionation is also considered to account for the variation in high field strength elements (HFSE) in sandstones (Fig. 4.16a). Th, Nb, LREE, Zr, and Ti all show enrichment in samples 858 and 222 (located in central and eastern areas) relative to 835 and 839, however the slopes of the multi-element patterns defined by these elements are comparable for all samples. The parallel increases of Th, LREE, Zr and to a lesser extent Th, are likely to reflect concentration of these elements in zircons, whereas Ti and Nb enrichment is considered to indicate fractionation of rutile or Fe-Ti oxides. These interpretations are consistent with petrographic evidence, which shows an abundance of both zircons (in particular euhedral grains), rutiles as well as chromites in sandstones from the eastern parts of the Dundas region. As phosphates were not recognised as part of the heavy mineral assemblage in suite 3 sandstones, enrichment of HFSE relative to P would be expected in sandstones in which the heavy mineral fraction has affected absolute element abundances. The anomalous trough at P

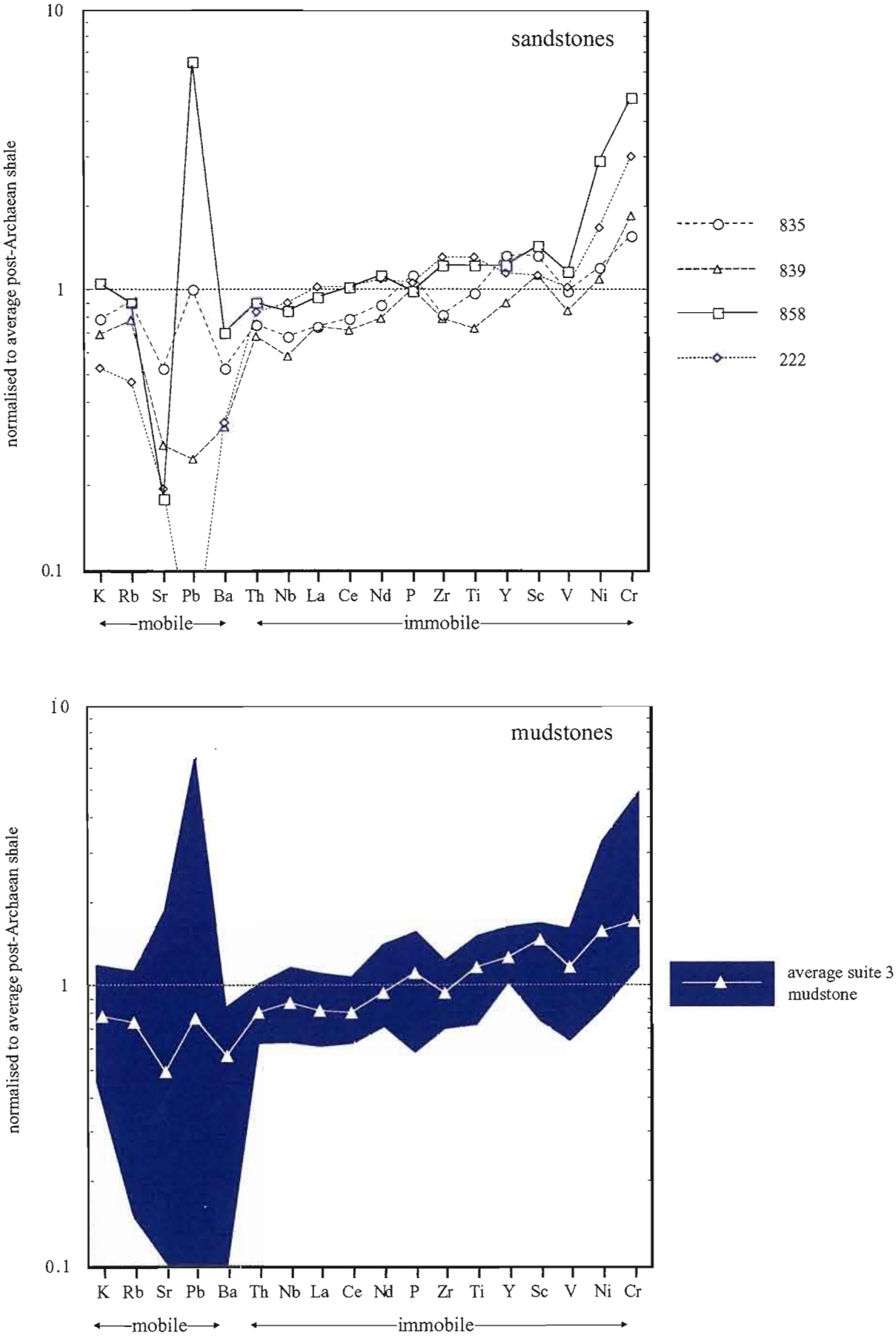

Figure 4.16. Average post-Archaean shale normalised extended trace element and LREE plot for suite 3 sandstones and mudstones. The coloured field in (**b**) encompasses 17 samples.

shown in the patterns of samples 858 and 222, is thus not a true reflection of source characteristics, but an artefact of heavy mineral concentration.

Berry and Fulton (1994) suggested that high abundances of heavy minerals could be achieved by pre-erosional concentration of resistant phases within the weathering profiles of tectonically inactive, low-lying source terrains. This mechanism could in part have attributed to the inferred high concentrations of resistant mineral phases in some suite 3 sandstones. Alternatively, heavy mineral concentration could have resulted from intrabasinal reworking of sandstones by bottom current activity. Stow and Lovell (1979) indicate that winnowing of fine-grained detritus (from sediments possibly originally deposited from turbidity currents) by bottom currents can produce a concentration of dense detrital components in residual sands. This interpretation is particularly attractive for sample 858 which occurs as part of a succession which displays a range of sedimentary textures consistent with bottom current reworking (ie. sub-facies 3B: section 3.4.2).

4.7.4 Discussion of likely sources

Unlike the dominantly mono-genetic source signatures characterised by suites 1 and 2, the provenance of suite 3 appears more complex with significant contribution from two or more source terrains. Evidence from petrographic studies suggests input of detritus from: i) mature siliciclastic sources (ie. abundant sub-rounded and strained quartz, muscovite, ultrastable heavy minerals, meta-sedimentary lithic fragments), ii) basaltic source terrains (ie. volcanic lithic fragments, feldspathic greywacke clasts, detrital chromites) and iii) minor acid to intermediate volcanic sources (ie. quartz and feldspar-phyric volcanic lithic fragments, euhedral zircons, quartz and feldspar grains of probable volcanic origin). In terms of the geochemistry, increased contribution from an 'acid' source (ie. mature basement sequences or felsic to intermediate volcanic sources) is indicated by elevated SiO_2 contents, reduction in the abundances of ferromagnesian elements and the 'flatter' patterns in PAAS-normalised spider diagrams compared to the more 'basaltic' suites 1 and 2. That the 'flat' multi-element patterns correspond to a single source with average upper crustal compositions is considered unlikely as the peak at Cr clearly indicates input of primitive mafic or ultramafic material. A mixing of discrete incompatible element enriched and depleted sources is the preferred interpretation for the shape of the patterns. As mixing of detritus has effectively masked the chemical signature of the various parent rocks however, determination of individual source terrains is difficult.

In a novel approach to determine the relative contribution from likely source areas in sediments of mixed provenance, Floyd et al. (1989) applied mixing equations originally formulated by Langmuir et al. (1978) to identify magma and source mixing in igneous rocks. On a bivariate trace element plot, data representing varying degrees of

mixing between two chemically distinct sources would be expected to scatter along an asymptotic curve linking the two source compositions. Floyd et al. (op cit.) calculated the mixing curves for their sediment groups on the basis of the most extreme compositions of the chemical data set. They considered that extrapolation of the curve away from the extreme sediment compositions would point towards the dominant "end member" sources and that deviation of data from the simple mixing curve indicated variation in the composition of the source area or contamination from an additional component.

The Cambrian system in western Tasmania is well suited for this method of provenance analysis as not only are the compositions of potential sources areas highly variable and distinctive, but they are also well constrained. The P/Zr vs Ti/Sc plots in Figure 4.17 show mixing curves calculated from average compositions of potential source terrains: Crimson Creek Formation; MUC; 'shoshonitic' lava suite of the Mt Read volcanics; Oonah Formation mudstone (mature continental basement). The method used here is thus opposite to that of Floyd et al. (op cit.) with curves constructed on the basis of assumed source compositions rather than chemical trends in the sediments. This is mainly due to fact that suite 3 data does not conform to simple mixing of two sources. Element ratios used in the plot were chosen to best discriminate between the inferred source regions. Arc-type volcanic sources (ie. MUC and shoshonitic lavas) are effectively discriminated from the tholeiitic rocks of the Crimson Creek Formation using Ti/Sc (compare Figs 4.10b, c and d), whereas strong depletion of P coupled with enrichment of Zr in mature continental basement terrains allows discrimination from basaltic sources using P/Zr (see Appendix A). Included in these plots are mudstone data from all suites. As expected, suite 1 data plot close to or within (ie. suite 1B) the Crimson Creek tholeiite field (Fig. 4.17b). Two thirds of this data lies along the curved predicted for mixing of *average* Crimson Creek tholeiite and Oonah Formation, with deviation of the remainder probably reflecting variation in source area composition (which in the Crimson Creek Formation is considerable). Suite 3 mudstone data shows a larger spread, but plots neatly within the 'wedge' defined by mixing curves between 'arc-type' lavas, Crimson Creek Formation and the Oonah Formation. It is unclear as to whether there is true mixing of all three components or whether the vertical scatter between the two curves reflects compositional variation within a single mafic/ultramafic source. There does appear to be a clear distinction in mafic/ultramafic source shown by some data however, with several mudstones displaying clear affinities with an arc-type volcanic component and others plotting close to the Crimson Creek tholeiite curve. Those which display 'arc-type' affinities are generally positioned low in the stratigraphy (eg. Hodge Slate and mudstones intercalated with suite 2 rocks), however two samples of probable latest Middle Cambrian age (ie. 22 and 390) also occur within this group (Table. 4.3). Mudstones containing a probable Crimson Creek Formation input are mainly from the

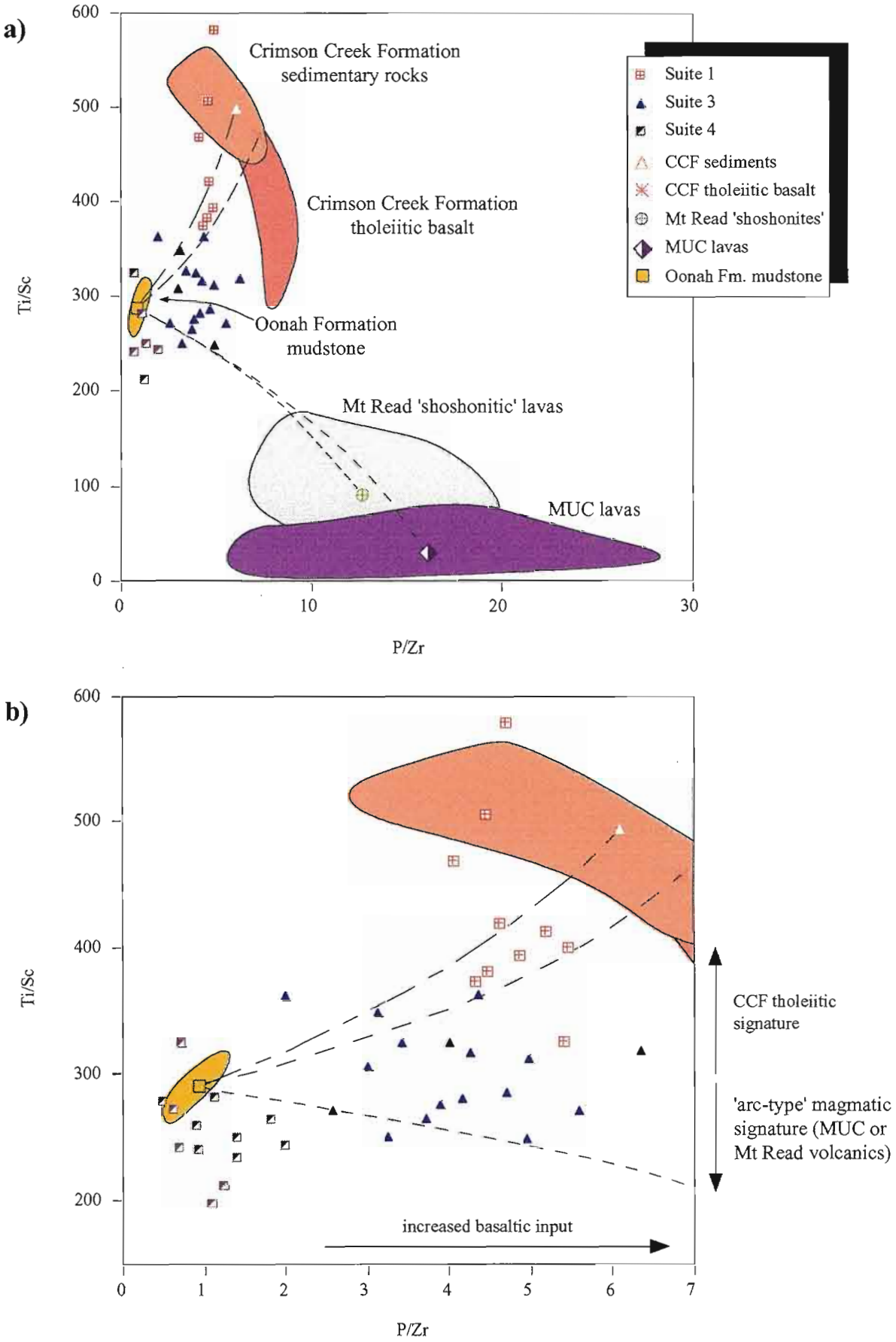

Figure 4.17. P/Zr vs Ti/Sc mixing plot for mudstones. Mixing curves are calculated from the equations of Langmuir et al. (1978) on the bases of average compositions of potential source terrains.
Data sources: i) Oonah Formation - this study
ii) Crimson Creek Formation sediments - Brown (1986), Haines (1991), this study
iii) Crimson Creek Formation tholeiitic basalts - Brown (1986)
iv) Mt Read volcanics - Crawford et al. (1992)
v) MUC - Brown (1986), Crawford and Berry (1992)

central area and occur at a variety of stratigraphic levels. Plotting closest to the Oonah Formation "end member" are samples from the Upper Cambrian Climie Slate from the western area. These data show significant vertical scatter with possible input from either mafic/ultramafic source.

Sandstones show a similar distribution on the P/Zr vs Ti/Sc plot (Fig. 4.18). The increased scatter and deviation of suite 1 samples from the Crimson Creek tholeiite field is interpreted to result from heavy mineral fractionation of Zr and Ti. Suite 1C sandstones in particular appear effected by heavy mineral fractionation, with high Ti/Sc and generally low P/Zr values. Similarly, the two suite 3 sandstone samples which were interpreted in the previous section to show evidence of zircon, rutile and/or Fe-Ti oxide concentration (ie. 858 and 222) plot towards lower P/Zr. Although there is some petrographic evidence for input from a Crimson Creek Formation-type source in the eastern parts of Dundas region (ie. feldspathic greywacke clasts and feldspar/Fe-Ti oxide bearing basalt fragments) it is uncertain as to whether the moderate Ti/Sc values shown by these sample truly indicate a dominant tholeiitic component. The remaining suite 3 samples appear to show greater affinities with an 'arc-type' volcanic component, with possible mixing of tholeiitic material in sample 835. Both 835 and 839 are situated towards the lower part of the Dundas Group stratigraphy in the type area (Razorback Conglomerate) and match well with the 'arc-type' signature shown in mudstones positioned at similar stratigraphic levels. Note also the very good fit of suite 2 sandstones along the 'arc-type' volcanic - Oonah Formation mixing curve.

Discrimination between a MUC or a Mt Read volcanic source in those samples interpreted to contain an 'arc-type' magmatic signature is not so straightforward. Cr-bearing basaltic fragments are so intensely altered, that primary mineralogies and textures are effectively destroyed and petrographic techniques cannot be used to identify parental volcanic rocks. In terms of the geochemical signature of the two potential source lithologies however, Mt Read volcanics 'shoshonitic' lavas are clearly distinguishable from MUC lavas through extreme enrichment of incompatible elements (ie. LREE, P and possibly Th: see Fig. 4.10). In support of an MUC-derived component, are the generally low values of P_2O_5 and LREE relative to suite 1 and suite 3 mudstones interpreted to contain an input from the Crimson Creek Formation. Very subtle 'enrichment' of these elements in one (824) sample however, combined with slight elevation of La/Sc and P_2O_5/TiO_2 may indicate contribution of a more enriched basaltic source. Although evidence for a 'shoshonitic' input is admittedly weak, such material would not be unexpected considering the recognition of a volcaniclastic deposit of late Middle Cambrian age containing proximally derived 'shoshonitic' debris (see section 3.7).

A compositional study of chromites contained in suite 3 sandstones would aid in resolving the problems regarding the parentage of the 'arc-type' basic component. As shown in Figure 4.11, chromites derived from the MUC are likely to be distinguishable

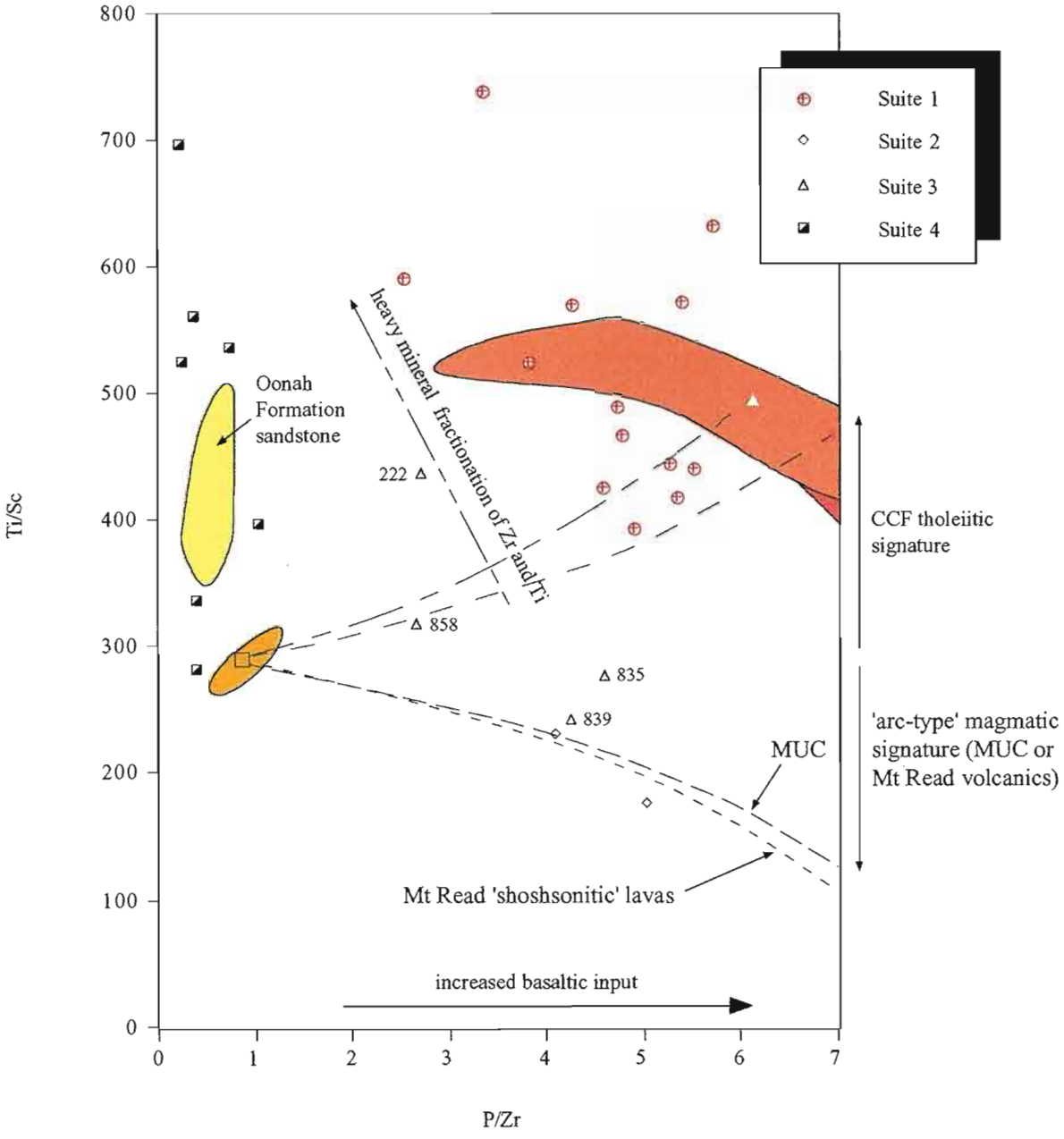

Figure 4.18. P/Zr vs Ti/Sc mixing plot for sandstones. Trend towards higher Ti/Sc and lower P/Zr in sandstones from the Dundas region is interpreted to reflect heavy mineral fractionation of Ti and Zr. Increased Ti/Sc values for mature Oonah Formation sandstones relative to mudstones results from significant Sc 'depletion' in the former. This is due to the partitioning of ferromagnesian elements into clay minerals and hence finer-grained lithotypes. Legend for compositional fields of potential sources is shown in **Figure 4.17**.

from those contained within shoshonitic lava fragments on the basis of the TiO_2 contents. Unfortunately, such a study was prevented by time constraints. What can be inferred with confidence however, is that the mafic detritus was derived from a proximal source, as indicated by the highly irregular, unreworked shape of the lithic fragments.

4.8 Suite 4

Suite 4 involves compositionally and texturally mature, sandstones, mudstones and fine-grained meta-sedimentary rocks (schist). The suite is defined by P/Zr values ≤ 2 and Ti/Th ≤ 425 (Table 4.4). High end member values are shown by fine-grained lithotypes. These values are only slightly lower than those of the most "felsic" suite 3 mudstones and are interpreted to indicate a close compositional association between these rocks. In contrast, chemical distinction between suite 4 sandstones and the remaining suites is readily achieved on the bases of absolute element abundances and incompatible-compatible element ratios, principally due to the lack of a basaltic component in the former.

4.8.1 Sample distribution

Suite 4 samples were collected from: a) the Moores Pimple-Comet Maestries region (shown in Figure 4.1 as the "Comet area"), b) a fault bounded block which crops out in the Ring River (eastern area) and c) the Farrell Rivulet 'quartzwacke'/conglomerate package (as defined by Corbett and Lees, 1987) situated approximately 5km south of the Dundas region. Additional unpublished data from the ?Middle Cambrian Stitt Quartzite situated to the east of the Rosebery Mine (approximately 7km NNE of the study area) are included from Berry et al. (1995).

The stratigraphic position of some of these units has been the focus of controversy for some years. For instance, the intercalated succession of quartz arenites, mudstone and schistose sediments (ie. Concert Schist) at Moores Pimple have been traditionally interpreted as a basement inlier comprising correlates of the Precambrian Oonah Formation and metasediments of the White Schist (Elliston, 1954; Turner, 1979; Brown, 1986). More recently however, workers have highlighted the textural and compositional similarities between units contained within this package and the ?Middle Cambrian Stitt Quartzite (Findlay, 1994; Brown et al., 1994). The aim of the present study is to compare the petrographic and compositional characteristics of these less well constrained units with samples from the type areas of the Stitt Quartzite and Oonah Formation in order to identify any systematic variations between basement and Dundas trough lithologies.

4.8.2 Sandstone Petrography

The petrographic features of sandstones from all areas are remarkably consistent. Quartz comprises the bulk of the framework component. In some instances strain

Table 4.4 Whole rock geochemical data for Suite 4.

Lithology	**Sandstone**												**Mudstone**					**Schist**							
	Comet area								*Stitt Quartzite and correlates*															
Sample #	**D3**	**D4**	**D9**	**D16**	**D35**	**D59**	**D7**	**D32**	**F7**	**Henry**	**SQ1****	**SQ2****	**D2**	**D22**	**D33**	**D34**	**D52**	**402**	**446**	**465**	**472**	**477**	**D45**	**D48**	**D50**
SiO2	92.86	90.57	96.09	91.42	94.23	91.02	93.13	94.23	80.74	84.32	94.47	91.35	67.07	68.54	74.34	71.26	72.17	65.01	69.94	66.62	65.01	63.34	64.26	64.12	63.13
TiO2	0.26	0.27	0.39	0.35	0.28	0.40	0.28	0.19	0.52	0.51	0.26	0.37	0.71	0.69	0.81	0.88	0.71	1.34	1.12	1.04	1.28	1.06	1.10	1.22	1.06
Al2O3	3.34	3.97	2.55	3.91	4.02	6.20	3.53	2.52	12.09	8.71	3.62	5.75	18.97	20.03	17.53	20.84	16.27	23.90	18.92	19.41	21.36	20.54	19.63	20.67	24.32
Fe2O3 (tot)	2.29	3.45	0.17	2.47	0.18	0.29	1.81	1.87	2.18	3.29	0.28	0.41	6.10	4.76	1.62	0.71	4.72	1.87	2.14	6.24	4.38	7.40	7.81	5.58	2.07
MnO	0.01	0.04	0.00	0.04	0.00	0.00	0.06	0.04	0.00	0.01	0.00	0.00	0.08	0.03	0.02	0.00	0.04	0.00	0.00	0.01	0.00	0.02	0.04	0.00	0.00
MgO	0.58	0.78	0.09	0.80	0.15	0.21	0.15	0.39	0.85	1.03	0.20	0.27	1.84	0.63	0.89	0.71	1.50	0.90	1.70	1.68	1.67	2.30	2.28	2.05	1.63
CaO	0.07	0.09	0.01	0.03	0.01	0.06	0.02	0.08	0.01	0.04	0.01	0.03	0.12	0.00	0.04	0.01	0.11	0.00	0.01	0.00	0.15	0.05	0.04	0.01	0.03
Na2O	0.09	0.10	0.04	0.02	0.05	0.11	0.05	0.04	0.11	0.12	0.01	0.03	0.34	0.26	0.29	0.23	0.17	0.48	0.25	0.32	0.31	0.29	0.26	0.29	0.37
K2O	0.45	0.68	0.63	0.93	1.05	1.62	0.92	0.58	3.46	1.94	1.12	1.75	4.68	5.02	4.38	5.26	4.23	6.42	5.88	4.61	5.70	4.90	4.45	6.00	7.32
P2O5	0.04	0.04	0.03	0.02	0.02	0.08	0.03	0.06	0.03	0.03	0.02	0.03	0.10	0.04	0.07	0.11	0.08	0.07	0.04	0.06	0.15	0.09	0.13	0.05	0.07
La	22	20	27	22	19	27	18	18	38	36	15	24	48	47	49	62	48	69	52	46	60	57	52	62	63
Ce	49	45	60	45	43	61	55	47	84	73	39	57	102	96	105	141	99	145	107	85	122	113	101	125	124
Nd	21	19	25	22	17	25	21	22	37	32	15	24	45	45	48	68	44	62	48	41	59	53	50	57	56
Nb	8	9	8	8	7	10	6	4	13	13	6	8	21	13	19	21	21	29	23	20	25	26	22	26	24
Zr	242	195	492	313	193	273	257	171	272	267	273	290	238	203	344	313	255	276	296	231	275	233	218	277	228
Sr	20	19	31	18	20	18	11	17	27	16	8	9	73	51	70	85	43	194	84	120	355	265	97	121	120
Cr	15	16	11	15	14	26	12	9	62	37	36	34	75	108	66	82	65	166	110	119	143	137	133	133	137
Ba	48	75	77	103	106	190	74	74	684	206	294	386	549	508	594	592	432	620	478	387	864	663	551	305	511
Sc	1	3	1	3	1	6	2	1	11	9	3	4	17	17	15	25	15	31	24	26	29	27	27	27	32
V	20	24	13	19	17	30	17	18	58	46	22	28	102	121	85	112	101	228	157	189	203	193	190	166	188
Y	17	17	23	21	15	24	16	13	33	29	17	24	40	44	47	83	40	49	47	40	50	42	44	50	55
Rb	35	48	35	42	43	75	80	28	154	88	46	70	212	200	185	222	187	275	214	189	248	230	194	250	273
Th	7	7	7	6	5	10	7	3	15	11	5	9	19	17	18	24	17	22	19	19	18	18	17	18	19
Ni	15	14	3	3	2	3	5	4	25	17	4	6	20	42	11	15	18	6	9	27	55	53	35	1138	21
Pb	59	26	82	4	9	8	1175	3	109	3	8	60	6	45	11	5	12	56	34	9	9	34	6	5	5
Ti/Zr	6.37	8.25	4.79	6.67	8.85	8.69	6.63	6.75	11.43	11.34	5.76	7.74	17.91	20.25	14.14	16.91	16.59	29.12	22.63	26.99	27.86	27.17	30.16	26.50	27.80
Ti/Y	90.70	94.61	102.51	99.45	113.87	98.90	106.57	88.84	94.19	104.41	92.54	93.49	106.56	93.42	103.50	63.77	105.76	164.01	142.54	155.88	153.26	150.73	149.45	146.82	115.25
Zr/Sc	242.00	65.00	492.00	104.30	193.00	45.50	128.50	171.00	24.73	29.67	91.00	72.50	14.00	11.94	22.93	12.52	17.00	8.90	12.33	8.89	9.48	8.63	8.07	10.26	7.13
Ti/Sc	1541.98	536.15	2357.70	696.16	1708.04	395.58	852.54	1154.91	282.57	336.43	524.41	560.95	250.73	241.78	324.30	211.71	282.03	259.24	279.14	239.81	264.23	234.46	243.54	271.88	198.08
Cr/Nb	1.88	1.78	1.38	1.88	2.00	2.60	2.00	2.25	4.77	2.85	6.00	4.25	3.57	8.31	3.47	3.91	3.10	5.72	4.78	5.95	5.72	5.27	6.05	5.12	5.71
Ni/Nb	1.88	1.56	0.38	0.38	0.29	0.30	0.83	1.00	1.92	1.31	0.67	0.75	0.95	3.23	0.58	0.71	0.86	0.21	0.39	1.35	2.20	2.04	1.59	43.77	0.88
La/Sc	22.00	6.67	27.00	7.33	19.00	4.50	9.00	18.00	3.45	4.00	1.88	2.67	2.82	2.77	3.27	2.48	3.20	2.23	2.17	1.77	2.07	2.11	1.93	2.30	1.97
Th/Sc	7.00	2.33	7.00	2.00	5.00	1.67	3.50	3.00	1.36	1.22	1.67	2.25	1.12	1.00	1.20	0.96	1.13	0.71	0.79	0.73	0.62	0.67	0.63	0.67	0.59
P/Zr	0.58	0.73	0.21	0.22	0.36	1.02	0.41	1.22	0.39	0.40	0.25	0.36	1.40	0.72	0.73	1.25	1.13	0.91	0.48	0.94	1.83	1.39	1.99	0.64	1.10
Ti/V	77.10	67.02	181.36	109.92	100.47	79.12	100.30	64.16	53.59	65.82	71.51	80.14	41.79	33.97	57.23	47.26	41.89	35.25	42.67	32.99	37.75	32.80	34.61	44.22	33.72
Ti/Th	220.28	229.78	336.81	348.08	341.61	237.35	243.58	384.97	207.22	275.26	314.65	249.31	224.34	241.78	270.25	220.53	248.85	365.29	352.59	328.17	425.71	351.70	386.80	407.82	333.60
Cr/Zr	0.06	0.08	0.02	0.05	0.07	0.10	0.05	0.05	0.23	0.14	0.13	0.12	0.32	0.53	0.19	0.26	0.25	0.60	0.37	0.52	0.52	0.59	0.61	0.48	0.60
Nb/La	0.36	0.45	0.30	0.36	0.37	0.37	0.33	0.22	0.34	0.36	0.40	0.33	0.44	0.28	0.39	0.34	0.44	0.42	0.44	0.43	0.42	0.46	0.42	0.42	0.38
P2O5/TiO2	0.15	0.15	0.08	0.06	0.07	0.20	0.11	0.32	0.06	0.06	0.08	0.08	0.14	0.06	0.09	0.13	0.11	0.05	0.04	0.06	0.12	0.08	0.12	0.04	0.07
Zr/Nb	30.25	21.67	61.50	39.13	27.57	27.30	42.83	42.75	20.92	20.54	45.50	36.25	11.33	15.62	18.11	14.90	12.14	9.52	12.87	11.55	11.00	8.96	9.91	10.65	9.50

* major elements presented as volatile-free percentages

** data from Berry et al. (1995: unpublished AMIRA report)

features such as sub-grain development, deformation lamellae and deformation bands are developed. The original outlines of grains are obscured in most samples due to secondary silicification and grain-grain suturing. Where detrital cores were observed however, they involved rounded to sub-angular forms. There is no evidence to suggest that quartz of volcanic origin is included in these sandstones. Feldspar grains are uncommon and include untwinned albite and K-feldspar. Much of this material has probably degraded to clays as a result of source area weathering and polycyclic reworking. Some of the sericite-altered grains with poorly defined margins are thus probably relict feldspars. Apart from these grains, unstable mineral assemblages such as ferromagnesians are absent. The micaceous component includes muscovite flakes ranging in thickness from <0.01mm to 0.05mm in their shortest dimension and rare books of biotite which have been partially altered to chlorite.

Sedimentary rock particles comprise the bulk of the lithic fraction. These include fine-grained, light coloured 'cherty' fragments comprising textureless aggregates of equant microcrystalline quartz. Slightly darker pelitic fragments containing fine detrital white mica and quartz grains are interpreted to be derived from partly silicified mudstones. Low grade metamorphic fragments including quartz-mica schist, ribbon quartz and metaquartzite are generally subordinate to non-metamorphosed material. The highest concentration of these clast-types were observed in sandstones from the Farrell Rivulet 'quartzwacke'.

The heavy mineral assemblage is ultra-mature and includes yellow-green and blue-green euhedral to rounded tourmaline, rounded zircon, minor rutile and rare skeletal opaques. Fine, radiating needles of rutile were observed as inclusions in detrital quartz grains. Authigenic pyrite and epidote comprise are common in some samples.

4.8.3 Chemical composition and source characteristics

Whole geochemical data for suite 4 is shown in Table 4.4. Sandstones are characterised by high SiO_2 (80-96 wt%), low abundances of P_2O_5, TiO_2 and ferromagnesian elements. Sr, CaO and Na_2O concentrations are also well below the ranges shown by other sandstones and reflect the paucity of labile constituents coupled with the dilution effect of quartz. In contrast to the remaining suites, there is poor correlation between the composition of sandstones and mudstones, with the latter showing relative enrichment in most trace elements (Zr is a local exception). Mudstones and schists involve moderate to high SiO_2 abundances (63-74 wt%) but are markedly enriched in Al_2O_3 and K_2O indicating the predominance of illites in the primary mineral assemblage. Enrichment of trace elements within fine-grained lithotypes relative to sandstones is unlikely to reflect any fundamental differences in source characteristics. In Figure 4.19, elements are plotted against Al_2O_3. As the feldspar content in these lithologies is very low, Al_2O_3 concentrations provide a rough estimate of the clay content

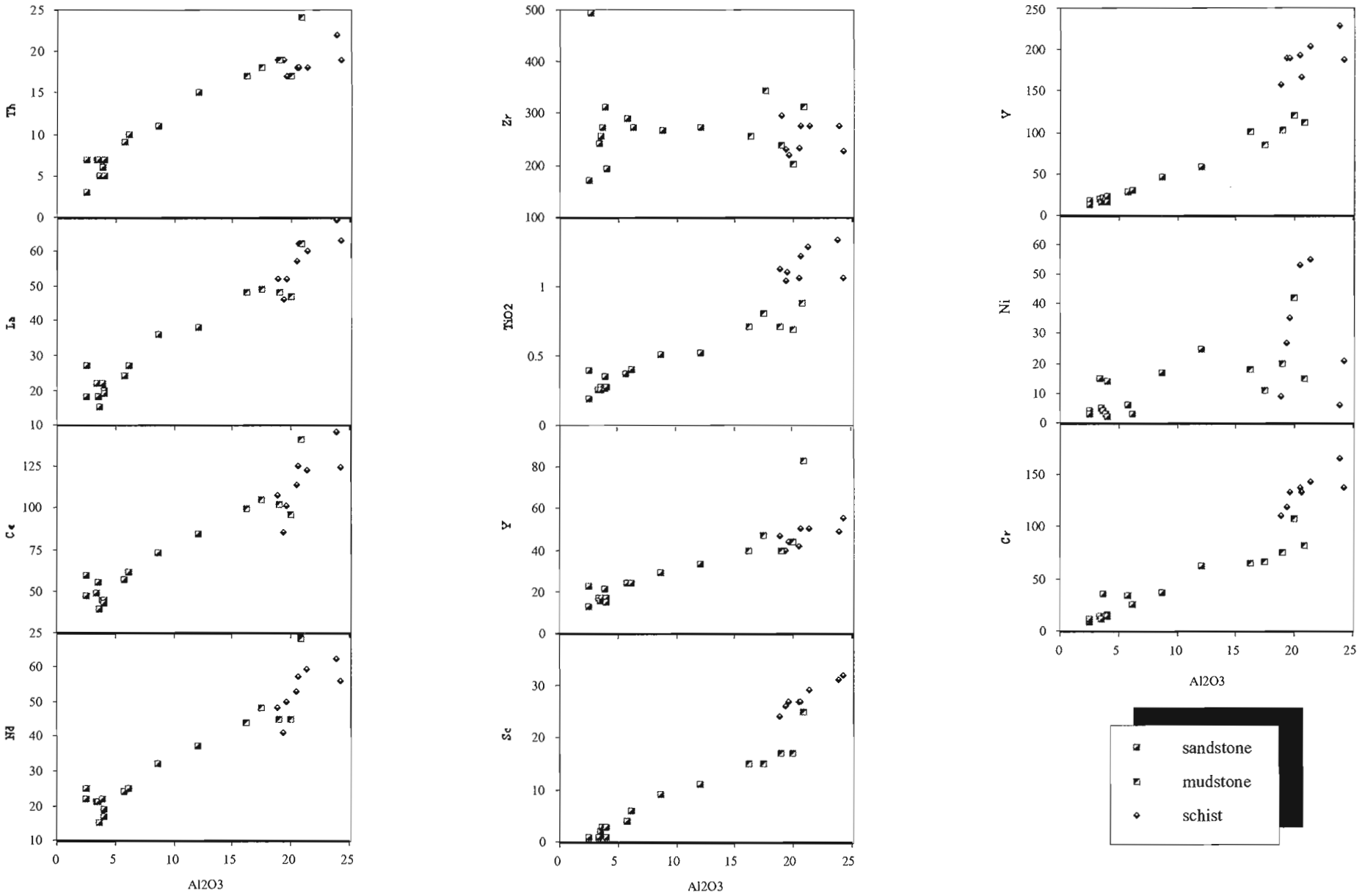

Figure 4.19. Plots of Al_2O_3 vs trace elements and TiO_2 for suite 4. Positive linear correlations are shown in most plots, with higher trace element abundances in fine-grained sediment and schist.

in the original unmetamorphosed sediment. The positive linear correlations shown in most of the plots are interpreted to indicate that trace elements abundances are controlled primarily by concentration in clay minerals (cf. Taylor and McLennan, 1985; McLennan et al., 1990). Exceptions to this rule include Zr and Ni. Zr abundances are fairly uniform regardless of grain-size or Al_2O_3 content, indicating that concentration of this element by zircons in sandstones roughly matches that by clays (or fine-grained zircons) in fine-grained lithotypes. The slight vertical scatter of Th, and LREE in sandstones suggests that these elements may also be housed within zircons. Ni abundances are highly variable, with the greatest range shown by the schistose rocks (up to 1138ppm). The high abundances of this element in fine-grained rocks would tend to indicate that heavy mineral fractionation is not responsible for anomalous values. Note also the higher absolute abundances of other ferromagnesian elements (Sc, V, Cr) as well as TiO_2 in the schists relative to mudstone samples. Enrichment of these elements is paralleled by trends towards lower Th/Sc, La/Sc, Zr/Sc, Ti/V, P/Zr and increased values of Ti/Zr, Cr/Nb and Cr/Zr in the schistose rocks, indicating an additional basic component (Table. 4.4).

PAAS-normalised spider diagrams for suite 4 are presented in Figure 4.20. The shape of the patterns for sandstones are remarkably similar (Figs. 4.20a, b), with slight vertical displacement shown by two Stitt Quartzite correlate samples (F7 and Henry). These two samples are anomalously low in SiO_2 and higher than other suite 4 sandstones in Al_2O_3 and K_2O (Table. 4.4). A higher 'clay' matrix content is indicated by these values, which may account for relative enrichment in most trace elements. However, Cr values are also slightly enriched in the 'cleaner' Stitt Quartzite samples relative to the sandstones from the Comet area. Furthermore, very slight but consistent relative increases in values of Cr/Zr and Cr/Nb, as well as a decrease in La/Sc for Stitt Quartzite samples (Table 4.4) tend to indicate subtle differences in the composition of suite 4 sandstones (ie. increased basic input for Stitt Quartzite samples). It should be noted however, that as the absolute abundances of most trace elements (in particular ferromagnesian elements) are so low in these rocks, ratios are likely to be very sensitive to localised enrichment due to heavy mineral concentration or increased clay content. As such, the chemistry of mudstones, which involve higher absolute trace element abundances and are less prone to anomalies due to heavy mineral concentration are considered to be more reliable in establishing variation in provenance characteristics.

Differences in the PAAS-normalised patterns of Comet area mudstones and the Concert Schists are shown mainly by greater enrichment of Sc, V and Cr relative to incompatible elements in the latter (Fig. 4.20c, d). Unfortunately, no mudstone samples from the Stitt Quartzite and correlates were analysed for whole rock chemistry and hence no direct comparison can be made.

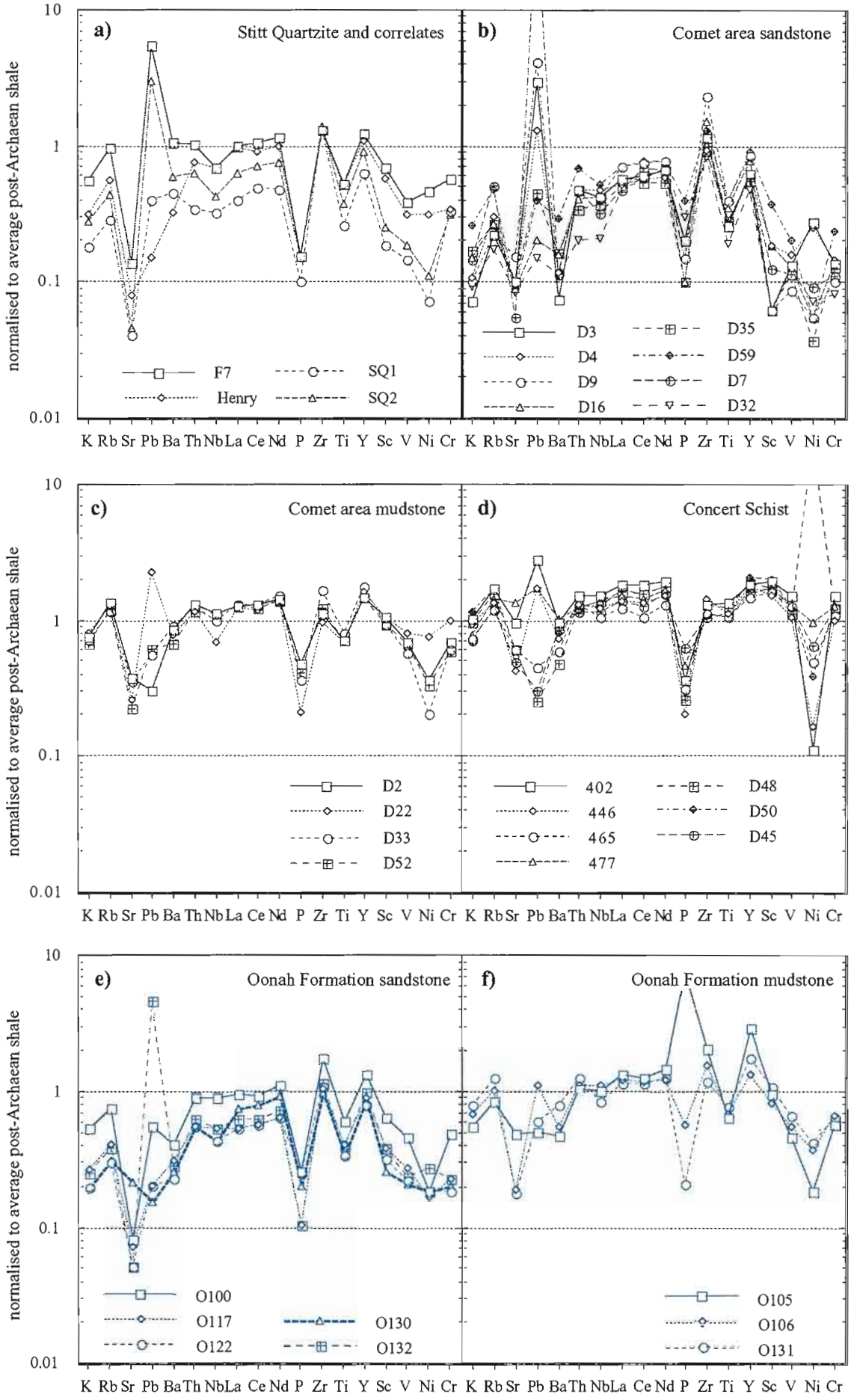

Figure 4.20. Average post-Archaean shale normalised extended trace element and LREE plot of suite 4 sandstones, mudstones and schists (**a-d**) and sedimentary rocks of the Oonah Formation (**e-f**).

Comparison of suite 4 with sandstones and mudstones of the Precambrian Oonah Formation (Fig. 4.20 e, f) reveals few differences. Oonah Formation sandstones are slightly lower in SiO_2 compared to Comet area sandstones and may have originally been richer in clay minerals. Although Cr/Zr and Cr/Nb values are generally higher than the ranges shown by Comet area sandstones, they are lower that Stitt Quartzite samples of equivalent SiO_2 content. Oonah Formation mudstones are indistinguishable in terms of the geochemistry from Comet area mudstones. Furthermore, the chemistry of Oonah Formation mudstones deviate from that of the Concert Schist in an identical fashion to the Comet area mudstones.

These results indicate good chemical correlation between the Oonah Formation and sandstones and mudstones of the Comet area. An additional basic component is indicated for the Concert Schist, and is also tentatively suggested for the Stitt Quartzite and correlates. It is emphasised however, that due to the dilution effect of quartz and the degradation of labile constituents, there is probably very little difference (in terms of whole rock geochemistry) between most compositionally mature sandstones. A more rigorous technique for discrimination between compositionally mature sediments is the chemistry of specific mineral phases (ie. zircons and if present, chromites). In order to definitively establish the relationship between the Oonah Formation and rocks of the Comet area, a detailed chemical study of the heavy mineral assemblages should be undertaken (cf. Berry and Fulton, 1994). If the Comet area rocks are of Cambrian age and post-date the emplacement of the MUC, then low-Ti Cr-spinels should be evident.

4.9 Summary of provenance characteristics

Contribution of detritus from sources of mafic composition is apparent in all suite 1-3 samples. Evidence for input of mafic detritus is provided from the petrographic characteristics of many of the studied sandstones (eg. basaltic lithic fragments, chromites), and is also shown in PAAS-normalised trace element plots, which involve ubiquitously 'enriched' concentrations (ie. normalised values >1) of ferromagnesian elements.

The chemistry of those sediments which contain a significant mafic component (ie. suite 1 and suite 2 sandstones) is strongly dependant on the composition of the mafic source(s). In a setting such as the Dundas Trough, where sediments have been derived from several *chemically distinct* mafic sources, ie. CCF, MUC and MRV, this feature is potentially useful provenance determination. Sediments which have most faithfully recorded the compositions of their mafic precursor involve suites 1A and 1B. These all show SiO_2 values $\leq 62\%$ and possess a geochemical signature which can be closely approximated with volcanic facies and volcanogenic sediment of the Crimson Creek Formation (CCF). In terms of absolute element abundances, the most distinctive feature of the CCF signature recorded in these sediments involves anomalously high values of

both Ti (>11000 ppm) and Nb (≥21ppm) relative to other incompatible element abundances. Accordingly, sediments which contain significant contribution from the CCF are effectively discriminated by their elevated values of Ti/Zr, Ti/Y, Ti/Sc, Nb/La and low Zr/Nb. Petrographically, coarse-grained sediments contain high concentrations of detrital Fe-Ti oxides, fractured feldspar grains and quench-textured basalt fragments. Samples examined in this study did not contain fresh ferromagnesian grains, however the composition of detrital clinopyroxene in sediments derived from less altered precursors may prove to be a useful tool in discriminating between basaltic sources.

Identification of MUC-sourced detritus from whole rock geochemical data alone is less effective than defining a CCF component. In samples which have been interpreted to involve a significant MUC input using this technique (eg. suite 2 sandstones), PAS-normalised multi-element plots show depleted values of incompatible elements (notably Th, Nb, LREE, Zr and Ti) and elevated concentrations of Sc and Cr. In addition, Ti and Zr concentrations are well below the ranges shown by sediments which involve a significant contribution from the CCF. Ratios involving elements with markedly different compatibilities are therefore considered to provide a good method of identifying an MUC source: Ti/Sc, La/Sc, Th/Sc, Nb/Sc, Nb/Ni, Nb/Cr and Zr/Cr all show low values. P_2O_5/TiO_2 and P/Zr are also useful in discriminating between MUC and CCF sources, with a trend towards higher values shown by the former. However, due to the very low concentrations of incompatible elements characterised by the MUC most of these ratios are prone to significant modification by only minor levels of contamination from other sources, particularly if heavy mineral concentrations have effected the composition of sediments. This problem is manifested in coarse-grained sandstones from Black Hill and in particular the Que River member (suite 1A). Despite evidence from petrographic features and chromite composition for a significant MUC input in these sediments, incompatible element enrichment due to zircon and Fe-Ti oxide concentration have caused the MUC signature to be masked. This can be overcome to some extent by employing ratios involving elements whose abundance is likely to be strongly controlled by heavy mineral concentration, such as Cr/Zr, or Cr/Nb. The values shown by these ratios essentially monitor the relative contribution from MUC (Cr in chromites), felsic volcanic/quartzose basement (Zr in zircon) and CCF (Nb in Fe-Ti oxide) sources.

Unequivocal evidence for an MRV mafic component has not been established. A possible contribution from this source has been identified in suite 3 siliciclastics. Features which might be attributable to a mafic MRV source include progressively increasing La with P_2O_5 and high values of P_2O_5/TiO_2 in some mudstones. The presence of scoriaceous debris and texturally immature feldspar-phyric basaltic/andesitic lithic fragments in suite 3 sandstones and conglomerates may also derived from MRV-sourced detritus. A compositional study of detrital chromites contained in suite 3

sandstones is considered as the best method for determining whether mafic successions of the MRV were active sources for Dundas Group sediments.

Contribution from mature basement siliciclastics and felsic volcanic sources of the MRV is best established from petrographic analysis. The association of stable minerals such as rounded zircon, tourmaline, rutile, coupled with detrital muscovite and metamorphic quartz grains with rounded cores in sandstones is considered to indicate contribution from mature basement sources. Conversely, assemblages including euhedral zircon, volcanic quartz and quartz-phyric volcanic fragments provide evidence for felsic volcanic input (eg. suite 1A, 3). Although simple incompatible/compatible trace element ratios (eg. Th/Sc, La/Sc, Ni/Nb, Zr/Cr etc.) provide a rough estimate of the relative contribution from mafic and 'felsic' sources, care must be taken to ensure that variation of these ratios is not merely recording changes in the chemistry of basic detritus. For instance, La/Sc values for a sediment containing a significant component of LREE-enriched shoshonitic detritus derived from the MRV would be extremely high compared to MUC-derived sediments.

4.10 Conclusions

1) Suite 1B siliciclastics from the eastern domain are distinguished from other CCF-derived suite 1 members by their textural and compositional immaturity. Furthermore, there is no evidence to indicate that source terrains of younger age than the CCF (ie. MUC or MRV) have contributed to detritus contained in these sediments. Although only one sandstone sample has been analysed in terms of detrital Cr-spinel composition, only high-Ti chemistries were found indicating exclusive contribution from the CCF. These features could possibly be explained by derivation from a proximal CCF source which was dominated by coherent volcanic facies. More likely however, is the interpretation that these sediments represent basement inliers which were structurally emplaced during Cambrian and/or Devonian phases of deformation. If this interpretation is correct, then other units located in the structurally complex eastern domain may also comprise uplifted slices of basement material (eg quartz-rich siliciclastics of suite 4).

2) The western-most exposures of the Dundas Group involve petrographically and chemically similar conglomerate-greywacke-mudstone successions which crop out at Dundas and at Que River to the north (Suite 1A). These are derived principally from basement sources (CCF and mature siliciclastic basement), however minor input from a felsic volcanic source is indicated from the presence of euhedral quartz grains. Contribution from the MUC in the Black Hill and Que River members is evident from low-Ti Cr-spinels, boninitic lava fragments and anomalously low Zr/Cr values. The most volumetrically significant suite 1A deposits include the Brewery Junction, Fernfields and Que River members. These range in age from latest Middle Cambrian to probable Late

Cambrian and represent a marked change in basin geometry characterised by rapid basement uplift. This phase of tectonism and associated sedimentation is slightly older than, to coeval with, the onset of Denison Group deposition further to the east. The Black Hill member is anomalous in that it is appears to be considerably older than other suite 1A siliciclastics. This is interpreted to indicate that repeated episodes of basement uplift and deposition of proximally derived debris occurred throughout the depositional history of the Dundas Group, particularly along the western margin.

3) The less distinctive, homogeneous geochemical signatures of suite 3 siliciclastics are interpreted to result from mixing of components from several different sources. This is indicated from the association of i) ultrastable heavy mineral assemblages, metamorphic and quartz-rich sedimentary lithic fragments derived from basement sources; ii) euhedral zircons and felsic volcanic lithic fragments derived from either felsic MRV terrains or reworked intrabasinal felsic tuffs; and iii) detrital chromites and mafic volcanic lithic fragments. The origin of the latter is uncertain, however the lack of rounding shown by the fragments indicates a proximal derivation. This complex provenance may have been achieved via mixing of several different sources in a shoreline setting prior to redeposition as turbidity currents. Alternatively, mixing may have occurred intrabasinally, either from the activity of strong bottom currents or reworking of sediment due to gravitational collapse of slope deposits.

4) Deposition of suite 3 siliciclastics occurred during the middle Middle Cambrian in the western domain, but continued into the latest Middle Cambrian in the central domain. During this latter period, suite 1A sediments were being deposited along the western margin of the basin, whereas coeval finer-grained suite 3 sediments occupied central or eastern portions of the basin. This asymmetry in lithofacies distribution from west to east probably reflects proximal derivation of suite 1A conglomerates and sandstones from rapidly uplifted basement sources to the west, with either reworking and mixing of slope sediments or supply of thoroughly mixed sediment along basin axial drainage systems (suite 3) to the east.

Chapter 5
Melange-type domains

5.1 Introduction and previous studies

Structural relationships in the Dundas region are most complicated towards the east and culminate in tightly folded and disrupted strata positioned within the footwall of the Rosebery Fault. The macroscopic geometry of these rocks is characterised by the dissection of a N-S trending generation of presently upright folds by an anastomosing array of steeply dipping faults (Corbett & Lees, 1987). Faulting out of major hinges has resulted in abrupt facing changes between adjacent blocks and in many instances, obscured the original geometry of large scale folds.

Recent mapping of this region has revealed a complex association of mesoscopic structural elements (Green, 1983; 1984; Corbett, 1984a; Corbett & Lees, 1987). In each study, workers have emphasised the disparity between the style of many of these structures and those developed in post-Cambrian sequences during Devonian deformation. The most conspicuous of these 'anomalous' structural elements involves zones of intense disruption in which sedimentary layering is commonly annihilated. These zones range between 5-150 m in width and in most cases have been recognised at the margins of fault bounded blocks. In the Ring River - Moores Pimple region however, they may also occur within discrete fault blocks. They are oriented either sub-parallel or at a low angle to bedding in neighbouring coherent strata and are positioned within steeply to moderately dipping limbs of major folds. To some extent, this style of deformation appears to be dependant upon the rheological properties of the sedimentary precursor. Loss of stratal continuity is most evident within originally well bedded sequences of mudstone and sandstone (eg. mudstone-dominated portions of correlates of the Stitt Quartzite). In these sequences, a mesoscopic 'block-in-matrix' fabric is characteristically developed in which dismembered sandstone horizons are enclosed within a matrix of pervasively sheared and foliated mudstone. Although fabrics of this type would clearly be difficult recognise in more massive units, it should be noted that they have not been described from volcanic lithologies or thickly bedded, conglomeratic sediments. In addition to the disrupted zones, a variety of mesoscopic fold styles have been described. Many of these exhibit 'chaotic' geometries and have been interpreted as having resulted from soft sediment deformation (Corbett and Turner, 1989). In the region to the west and northwest of Rosebery Mine, minor folds of likely 'tectonic' origin exhibit shallow to subvertical N and S plunges and locally may be downward facing (Green, 1983; Aerden, 1991). The dominant cleavage in this region (S_2 in this

study) is sub-vertical and strikes roughly parallel to the trend of minor folds. However, no direct relationships have been described between this cleavage and axial surfaces of folds.

Green (1983) and Corbett & Lees (1987) considered much of the deformation within the disrupted zones to be genetically related to a Cambro-Ordovician period of accretionary tectonics (see also Chapter 1). Their arguments were based largely on gross similarities between the mesoscopic fabric associations within these zones and descriptions of melange terrains from both modern and ancient accretionary complexes. The timing of this event was supported partly by the apparent lack of similar fabrics in the Siluro-Devonian sequences, and the local association of structures interpreted to have formed during soft sediment deformation. In addition, radiometric K-Ar dating of micas from cleaved Stitt Quartzite have provided ages ranging 485-475 Ma (Lower-Middle Ordovician) (Adams et al., 1985). Corbett and Turner (1989) have conceded however, that these ages may reflect partial resetting of detrital mica of Precambrian origin during the Devonian phase of orogenesis.

This tectonic model has been criticised by subsequent workers (Leaman et al., 1987; Berry and Crawford, 1988; Corbett and Turner, 1989) and is now generally considered to be unviable in the early Palaeozoic tectonic framework of western Tasmania. The nature and significance of the highly disrupted zones, however, remain poorly understood.

Since Green's (1983) description of 'melange-type' deformation in the footwall of the Rosebery Fault, this term has been applied to many disrupted units within Late Proterozoic to Middle Cambrian sediment-dominated sequences throughout Tasmania (Bischoff, 1983; Brown, 1986; Elliot et al., 1993; Findlay, 1994). In each of these studies, the 'melange-type' zones have be used to support palaeo-geographic and tectonic models. Despite the widespread usage of the term and the many models put forward to explain their genesis, none of these studies have properly addressed the structural geometry, mechanics of fabric development or the rheological properties of the sediment at the time of deformation. In her review of melange terrains, Raymond (1984) stressed that much confusion has arisen from many worker's attachment of a genetic significance to these elements. She strongly suggested therefore, that for the term to remain useful in structural geology, it should be applied primarily in a descriptive sense if the tectonic setting and mechanisms of formation are poorly constrained. Although I agree with Raymond's philosophy, from my reading of many recent studies on melanges, a seemingly unavoidable genetic connotation of the term, is that at least some component of the strain accumulated within melanges occurred *early* in the rock's history. Description of melange development late in the structural history of a deformation zone involving well-lithified sediments (eg. Hammond, 1987; LaFrance, 1989) are, in comparison, very rare.

Considering the widespread distribution of melange-type fabrics in Tasmanian rocks and the poor understanding of their nature and significance, it is timely that a detailed study of these fabrics be undertaken. In this section I describe the geometry and kinematics of meso- and microscopic fabrics associated with one of the best exposed disrupted zones from the Ring River. Comparisons are made with some of the more recent studies on the textures and mechanisms associated with melange development. I also present a discussion of their significance in terms of the structural evolution of lithologies contained within the footwall of the Rosebery Fault.

5.2 Ring River disrupted zone

Domains of melange-type deformation are well exposed in the Ring River, approximately 300 m east of the Ring Valley Mine (Figs. 2.1 and 5.1). They occur within a fault-bounded sequence of intercalated mudstone and sandstone which forms part of a strongly dismembered unit which extends discontinuously from Moores Pimple, NNE to the Pieman River area (Corbett and McNeill, 1986). Although more than 80% of the 400m thick sequence in the Ring River is disrupted, stratally coherent domains are locally preserved and provide the best insight into the lithological character of the unit prior to deformation. These reveal a well-bedded succession dominated by argillaceous lithotypes with subordinate massive and parallel laminated micaceous quartz sandstone beds which locally exceed 1 m in thickness. Fine grained portions involve thinly bedded intervals of black carbonaceous mudstone, phyllosilicate-rich mudstone and normally graded siltstone. Facing directions indicated from the latter are consistently to the ESE or SE, suggesting that the disrupted unit is situated on the eastern limb of a major NNE-trending anticline.

Movement on late-stage brittle faults has locally obscured the original geometry of both melange-type and coherent domains (Fig. 5.1). This is most apparent in the west of the section, where late stage structures are oriented at a high angle to the pre-existing structural grain. In this region, relict bedding and early deformation fabrics are either rotated into parallelism with major E-W striking faults or strongly modified. To the east however, strain associated with brittle faulting is less intense and early fabrics have suffered only minor modification. Due to the particularly good exposures in the eastern region, and the relative lack of additional complexity from late stage deformation, sampling and the descriptions presented below are largely confined to this portion of the section.

The strike of bedding within stratally coherent domains is locally variable due to rotation during late-stage brittle faulting and dips are moderate, rarely exceeding 65°. Small scale angular box-shaped folds with upright or steeply E-dipping axial planes and wavelengths ranging 2-300 mm are locally observed in thinly bedded units. Fold

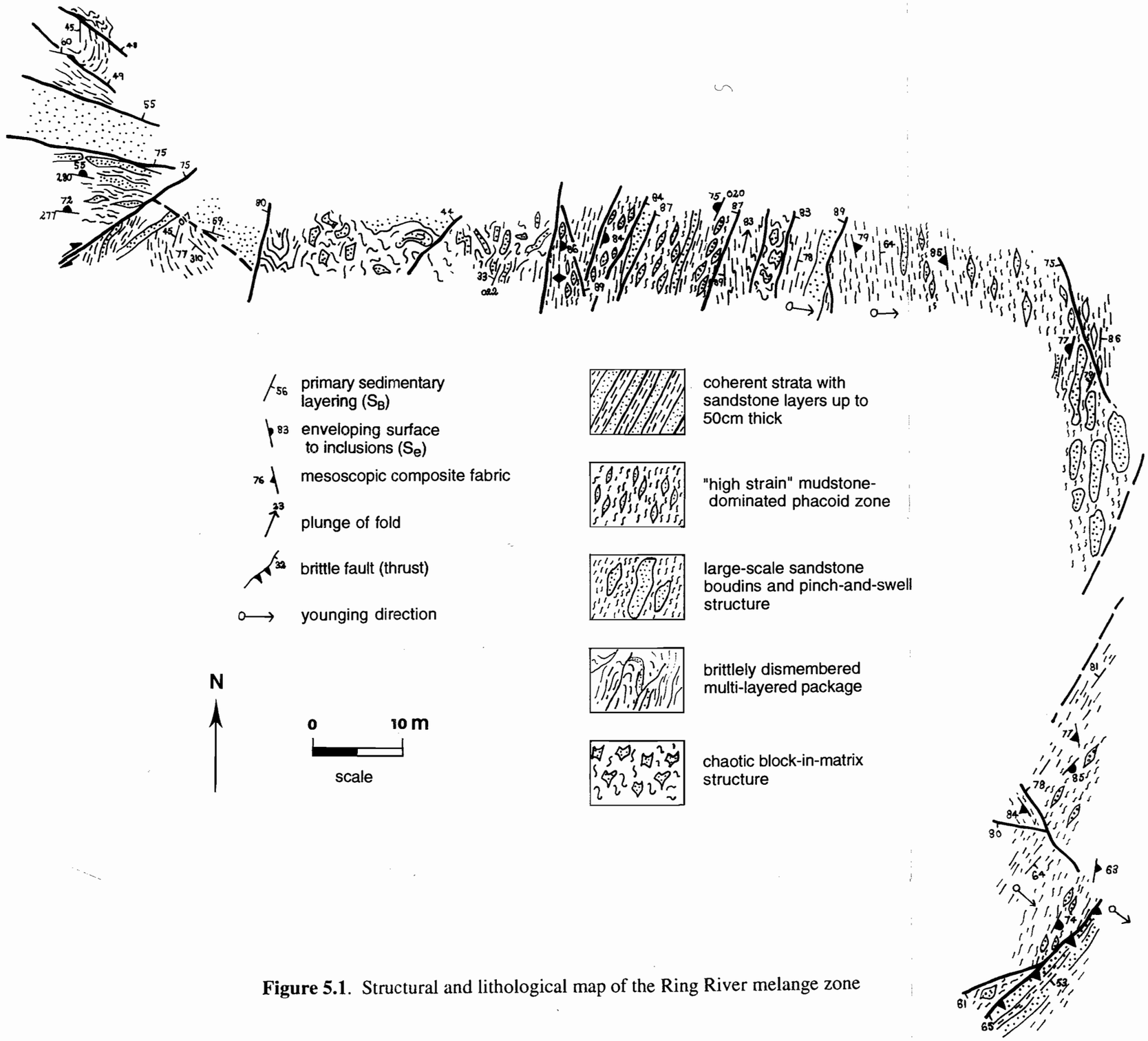

Figure 5.1. Structural and lithological map of the Ring River melange zone

profiles are both symmetrical and asymmetrical, the latter exhibiting northwesterly vergences. An associated closely spaced cleavage crenulates bedding laminations.

The dominant texture common to all disrupted units is characterised by partially to completely fragmented sedimentary layers enclosed within a fine-grained and frequently fissile matrix. The degree to which fragmentation has destroyed primary sedimentary layering and the style of deformation is variable throughout the section. This 'block-in-matrix' texture is developed at both microscopic and mesoscopic scales, with isolated fragments ranging in size from discrete sand grains to elongate inclusions with cross-sectional areas exceeding 2 m^2. Without exception, inclusions are coarser-grained than the matrix which immediately surrounds them, however they may comprise one of several lithotypes. In most cases they involve pale grey arenaceous lithologies (massive or laminated quartzose sandstone), however small phyllosilicate-rich silty mudstone blocks and quartz vein fragments are recognised microscopically. Matrices are always argillaceous and range in coarseness from extremely fine-grained, homogeneous black mudstone to dark grey silty mudstone. All of these lithotypes are represented in the neighbouring coherent domains and there is no evidence to suggest that material foreign to the unit has been incorporated into the disrupted domains. As such, the latter are considered to reflect disaggregation of a single, initially intact sedimentary sequence. This style of deformation has been referred to as broken formation (Hsu, 1974) or Type I melange (Cowan, 1985). In accordance with many other examples of melange zones, I will argue that the Ring River disrupted zone represents a domain of significant, but localised accumulation of bulk non-coaxial strain resulting from layer-parallel shear.

5.3 Penetrative planar fabrics associated structural elements in melange-type domains

Although the primary depositional geometry is usually annihilated or at least strongly modified during deformation, the original thickness and spacing of coarse-grained horizons is grossly reflected in the dimensions of sandstone inclusions and relative proportions of these inclusions to matrix respectively. In areas of low strain, inclusions of roughly equal dimensions and similar composition are commonly arranged in semi-continuous trains. These trains can be traced over distances up to 3 m and are interpreted as having formed from the disaggregation of discrete sedimentary horizons. The enveloping surface of these inclusions is therefore considered to represent 'bulk' sedimentary layering and is measured in outcrop as a sub-planar, generally steeply dipping and N to NNE-striking penetrative fabric, S_e (Figs. 5.1; 5.2a, b; 5.3a). The spacing of S_e ranges from a few mm to 1m depending on the original thickness of the layers. This fabric is distinguished from 'primary' sedimentary layering (S_B), which is locally preserved in the form of delicate laminations within sandstone blocks and

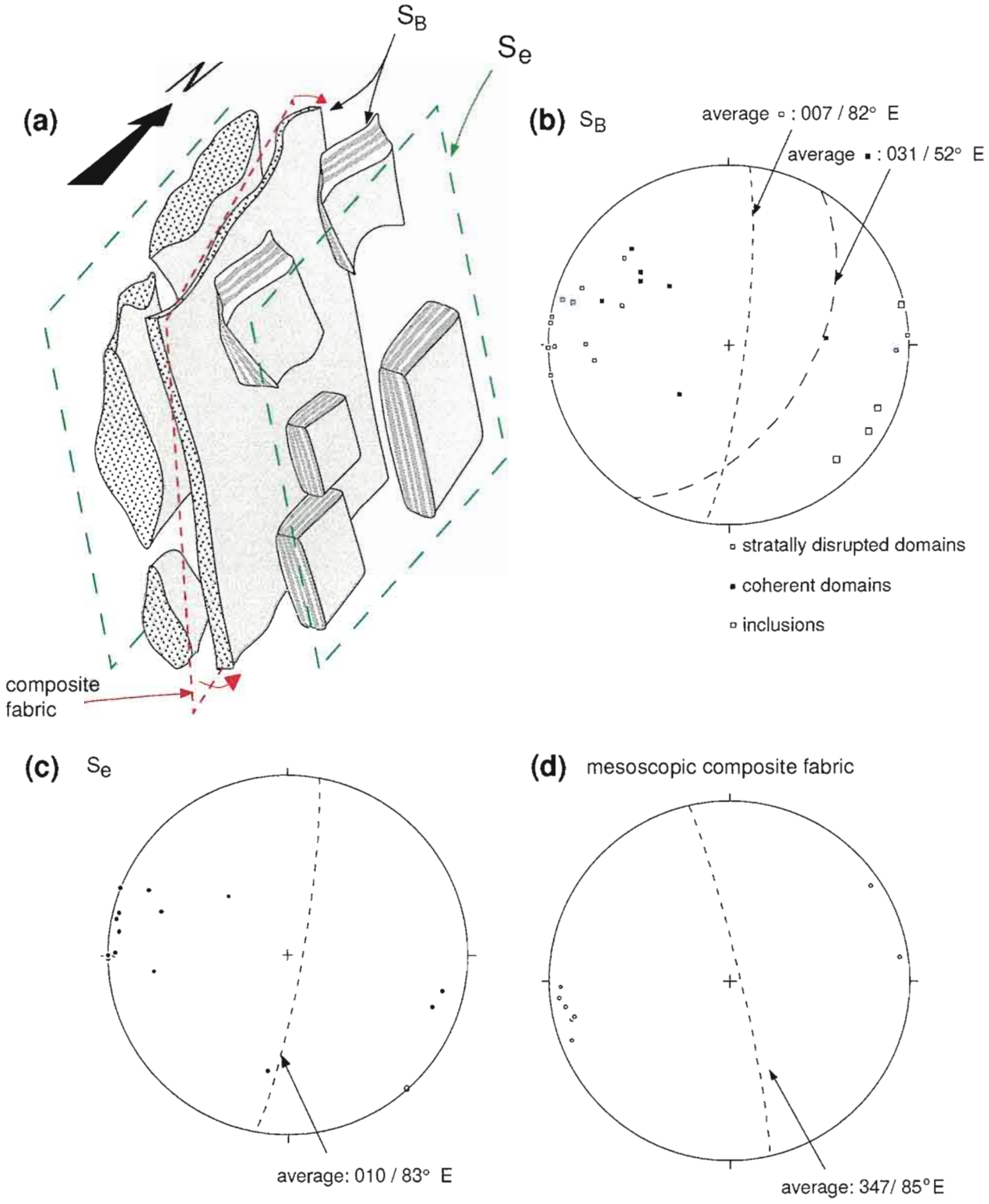

Figure 5.2. Mesoscopic planar fabrics from the Ring River melange zone. (**a**) Components of the "melange fabric". Lozenges and blocks represent sandstone inclusions 'floating' within an argillaceous matrix. Shown also is the geometric relationship between S_e and the mesoscopic composite fabric. (**b**) Poles to S_B: primary sedimentary layering preserved in coherent domains, stratally disrupted domains and within isolated sandstone inclusions. (**c**) Poles to S_e: defined by the enveloping surface of inclusions derived from fragmentation of a discrete bed. (**d**) Poles to the mesoscopic composite fabric.

Figure 5.3. Penetrative planar fabrics in melange-type domains

(**a**) Trains of isolated inclusions and pinch-and-swell structure positioned close to the margin of a large massive sandstone inclusion. Exposure photograph on left, line drawing on right. The enveloping surface of these smaller inclusions defines S_e. Length of pencil is 15cm.

(**b**) Photomicrograph displaying the relationship between S_{SL} slaty cleavage and the S_{SP} spaced fabric. S_{SL} is defined here by a weak grain shape preferred orientation of quartz and white mica grains . S_{SP} is shown by dark residual seams which crenulates S_{SL}. (plane polarised light: sample 12)

(**c**) Strongly developed S_{SL} cleavage defined by fibrous tails on quartz vein inclusions, flattened detrital quartz grains and fine-grained recrystallised white mica. The S_{SP} cleavage is also well-developed and occurs as a spaced, continuous fabric. Obliquity of both fabrics to relict S_B is shown by the folding of delicate compositional bands. (plane polarised light: sample H3A)

(**d**) Sketch from thin section showing transposition of S_{SL} by S_{SP} at diametrically opposing corners of an asymmetric sandstone inclusion. Note also the obliquity of 'internal' S_{SL} to the fabrics in the matrix, indicating rotation of the inclusion in response to non-coaxial flow in the matrix. (sample H3A)

(**e**) History of fold development in (c). Close inspection shows that although the S_{SP} surface appears axial planar to this structure, the S_{SL} cleavage is not folded about the closures. The interpretation shown involves oblique superposition of the S_{SP} pressure solution cleavage on a pre-existing structure with S_{SL} as axial planar.

(**f**) Development of the S_{SP} in a cataclastically deformed sandstone inclusion. The cleavage is restricted to suitably oriented deformation bands. (plane polarised light: sample H2C)

(**g**) Asymmetric shear bands cross-cutting the earlier melange fabrics. (plane polarised light: sample 12)

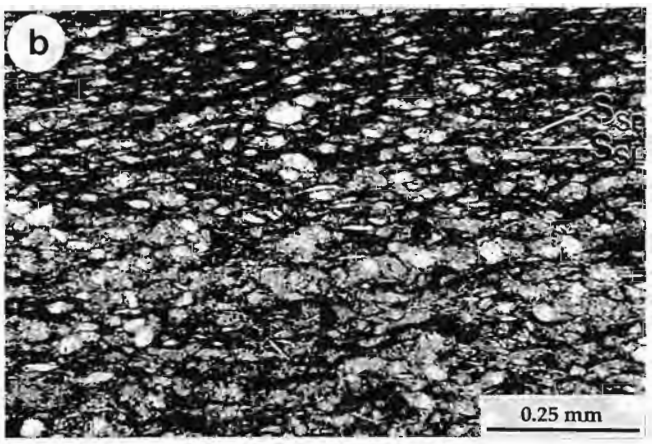

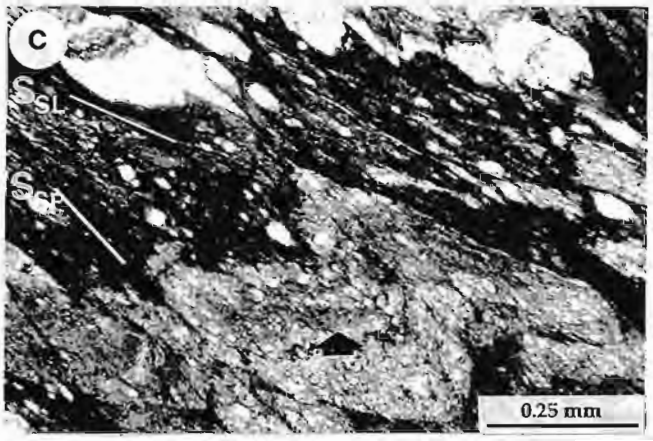

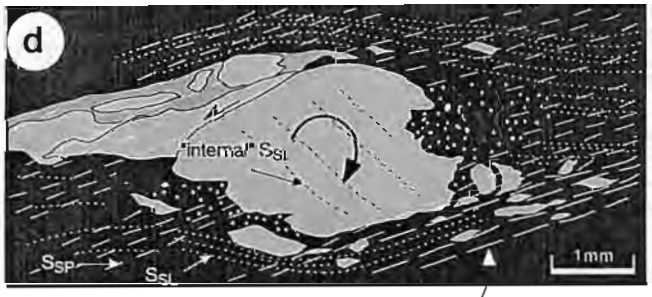

transposition of S_{SL} by S_{SP} on diametrically opposing faces of inclusion

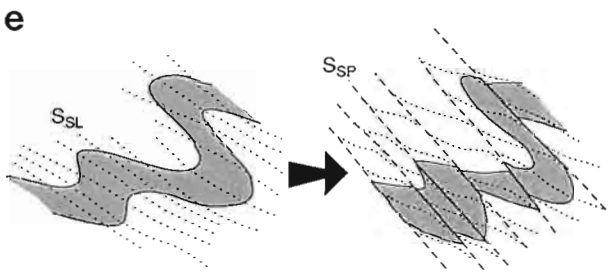

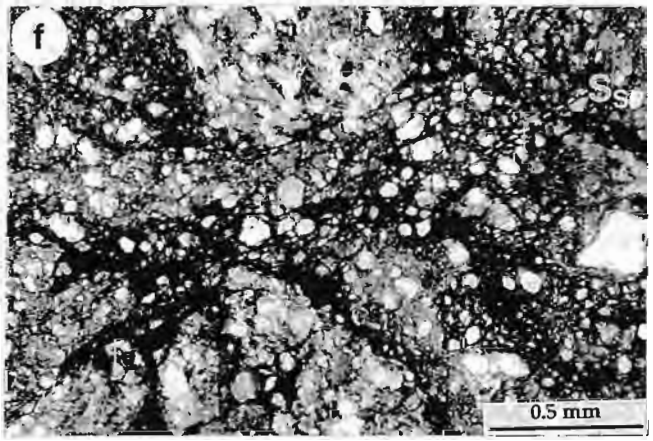

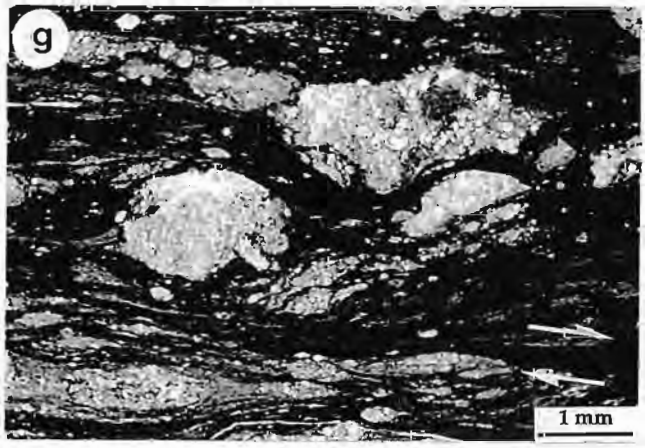

apparently unmodified sedimentary contacts along the margins of weakly deformed blocks. Although the average orientations of S_e and S_B (within melange-type domains) are shown to be sub-parallel in Figure 5.2 b and c, direct observation of the relationship between the two surfaces in the field reveals that they are commonly oblique to each other (Fig. 5.3a).

Oriented at low to moderate angles to S_e and S_B (generally less than 35°) is a sub-vertical, NNW to N-striking mesoscopic composite foliation (Fig. 5.2a, c). It cross-cuts both S_e and S_B in an anticlockwise fashion on horizontal surfaces and in a clockwise fashion on northerly facing vertical sections. In outcrop, this foliation is best developed in mud-rich lithotypes where it occurs as a complex anastomosing network of closely spaced, planar and curviplanar surfaces which closely resembles typical scaly fabrics described from ancient melange belts (eg. Vollmer and Bosworth, 1984; Needham and Mackenzie, 1988; Waldron et al., 1988; Jeanbourquin, 1994; Onishi and Kimura, 1995). Separation of this composite foliation into morphologically distinct fabrics is most easily achieved at the microscopic scale (see below), however in zones of relatively low strain at least two components can be identified including an early, smooth to rough disjunctive cleavage (*sensu* Powell, 1979) which is overprinted obliquely by mesoscopic scale semi-ductile and brittle shear zones.

In thin section, mesoscopic composite fabric is observed to comprise two morphologically distinct continuous cleavages (Figs. 5.3b, c). The first of these, S_{SL}, is pervasively developed in fine-grained lithotypes, but only crudely developed in coarse-grained, matrix-poor sandstones. In silty mudstone and mudstone lithotypes, S_{SL} occurs as a closely spaced slaty cleavage defined by the moderate to strong preferred alignment of both detrital and recrystallised grains. Detrital white mica flakes with ubiquitous undulose extinction have been mechanically rotated towards parallelism with S_{SL}, whereas the preferred dimensional orientation of detrital quartz grains and small inclusions has resulted mainly from a combination of boudinage and diffusive mass transfer processes (DMT). Grains interpreted to have been deformed via DMT show straight to mildly undulose extinction and truncation of grain faces oriented parallel to S_{SL} by dark pressure solution surfaces. Strongly oriented cleavage films comprising extremely fine-grained recrystallised phyllosilicates are very thin and closely-spaced in mudstones but form less continuous, more widely-spaced films in coarser-grained lithotypes. In zones of high strain, S_e is locally transposed by S_{SL}, with re-orientation of small inclusions into parallelism with the latter. Growth of oriented phyllosilicates grains and fibrous quartz in pressure shadow regions at the terminations of detrital grains and within dilational intragranular microfractures also locally defines S_{SL}, however microstructures of this type are not diagnostic of this fabric and also develop in association with the overprinting cleavage.

Although the S_{SL} cleavage in the melange-type domains is considerably more intense than the regionally developed Devonian cleavage (S_2), the orientation of these fabrics, their morphologies and inferred conditions of formation are grossly similar (a description of the S_2 cleavage is given in Chapter 2). I therefore interpret the two fabrics as correlates. Intensification of the regional Devonian cleavage within the melange-type domains is significant in that it indicates that the structural fabric of the melange was actively developing during the Devonian phase of orogenesis.

The second continuous cleavage S_{SP} (spaced cleavage) was observed in narrow zones of high strain and cross-cuts S_{SL} with an anticlockwise sense in horizontally oriented thin sections and with a clockwise sense in northerly facing, vertically oriented thin sections. The angle between these two fabrics on either surface is usually very small (< 10°) and transposition of S_{SL} by S_{SP} in the fine-grained matrix of the melange is common. Transposition is most noticeable on diametrically opposing faces of sandstone inclusions with long axes oblique to S_{SP} (Fig. 5.3d). Intense flattening has occurred in these regions, with detrital quartz grains showing aspect ratios as high as 10:1. Local preservation of S_{SL} occurs in small pressure shadows at the terminations of elongate inclusions or where deflection of S_{SL} around large inclusions has resulted in anomalously high angles between the two cleavages. The angle between S_{SL} contained within inclusions and the external transposition foliation is also very high in some cases (up to 60°). This is interpreted to indicate that inclusions have rotated with respect to the external fabric, providing evidence for non-coaxial flow during cleavage development.

In coarser-grained lithotypes, inter-cleavage angles are generally wider and two distinct cleavage surfaces are usually preserved. In Figure 5.3b for example, S_{SP} is defined by a parallel array of spaced, semi-continuous dark seams which crenulate S_{SL} (oriented horizontally) and result in bending or re-orientation of detrital mica flakes. With increasing strain and decreasing grainsize, S_{SP} becomes more closely spaced and continuous (Fig. 5.3c). In such cases, the morphology of S_{SP} begins to resemble that of S_{SL}, however spacing of the former is slightly greater and a grain shape preferred orientation is less well developed. Elongate inclusions that were previously oriented parallel to S_{SL} have been modified by S_{SP} to produce asymmetric or rhombic cross-sectional geometries. Where fabric development is particularly intense, inclusions are completely re-oriented into S_{SP}.

In matrix-poor sandstone layers and inclusions, S_{SP} is weakly developed, irregularly spaced, and anastomosing to rough. Detrital quartz grains show a crude dimensional orientation defined by elongate grains with truncated margins and less commonly by beard overgrowths of fine phyllosilicates and quartz. Dark, crenulate seams anastomose about detrital grains and commonly die out into the central portions

of layers. In many cases the seams follow suitably oriented pre-existing cataclastic deformation bands (Fig. 5.3f) within which grainsize has been mechanically reduced.

Shear bands and shear fractures

Ductile shear bands and brittle shear fractures cross-cut S_e, S_{SL} and S_{SP}. In most cases, they are oriented at low angles (< 30°) to the "S"-surfaces, however rare high angle sets were also observed. The latter are demonstrably late and displace pre-existing low angle shear surfaces. Low angle shear fractures are commonly polished and slickensided with striations consisting of fine grooves or quartz-chlorite-epidote fibre veins. Up to two sets of striations were observed on any one of these surfaces, commonly at high angles to one another. One set plunges shallowly to moderately to the north and the other is subvertical. Generally it is difficult to establish overprinting relationships, however in a few examples, the steeply plunging lineation appears to be youngest. The spacing of shear bands and fractures is mainly dependant upon the dimensions of coarse-grained inclusions. Only rarely do these surfaces penetrate inclusions.

In thin section, ductile shear bands were observed to be pervasively developed in the fine-grained matrices of the melange fabric. Displacements along shear bands indicated from the drag of pre-existing foliations are invariably extensional and in most cases small (< 5 mm) (Fig. 5.3g). The orientation of shear bands with respect to the melange fabric is commonly contradictory however and they cross-cut S_e, S_{SL} and S_{SP} with either clockwise or anticlockwise senses on both vertically and horizontally oriented surfaces. In some cases, conjugate shear band sets are developed within a single thin section, with symmetrical or less commonly asymmterical disposition about S_e. Single, *en echelon* shear band sets were also observed, with opposing shear senses indicated in different parts of the melange. There is no evidence however, which indicates that shear bands with opposing shear senses are related to different movement events. No consistent cross-cutting relationships were observed and the morphologies of most shear bands are remarkably similar. The development of conjugate shear bands could be taken to indicate a bulk coaxial strain path during melange development (eg. Platt and Vissers, 1980), however this interpretation is not supported by more reliable kinematic indicators such as porphyroclast systems, asymmetric boudinage and asymmetric folds, all of which are indicative of bulk non-coaxial flow (discussed below). Behrmann (1987) argued that conjugate shear band sets or single sets of antithetic extensional shear bands potentially develop in shear zones in which the strain is non-plane or mechanical heterogeneities result in localised perturbation of flow. Similarly, Gaudemer and Tapponier (1987) documented meso-scale antithetic shear zones within the Snake Range décollement, Nevada, which they attributed to perturbation of flow by large asymmetric boudins. In view of the heterogenous nature

of the melange fabric in this study (Fig. 5.3f), a similar mechanism could account for the variation in geometry and shear sense shown by shear bands.

Folds

Folds are rare and characteristically small-scale with wavelengths less than 20cm. There is no evidence for large scale folding within the melange, as younging directions are consistently to the ESE or SE and vergence relationships between cleavages and relict sedimentary layering remain unchanged throughout the section. In most cases, folds are intrafolial and have rootless geometries. Apart from five steeply plunging mesoscopic folds, all were identified in thin section. Closures were observed in both horizontal and vertical sections cut perpendicularly to the principal planar fabric (ie. S_e or S_{SL}). Due to the small scale of the folds however and the difficulty of examining them in three dimensions, the degree of cylindricality is poorly constrained. I am uncertain as to the angle of obliquity between the hinge line and the plane in which the folds were observed, however within each plane, the 'profiles' are characteristically asymmetric and the sense of vergence is consistent. "Z"-vergences are shown on horizontal surfaces whereas profiles on northerly facing vertical sections have "S"-vergences, indicating bulk dextral-reverse sense of shear (E-side up). No evidence for sheath-like geometries was observed. Apparent interlimb angles range from 140° to isoclinal and decrease progressively as the axial trace rotates towards parallelism with the principal planar fabric.

In many cases fold hinges were observed to have nucleated on the 'neck' regions of pinch-and-swell structure (Figs. 5.4 a-c). Commonly only one hinge from a synform-antiform pair is preserved or was ever developed (usually the synformal closure). The folding of pinch-and-swell structure, coupled with the rootless morphologies are significant in that they indicate that folding post-dates an initial phase of layer-parallel stretch and developed relatively late in the process of layer fragmentation. Folds of this type probably formed as a result of amplification of flow perturbations during shearing parallel to S_e (cf. Lister and Williams, 1983). Note that the amplitude of the folded 'neck' in Figure 5.4c is very low compared to folds developed in association with isolated inclusions or close to the terminations of semi-continuous pinch-and-swell structure. This is interpreted to indicate that the swells on either side of the neck were back-rotated with respect to the bulk shearing direction, preventing amplification of the fold (cf. Lister and Williams, op cit.).

Both S_{SL} and S_{SP} occur as axial planar fabrics to folds. Regardless of which cleavage is axial planar, the movement sense indicated from fold vergence remains unchanged. In general however, folds associated with S_{SL} are tighter that those with S_{SP} axial planar fabric. Tightening and/or modification of pre-existing folds by S_{SP} was observed locally. An example is shown in Figures 5.3c and e. Close inspection of the

Figure 5.4. Photomicrographs of intrafolial folds from the melange-type domains.

(a) Isoclinally folded pinch-and-swell structure with S_{SL} axial planar cleavage (only weakly developed in sandstone). (plane polarised light: sample H3B)

(b) Gentle closure centred on neck region of pinch-and-swell structure. The S_{SL} cleavage refracts markedly through the hinge region.

(c) Back rotation of 'swells' in this semi-continuous boudinage layer prevents amplification of the fold in the intervening 'neck' region. A rough S_{SP} fabric is developed in the 'closure' region. (plane polarised light: sample H5A)

(d) Poorly developed fold with rough S_{SP} axial planar fabric. This structure probably results from the impingement of thin sandstone and mudstone layers by the larger sandstone inclusion to the left. (plane polarised light: sample H3B)

* Note that horizontally sections (b-d) show consistent dextral asymmetries regardless of the age of the axial planar fabric. The vertically oriented section (a) shows E-side up reverse movement.

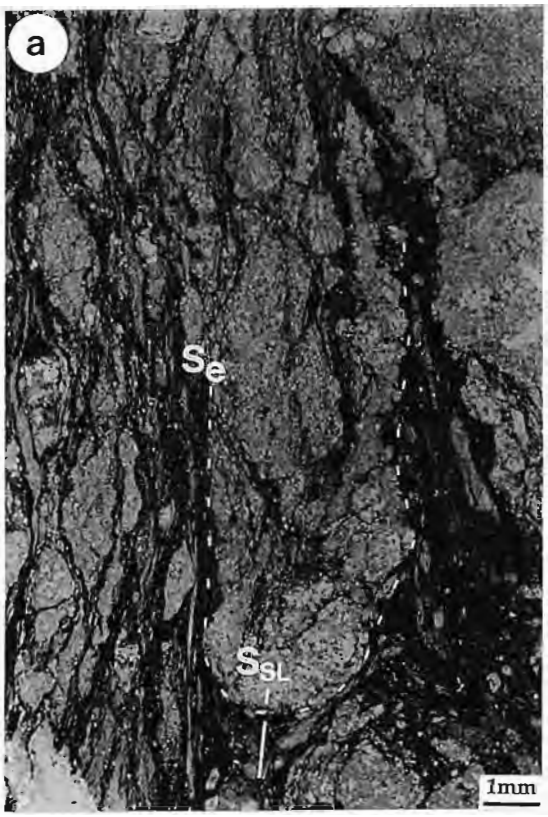
a
Se
SSL
1mm

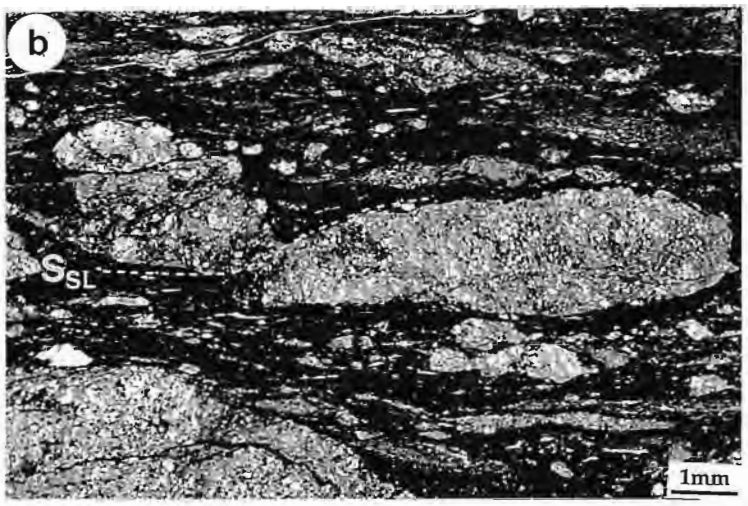
b
SSL
1mm

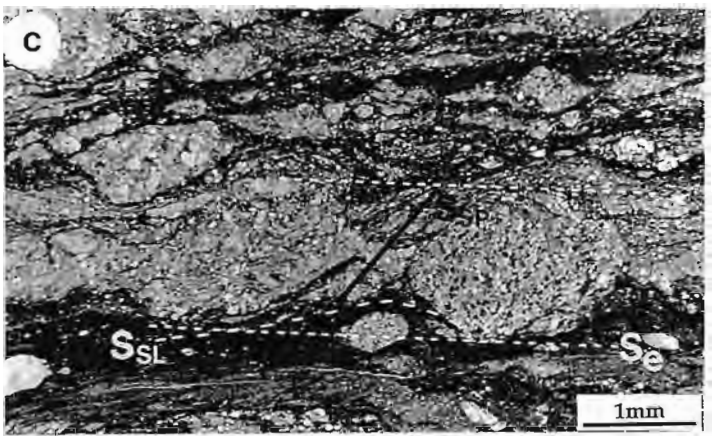
c
SSL
Se
1mm


d
SSP
1 mm

folded layer reveals that S_{SL} is not folded about the hinge of the fold even though S_{SP} approximates the axial surface. Such cleavage-fold relationships may have resulted hinge migration of earlier folds (either pre- or syn-S_{SL}), in response to oblique flattening by S_{SP} (cf. Hudleston, 1973). Alternatively, as shown in Figure 5.3e, modification of an early closure has resulted from dissolution of hinges and limbs during imposition of the S_{SP} pressure solution cleavage.

The consistent geometric relationships between S_{SL} and S_{SP} and their association with folds of similar vergence and style are interpreted to indicate that both cleavages are kinematically and genetically related. They are considered to have developed progressively during a single deformation event which involved shearing parallel to S_e. Development of the younger S_{SP} cleavage occurs in regions where deflection of S_2 is such that it can no longer accommodate strain, (ie. it failed to track the path of the XY plane of the finite strain ellipsoid during progressive deformation).

5.4 Mesoscopic deformation styles and geometry of inclusions in the Ring River melange

Partitioning of strain and variation of deformation styles throughout the disrupted domains occur primarily as a function of the original sedimentary lithotypes. Three broad mesoscopic styles are defined: i) "high strain" phacoid zones containing inclusions < 30cm in length, ii) domains of large-scale boudinage and pinch-and-swell structure and iii) chaotic block-in-matrix structure. Despite significant difference in the scale of inclusions in i) and ii), the geometry of inclusions at a given stage of layer disaggregation are remarkably similar. Figure 5.5 summarises the various cross sectional geometries of inclusions (independent of scale) observed no meso- and microscopic scales.

5.4.1 "High strain" phacoid zones

The most spectacular examples of stratal disruption occur in narrow, "high strain" mudstone-rich zones which range in thickness from 35-70 cm. The original lithologies in these zones are interpreted to have been mudstone-dominated multilayered units, which contained thin (< 1 cm to 10 cm in thickness) sandstone and silty mudstone horizons. In rare domains of relatively minor disruptions, this primary sedimentary fabric is preserved with only minor modification. Throughout the main part of these zones however, sedimentary layering is thoroughly disrupted to form a block-in-matrix fabric (Fig. 5.6a). Sandstone layers, siltstone layers and quartz ± chlorite veins show progressive fragmentation via pinch-and-swell (or "flow" boudinage: *sensu* Smith, 1975) or fracture boudinage to produce isolated inclusions which possess a variety of geometries ranging from rounded oblate or prolate forms to more angular forms with rectangular or rhombohedral cross-sections. The thinly

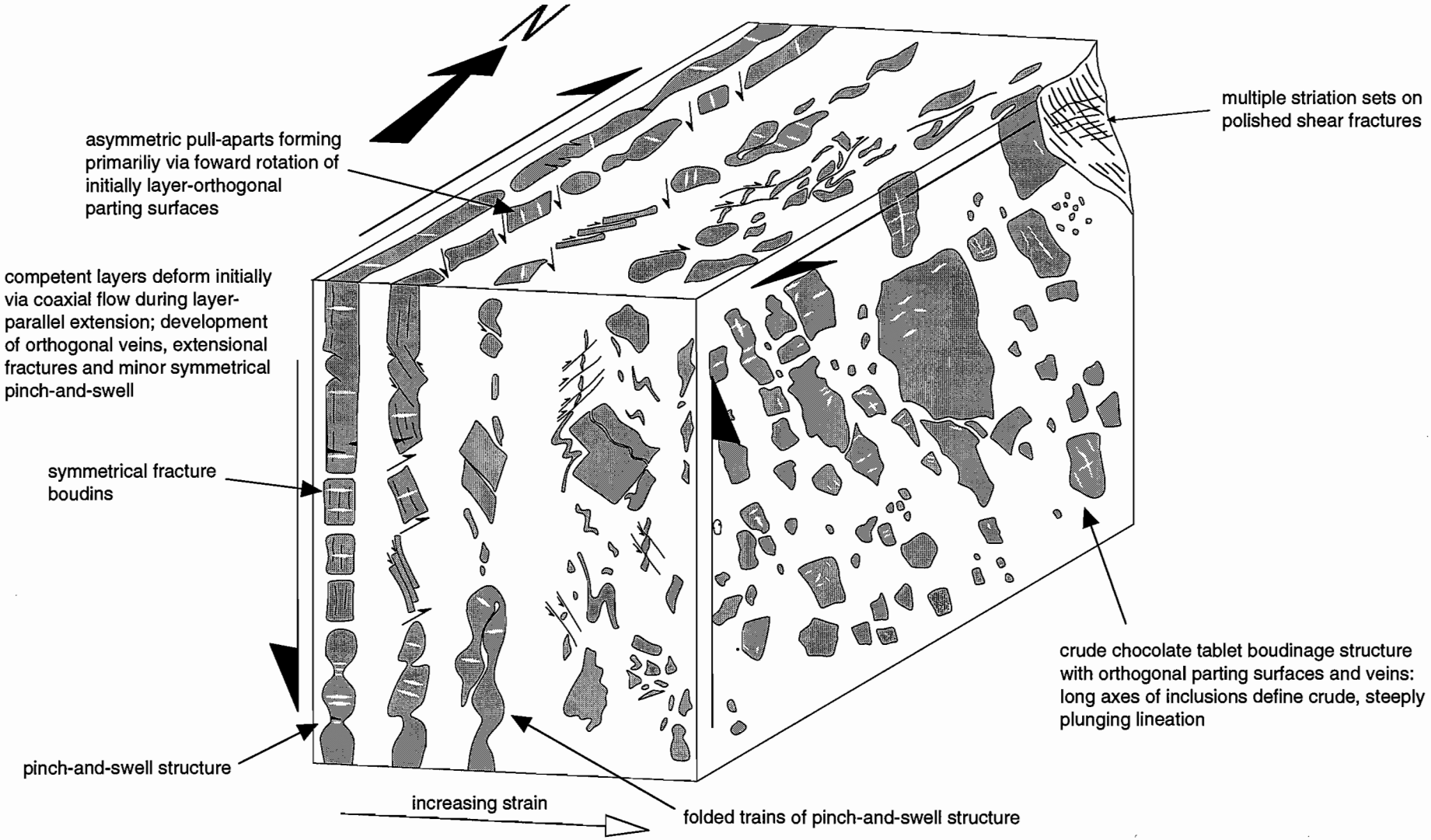

Figure 5.5. Composite diagram displaying geometry of mesoscopic and microscopic inclusions from Ring River melange zone.

Figure 5.6 Inclusion geometry in "high strain" phacoid zones.

(**a**) Typical outcrop appearance of "high strain" zones. The photograph shows a strongly developed planar fabric defined by elongate lenticular inclusions. S_e is transposed completely by the mesoscopic composite fabric. Lens cap is 60mm in diameter.

(**b**) Section cut parallel to S_{SL} showing chocolate tablet boudins of sandstone enclosed by the fine-grained matrix. (sample H2)

(**c**) Sub-orthogonal vein generations in a chocolate tablet boudin. Note the weak boudinage of both sets of quartz veins. (sample H2)

(**d**) Section cut parallel to S_{SL} showing quartz vein fragment which is itself veined. Fibrous quartz and chlorite 'beards' extend from the terminations of the inclusion and are considered to represent a weak, steeply plunging stretching lineation. (sample H3)

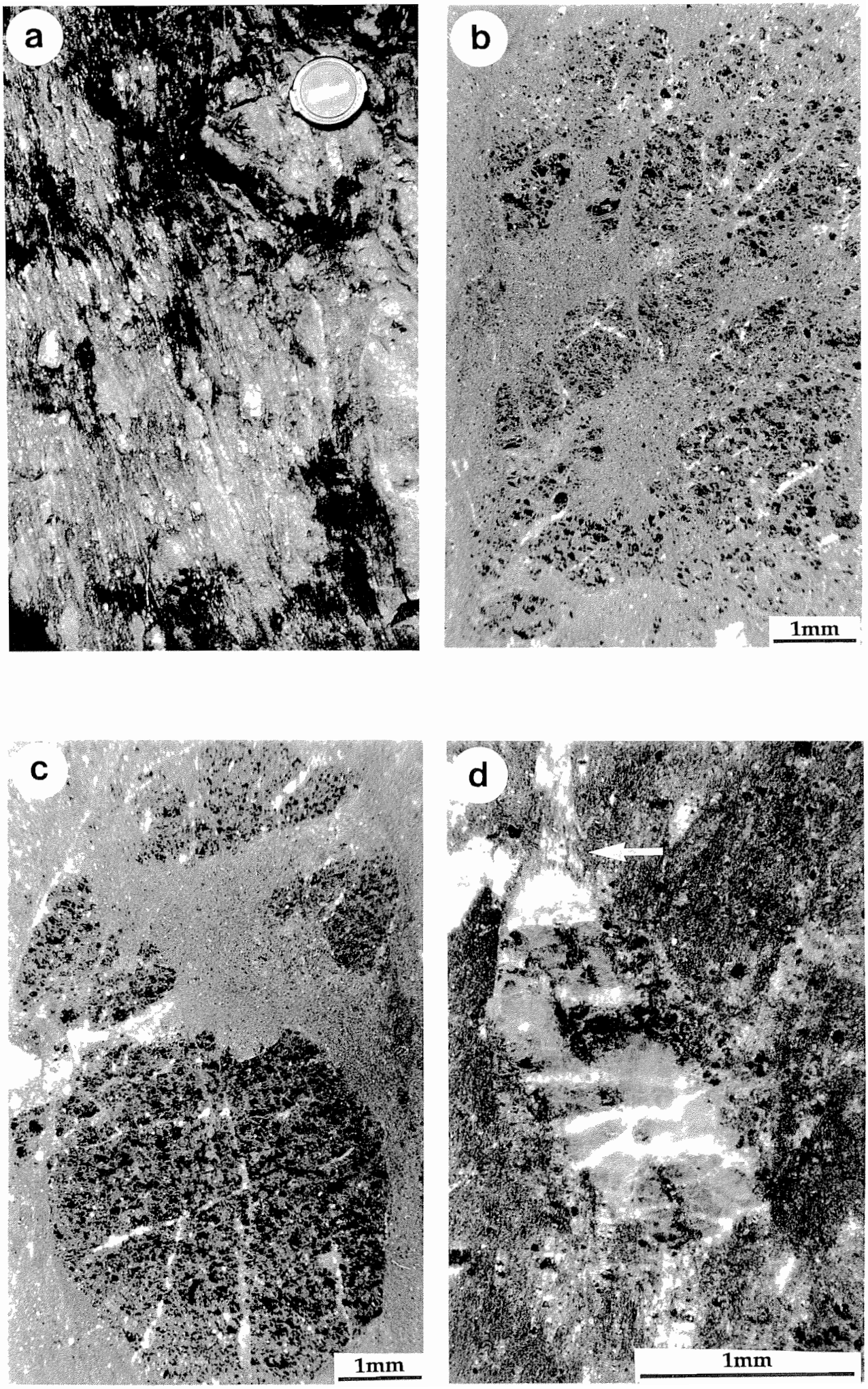
a
b
1mm
c
1mm
d
1mm

bedded character of the pre-deformed lithology is reflected in the dimensions of inclusions, which are generally less than 2cm in their longest dimension, but were observed to exceed 25cm in rare cases. Primary sedimentary layering even graded bedding is locally preserved within some inclusions. Within most however, these textures have been obliterated.

The inclusions are closely spaced within the argillaceous matrix and show a strong preferred dimensional orientation. Alignment of flattened and elongate inclusions defines S_e where it can be shown that trains of inclusions were derived from fragmentation of a single sedimentary layer. More commonly however, S_e is transposed by the mesoscopic composite fabric (ie. S_{SL} and/or S_{SP}) which is then defined as the principal planar fabric. The shortest axes of inclusions are invariably oriented at a high angle to either S_e or the mesoscopic composite fabric. In cross sections oriented perpendicularly to the principal planar fabric (both down-dip and along strike directions), the inclusions show either symmetrical or asymmetrical forms. The degree of symmetry is in many cases enhanced through the development of tapered appendages or 'tails' which consist primarily of granulated material and lie within or close to the principal planar fabric. In terms of their geometries, 'tailed' inclusions closely resemble porphyroclast systems described from mylonites (eg. Passchier and Simpson, 1986) and thus potentially provide insight into the kinematic history of the "high strain" zones .

In sections cut parallel to the principal planar fabric, an association of equant and elongate inclusions with roundish, polygonal and tabular outlines was observed (Fig. 5.5). A uniform arrangement of inclusions is generally lacking throughout most sections cut in this orientation, however locally a chocolate tablet boudinage structure is developed. This structure is defined by small clusters of similarly composed sandstone inclusions which are separated from each other on all sides by extension fractures and less commonly tensional veins or pinched 'necks' (Fig. 5.6b). The margins of the inclusions with matrix are either sharp or diffuse, the latter exhibiting a mantle of loosely packed detrital quartz grains. Neighbouring inclusions occasionally exhibit 'jigsaw-fit' arrangements, suggesting that there has been little or no rotation (about axes oriented at a high angle to the principal planar fabric) once the boudinage structure has developed. In terms of rheology and strain, chocolate tablet boudinage indicates that sandstone layers behaved competently relative to the enclosing argillaceous matrix and that they were oriented within the extensional field of bulk flattening-type deformation: ie. $\lambda_1>\lambda_2>1$, where λ_1 and λ_2 represent the maximum and intermediate quadratic elongation of finite strain partitioned within the competent layer (cf. Casey et al., 1983; Ghosh, 1988).

Although inclusions appear rather randomly distributed on surfaces parallel to the principal planar fabric (partly due to their variation in shape and dimensions), statistical measurement of the orientation of long axes and fractured margins of

inclusions reveals a crudely systematic pattern. Figure 5.7a shows the orientation of long axes measured in the plane of S_{SL} from two oriented hand specimens. The attitude of these axes ranges markedly from horizontal to vertical, however the bulk of the data pitches steeply on the S_{SL} surface (averaging 76° to the N) and defines a crude linear fabric(see also Fig. 5.5). The orientations of fractured margins (measured from both elongate and equant inclusions) (Fig. 5.7b) show a less focused distribution, from which two broad populations can be discriminated: population I pitches shallowly to moderately to the S and accounts for 29% of the data, whereas population II (71% of the data) exhibits a wide range in pitch from moderately to the south to shallowly to the N. The average orientation of each population are roughly orthogonal, with coincidence of population II and the linear fabric defined by the long axes of inclusions. The relationship between margins and long axes of inclusions is interpreted to indicate a fundamental orthogonal fracture pattern (Fig. 5.7d), resembling the more "classical" chocolate tablet boudinage structure documented from lesser strained naturally deformed rocks (eg. Coe, 1959; Fyson, 1962) and that produced in laboratory experiments (Ghosh, 1988). According to Ramsay (1967, p. 112) it is reasonable to expect that the numerically predominant fracture set and hence the long axes of the inclusions will be oriented sub-perpendicularly to the principal extension direction. If such an interpretation is valid, a sub-horizontal maximum principal stretch (λ_1) is indicated.

In addition to the fractures developed around the margins of inclusions, fracturing has occurred internally in the form of quartz- and chlorite-filled extension veins and thin, deformation bands (*sensu* Aydin, 1978). Veins were observed on both horizontal and vertical sections oriented normal to the principal planar fabric. On each of these planes, the traces of veins are oriented at a high angle to the principal planar fabric (and hence at a low angle to the short axes of the inclusions). On surfaces parallel to the principal planar fabric, one or frequently two sets of veins are revealed (Fig. 5.5, 5.6c). Where two vein sets are developed, they are usually (but not always) of similar composition and at high angles to one another (ie. >60°- 90°). In general, where the inclusions are elongate, the numerically dominant vein set is developed normal to the long axis. The orientations of vein traces parallel to the S_2 surface are largely shallowly to moderately pitching (Fig. 5.7c), however a relatively small proportion pitch down-dip in the direction of inclusion long axes. Veins themselves are commonly boudinaged to form semi-continuous trains and in some cases even form discrete inclusions within the matrix (Fig. 5.6c, d). In rare examples, elongate vein fragments are themselves cross-cut by later vein sets and exhibit fibrous quartz developed in pressure shadow regions which extend in a down-dip direction from the tips of their long axes (Fig. 5.6d). Pressure shadow regions at the tips of inclusion long axes are interpreted to indicate the embryonic development of a stretching lineation. Note

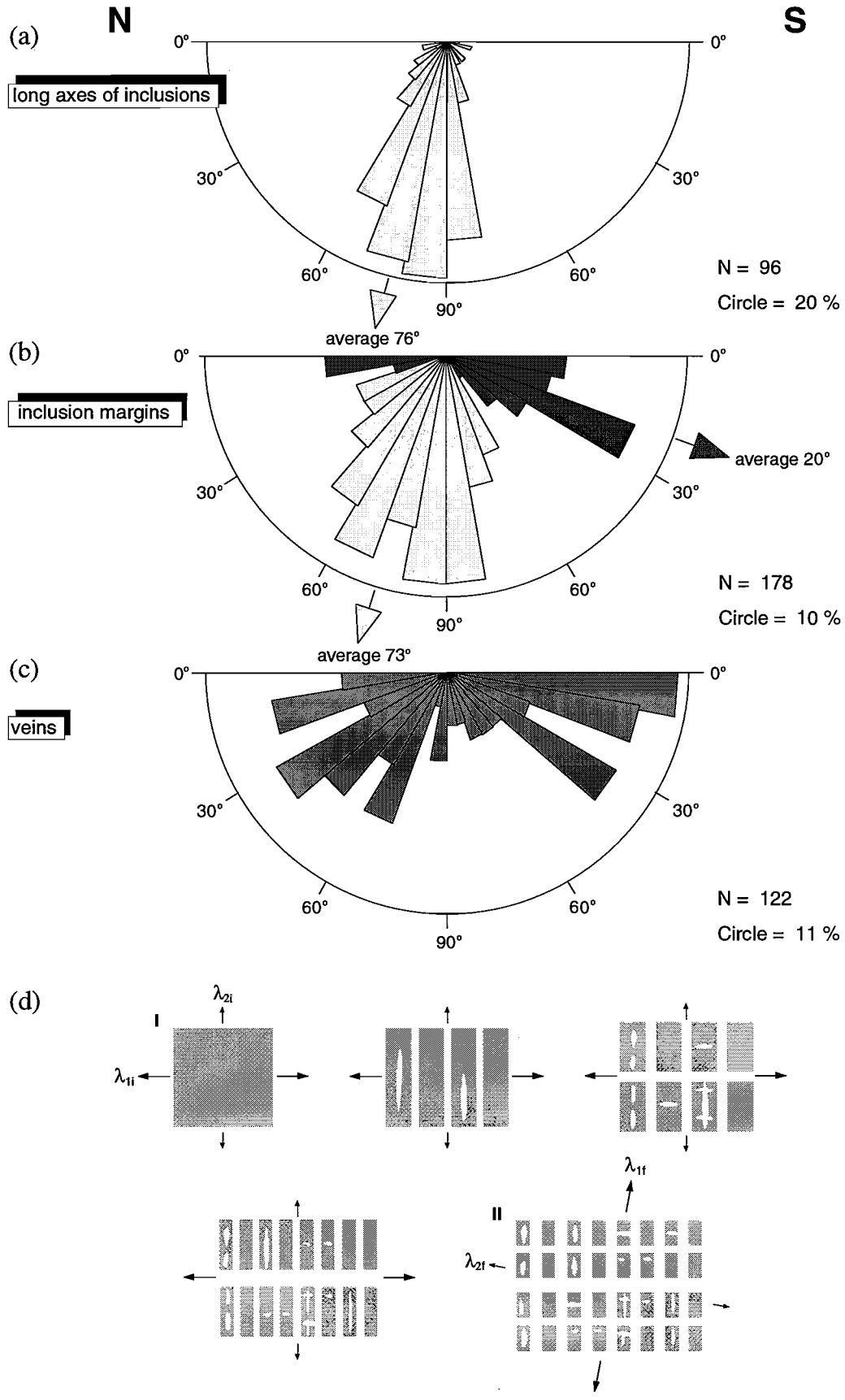

Figure 5.7. Geometry of inclusions shown in the plane of S_{SL}. (a) - (c) Rose diagrams showing orientations of structural elements in inclusions (see text for discussion). (d) Schematic diagram illustrating progressive formation of chocolate tablet boudins. The orientations of parting surfaces and veins are dependent on pre-existing boudin geometry rather than the orientation of the far field stresses in the matrix (modified from Ghosh, 1988).

however, that the steep pitch of this fabric conflicts with the inferred sub-horizontal orientation of λ_1 deduced from long axes and fracture patterns.

Chocolate tablet boudinage (or the development of orthogonally arranged extensional fractures in the plane of layering) has been considered by many workers as a fundamental structural element formed during the development of melange (eg. Byrne, 1984; Needham and Mackenzie, 1988; Waldron et al., 1988; Kimura and Mukai, 1991; Onishi and Kimura, 1992). A systematic geometric relationship between both the orientation of principal extensional fractures and long axes of inclusions and the principal axes of strain during progressive deformation has also be inferred in most of these studies. Byrne (op cit.) and Fisher and Byrne (1987) for example, have described an orthogonal arrangement between the long axes of inclusions and the inferred principal extension direction during the initial stages of layer fragmentation from melange belts in Kodiak Island, Alaska. In studies of melange within the Shimanto Belt, Japan however, conflicting results have been presented in the literature, with Kimura and Mukai (1991) and Onishi and Kimura (1995) indicating orthogonality between long axis of inclusions and the extension direction, whereas Needham and Mackenzie (1987) suggest that the long axes are coincident with the extension direction. In his description of melange developed within Franciscan sediments, California, Cowan (1982) considered that no systematic lineation was defined either by boudin long axes or "neck lines", which he argued indicates axially symmetric extension (ie. $\lambda_1=\lambda_2>1$) within the plane of layering.

Ghosh's (1988) experimental and mathematical investigation of chocolate tablet boudinage structure however, has shown that the geometric fracture pattern developed during progressive fragmentation of the competent layer is dependant primarily upon the initial shapes of boudins developed during the early stages of deformation rather than the orientation of the far-field principal strain during the course of deformation. Figure 5.7d shows a very simple, hypothetical example of development of chocolate tablet boudinage during which the far-field principal axes of layer-parallel strain vary throughout deformation history. Ghosh (op cit.) showed that if fracturing normal to the initial far-field maximum stretch (λ_{1i}) produced boudins which were sufficiently long and narrow, the tensile stresses directed along the length of the boudins can outweigh the forces imposed by viscous drag of the matrix. Consequently, progressive vein development and break up of the layer occurs along surfaces oriented normal to the long axes of the boudins, regardless of the orientation and relative magnitudes of the principal stretches in the matrix. This process of orthogonal fracture development will continue until the boudins attain a stable geometry. In the final stages of deformation shown in the example, the bulk orientation of inclusion long axes and the numerically dominant fracture set remains sub-perpendicular to λ_{1i} , but is oblique to far-field final maximum incremental stretch (λ_{1f}). Accordingly, interpretation of strain paths in

melange-type belts structured on the basis of fracture patterns and vein orientations in chocolate tablet boudins should be approached with caution.

5.4.2 Zones of large-scale boudinage and pinch-and-swell structure

Packets of deformed strata which are inferred to have originally comprised thickly- to very thickly-bedded, massive or poorly-laminated sandstone units are characterised by the development of large-scale pinch-and-swell structure interpreted to have developed in response to layer-parallel extension. Sub-parallel, semi-continuous inclusions of pale grey massive sandstone (some of which can be traced for more than 10m along strike), are separated by argillite-dominated regions which originally contained thin- to medium-bedded sandstone horizons and now exhibit various degrees of layer disaggregation (Fig. 5.8a). Strain is heterogeneously distributed throughout the argillaceous regions, with localised areas within which layering is only very weakly deformed and most primary sedimentary structures are preserved, juxtaposed with others in which layer fragmentation is particularly intense. In terms of inclusion geometries, the latter resemble "high strain zones", however inclusions are generally larger, less densely-packed and the development of a well-developed 'scaly' cleavage is lacking. In the presently deformed state, the distance separating adjacent large-scale pinch-and-swelled sandstone layers ranges from 3m to less than 1cm, however in consideration of the degree of shortening across layering which was likely to have accompanied layer-parallel extension, the original range of layer spacing was probably considerably greater.

The cross-sectional geometry of sandy inclusions is dependant not only on the degree of strain and layer separation, but also the nature of the original lithotype. Those which are inferred to have been derived from medium to very thickly-bedded, massive or poorly-laminated sandstone beds have deformed in a mesoscopically ductile fashion. They have sub-rounded lenticular shapes and form isolated bulbous inclusions or semi-continuous trains of pinch-and-swell structure (Fig. 5.8b). In contrast, inclusions which preserve fine internal bedding laminations are characteristically blocky in shape, with rectangular or more commonly rhombohedral cross sections (Fig. 5.8c). Sub-planar margins and parting surfaces associated with internally laminated inclusions are suggestive of a more 'brittle' style of fragmentation. In some cases, inclusions exhibit a style which is intermediate between these two end-members. Such inclusions contain weakly preserved internal laminations, however their external geometries are more compatible with internally massive varieties, with sub-rounded bulbous forms. In the following sections, I discuss the geometries and strain features associated with each style of inclusion.

Figure 5.8 Inclusion geometry in zones of large-scale boudinage and pinch-and-swell structure.

(**a**) Semi-continuous inclusions of massive sandstone. Intervening matrix contains isoclinal folds oriented sub-parallel to S_e, brittle shear fractures and smaller isolated sandstone inclusions.

(**b**) Mesoscopically ductile pinch-and-swell structure positioned adjacent to the boundary of a larger massive sandstone inclusion. Intervening matrix is squeezed out from between amalgamated inclusions and forms discontinuous wisps oriented sub-parallel to S_e. Note also the abundant quart veining and the development of dark fractures in neck regions.

(**c**) Blocky asymmetric inclusion with mesoscopically brittle appearance. Internal laminations are well preserved and are rotated forward with respect to S_e. Thin quartz veins are positioned close to the centre of the inclusion and oriented sub-perpendicularly to internal laminations.

(**d**) Similar contact relationship to (**b**) between pinch-and-swelled sandstone trains along the margin of a massive inclusion. In this case however, the margin is oblique to bulk Se. Marginal sandstone inclusions and intervening mudstone have been buckled in response to rotation into the shortening quadrants of flow. Note also the "podding off" of sandstone inclusions into the matrix and parallelism with S_e.


a

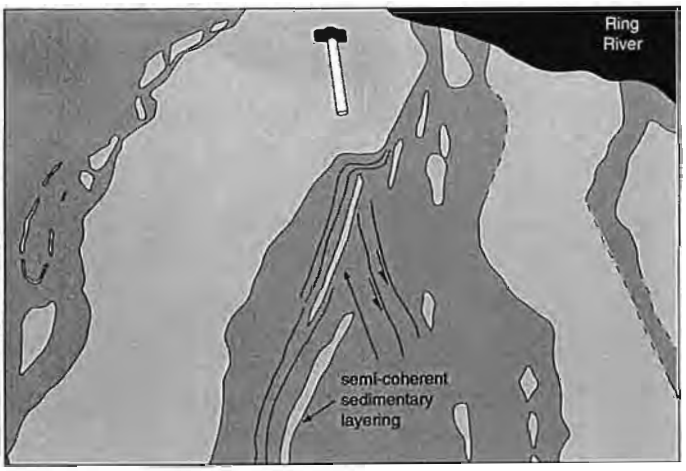
Ring
River
semi-coherent
sedimentary
layering


b


c
Nikon

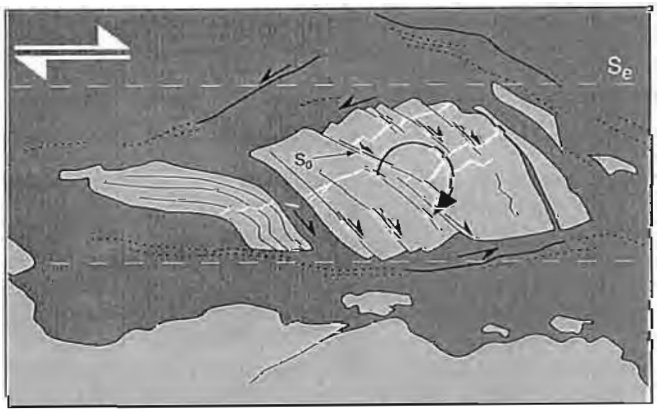
Se
So


d

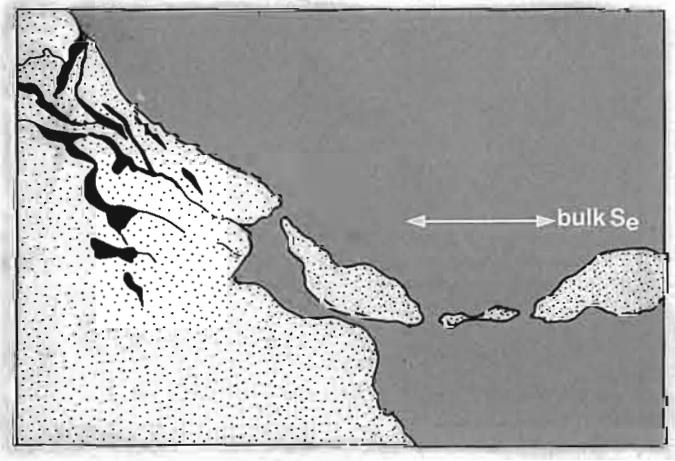
bulk Se

Internally massive pinch-and-swell structure and lenticular inclusions

Pinch-and-swell structures and lenticular inclusions generally show symmetrical cross-sections when viewed on horizontal exposure surfaces, however markedly asymmetric forms were observed locally where the long axes have been rotated away from bulk S_e. Elongate tails extend from terminations of pinch-and-swells and isolated inclusions and are aligned within S_e. Due to the paucity of suitably oriented exposures, the down-dip geometry of these inclusions is difficult to constrain. In the few sub-vertically oriented exposed surfaces down-dip separation of thin layers was observed, suggesting a similar three-dimensional geometry to the chocolate tablet boudinage structure documented from "high strain zones". The margins of inclusions dug out from field exposures exhibit crude oblate forms and are enveloped by a thin mantle of silty mudstone. The S_{SL} foliation closely follows the inclusion margins and has a 'shiny' appearance in hand specimen due to the strong alignment of detrital white mica flakes.

Tensional quartz veins and rare mud-filled veinlets oriented at high angles to inclusion margins are commonly developed within the 'tails' of isolated inclusions and in the 'neck' regions of semi-continuous pinch-and-swell structure. Veins with more random orientations were also observed within the interiors of thick inclusions. In general, veins terminate at the margins of sandstone inclusions and do not propagate into the enclosing matrix. Thin, dark deformation bands forming either systematic arrays oriented sub-perpendicularly to the long axes of inclusions (Fig. 5.8b) or complex cross-cutting networks occur within the interiors of many inclusions. These structures bear a striking resemblance to the "web structures" of Byrne (1984) and cataclastic shear zones described by Lucas and Moore (1986) from melange belts interpreted to have formed in accretionary environments. Their origin and significance will be discussed further in the section on grain-scale deformation (5.5.2.3).

Where the original spacing of sandstone layers was small, intervening argillaceous material appears to have been 'squeezed out' such that the long margins of inclusions derived from successive layers are now in direct contact. An example of this style of structure is shown in Figure 5.8b where massive sandstone inclusions have amalgamated along the long margin of a very thick pinch-and-swelled sandstone body and relict portions of mudstone layers and thin silty horizons are preserved as thin distorted slivers oriented sub-parallel to the outer surface. Such structures demonstrate the component of shortening directed at a high angle to primary layering. Figure 5.8d shows the same amalgamated contact, however in this case at a 'necked' region of the thick sandstone body. Deflection of the contact into the shortening field of the bulk deformation has resulted in folding of pre-existing pinch-and-swell structures as well as the intervening relict mudstone layers. Due to the originally complex geometry of the amalgamated contact, the folds have a rather disharmonic and convoluted appearance. If the early history of boudinage and inclusion amalgamation along the outer surface of

the sandstone body was unknown, such textures could easily be misinterpreted as the effects of soft sediment deformation such as slumping or liquefaction. Note also the apparently ductile "podding off' of the outer-most disrupted sandstone layer into the matrix parallel to S_e.

On the scale of individual inclusions, the interface between sandstone and the enclosing mudstone matrix is also characteristically irregular. On smooth river-worn exposures, rounded to sub-angular 'lobes' of sand were observed to alternate with cuspate or graben-shaped mud-filled indentations (Fig. 5.9a). Thin, semi-continuous sandstone layers contained within the matrix are shortened and folded within the indentations and pinch out over the sandy 'lobes'. Note also the folded quartz vein (arrow above lens cap) within the mud-filled indentation in the centre of field of view. In extreme cases, mudstone-filled cusps appear as small veinlets extending up to 5cm into sandstone inclusions (< 1/10 thickness of inclusions). Such veinlets are distinguished from dismembered mudstone horizons formed during inclusion amalgamation partly through the folding of the matrix, but mainly as they are oriented at high to moderate angles to the long margins of inclusions (ie. S_e). In cases where veinlets and cusps are oriented obliquely to S_e, they may show evidence for activation as small shear zones.

Similar irregularities along the margins of sandstone bodies have been described from many ancient melange zones, however there is little consensus regarding their origin and significance. Most workers have drawn analogies between these structures and soft sediment deformation features including load and flame-type structures, sand volcanoes or sedimentary dykes (eg. Cowan, 1982; Lash, 1985; Needham and Mackenzie, 1988; Jeanbourquin, 1994; Needham, 1995). They have argued that their appearance on both upper and lower surfaces of dismembered sandstone layers indicates that they were not developed as a result of 'typical' sedimentary processes (ie. sedimentary loading or scour-and-fill) but rather during the onset of layer fragmentation and melange development. Sandstone 'lobes' have been regarded as *protrusions* which grew via particulate flow of unlithified, overpressured sand. Many of the arguments put forward for initiation of melange development whilst sediments were unlithified have relied heavy on a "soft sediment" interpretation of these structures.

On the other hand, careful examination of surface irregularities on competent inclusions by Byrne (1984) and Waldron et al. (1988) have demonstrated that structures were initiated and later amplified by dilation and/or offset along brittle fractures developed at high angles to the inclusion-matrix interfaces. Furthermore, Waldron (op cit.) noted that mud-filled tensional fractures formed in boudinaged limestone layers contained in melange from Newfoundland, cross-cut pre-existing calcite veins, providing evidence, they suggest, for lithification at the time of layer extension. Byrne (op cit.) described wavy irregularities on sandstone inclusions from the Kodiak Islands,

Figure 5.9 Detailed contact relationships between massive sandstone inclusions and matrix.

(**a**) Irregular contact between sandstone inclusion and matrix. The interface is shown by alternating sandstone lobes and mud-filled cusps. Thin siltstone layers contained within the matrix are folded into the cusps. Note also the folded quartz vein contained within the matrix (arrow). Lens cap is 60mm in diameter.

(**b**) Brittle disaggregation of sandstone at the interface with mudstone. Thin quartz veins are developed sub-perpendicularly to the interface in the sandstone (black arrow). The white arrow highlights angular fragments of sandstone which have dislodged from the corners of 'horsts' and accumulated at the base of matrix-filled cusps.

(**c**) Photomicrograph showing a small mud-filled apophysis extending into sandstone from the margins of a large matrix-filled veinlet. The apophysis cuts across a quartz vein (black arrow) indicating that the sandstone was well-lithified at the time of mudstone injection. (plane polarised light: sample 354)

(**d**) Photomicrograph of a thin mudstone veinlet cutting across a quartz vein in sandstone, with entrainment of quartz vein fragment (arrow). (plane polarised light: sample 354)

(**e**) Schematic diagram showing cusps forming at the margins of sandstone inclusions due to high tensile stresses in this lithology compared to the more rapidly extending ductile matrix. Flow of matrix into the cusps induces high shear stresses and disaggregation at the corners of sandstone 'horsts', producing rounded lobes.


a
Nikon

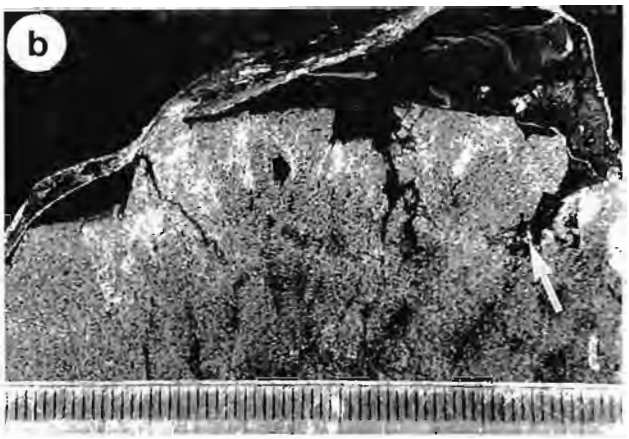
b


c
1mm

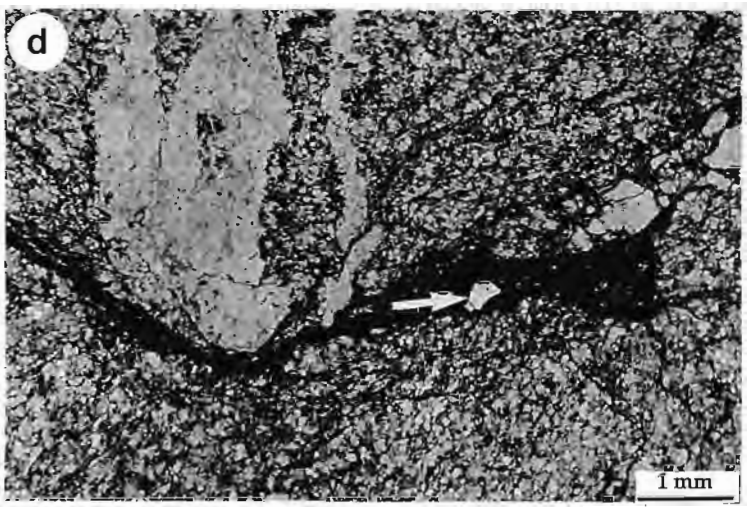
d
1 mm

e

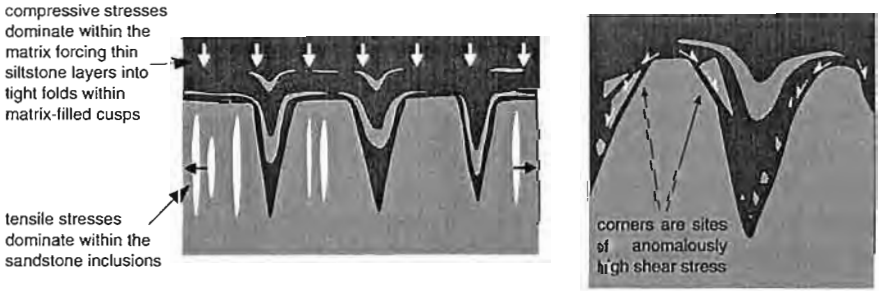
compressive stresses dominate within the matrix forcing thin siltstone layers into tight folds within matrix-filled cusps
tensile stresses dominate within the sandstone inclusions
corners are sites of anomalously high shear stress

Alaska, as mullion-type structures, which he considered to have been formed in part by offset along cataclastic shear zones contained within the sandstone. Although the structures shown in Figure 5.9a superficially resemble mullions (cf. Ramsay, 1967, Fig.7-45), I consider this term to be misleading as the formation of mullions requires particular rheological and strain conditions which are inconsistent with most structural observations in melanges. Specifically, mullions form at the margins of incompetent layers which firstly are volumetrically sub-ordinate to an enclosing competent host and secondly occur oriented within shortening quadrants of flow (Smith, 1975; Talbot and Sokoutis, 1992). Neither of these features are consistent with descriptions of melange from the literature or my own observations, which indicate that competent sandstone inclusions are on the whole volumetrically sub-ordinate to the surrounding mudstone matrix and the fundamental structural element in melange (namely boudinage) is indicative of layer-parallel extension. Small cusps, or "inverse-necks" of Talbot and Sokoutis (op cit) may also develop during extension of relatively thin incompetent layers, however their amplitudes are characteristically small and as such would be unlikely to account for penetrative 'veinlets' observed in this study.

Examination of the margins of inclusions on slabbed surfaces reveals a considerably more angular shape of the sandstone 'lobes' compared to their appearance on surface exposures. Figure 5.9b shows a sample collected adjacent to the intersection of mud-filled veinlet and the outer margin of a thick sandstone inclusion. In detail, the interface of sandstone and mudstone is ragged with blocky 'horst-like' protuberances of sandstone separated by tensile fractures into which mudstone has flowed ductilely. Angular sandstone particles have dislodged from the corners of the 'horsts' and accumulated towards the bases of intervening cusps (white arrow). The bounding surfaces of sandstone protuberances are defined by narrow (<0.5mm in width), sub-planar shear fractures which are oriented at a high angle to the interface and extend a short way into the inclusion (cf. Byrne, 1984). Thin quartz veins are also developed perpendicularly to the outer margin of the inclusion and parallel the edge of the mud-filled veinlets. Note also how the brittle style of deformation shown within the sandstone contrasts with the more ductile folding of darker silty inclusions contained within the mudstone matrix (black arrow). In Figure 5.9c, microscopic textures developed along the margin of a relatively large (4cm in length) mudstone veinlet are shown. Much of the original fabric within the large veinlet has been obscured by late-stage shearing, however small mud-filled apophyses which extend into the inclusion appear relatively undeformed. In this example, the fracture into which mudstone has flowed cross-cut pre-existing quartz veins. Similarly, the small mud-filled apophysis shown in Figure 5.9d truncates quartz veins, fragments of which have been entrained with mud during injection.

On the basis of textures described above I interpret that irregularities on the sandstone-mudstone interface developed as a result of brittle disruption and tensional failure. Although the form of the interface shown on river-worn exposure surfaces superficially resemble pre-lithification deformation features, no evidence was observed to indicate that the sandstone responded ductilely to deformation. The presence of swirled and folded siltstone adjacent to the interface (Fig. 5.9b) could however be taken to indicate that dominant brittle phase of deformation is imposed upon pre-existing soft sediment deformation features. Although it is difficult prove that this not the case, the lack of clear evidence for ductile flowage of the sandstone, coupled with the presence of folded quartz veins contained within the mudstone matrix (eg. Fig. 5.9a) suggests that this is unlikely. The variation in style of deformation shown by matrix and inclusions is therefore interpreted to reflect rheological contrast between incompetent mudstone and rigid sandstone.

Amplification of the matrix-filled cusps to form elongate veinlets is inferred to have resulted from propagation of tensional fractures towards the interior of the inclusion, rather than intrusion of sandstone into the less-competent surroundings. The dilatant cusps form as sites of low mean stress, whereas the dominant component of stress distributed throughout the majority of the surrounding matrix is a compressive force directed at a high angle to layering (cf. Selkman, 1978). Once dilatant fractures nucleate at the margins of inclusions, the matrix is progressively squeezed into the opening cusps (down a stress gradient), producing drapes or folds if thin sandstone layers are able to flow at a rate comparable to that of the mudstone (Fig. 5.9e). The effect of the flow of matrix into cusps is to impose anomalously high component of shear stress at the corners of the sandstone 'horsts'. Corner regions respond by disaggregation along shear fractures, releasing small aggregates of sand grains which become entrained within the more mobile matrix and migrate towards the region of low mean stress (ie. towards the base of the cusp). This processes of denudation of the corners of 'horsts' may eventually lead to the more rounded, lobe-like form of the sandstone protuberances seen in field exposures.

Inclusions with internal bedding laminations

As mentioned in the beginning of this section, internally laminated inclusions have shapes which range from distinctly blocky styles with sub-planar margins and angular corners to less regular geometries more typical of internally massive sandstones. As a general observation, as external geometries become less regular, internal laminations become less easily distinguishable. In extreme cases, only the local preservation of very faint relict laminations indicates that inclusions were derived through fragmentation of an originally finely laminated sandstone horizon. Variation in inclusion geometry can occur randomly throughout a disrupted package and in some

cases between neighbouring inclusions derived from a single fragmented layer. The string of inclusions shown in the middle of Figure 5.3a for instance, show a marked variation in geometry, with almost complete obliteration of bedding laminations in the central, irregularly-shaped inclusion but excellent preservation of S_B within the two neighbouring blocky fragments. On the basis of their spatial distribution, all three inclusions are considered to have been derived from the same layer. Such a marked difference in finite strain within a single layer is significant in that it shows that in this case at least, there is no simple relationship between rheological response of sandstone layers and primary lithological attributes (eg. degree of lithification, matrix content of sandstone, bedding thickness, grainsize, composition, viscosity contrast between inclusions and the surrounding matrix etc.). What then are the main factors which influence inclusion geometry and at what point of the deformation history do strain paths begin to deviate? In an attempt to try and explain these problems, I start by looking at the more simple strain paths leading to the formation of blocky inclusions.

The relatively small dimensions of blocky inclusions indicate the original thicknesses of finely laminated sandstone horizons were generally less that 10cm, however in rare cases inclusions were observed with dimensions perpendicular to internal bedding in excess of 50cm. Some very thin (<0.5cm), originally massive sandstone horizons which lack internal laminations have also disaggregated to form blocky inclusions. Aspect ratios ($R=a/b$, where a and b represent the axial dimensions measured parallel and perpendicular to internal laminations respectively) measured on planar surfaces oriented normal to S_e range from 4 to 0.5. In some cases therefore, the longest axis of inclusions in two dimensions occurs perpendicular to primary layering. Layer fragmentation has been initially accomplished by extension fracture boudinage in response to layer-parallel stretching. In rare cases, inclusions can be shown to possess a chocolate tablet geometry with two sets of parting surfaces oriented at high angles (60°-90°) to one another. Due to the horizontal attitude of most exposures however, only one set of steeply-dipping parting surfaces was usually observed.

Both symmetric and asymmetric trains of inclusions occur, the former closely resembling "classical" boudinage with the development of rectangular segments separated by matrix- or less commonly vein quartz-filled gaps. Internal fracturing occurs in the form of quartz- or mud-filled tension veins which are mostly (but not always) oriented sub-perpendicular to internal bedding laminations. The degree of asymmetry is manifested either in terms of the external shape of inclusions, or obliquity of internal bedding and extensional structures relative to bulk S_e. In most cases, asymmetric inclusions have not developed in response to offset along structures which were originally oblique to primary layering (eg. shear fracture boudinage), but rather through the modification of initially symmetric structures during progressive deformation. Evolution from symmetric to asymmetric inclusions is demonstrated by

the local preservation of initially orthogonal relationships between extensional structures (eg. veins and parting surfaces) and primary layering (eg. Fig. 5.8c). This modification of initially symmetric boudins is analogous to Type 1 asymmetric pull-apart structures of Hanmer (1986). Structures of this type have been widely documented from ductile shear zones (eg. Mawer, 1987; Malavieille, 1987; Swanson, 1992) and it is generally agreed that they develop in response to a component of shear directed parallel to bulk layering: ie. S_e in this terminology.

The asymmetry of inclusions with high aspect ratios (ie. $R \geq 2$), is manifested primarily in the modification of parting surfaces such that the ends of inclusions appear oblique to internal laminations (Fig. 5.10a). With the exception of the corners of these inclusions, long axes and bulk internal layering remain sub-parallel to S_e, resulting in rhombohedral external geometries. Examination of the parting surfaces in detail however, reveals a stair-step geometry (Fig. 5.3a, Fig. 5.10a), suggesting that apparent obliquity of parting surfaces has resulted from minor offset of an originally layer-orthogonal fractures along internal bedding surfaces. The two-dimensional modification of initially rectangular structures to produce asymmetric rhombohedral geometries can therefore be approximated with progressive simple shear. Folding of internal layering in corner regions positioned within the extensional quadrants of flow results from locally high stress gradient between the corner of the inclusion and the matrix-filled gap separating successive inclusions (cf. Hanmer and Passchier, 1991). In contrast, inclusions with initially low aspect ratios respond by bulk rotation sympathetic to the flow in the matrix, with little or no component of internal shearing (Fig. 5.10b). Originally layer orthogonal parting surfaces and tensile fractures remain perpendicular to internal layering. Inclusions continue to rotate until they attain a stable geometry within the bulk flow. The more general case, however involves components of spin plus internal shear (Fig. 5.10d). Hanmer and Passchier (op cit.) noted that the effect of shear along anisotropy which is oriented within the shortening quadrants of flow, is to produce an component of spin antithetic to the bulk shear plane. The anisotropy will attempt to rotate back towards the bulk shear plane (Freund, 1974) and thus counter the sympathetic rotation caused by the viscous drag at the inclusion interface. If internal layering is not suitably oriented for easy slip once rotation has ceased (for instance if back-rotation results in a layer orientation with high normal stress component), strain may become more homogeneously distributed throughout the inclusion, resulting in internal ductile flow. Alternatively, new shear fractures oriented at a high angle to internal layering may form. Either of these processes would be expected to disrupt internal layering and destroy the regular or blocky shape of the inclusion.

The mechanisms of inclusion modification outlined above are very simplistic. They do not take into account the degree of separation between adjacent inclusions or the possible effects of differing partitioning of vorticity in neighbouring inclusions. It is

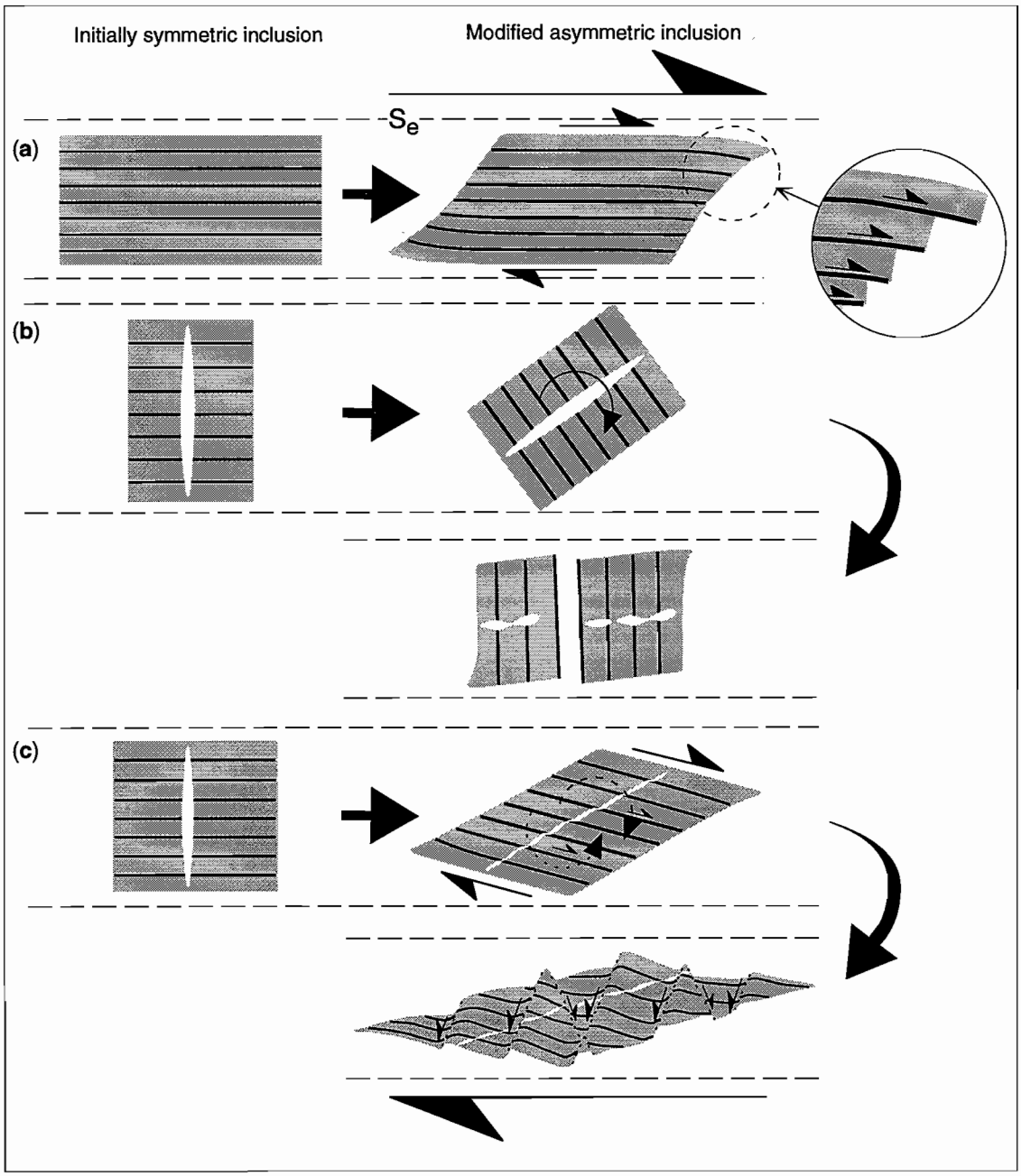

Figure 5.10. Modification of initially symmetric, internally laminated inclusions in response to shearing directed parallel to bulk layering (S_e). Initial aspect ratios are shown to influence the partitioning of vorticity into spin and internal shear-induced components (cf. Lister and Williams, 1983). (**a**) and (**b**) represent two end-members in which inclusions deform via internal layer-parallel shear and rotation sympathetic to the bulk flow respectively. The more general case is shown in (**c**) where vorticity is paritioned into components of both spin and layer-parallel shear. In this case antithetic spin induced by slip on layer counters the foward spin resulting from viscous drag of the flowing matrix.

presented mainly to highlight the inferred influence of initial mechanical properties (ie. presence or absence of internal anisotropy, initial spacing of parting surfaces and inclusion aspect ratio) on the finite strains shown by inclusions.

"Brittle" vs "ductile" inclusions: causes of variation in cross-sectional geometry

Similar relationships between inclusion geometry and the presence or lack of an internal anisotropy defined by primary sedimentary layering have been described from ancient melange belts (eg. Cowan, 1990; Needham, 1995). Needham (op cit.) considered that the contrast in deformation style exhibited by lenticular and rectangular inclusions in melange belts from the Southern Uplands of Scotland was primarily a function of the degree to which sediments were lithified at the time of layer fragmentation. He states that..." The rectangular blocks are suggestive of deformation of a lithified bed whilst the lenticular blocks formed in a more ductile manner and possibly represent less well cemented layers."... . Although the massive sandstone inclusions involved in this study display features which superficially resemble textures developed during the deformation of unlithified sediment, I have found no conclusive evidence which indicates that laminated sandstone horizons were at a more advanced stage of lithification compared to their massive counterparts, or indeed that either were not entirely consolidated during layer fragmentation.

Factors which determine whether extending competent layers embedded within a less competent matrix will respond in a brittle or ductile fashion (ie. fracture or flow boudinage respectively) are varied and include: i) viscosity contrast between the competent and incompetent material, ii) degree of cohesion at the interface of the two materials (ie. potential for decoupling at the interface), iii) strain rate, iv) length of the competent layer relative to its thickness (Smith, 1975, Lloyd et al., 1982). Each of these factors would be expected to vary considerably within melange and could potentially account for differences in inclusion geometry. The correlation between inclusion geometries and particular lithotypes however (shown in a number of different melanges), may indicate that the response to deformation is dependant upon primary sedimentary fabrics. Textural features which would be expected to enhance ductility include loose grain packing and high matrix content. Alternatively, the content of ductile 'matrix' in sandstones may increase during the deformation, with progressive degradation of labile or mechanically weak constituents (cf. Mitra, 1978). Thus, the 'cleanness' of sandstones as well as the tightness of grain packing may be important in determining inclusion geometry both at the initial stages of deformation and as deformation proceeds. Intuitively, thick, massive sandstones deposited rapidly from mass flows would be expected to show poorer sorting, grain orientation and compositional maturity compared to laminated beds involving traction current deposition. However, examination of both massive and laminated sandstone inclusions

in thin section however, shows little variation in 'matrix' content between these two lithotypes.

The presence of a planar anisotropy (ie. closely spaced bedding laminations) within some sandstones may also have an effect on ductility. In their study of foliation boudinage, Platt and Vissers (1980) argued that the ability of a rock to deform in a ductile manner is reduced if a component of stretch is applied in the direction of a strong planar anisotropy. They predicted that brittle failure along extension fractures oriented at a high angle to the anisotropy would occur under such conditions. If bedding laminations contained within sandstone exert a similar effect on ductility during layer-parallel extension, this may account for the variation in deformation style shown between inclusions in the Ring River melange zone.

5.4.3 Chaotic block-in-matrix structure

Domains in which sandstone blocks or inclusions are arranged in a totally random fashion (Fig. 5.1, 5.11) were observed locally within the eastern portion of the mapped section. These domains occur up to 5m in width and are bounded by steeply dipping, late stage brittle faults. They are characterised by a high proportion of sandstone lithotypes, many of which were originally medium- to thickly bedded and contain a well-preserved internal anisotropy defined by closely spaced, sub-parallel mudstone laminations (S_B). No preferred orientation of inclusions is evident within these domains and the trace of S_B within neighbouring inclusions is discordant by angles of up to 90°. As is the case with zones of large-scale boudinage, those blocks which possess an internal anisotropy exhibit a mesoscopically 'brittle' style involving blocky tabular forms, whereas inclusions derived from massive layers show more rounded margins and 'ductile' pinch-and-swell structures. Isolated fold hinges, with highly variable orientations were also recognised locally.

Evidence for initial fragmentation via layer-parallel extension is provided by quartz and mud-filled tension veins oriented at a high angle to S_B within some inclusions and the development of rectangular cross-sectional geometries which closely resemble classical blocky boudinage structure (Fig. 5.11b). Although minor rotation and offset of veins along bedding surfaces (mm to cm scale) has occurred, few inclusions show markedly asymmetric forms suggesting that layer parallel shear has not played a significant rolé in controlling the shapes of inclusions. The high degree of block rotation coupled with the overall lack for internal shearing indicates that vorticity was partitioned entirely into spin. Such a strain history may have been brought about by anomalously turbulent flow within the matrix.

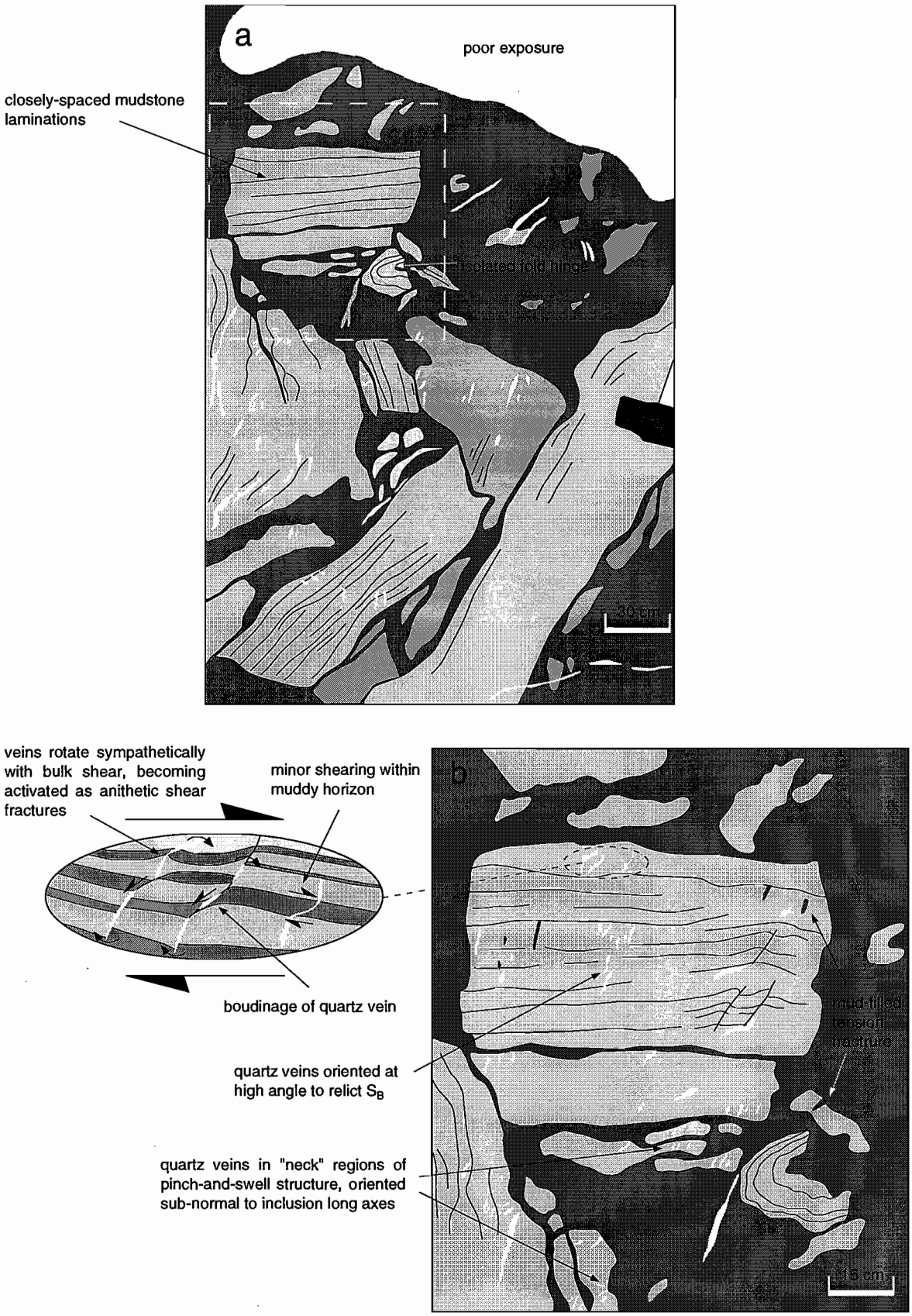

Figure 5.11. Field sketches of chaotic block-in-matrix structure. Sandstone inclusions are shown in pale grey and the mud-rich matrix is dark grey. White lenses represent quartz veins. Although the present arrangement of inclusions is apparently random (**a**), initial fragmentation via layer-parallel extension is interpreted on the basis of rare rectangular inclusion shapes and the development of tensional structures at a high angle to relict bedding (**b**). Evidence for minor layer-parallel shearing, probably preceding chaotic jumbling of inclusions, is preserved locally (inset of (**b**)). The position of (**b**) is indicated by the dashed white box in (**a**).

5.5 Microstructural fabrics and grain-scale deformation processes

The purpose of this section is to characterise grain-scale structures related to the development of the Ring River melange. Through the examination of microstructures, constraints can be placed on the deformation mechanisms responsible for the localisation of strain. The interaction between competing mechanisms can in turn provide valuable information on environmental conditions as well as the physical character of the rock.

Faulting at upper crustal conditions and the production of cataclasites or microbreccias can be complex as more than one process is likely to be active throughout the deforming medium. Grain breakage, for instance, is only one potential mechanism involved in the formation of these textures and characteristically crystal-plasticity, diffusion mass transfer (DMT) and particulate flow (ie. grain boundary sliding), all play important rolés in fabric development (eg. Knipe, 1989; Stel, 1981; Rutter and White, 1979). Moreover, a cyclic or evolutionary deformation path is likely, in part due to fluctuations in environmental conditions, but also in that the development of microstructures themselves causes changes in the behaviour of rocks during deformation.

The following sections concentrate on grain-scale processes within deformed sandstone inclusions (section 5.5.2) and contrasts these with the limited deformation features in sandstones outside the melange zones (section 5.5.1). Through the discussion, sedimentary matrices are referred to as 'groundmass' to avoid confusion with the matrix component of melange domains.

5.5.1 Low strain sandstone

A sample of medium grained sandstone was collected from coherent strata positioned along the eastern margin of the Ring River melange zone. Detrital modes are dominated by quartz (>70%), with the remainder comprising a highly altered 'groundmass' of sericitised feldspar, rock fragments, muscovite, zircon, tourmaline and minor rutile. Sorting is moderate to good, with most quartz grains having sub-rounded to angular forms with relatively sharp and easily-definable margins (Fig. 5.12a). Textures in quartz include straight to mildly undulose extinction, with sutured margins developed in a few grains. Undulose extinction may be partly inherited from a metamorphic precursor, however as the degree of undulosity increases within sutured grains much of this strain is considered to have accumulated *in situ*. In some cases, the boundaries between adjacent quartz grains are diffuse or have patchy extinction, which is interpreted to indicate the onset of sub-grain development (Fig. 5.12b). No grain elongation fabric is developed in quartz, however crude alignment of detrital white micas parallel to S_{SL} is shown locally. Mica flakes have weak undulose extinction and are commonly kinked or displaced along (001) partings due to minor rotation due to

Figure 5.12 Photomicrographs of low strain sandstone and pervasive microfracturing in more highly strained sandstone inclusions.

(a) Low strain sandstone showing detrital quartz grains set in a 'groundmass' of altered labile constituents and primary sedimentary matrix. Quartz grains have well-defined margins and low degrees of internal strain. (crossed polars: sample 350)

(b) Minor grain-grain suturing in low strain sandstone with the diffuse margin indicated by the arrow showing early stages of grain boundary migration and small sub-grain development. Note also the preservation of the rounded detrital core in the central quartz grain. (crossed polars: sample 350)

(c) Intragranular microfractures in quartz delineated by fluid inclusion trails. Note also the irregular margins of the quartz grains with overgrowths of fibrous quartz and minor chlorite (crossed polars: sample 12)

(d) Multiple intragranular microfracture sets with obliquity of approximately 40°. Fibrous phyllosilicate overgrowths are perpendicular to the younger of these microfracture sets. (plane polarised light: sample H2B)

(e) Well-developed phyllosilicate fibres forming within intergranular microfractures. (plane polarised light: sample H2B)

(f) "Stretched fibre" vein consisting of chlorite and quartz. The fibres track the displacement vector of the intragranular fracture. (plane polarised light: sample H3A)

(g) Zircon grain engulfed by quartz overgrowth. (crossed polars: sample 15)

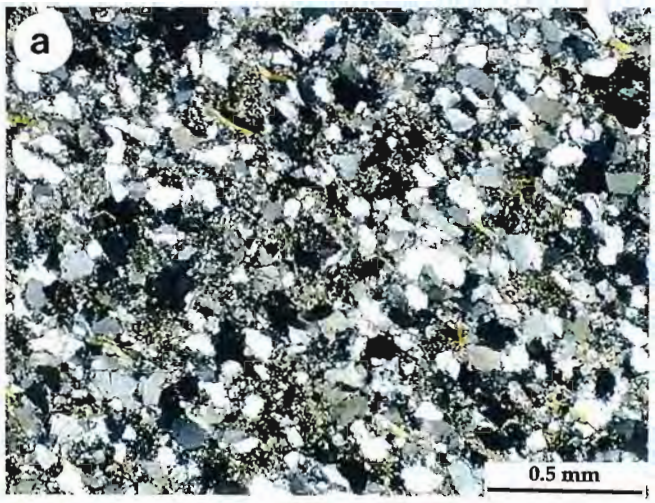
a
0.5 mm

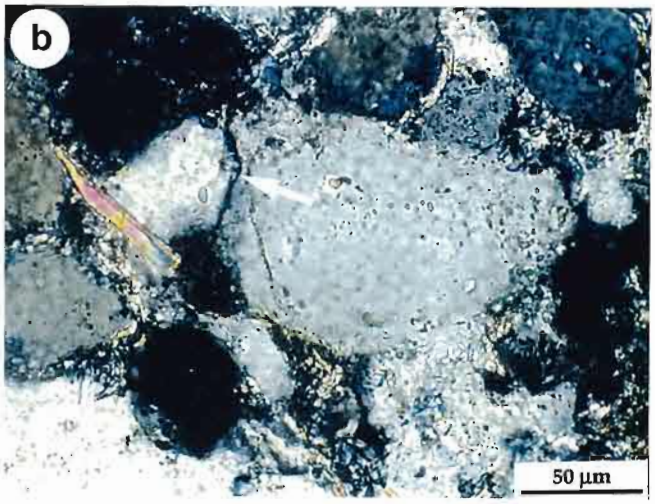
b
50 µm

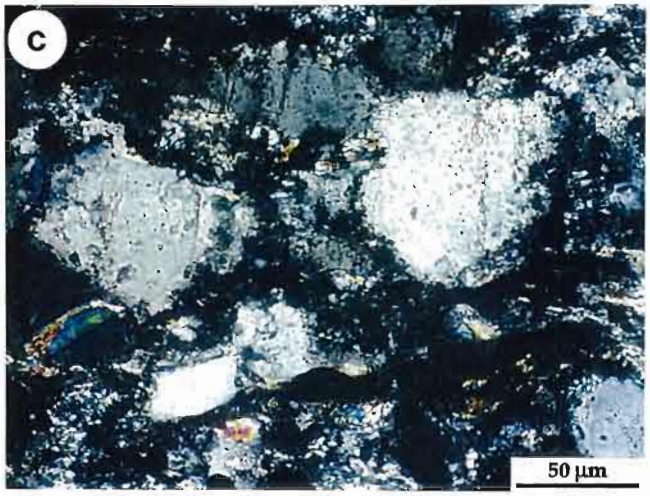
c
50 µm


d
1
2
50 µm

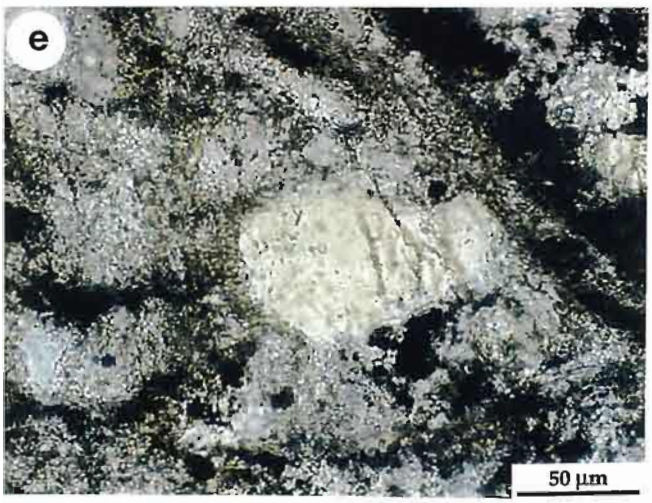
e
50 µm


f
50 µm

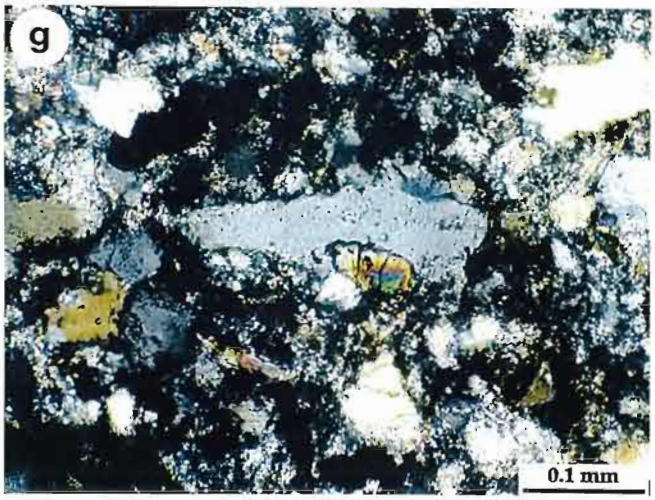
g
0.1 mm

impingement of neighbouring rigid grains. A few mica grains are broken, with serrate fractures developed perpendicular to (001). Apart from these mica grains, evidence for cataclastic deformation processes is lacking.

5.5.2 Deformation of sandstone inclusions

In contrast to low strain sandstone, inclusions contained within melange domains are characterised by cataclastic textures. Grain breakage has not occurred in isolation however and in most examples grain breakage is closely related to microstructures formed in response to DMT and crystal plastic processes. Three main styles of cataclastic behaviour have been identified: i) incipient ductile cataclastic flow (IDCF), ii) brittle failure along extension fractures and shear fractures and iii) transitional brittle-ductile cataclastic flow. The characteristics and origin of microstructures associated with each of these deformation styles are discussed below.

5.5.2.1 Incipient ductile cataclastic flow

Microfractures

Inclusions with incipient ductile cataclastic flow (IDCF) are characterised by pervasive extensional microfracturing. The development of microfractures is readily demonstrated within detrital quartz grains (intragranular microfractures), however fracturing along grain boundaries (intergranular fractures) has also occurred. Although a few quartz grains are in direct contact with their neighbours, the vast majority are enclosed by fine-grained recrystallised 'groundmass'. There is generally only minor translation and/or rotation of fractured grains associated with this style of deformation, and primary internal laminations are commonly weakly preserved. Separation across microfractures is typically less than 10 μm and they are invariably healed. In most cases, the microfractures are defined by narrow planar arrays of fluid inclusions, however microveins comprising silica and/or extremely fine-grained phyllosilicates are also common (Fig. 5.12c). Intragranular microfractures were most commonly observed in vertically oriented thin sections (cut perpendicular to the principal planar mesoscopic fabric), however a numerically subordinate population is also shown in horizontally oriented thin sections. They penetrate only part way, or truncate grains completely, but generally do not propagate into the surrounding groundmass, terminating at grain boundaries. Exceptions occur where neighbouring quartz grains are in direct contact and share a common, sutured grain margin. In such cases, microfractures can be traced across the grain aggregate (up to three grain diameters have been observed to be truncated) and they clearly cross-cut the pre-fracture sutured margins.

Individual detrital grains contain between one and fifteen microfractures, with multiply fractured grains most commonly observed in vertically oriented thin sections. Where several microfractures are developed within a single grain, they are typically

arranged in relatively evenly spaced, sub-parallel sets. Up to three generations of microfracture sets can be seen within any one grain, with each generation distinguished by slight differences in orientation (generally less than 30°) and clear overprinting relationships (Fig. 5.12d). The sense of transection exhibited by successive microfracture generations is consistent throughout cohesive portions of inclusions, with the demonstrably youngest fracture generation oriented sub-perpendicular to the long axes of inclusions. Where this style of deformation is associated with conjugate arrays of brittle extensional shear fractures, the trace of the youngest microfracture generation is oriented close to the linear bisector of the conjugates.

Quartz overgrowths and fibrous microstructures

Apart from the development of intragranular microfractures, the most striking feature which distinguishes IDCF from the microstructural fabric seen in the least deformed inclusions is the development of quartz and phyllosilicate overgrowths on detrital quartz grains (Figs. 5.12c-e). Overgrowths of quartz are commonly optically continuous with the original detrital core, resulting in markedly angular grains with serrate margins. In some cases however, overgrowths can be distinguished from the core by slight differences in incidence, crude fibrous texture, or an anomalously high density of fluid inclusions. Evidence of silica overgrowth can also be manifested in the incorporation of different mineral phases within the outer portion of grains. In Figure 5.12g for example, a detrital zircon grain is partly enclosed by the neighbouring quartz grain. Note that there is no apparent increase in intragranular distortion towards quartz grain margin as would be expected if this relationship had resulted from crystal-plastic grain migration (cf. Urai et al., 1986). Incorporation of the zircon grain must therefore have resulted from the growth of quartz from the original interface of the two grains. Phyllosilicates which have grown along the margins of quartz grains include fine-grained chlorite or white mica and show a well developed fibrous texture (resembling mica beards) in vertically oriented thin sections (Fig. 5.12e). They are commonly interspersed with fine fibres of quartz and in many cases there is a gradation at the margins of detrital cores from textureless silica overgrowth $\rightarrow$ intergrown fibres of quartz and phyllosilicate $\rightarrow$ extremely fine-grained fibres of phyllosilicate.

The composition and texture of overgrowths on grain margins is identical to the vein material precipitated along intragranular microfractures. As is the case with overgrowths, where intragranular vein material consists of recrystallised phyllosilicates they are seen as bundles of parallel fibres which connect originally joined points on the walls of the microfracture (Fig. 5.12f). Furthermore, the orientation of fibres developed in overgrowth regions is usually parallel to those associated with intragranular microveins and/or sub-orthogonal to the trace of microfractures. Multiple generations of sub-planar fibrous microstructures are locally developed in a similar fashion to

microfractures. Preservation of earlier fibrous microstructure generations is poor however, probably due to recrystallisation during successive fracture/crystal growth events. Generally only the youngest generation of fibrous microstructure is preserved, which in accordance with their characteristic orthogonality to the each microfracture generation, defines a crude linear fabric in vertically oriented thin sections that is roughly parallel to the trace of S_{SP} in the matrix (ie. roughly perpendicular to the youngest microfracture generation). This fabric is either absent or only very weakly developed in horizontally oriented thin sections. This lineation/foliation relationship is consistent with the observation of a steeply pitching fibrous mineral lineation developed at the tips of elongate inclusions on cleavage surfaces in polished hand specimens (see sections 5.4.1). The observations outlined above are interpreted to indicate genetic and temporal relationships between fibrous overgrowths, intragranular microveins and extensional microfractures.

"Extended" quartz grains

The combined effects of displacement associated with extensional grain breakage and quartz growth at the termination of grains and as intragranular microveins has locally resulted in the development of a grain elongation fabric. This fabric was observed in a few inclusions within vertically oriented thin sections, but is absent in horizontal sections. It is not pervasively developed throughout inclusions however, and only affects a small number of detrital grains. Examples of elongate grains can be quite spectacular (Fig. 5.13a), with aspect ratios in excess of 10:1. Many show smooth, sweeping undulose extinction, suggesting that they were derived from a single parent grain. Others however, show a patchy or "blocky" extinction, with slight (5°-25°) deviation in optical continuity across extensional microfractures. These grains may formed as a result of "fusion" of a linear series of favourably oriented grains (ie. healed intergranular fractures), or alternatively mis-orientation across microfractures may be attributable to slight rotation of fragments accompanying grain breakage. The rather randomly distributed, discontinuous traces of these elongate grains tends to suggest that they do not represent fragmented quartz veins. In cases where elongate grains appear to have been derived from a single parent grain, they are interpreted to have "extended" during repeated episodes of tensile failure and healing of fractures. Portions of grains that comprise new mineral growth are distinguished by high densities of fluid inclusions. These occur at the ends of grains, where they may form delicately tapered "tails", and at regularly to unevenly spaced intragranular locations (Fig. 5.13b). A few elongate grains show undulatory margins which are interpreted to have resulted from ductile "necking" of pre-existing microvein regions during progressive extension (Fig. 5.13c). This style of structure superficially resembles 'bone-shaped' boudins of Malavieille and Lacassin (1988), however in contrast to descriptions from these

Figure 5.13 Photomicrographs of "extended" quartz grains.

(**a**) Series of extended quartz grains with long axes oriented horizontally. The lower grain has an aspect ratio in excess of 10:1. (plane polarised light: sample H2A)

(**b**) Delicately tapered tail of an extended quartz grain with density of fluid inclusion trails increasing towards the tip. (crossed polars: sample H2A)

(**c**) Boudinaged quartz grain with serrate margins typical of bone-shaped boudins. (crossed polars: sample 12)

(**d**) Long axis of elongate quartz grains re-oriented by oblique intragranular microfracturing. An early set of microfractures can be seen to be sub-perpendicular to the long axis. (crossed polars, sample H2B)

(**e**) Parallelism of extended quartz grain fabric with internal S_{SL} defined by discontinuous phyllosilicate films. External S_{SL}: is oriented horizontally. (crossed polars: sample H2B)

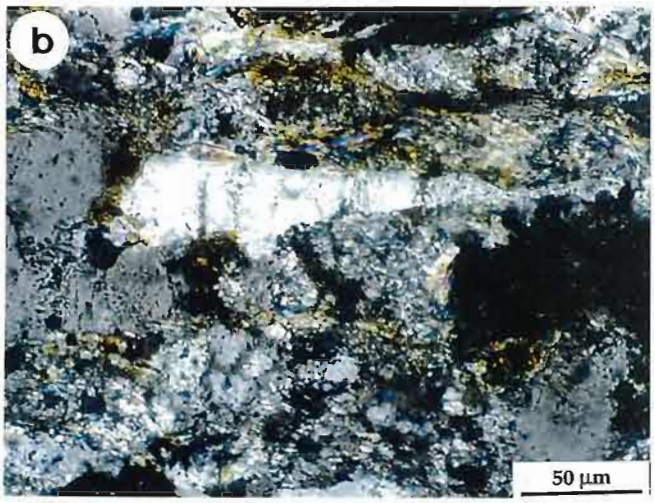

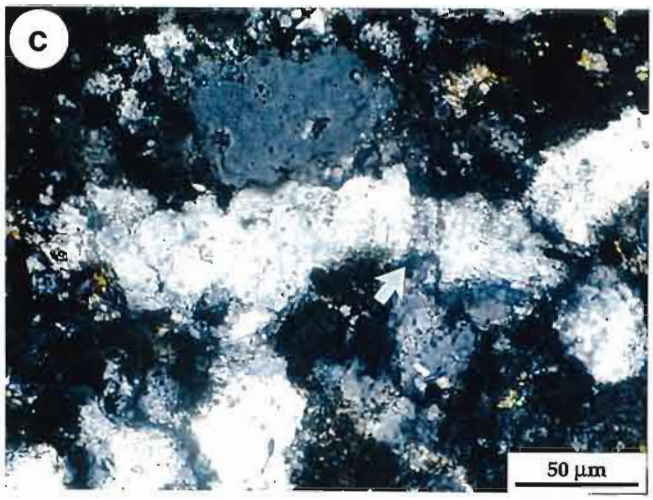

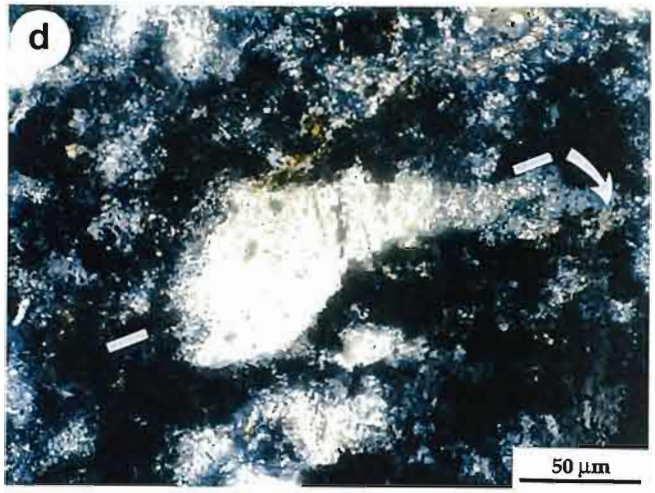

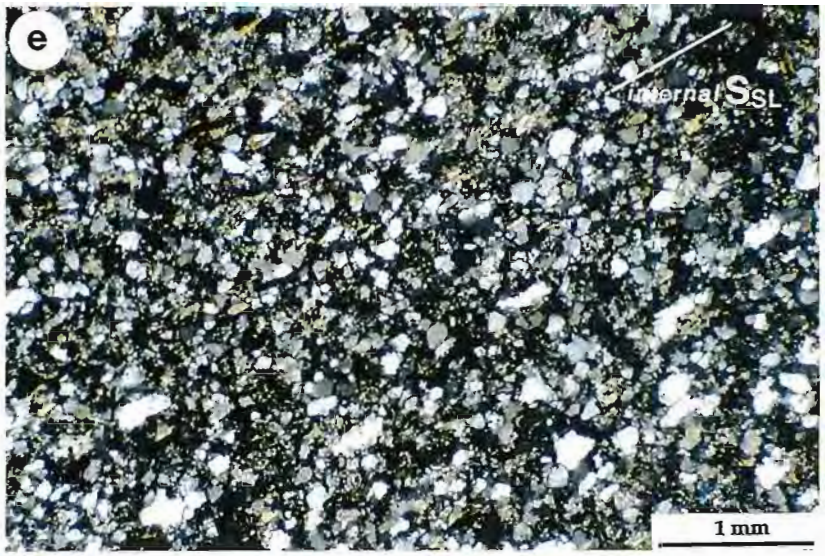

external S_{SL}

workers, ductile stretching is accommodated in the mineralised partings rather than 'boudin' segments.

The orientation of grain long axes in vertically oriented thin sections varies by up to 40° throughout individual inclusions. The largest population of long axes are oriented sub-perpendicular to older extensional microfracture generations contained within a given inclusion, suggesting that they developed early during the fracture history. As a result, most grains are oblique to the external S_{SP} cleavage and the lineation defined by fibrous microstructures, however a few have been partially or completely re-oriented into this direction. This has been accomplished by bending of "tails" or truncation of grains by later episodes of microfracturing along surfaces oriented obliquely to long axes (Fig. 5.13d). Grains which possess the highest aspect ratios are least affected by this process of mechanical re-orientation.

Mechanisms of grain breakage

Over the last 25 years, our understanding of cataclastic processes in quartz-dominated grain aggregates has advanced significantly through both experimental studies performed under controlled environmental conditions (Dunn et al., 1973; Rutter and White, 1979; Zhang et al., 1990; Scott and Nielsen, 1991; Menendez et al., 1996) and detailed investigation of natural fault rock deformed at upper crustal levels (Aydin, 1978; Aydin and Johnson, 1978; Jamison and Stearns, 1983; Lucas and Moore, 1986; Antonelli et al., 1994; Lloyd and Knipe, 1992). Overwhelming evidence presented in many of these studies has demonstrated that the dominant mechanism of grain breakage during at least the early stages of cataclastic deformation involves stress concentrations induced by point loading across grain-grain contacts (cf. Gallagher et al., 1974). Strain induced by this mechanism is manifested as 'Hertzian-type' fractures (Zhang et al., op cit) which develop as intragranular tensile microcracks propagating from isolated grain contacts or connecting contact points between neighbouring grains. Pervasively developed microfractures of this type may form in systematic arrays, with cracks preferentially oriented parallel to the far-field maximum compressive stress direction (σ_1), or more complex, random patterns controlled principally by grain contact geometry and localised stress concentrations.

Although this process of grain point loading has probably contributed in part to the development of microfractures observed in this study (ie. in those cracks which propagate across quartz grain contacts), the majority of fractured quartz grains are enclosed by 'groundmass' and do not involve grain-grain contacts. Furthermore, microfractures related to a discrete generations are strongly aligned and do not show the variability in orientation expected from Hertzian-type microfracturing.

A second, but considerably less well-documented style of microfracturing involves the fragmentation of brittle grains which are set within a weaker groundmass

(cf. Aydin, 1978, p. 921; Lloyd and Knipe, 1992, p.138). Fracturing of this type involves localised stress concentrations induced by the different rates of extension between rigid particles set within a weaker, ductilely flowing groundmass. This mechanism can be approximated with fibre-loading and has been invoked to explain grain-size reduction of brittle mineral phases set within ductile matrices in mylonites (eg. White et al., 1980; Boullier, 1980). Fibre-loading theory is based upon the balancing or transfer of tangential stresses at the interface of an elongate rigid particle set in a ductilely extending groundmass by tension in the rigid particle (White et al., op cit; Lloyd et al., 1982). Tensile stresses increases towards the centre of the rigid particle, the magnitude of which is controlled by the particle length. The particle will deform via progressive mid-point extensional fracturing until fracture segments attain a geometry that prevents tensile stresses from exceeding the tensile strength of the material. As is the case with some Hertzian-type fractures, microfractures attributable to fibre-loading would be expected to show a strong preferred orientation parallel to σ_1, however they do not require rigid grains to be in point contact to initiate fracture. Moreover, microfracturing would be most pronounced in elongate grains oriented in the direction of the maximum incremental stretch, with initial fracturing concentrated around the centre of these grains.

Probably the best evidence for a mechanism of grain breakage via fibre-loading is the development of elongate grains with quartz-sealed microfractures. Consider an elongate quartz grain which is oriented sub-parallel with the direction of maximum incremental stretch imposed upon ductilely extending groundmass. If rate of displacement along intragranular fractures is matched by the rate of crystallisation of quartz microvein material, separation of the grain into discrete fracture segments will not be achieved. Instead, the grain will appear to be 'drawn out' in the direction of maximum stretch. The effective length of the grain will thus be *increased* via repeated episodes of fracture and healing as long shear stresses are maintained at the interface with the groundmass. As the length of the grain is not reduced, tensile stresses will persist in exceeding the tensile strength of the grain and as such it will continue to fracture, primarily along its centre. Thus the process of repeated grain breakage and fracture healing is self-feeding and may be expected to continue until the rate of crack sealing can no longer match the rate of separation along microfractures. This could result from a reduction in the volume of saturated fluids percolating through the sandstone due to progressive cementation of voids and loss of permeability. Alternatively, the composition of the fluid may change with time, potentially resulting in the precipitation of mineral phases which are weaker than the host grain. A possible example of such a growth history is shown in Figure 5.12a, where the maximum separation of the fracture segments has occurred towards the centre of the elongate grain along cracks healed with fibrous phyllosilicate material.

In terms of the physical character of the rock at the time of deformation, the recognition of a fibre-loading fracture mechanism is significant in that it indicates that there was sufficient cohesion between the framework grains and the enclosing groundmass to allow shear stresses to be maintained at the interface of these components. Accordingly, the sandstone can be regarded as having been lithified during the course of the deformation (cf. Maltman, 1984). If the rock was unlithified during deformation, decoupling between the groundmass and the quartz grains would prevent the transfer of tensile stress to the latter and consequently fracturing would be inhibited. In contrast, Hertzian-type fractures are not necessarily confined to lithified sandstone and can be formed in unconsolidated sediment during transient elevation of effective confining stress in response to pore pressure reduction. Examples of cataclasis resulting from impingement of rigid grains (ie. point loading) in unlithified sediment sampled from the Middle America Trench have been presented by Lucas and Moore (1986).

5.5.2.2 Through-going brittle extensional and shear fractures

Extensional fractures

Through-going microfractures with little or no shear offset or associated zone of grain comminution were observed in a few weakly deformed inclusions. They consist of irregular to sub-linear arrays of linked microfractures which propagate both through isolated quartz grains and along the interfaces of grains and groundmass (Fig. 5.14a). Rare examples of cracks propagating through the groundmass were also observed, indicating that the fracture strength of both grains and groundmass were locally comparable during deformation. Intragranular microfractures are usually defined by linear tails of fluid inclusions or healed surfaces which either terminate at the margins of grains or link to intergranular fractures. Rarely, fibrous microfracture infills were observed with fibres oriented perpendicular to fracture walls. These microstructures coupled with lack of shear offset associated with linked arrays are interpreted to indicate an extensional history. The fracture mechanism is considered to be similar to that associated with IDCF.

Where linked extensional fractures occur within rectangular inclusions, they are oriented sub-perpendicular to internal bedding laminations and cluster towards the centre or near the terminations of inclusions (Fig. 5.14b). Those positioned in the centre of elongate inclusion are interpreted to represent sites of incipient mid-point fracturing during progressive extension fracture boudinage of sandstone layers and provide evidence that grain fracture mechanisms were active during the early stages of layer fragmentation.

In cases where dilation has accompanied microfracturing, fine-grained matrix or quartz veins with blocky crystalline interiors and irregular margins follow the trace of

Figure 5.14 Photomicrographs of brittle through-going fractures

(a) Linked extensional fracture shown in the centre of field of view and highlighted by black dashed line. Intragranular microfractures cluster around the through-going fracture and show similar orientations. (plane polarised light: sample 12)

(b) Development of linked extensional microstructures within central portions and along margins of blocky inclusions. Notice the offset of the fracture due to sliding along lamination surfaces. (plane polarised light: sample H2A)

(c-g) Progressive magnification of shear fractures (plane polarised light: sample H2B)

(c) Conjugate sets of shear fractures offsetting inclusion margins but not penetrating the matrix. Dextral set is oriented sub-perpendicular to internal laminations .

(d) En echelon array of shear fracture segments linked by compressive bridges (arrow). An internal 'fluxion' texture reflects the sense of shear .

(e) Development of linked arrays of intragranular microfractures in the walls of the shear fractures. These fractures are oriented sub-perpendicular to the external melange fabric.

(f-g) "Spalling" of a quartz grain along the margin of the shear fracture: **(g)** shows increased component of crystal plastic deformation towards the fracture with sub-grain development at the contact. (**f** taken under plane polarised light; **g** taken under crossed polars)

(h) Wavy linked microfractures. Extensional microfractures filled with stretched fibre veins are linked across intergranular fracture surfaces. (plane polarised light: sample H3B)

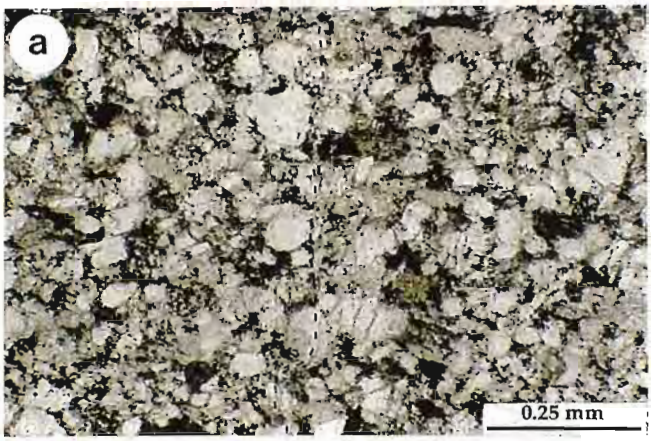
a
0.25 mm

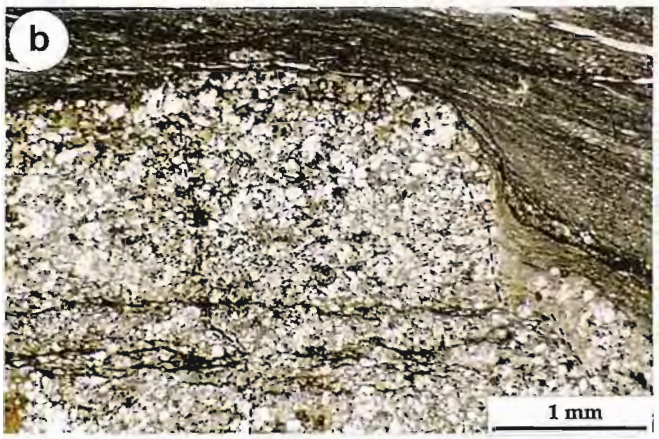
b
1 mm

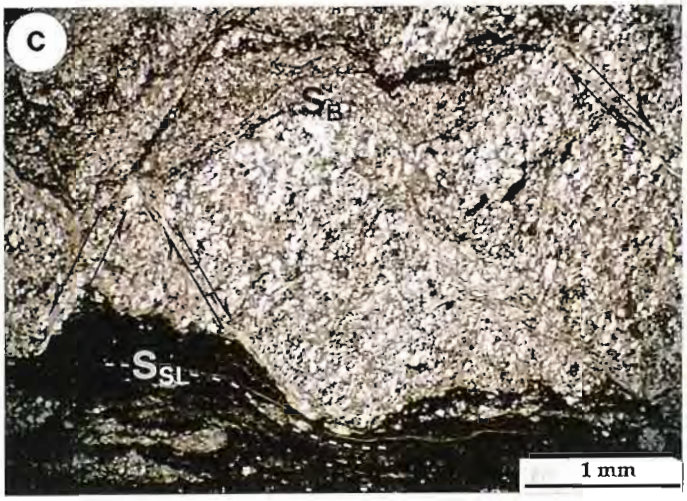
c
S_B
S_{SL}
1 mm


d
0.5 mm


e
36°
0.25 mm


f
0.1 mm

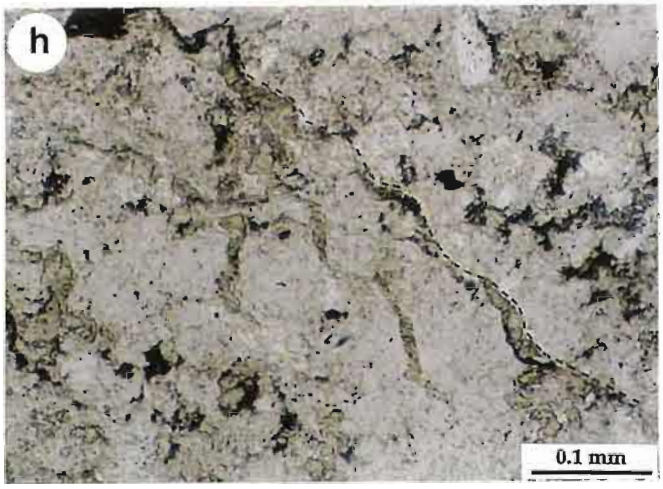
h
0.1 mm

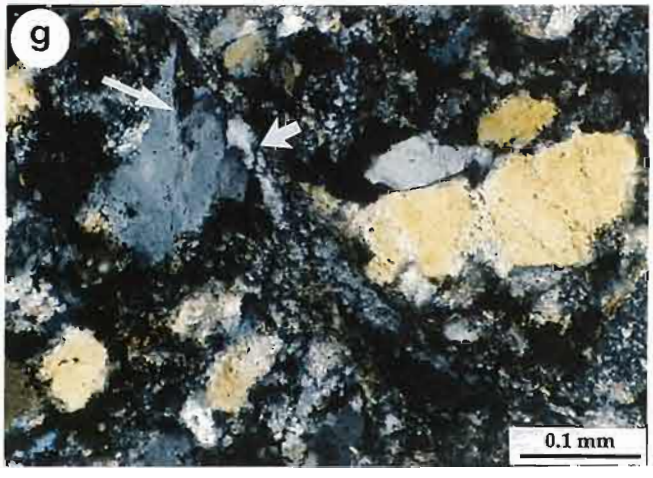
g
0.1 mm

extensional microfractures. Continued extension has resulted in fracturing of quartz vein material, producing narrow, linked tensile microfractures defined by fluid inclusions or healed by cryptocrystalline quartz. If dilation associated with re-opening of veins is significant, composite crack-seal veins develop with successive infilling of quartz, calcite, Fe-oxides or mud. Re-opening of veins generally occurs close to the vein-wall contact so that the younger mineral species occupies the margin of the vein, however median fracturing and vein infilling was also observed locally.

Shear fractures

Fractures displaying shear offset are only developed in inclusions which have experienced a prior component of rotation (usually sympathetic with the bulk flow in the matrix) such that internal bedding laminations are no longer parallel to melange fabric. They represent discrete surfaces across which cohesion of the sandstone is lost and have resulted in visible offset along the margin of the inclusion (Fig. 5.14c). Brittle fractures do not usually extend into the matrix, with the fabric in the latter wrapping ductilely around the corrugated inclusion-matrix interface. In cases where the amount of displacement on the shear fractures has resulted in complete separation of inclusions (ie. where displacement exceeds to the length of fracture in the sandstone), fractures may propagate a short way into the matrix as shear bands. The sense of displacement is invariably extensional in the plane of the melange fabric.

Incipient shear fractures are developed as both single sets or conjugate pairs, the latter commonly displaying symmetrical disposition about the principal axes of elongate inclusions (ie. longest and shortest axes seen in two dimensions). The acute angle between incipient conjugate fracture sets is about 60°, the bisector of which is oriented sub-perpendicular to both the long axes of inclusions and the external cleavage (S_{SL} or S_{SP}). Similarly, when only one fracture set is developed, it is initially oriented at 30° to the shortest axis of the inclusion. Asymmetric conjugate pairs have initiated in a few cases where the orientation of one of the sets is controlled by a pre-existing anisotropy such as primary lamination surfaces. In general, conjugate fault sets are unequally developed, with the numerically dominant set showing antithetic shear sense with respect to the inferred bulk vorticity in the matrix. This set was commonly observed to be oriented perpendicular to internal lamination surfaces (Fig. 5.14c). With increasing strain, shear fractures are progressively rotated towards parallelism with the inferred bulk shear plane, accompanied by rotation of the intervening cohesive blocks and generation of new fractures at roughly 30° to the short axis of inclusions. Conjugate pairs initially show opposing senses of rotation, however the synthetic set usually becomes inactive early in the deformation history and as a result may be rotated sympathetically with the cohesive block as deformation proceeds. Furthermore, only along antithetic shear fractures has displacement been sufficient to achieve complete

separation of internally cohesive inclusions. As a result, isolated inclusions formed by this mechanism of shear fracture boudinage invariably show bulk forward rotation (sympathetic component of spin) with respect to the flow in the matrix. This observation conflicts with many recent studies of the fragmentation mechanisms associated with melange belts, which have demonstrated that synthetic Riedel shears form the fundamental fracture geometry along which layers separate, resulting in an antithetic rotation of intervening inclusions with respect to the bulk vorticity in the matrix (eg. Needham, 1987; Kimura and Mukai, 1991; Onishi and Kimura, 1995; Needham, 1995).

At the grain-scale, brittle shear fractures are seen as narrow bands (40-750μm in width) of marked grain-size reduction . The margins of the bands are generally sharp, sub-planar and wall-rock grains are commonly truncated by fractures. Some fractures have developed as discrete, though-going surfaces, however a significant proportion appear as a series of slightly offset *en echelon* segments linked by compressive bridges (Fig. 5.14d). At the terminations of fractures near inclusion boundaries, a series of fish-tail splays commonly develop on the extensional side of the fracture-tip. There is a close spatial and temporal relationship between the development of shear fractures and microstructures associated with IDCF. Intragranular extension microfractures are pervasively developed in the wall rocks adjacent to shear fractures and are usually oriented at 30° to 65° to the latter (Fig. 5.14e). In a few grains however, an early generation of intragranular extension microfractures was observed sub-parallel to shear fractures.

Many of the fractures possess an internal anisotropic fabric which is oriented at acute angles (5°-40°) to the fracture walls. This fabric involves a distinct *en echelon* banding or 'fluxion' texture which imparts a sense of flow that is consistent with the overall shear sense indicated by offset at the margins of inclusions (Figs. 5.14d, 5.15a). The 'fluxion' texture is defined in part by elongate, wavy stringers of relatively weak opaque materials such as oxides, sulphide aggregates and phyllosilicate-rich particles, which have been progressively extended and rotated towards parallelism with fracture walls as shear strain increases. Separating these dark bands are elongate augen-shaped lozenges containing highly comminuted quartz grain fragments in an extremely fine-grained ground mass of quartz and chlorite. Delicate 'tails' (some of which are fibrous) extend from diametrically opposing corners of many lozenges in a manner similar to σ-porphyroclast systems in mylonites. Within the fractures, the size of the fragmented particles increases markedly from planar fracture segments to compressive bridges, wherein grains have ubiquitous intense undulose extinction, local sub-grain and high angle grain boundary recrystallisation and extension microfractures oriented at roughly 65°-85° to the shear zone margin. The high angle of the extension fractures within compressive bridges reflects the localised additional component of shortening directed

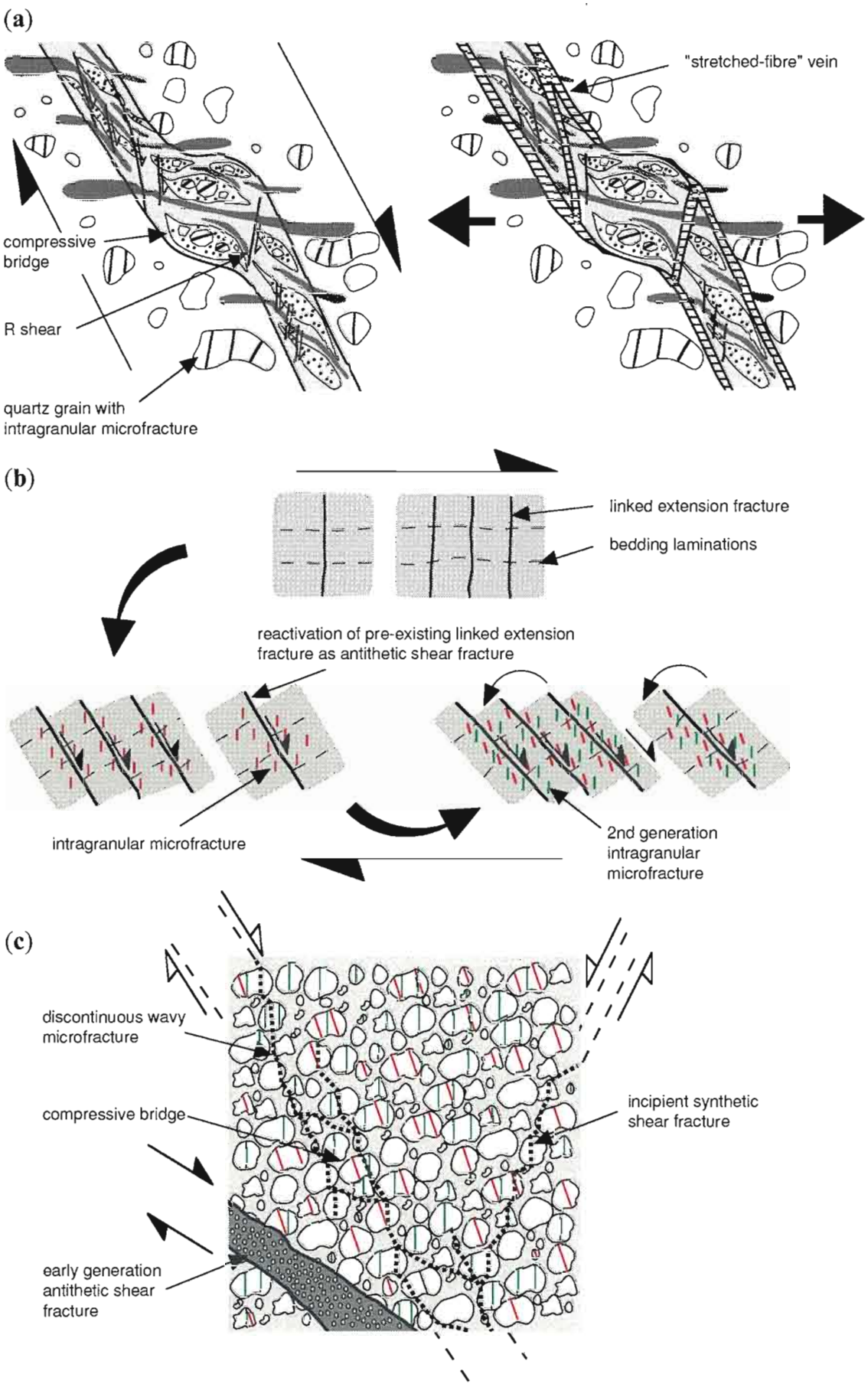

Figure 5.15. Through-going brittle fractures: microstructures and mechanisms. (**a**) Internal "fluxion" texture of brittle shear fracture. The diagram depicts *en echelon* segments linked by a compressional bridge (left). Late stage dilation of the shear fracture results in "stretched-fibre" veins forming along walls (right). (**b**) Mechanism for development of shear fractures via reactivation of linked extension fracture in response to inclusion rotation. (**c**) Initiation of shear fractures via linking of oblique generations of intragranular microfractures and propagation of microfractures through 'groundmass'.

across the shear fractures in these regions. Conversely, the orientation of the 'fluxion' banding with respect to the fracture walls decreases from 40° in compressive bridges to less than 5° in narrow planar shear segments, indicating the high shear strains accumulated within the latter. Along the margins of the fractures and in the immediately adjacent wall rock, the 'fluxion' texture is also contributed to via 'spalling' of particles from partially fragmented wall-rock grains and bending or pre-fractured quartz and detrital mica grains respectively. In Figures 5.14f, g for instance, the large quartz grain to the right of the field of view is drawn out against a shear fracture to produce an asymmetric tail indicating the sense of shear. Note that within the grain, the degree of strain which has been accommodated by crystal plastic processes increases markedly towards the shear fracture: patchy undulose extinction throughout much of the grain passes into a zone adjacent to the fracture which contains high angle (rotated) sub-grains with progressively increasing degree of misorientation across grain boundaries and small recrystallised grains formed along diffuse boundaries. Note also the intimate spatial (?and temporal) association of structures indicative of crystal plasticity and intragranular extension microfractures. The tail becomes too fine-grained within the shear fracture to determine whether grain-size is further reduced via fracture or dynamic recrystallisation.

Cross-cutting the components of the 'fluxion' texture is an *en echelon* array of micro-scale extensional shear fractures with displacements ranging 10-75mm (Fig. 5.15a). Arrays form at angles of between 25°-7° to the shear fracture margins; orientations which are compatible with synthetic Riedel fractures (R-shears) formed in brittle shear zones (cf. Tchalenko, 1970). The angle between the R-shears and the fracture walls decreases progressively from compressive bridges into shear fracture segments. In some cases they are healed by a thin quartz film.

Late-stage development of many shear fractures involves the growth of 'stretched-fibre' veins (cf. Ramsay and Huber, 1983) consisting of quartz, chlorite and sericite (Fig. 5.15a). These fibre veins are analogous to the fibrous microveins associated with IDCF and both structures commonly show similar orientations of crystal long axes. Veins usually form within dilational cracks positioned along the walls of the shear fracture, such that the pre-existing gouge (and 'fluxion' texture) appears to 'float' within a fibrous groundmass. In some cases however, favourably oriented R-shears are reactivated as dilational fractures, resulting in fibre veins cross-cutting the gouge fabric. Fibre orientations are consistently oblique to the 'fluxion' texture developed within adjacent gouges and generally lie with a few degrees of the external cleavage (and the long axes of inclusions). Thus assuming that the fibres have faithfully tracked the displacement vector during fracture opening, they indicate a dominant component of extension across the fracture.

Origin of shear fractures

There are two possible modes of shear fracture initiation, both of which contribute to their development in particular situations. The first is a mechanism which involves reactivation of pre-existing linked extensional fractures, which have been rotated passively during bulk rigid body rotation of the host inclusion (Fig. 5.15b). At the point where shear stresses exceed the frictional resistances along the fracture, brittle failure will occur. From the attitude of shear fractures within inclusions which demonstrate relatively low strains, shearing is initiated after approximately 30° of bulk rotation. Fluctuations in fluid pressure and its control on effective confining pressures and the ultimate strength of the inclusion is also likely to play an important role in determining at which point shearing will initiate. The most convincing evidence for this mechanism of shear fracture development is the observation that antithetic shear fractures are commonly oriented sub-perpendicular to internal bedding laminations and thus in the orientation predicted for linked extensional fractures prior to inclusion rotation. Furthermore, early generations of intragranular extension fractures positioned immediately adjacent to shear fractures were sometimes observed to be oriented sub-parallel to the latter, suggesting an early phase of extension associated with these structures.

Unless linked extensional fractures continued to develop after inclusion rotation and the onset of shear, for which there appears to be little evidence, the shear fracture initiation mechanism outlined above can only account for one set of fractures. Thus in order for multiple sets and indeed conjugate pairs to develop, it would seem that at least some fractures do not evolve via modification of pre-existing extensional structures but rather initiate directly as oblique shear fractures. In these cases, there is probably an important genetic relationship between intragranular extension fractures developed as a result of IDCF within blocks separated by early-formed brittle shear fractures and the propagation of secondary shear fractures. In Figure 5.14h, an example of inferred incipient shear fracture development is shown. Sub-parallel arrays of short, wavy microfractures can be seen to consist of two linked components: 1) intragranular extensional microfractures with fibre growth oriented sub-perpendicular to the fracture walls, and 2) microfractures oriented obliquely to the former (by angles up to 55°) and positioned either along grain boundaries (intergranular microfractures) or wholly contained within individual grains. The enveloping surfaces of the wavy microfracture arrays are inclined at between 20° and 30° to the intragranular microfracture set and the short axis of the inclusion (oriented vertically in the photograph) and are thus oriented close to the direction expected for shear fracture initiation. In cases where grains contain multiple generations of microfractures, linking of oblique sets may provide an effective mechanism for producing wavy microfractures (Fig. 5.15c). I suggest that linking of suitably oriented wavy microfractures significantly reduces the fracture

strength of the inclusion such that strain is accommodated principally along localised brittle shear surfaces at the expense of IDCF. Propagation of incipient shear fractures by linking of *en echelon* arrays of discontinuous wavy microfractures across compressive bridges can further increase the component of resolved shear stress along the fracture which may in turn enhance strain softening within these zones. These observations and inferences are very similar to those of Dunn et al. (1973) and Scott and Nielsen (1991) from their studies of experimentally induced brittle behaviour in low porosity sandstones. In both of these studies, the respective workers argued for an early episode of extensional microfracturing with subsequent linking of these microstructures to form oblique, through-going brittle shear fractures. If with progressive strain hardening within the shear fractures (potentially associated with increased frictional resistance as a result of grain comminution, cementation of fractured particles, or increased component of effective normal stress resulting from fracture rotation or fluid pressure decrease) they become inactive, IDCF may again become the dominant deformation processes and the cycle is repeated.

This second mode of shear fracture generation does not appear to be important during the initial stages of layer fragmentation. I have found no examples of sedimentary layers having been initially transected by brittle fractures oriented obliquely to primary bedding. Thus, although inclusions, formed by disaggregation along these secondary shear fractures, are strictly shear fracture boudins, it must be remembered that this is a secondary process and post-dates an initial fragmentation mechanism involving extension fracture boudinage. The combination of both IDCF and brittle fracturing can result in marked change in the external geometry of inclusions without complete destruction of internal sedimentary fabrics. As the fundamental process of grain breakage inferred for the development of these microstructures is fibre-loading, they are likely to form within lithologies containing relatively high abundances of 'groundmass' (in this case a combination of primary sedimentary matrix and altered labile constituents).

5.5.2.3 Inclusions showing transitional brittle-ductile behaviour: web structure

Inclusions which exhibit dominantly transitional brittle-ductile behaviour are characterised by loss of internal cohesion across a network of anastomosing cataclastic shear zones. Remarkably similar structural fabrics, commonly referred to as "web structure", have been well-documented from numerous studies of ancient melange belts (eg. Byrne, 1984; Lash, 1985; Lucas and Moore, 1986; Fisher and Byrne, 1987; Agar, 1988; Kimura and Mukai, 1991). The term "web structure" was originally coined by Cowan (1982) to describe the style and geometry of clay-rich seams and fractures developed in the Fransiscan melanges, however he considered that cataclasis played a sub-ordinate role to particulate flow during their development. In this thesis, I employ

the term in the sense of Byrne (op cit) who refined its usage to include only randomly oriented cataclastic shear zones developed within sandstone inclusions.

Web structure in the Ring River melange is developed at both meso- and microscopic scales and is generally restricted to massive sandstone inclusions. Mesoscopic fabrics were readily observed on smooth, river-worn surfaces as a series of dark, curviplanar seams (Fig. 5.16a) which were either pervasively developed throughout entire sandstone inclusions or concentrated within the neck regions of pinch-and-swell structure. The dark colour of the seams owes partly to the comminution of detrital sand grains, but mainly to the precipitation of a chlorite 'matrix', which commonly extends a short way into the zone walls resulting in a diffuse halo. The network of seams isolates lenses of less-deformed paler sandstone and shows a close spatial association with quartz vein arrays. Mutually cross-cutting relationships are shown by the shear zones and quartz veins, indicating that a temporal relationship between the two structures is also likely. Very similar fabrics are developed within micro-scale inclusions (Fig. 5.16b) where they occur in association with rare brittle shear fractures. In some cases grain comminution is not confined to discrete shear zones, but is pervasively distributed throughout the entire inclusion or concentrated within 'tails' of asymmetric inclusions (Fig. 5.16c). Inclusions exhibiting this latter style of internal strain are considered to have flowed in a ductile fashion with smoothly distributed deformation rather than loss of cohesion across discrete fracture surfaces. The degree of internal strain is considerably higher than those exhibiting brittle fracture and/or IDCF, with near complete destruction of the original grain fabric via a combination of fracture, crystal plastic and DMT mechanisms. It is unclear as to whether that the lack of internal sedimentary fabrics such as bedding laminations is solely a function of the high levels of strain or if it is a reflection of the original lithological character of the parent layer.

Many of the microstructural textures associated with web structure resemble those developed in brittle shear fractures, however three critical features have been observed which enables them to be distinguished. Firstly, although the individual shear zones associated with web structure show evidence for limited (mm-scale) displacements, they have not resulted in appreciable offset of inclusion margins. Secondly, shear zones rarely develop into through-going structures and characteristically form short, discontinuous segments which can be traced more than 5cm within even the thickest sandstone inclusions before being truncated by another shear zone. Thirdly, the relatively systematic geometries shown by brittle shear fracture sets are in marked contrast to arrays of web structure which exhibit a random disposition and complex cross-cutting relationships. I consider these features outlined above to indicate that web structure has not contributed significantly to the separation of

Figure 5.16 Transitional brittle-ductile cataclastic behaviour

(**a**) Complex network of cross-cutting cataclastic shear zones in a thick massive sandstone inclusion. These textures bear a striking resemblance to "web structure" described from melange developed in accretionary environments. Lens cap is 60mm in diameter.

(**b**) Similar complex network of cataclastic seams formed at the microscopic scale. The seams are slightly darker that the less-deformed wall rock material. (plane polarised light: sample H3A)

(**c**) Ductile cataclastic flow in the tail of an asymmetric inclusion. A progressive reduction in grainsize is shown from the core of the inclusion to the tail. (plane polarised light: sample H3A)

(**d**) Narrow cataclastic shear zone with a sharp, planar contact with significantly less deformed wall rock grains. (crossed polars: sample 354)

(**e**) Cataclastic shear zone with sub-planar margins and extreme grainsize reduction shown along the margins of the zone. (crossed polars: sample H3A)


a
Nikon


b
1 mm

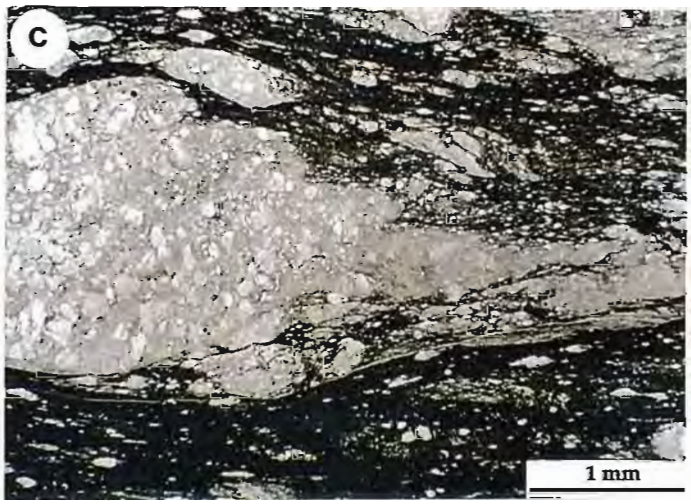
c
1 mm


d
0.25 mm


e
0.25 mm

sedimentary layers and inclusions, but rather have accommodated the change in external shape of inclusions.

At the microscopic scale, individual shear zones show sharp to irregular and diffuse margins. Those which possess less clearly definable, irregular margins have a fairly uniform internal fabric involving poorly sorted grain fragments cemented by fine-grained quartz and/or chlorite. Particle size increases transitionally towards less deformed wall rock accompanied by a reduction in authigenic cement. Sharply bounded shear zones were observed in only a few cases and involve discrete sub-planar surfaces or narrow bands positioned along one or both sides of the shear zone. These surfaces are defined by either healed tensile fractures along which little or no displacement has accumulated (Fig. 5.16d) or narrow domains of extreme grain-size reduction (Fig. 5.16e). In examples of the latter the dimensions of particles contained within the shear zone decreases rapidly towards the outer planar margin(s), resulting in an internal zonation which may be either symmetrically or asymmetrically disposed about the median line of the shear zone. Extensional microfractures oriented sub-parallel to the main shear zone are developed in the immediately adjacent wall-rock. The change from diffuse to sharply bounded shear zones is interpreted to reflect a transition in faulting mechanism from stable sliding to stick-slip behaviour during which slippage becomes progressively confined towards the margins. As strain hardening processes cause increasing resistance to shear, slippage is transferred to extensional microfractures contained within the wall rock, resulting in progressive widening of the shear zone. Alternatively, shear zones may become abandoned completely, with displacement being taken up along older reactivated surfaces or newly formed shear zones.

5.6 Discussion

5.6.1 Grain-scale processes

In the microstructural descriptions presented in the preceding sections, I have attempted to highlight the importance of fracture mechanisms operating throughout the strain history of coarse-grained lithotypes and their intimate association with both crystal plastic and DMT processes. Furthermore, I have suggested that the development of through-going fractures (linked extensional fractures and brittle shear fractures), structures which provide the principal control on layer separation and inclusion geometry, are at least partly dependant upon the mechanical instabilities formed at the grain-scale.

The interdependence of fracture and DMT processes during deformation at upper crustal conditions has been widely recognised from studies of both brittle faulting (eg. Rutter and White, 1979; Stel, 1981; Lloyd and Knipe, 1992; Knipe, 1993; Knipe

and McCaig, 1994) and cleavage development (Cox and Etheridge, 1989). Similarly, detailed analysis of microstructures developed within quartz-dominated grain aggregates from this study provides overwhelming evidence for the close temporal relationship between these two deformation mechanisms. This relationship is most clearly demonstrated by healed microfractures which occur as systematic arrays of fluid inclusion trails, micro-scale stretched-fibre veins which track the opening of both intra- and intergranular microfractures and the development of "elongate quartz grains" during IDCF. Pervasive precipitation of quartz and/or chlorite cements within brittle shear fractures and transitional brittle-ductile cataclastic shear zones is also considered to reflect the interaction of fracture, dilatancy and fluid transport mechanisms during cataclastic flow. The intimate association of these two processes suggests that development of microfractures provided a pathway throughout which fluids were able to migrate through and into sandstone units.

Effects of increased fluid pressure on rock strength

• The development of extension veins as both blocky quartz vein-fills within though-going dilatant cracks and fibre veins in microfractures indicates that fluid pressures were near lithostatic and hence resulted in a lowering of effective confining pressures ($s_{eff} = s_3 - P_{H20}$).

• As the fracture strength of materials increases with increasing effective confining pressure (Knipe and McCaig, 1994), an increase in fluid pressure may therefore induce brittle failure in a material might otherwise have possessed a tensile strength in excess of the imposed tensile stresses .

• Most examples of cataclastic deformation in melange and modern accretionary prisms have been attributed to a decrease in the effective confining pressure during dewatering of the incohesive sediment with progressively greater depths of burial (eg. Lucas and Moore). With decrease of fluid pressure, and consequential increasing confining pressure, grains are not effectively cushioned by the interstitial fluid and can no longer roll past each other as with independent particulate flow (cf. Borradaile, 1981). Where stress concentrations at grain-point boundaries exceed the grain strength, cataclasis is initiated. Thus, cataclasis under these conditions is considered to result from a progressive strengthening or cohesion of the sediment. This style of grain-point fracturing is inconsistent with the mode of grain breakage seen in this study.

Origin of fluids: relationships to cleavage development and its effect on deformation mechanisms

• The sub-parallel orientation of younger stretched fibre vein generations (consisting predominantly of extremely fine sericite fibres) with the external S_{SL} cleavage in

domains of IDCF suggests fluid migration and grain was effectively synchronous with cleavage development

• Earlier generations of fracture are aligned subparallel to the internal S_{SL} fabric defined by fine-grained recrystallised phyllosilicate films. Microfractures are healed primarily by quartz with minor chlorite and preservation and/or development of fibrous veins is poor. These early generations of cracks and vein fills are thus probably associated with the incipient development of S_{SL} and have been unable to track the XY plane of the finite strain ellipsoid due to rigid body rotation either accommodating displacements slip along shear fractures or spin of inclusions within the flowing matrix. The fluids associated with the precipitation of vein material associated with IDCF and brittle shear fractures are thus considered to be synchronous with S_{SL} and were probably sourced during degradation of hydrous phases (eg. kaolinite and smectite) during this fabric's development. Fluids may have been at least partially sourced from within sandstone layers, particularly if they were matrix-rich and contained abundant degraded phases such as feldspar and labile lithic fragments. Evidence for sites of dissolution within sandstone is shown by the presence residual phyllosilicate films defining S_{SL}. Most of the fluid volume (and dissolved mineral species) however, was probably sourced from the clay-rich matrix as evidenced by the extremely closely spaced layer silicate films and the truncated form of quartz grains within these regions. The sandstone units may therefore be considered to be mesoscale intercleavage domains.

• Once a fracture-controlled fluid pathway was established within the sandstone units and inclusions, these were likely to have become sinks or fluid reservoirs for the dehydrating matrix. Fluid flow within the sandstone is likely to be transient, with inevitable decrease in porosity accompanying either cementation of pore spaces (ie. microfractures) or granulation within cataclastic zones. Fracturing (and development of fluid pathways) may migrate to a different part of the inclusion or be abandoned completely. Inclusions may therefore be considered as transient fluid reservoirs.

• The relatively systematic vein and cement paragenesis: 1) quartz, 2) chlorite±Fe-oxides±quartz, 3) sericite and quartz - suggests that fluid compositions changed from being rich in Si, to Mg and Fe, to K and Al. This may relate to progressive stages of S_2 development during which Si was preferentially removed early and subsequent removal of the less soluble residue.

Significance of crystal plasticity and alternation of deformation mechanisms

• Although strain has been largely accommodated by fracture or DMT processes, at least some component of strain was initially accommodated by crystal plastic processes. In the least deformed sandstone, evidence for dislocation creep mechanisms is shown by undulose extinction, incipient grain boundary migration and rare deformation bands.

Similarly, during IDCF, microfractures transgress pre-sutured grain margins or in some cases follow the traces of high angle grain boundaries.

• Crystal plastic processes become increasingly more important in association with cataclastic shear zones and ductile cataclastic flow, where it not only precedes fracture as indicated by disegregation along sub-grain boundaries, but also overprints cataclastic textures. Deformation paths involving these fabrics appear to be very complex with strain being alternately accommodated by fracture±DMT and crystal plasticity.

• The alternation between mechanisms is likely to be dependant on strain rate, fluid pressure, and temperature. Each of these factors is potentially variable during the deformation history in melange, however the rather sporadic distribution of intense plastic deformation (and the apparently synchronous activation of different processes in different inclusions) would tend to suggest that fluctuation of any of these factors is very localised and not related to a wholesale change in the imposed environmental conditions during deformation.

5.6.2 Kinematic implications of melange

Bulk flattening-type strain in the Ring River melange is indicated by chocolate tablet boudinage structure and development of orthogonal extensional vein generations. The oblate geometry of many inclusions within the melange could be attributed to the superposition of unrelated plane strain deformation events or quasi-synchronous stretching of layering in two dimensions. In support of the first of these scenarios is the development of a weak, sub-vertically plunging stretching lineation during the latter stages of the deformation history. It could be argued that an early event involving sub-horizontal extension associated with a dextral wrench system was subsequently overprinted by an unrelated dip-slip event. However, the similarities of both orthogonal vein generations and the geometry and style of inclusions shown in both horizontal and vertical sections are interpreted to indicate that the fundamental character of the melange (ie. block-in-matrix fabric) was produced during a single progressive deformation event.

The favoured interpretation for the development of the Ring River melange involves tightening and rotation of upright, shallowly plunging, pre-D_2 NNE to NE trending folds (see Chapter 2) during oblique imposition of NNW to N striking slaty (S_{SP}) and spaced (S_{SL}) cleavages. The obliquity of these cleavages to bulk sedimentary layering (S_B and S_e) shown in both horizontal and vertical sections is interpreted to indicate they transect the axial surfaces of major folds in an anticlockwise sense. A similar cleavage-fold relationship has been interpreted for the eastern parts of the Dundas region in Chapter 2 on the basis of mesoscopic fold geometry and macroscopic domain analysis. The S_{SP} cleavage is considered to approximate the XY plane of the bulk strain ellipsoid during the earliest phase of Devonian deformation. Mechanisms

for folding about axes oriented obliquely to the XY plane of the bulk strain ellipsoid have been discussed in Chapter 2. These include: i) folding of initially inclined surfaces with principal stretching axes *within* the plane of bedding oriented obliquely to the principal stretching axes of the bulk strain ellipsoid (eg. Borradaile, 1978), ii) superposition of non-coaxial, but closely oriented fold generations (eg. Odonne and Vialon, 1987) and iii) rotation of folds away from the XY plane of the finite strain ellipsoid during bulk non-coaxial deformation associated with wrenching. The first two mechanisms initially involve bulk coaxial deformations, however with increased strain, folds will rotate towards the XY plane of the bulk strain ellipsoid. Relatively incompetent but well stratified packages of strata in the sub-vertical limbs of tightened folds are considered to have become activated as NNE-striking, layer-parallel shear zones involving components of both dextral wrench and dip-slip movement. Stretching in both horizontal and vertical directions results from initial hinge-parallel extension associated with fold rotation and subsequent vertical components of stretch associated with tightening and flattening of folds. Localised non-coaxial strain in the limbs of folds resulted in clockwise rotation of the S_{SL} cleavage towards parallelism with the bulk shear plane (ie. bulk sedimentary layering). When the S_{SL} cleavage was no longer able to accommodate strain, it was abandoned and overprinted by the S_{SP} cleavage. Dip slip movement and the development of a sub-vertical stretching lineation occurred during the latter stages of deformation as the folds became progressively dismembered with remnant limbs rotated towards parallelism with the XY plane of the bulk strain ellipsoid (ie. obliquity between the bulk sedimentary layering and S_{SP} was reduced to a point at which wrench movement became inactive). In this model, shear zones are rotated towards the axes of the bulk strain ellipsoid.

A mechanism of melange development during bulk non-coaxial deformation appears less likely. The component of wrench movement would be expected to increase as deformation proceeds, with extreme hinge-parallel elongation occurring as folds are rotated into parallelism with the bulk shear plane. This is inconsistent with the late stage development of a sub-vertical stretching lineation. Furthermore, if cleavages and folds were related to a NNE-striking dextral wrench system, they must have initiated in a NW to NNW orientation. Although this is consistent with the overprinting relationships of S_e, S_{SL} and S_{SP}, it does not explain why most coherent strata strike NE. This feature is interpreted to indicate that bedding was rotated in an anticlockwise direction with progressive tightening and dismemberment of the package.

Conditions required for melange development

Detailed examination of the melange in the Dundas region indicates that the melange textures formed under conditions of:

1) Intense flattening strains

2) Low effective confining pressure inducing brittle behaviour at the grain scale
3) Marked competency contrast, such that boudinage will develop as the dominant mesoscopic (and macroscopic?) deformation mechanism.
4) Relaxation of along strike boundary constraints to allow stretching in three dimensions.

These conditions are common in accretionary environments but are not restricted to them. Similar conditions can occur in other upper crustal tectonic environments and produce melange in well-consolidated ancient rocks. The spatial relationships in the Ring River and throughout the eastern part of the Dundas region provide no support for the model that this melange was developed in an accretionary environment as suggested by Corbett and Lees (1987). The textures developed in melanges cannot be used in isolation to indicate deformation within an accretionary environment.

Chapter 6
Summary and Synthesis

6.1 Introduction

The Dundas region has a complex geology involving a diversity of rock types. Four main litho-stratigraphic elements have been identified: 1) Late Proterozoic Concert Schist and correlates of the Oonah Formation, 2) Late Proterozoic to early Cambrian correlates of the Crimson Creek Formation, 3) ?early Middle Cambrian mafic-ultramafic complexes and 4) Middle to Late Cambrian Dundas Group and correlates. There has been considerable debate regarding the distribution and genetic relationships between these successions and these are the relationships which have been subject to detailed study in this thesis. This study concentrated on last of the these elements, the Dundas Group but also considered the relationship of this element to all the others both in a sedimentological and in a structural sense.

6.2 Facies

The previous stratigraphic nomenclature for the Dundas group was not supported by the work here. The previously described formations are not mappable on a regional scale. In order to proceed with the sedimentological study it was necessary to break the section into workable units. With the very limited outcrop available the study emphasised the textures and composition of discrete sedimentary assemblages. The first step was to define the textures and composition of individual rock types.

Four clastic sedimentary facies have been recognised from the Dundas region and distinguished primarily on the basis of grainsize. In addition, facies 5 is immature volcaniclastic deposits. Second-order classification is defined for most facies types on the bases of textures such as particle shape, degree of internal organisation and the presence or absence of distinctive sedimentary structures.

Facies 1: Conglomerates

Conglomerates are perhaps the most distinctive lithologies in the Dundas region. This is principally due to their greater resistance to weathering compared to finer-grained lithologies. Consequently in previous mapping studies of this region, conglomerates have been employed as litho-stratigraphic markers. They occur as very thick, laterally discontinuous bodies and less commonly as isolated thin to medium bedded units contained within finer-grained successions.

Subfacies 1A: Clast-supported, crudely- to well-stratified conglomerates comprise the bulk of the coarse-grained facies. The largely ungraded, disorganised units are considered to have deposited from highly concentrated debris flows. The presence of normal size grading in more organised conglomerates indicates that flow turbulence was an important particle-support mechanism. Many beds of this type show internal geometries consistent with gravelly and sandy high density turbidites but carry large intraclasts well above the base of some beds.

Subfacies 1B: Disorganised matrix-supported conglomerates are common in Late Cambrian strata. The thickness of individual depositional units ranges from < 30cm to at least 25m, with the most significant accumulations, in terms of volume, occurring close to the western limits of present Dundas Group distribution. Bed geometries are tabular to highly irregular. In the few examples where primary depositional contacts were observed, bounding surfaces were usually sharp with non-erosive bases and irregular, hummocky tops. Features including dominantly muddy matrix-support of clasts, lack of internal organisation, very poor sorting, inclusion of intrabasinal clasts and sharp upper and lower bounding surfaces are typical of cohesive debris flows.

Subfacies 1C: Open- to closed-framework mafic/ultramafic clast breccias are mainly restricted to the western limits of Dundas Group exposure, where they occur close to the base of the local stratigraphy. The breccia units form discrete, laterally-impersistent bodies which occur intercalated with both subfacies 1A and 1B conglomerates. The lack of organisation and in particular the matrix-support of some of these breccias resembles textures in subfacies 1B. The main distinguishing feature between the two lithofacies is clast composition. Whereas subfacies 1B involves polymict clast assemblages which include abundant intrabasinally-derived sedimentary fragments, subfacies 1C comprises clasts which are largely monogenetic, derived from the MUC.

Subfacies 1C exposures in the Ring River were originally mapped as intrusions of gabbro or fine-grained pyroxenite. More recently they were described as fragmented basalt flows. The evidence presented here indicates a sedimentary origin for the breccia units. Their disorganised fabric, immature clast shapes, restricted distribution and monogenetic provenance provide support for deposition proximal to the source.

Facies 2: Sandstones

Subfacies 2A: Thick-bedded poorly organised sandstone facies are poorly to moderately well sorted, coarse- to fine-grained and have a compositional range from relatively clean quartzo-feldspathic to less abundant lithic-bearing varieties. The latter comprise subrounded to angular sand- to granule-sized particles of pale to dark grey mudstone, chert and rare volcanogenic material. Depositional mechanisms of subfacies 2A sandstones were transitional between debris-flows and high-density turbidity currents. The dismembered form of mudstone lamellae near the tops of some beds

indicates some fluidisation. The relatively 'clean' quartz-dominated composition possessed by many sub-facies 2A units is in marked contrast to the lithic-rich composition of most other sandy lithotypes.

Subfacies 2B: Parallel stratified sandstones were commonly recognised in association with subfacies 1A conglomerates. Sandstone units are generally volumetrically subordinate to the enclosing conglomerates, however locally they were the dominant lithology. Beds range from 5-40cm in thickness, with stratification defined by alternating bands of fine-sand to granule-sized particles. Discrete bands are tabular to slightly lensoidal and range in thickness from 2-100mm. Grading within beds is complex and no systematic vertical variation in grain-size was observed. Individual coarse-grained bands, however, are commonly symmetrically graded, passing with inverse size grading from underlying finer-grained bands to normally graded tops. No evidence of bioturbation was observed in association with subfacies 2B, however layer disturbance inferred to have resulted from sliding and/or slumping is common. The internal stratification in subfacies 2B is grossly analogous to progressive 'freezing' of inversely-graded traction carpets developed in high-density sandy turbidites

Facies 3: Sandstone-mudstone couplets

Facies 3 consists of couplets of alternating coarse- to fine-grained sandstone and mudstone. The internal structure of sandstone-mudstone couplets shows a wide diversity, however two broad styles have been distinguished.

Subfacies 3A: Normally graded sandstone-mudstone couplets are interpreted to have been deposited from waning high- to low-concentration turbidity currents. They probably represent finer-grained, lateral (ie. inter-channel deposits) or perhaps distal equivalents of coarse-grained sub-facies 1A and 2B. Considering the close lateral and vertical relationships with 'proximal' coarse-grained facies, an inter-channel setting rather than a distal base-of-slope environment is considered most likely for this sub-facies.

Subfacies 3B: Ripple-laminated sandstone-mudstone couplets occur in packages up to 100m in thickness, and contain both mudstone- and sandstone-dominated intervals. Sandstones are generally medium- to fine-grained, moderately- to well-sorted and 'clean', consisting predominantly of quartz with subordinate feldspar, mica, heavy minerals and lithic fragments.

Subfacies 3B sandstone-mudstone couplets are distinguishable from subfacies 3A by their lack of features associated with turbiditic emplacement. In particular, normal grading is absent, or at best weakly developed in only a small percentage of sandstones. Furthermore, the upper surfaces of sandstone beds are invariably sharp and in some cases erosional. Bottom current activity provided an important mechanism for localised erosion and redeposition of these sandstones, however it was unlikely to have been responsible for supply of clastic material to the basin.

Facies 4: Fine-grained sediments

Included in this facies are mudstones and thinly interbedded siltstones. Facies 4 is widely distributed and voluminous throughout the Dundas region and occurs in association with all other facies types. Intervals dominated by facies 4 range from less than 2m to 350m in thickness. Thick, laterally continuous packages dominated by facies 4 reflect periods of relatively low sediment input into the basin. However, the more common occurrence of facies 4 as lateral equivalents of coarser-grained facies indicates that fine-grained sediment was actively depositing even during periods of high sediment influx.

Facies 5: Immature volcaniclastic deposits

Volcaniclastic facies comprise a volumetrically minor but distinctive association of sedimentary deposits. They have a wide spatial distribution throughout the Dundas region, but are restricted to low bio-stratigraphic levels: ie. pre-earliest Late Cambrian.

Subfacies 5A: Feldspathic crystal-rich volcaniclastic sandstone crops out in the Ring River near the Ring Valley mine as two thickly bedded volcaniclastic sandstone units interbedded with laminated dark grey mudstone. The relatively homogenous composition of volcanic debris contained within the lower crystal-rich portion of the unit, combined with crude normal grading and lack of internal bedding or amalgamation surfaces, is interpreted to indicate emplacement from a single depositional event. Deposition from large volume turbulent flows and the lack of evidence for shoreline reworking indicate a subaqueous, below wave-base depositional environment.

Subfacies 5B: Felsic vitriclastic sandstone consist of very thick (10-90m), crudely stratified beds of vitric tuff. Principal detrital components include formerly glassy juvenile volcanic particles including shards and pumice. Crystals and volcanic fragments are subordinate components. They are interpreted as rapidly emplaced mass flows comprising essentially unreworked, but redeposited pyroclastic debris.

Subfacies 5C: Quartz-feldspathic crystal-rich sandstone consists of units of unstratified, poorly-sorted crystal-rich sandstone. It is distinguished from facies 5A crystal-rich sandstone primarily through the presence of abundant detrital quartz, but also by the fact that matrices are composed primarily of mud. The thick, unstratified character of subfacies 5C, coupled with the texturally immature nature of the framework component, indicate that volcanic debris was rapidly resedimented after initial fragmentation of the parental magma, probably as cohesive debris flows or high-concentration turbidity currents.

Subfacies 5D: Basalt fragment-bearing mud-matrix breccia is located in the Ring River at Bonnie Point. The faunal assemblage at this locality is of Mindyallan age (latest Middle Cambrian) (Banks, 1956). Subfacies 5D can be distinguished from the previously discussed volcaniclastic facies by the presence of juvenile basaltic material. Clast shapes

suggests an association with peperitic facies. The only documented coherent mafic volcanic facies of late Middle Cambrian age in the Dundas region occurs 1km SSW of the subfacies 5D unit at Montezuma Falls (Curtin Davis Volcanics: Elliston, 1954; Corbett and Solomon, 1989). Although structural complexity and lack of good, continuous exposure between these two areas prevents a direct chrono-stratigraphic correlation from mapping, both subfacies 5D volcaniclastics and the coherent volcanics have similar geochemical affinities, indicating that they were likely to have been comagmatic .

Geochemical affinities of volcaniclastic deposits

Three distinct geochemical signatures for the volcaniclastic deposits have been identified: i) a felsic magmatic source like the Tyndall Group rhyolitic lavas (subfacies 5B and 5C); ii) a mafic tholeiitic source possessing subtle affinities with suite IV of the Mount Read Volcanics (subfacies 5A), and iii) a shoshonitic source component within subfacies 5D that compares well with both suite III lavas and the local Curtin Davis Volcanics.

6.3 Provenance

Provenance data was collected from siliciclastics located mainly in the Dundas region, with some additional samples from the Que River and Farrell Rivulet . The aim was to identify the nature and location of source regions which were actively supplying clastic material during the Middle and Late Cambrian. Any temporal and/or spatial variation in sediment provenance would allow constraints to be placed on the palaeogeography and structural evolution of the basin. Accordingly, samples were selected from a range of stratigraphic levels and geographic locations.

Fundamental differences in carefully selected chemical and petrological criteria of the analysed sedimentary rocks and in particular, the recognition of distinctive source signatures provide the bases for a first-order classification. Four broad compositional suites have been identified.

Suite 1 samples have a significant component of mafic detritus which showed compositional affinities with the Crimson Creek Formation. These were further subdivided. Suite 1A samples are located in the western area of the Dundas region and the Que River region. They have very high lithic component (>75% of the framework component) and in particular an abundance of sedimentary lithic fragments (between 64-88% of the lithic fraction). Suite 1A samples come from two chrono-stratigraphically and spatially distinct conglomerate-dominated packages. The oldest of these two packages is located on the northern slopes of Black Hill and lies with erosional contact on low-Ti pillowed lavas of the Serpentine Hill MUC . It is of probable Undillan age and is referred to herein as the Black Hill member. The younger package (?Mindyallan to Idamean)

occurs within the type section of the Dundas Group exposed in the Dundas River and totals 500m in thickness.

Suite 1B sandstones have a Crimson Creek tholeiite signature which is variably diluted by 'felsic' material . They are located in the eastern area of the Dundas region They are distinguished from suite 1A by a paucity of sedimentary lithic fragments and a lower degree of textural maturity (ie. poor sorting coupled with lack of abrasion or rounding of much of the framework component). The large component of chemically unstable volcanogenic debris contained in these sandstones suggests that the source was mineralogically immature and essentially unaffected by weathering and/or diagenesis prior to reworking. This feature, coupled with the abundance of texturally immature, monogenetic basaltic detritus (broken feldspar grains and basalt clasts), none of which is contained within reworked sedimentary clasts (cf. suite 1A) is interpreted to indicate a first-cycle origin for the volcanic component. That is, volcanogenic debris was either eroded directly from an older, uplifted volcanic massif, with negligible contamination from sedimentary sources, or derived from a genetically and temporally related phase of basaltic magmatism.

Suite 1C sandstones have an even higher component of 'felsic' source material as shown by moderate to high SiO_2 abundances. Relative to other suite 1 samples, they show a smaller component of basaltic detritus and a higher degree of mineralogical maturity. The resolvable lithic component is small in comparison to other suite 1 sandstones (0-17%) and consists of siliciclastic, 'chert' and volcanic rock fragments. Siliciclastic rock fragments include greywacke, mudstone and quartzose sandstone. Both mafic and felsic volcanic rock fragments were observed.

Cr-spinel data collected as part of this provenance study were derived from four coarse-grained suite 1A samples and two suite 1B sandstones. While the whole rock geochemistry can only identify the Crimson Creek Formation signature in these rocks there are some suite 1A samples with low Ti chromites indicating a substantial component of MUC in the provenance which is swamped in the whole rock chemistry by the more enriched tholeiitic signature of the Crimson Creek Formation.

Suite 2 involves sandstones which are characterised by a mixed sedimentary - basaltic input. Suite 2 comprises polymict conglomerate and lithic sandstone which form part of an easterly facing package in the Kapi Creek-Ring River area The sandstones are poorly sorted and rich in lithic fragments. Quartz is common, comprising up to 30% of the framework component of better-sorted sandstones. Grains are typically poorly-sorted, angular and anhedral, with straight to mildly undulose extinction. Sedimentary clast-types comprise the bulk of the lithic component in suite 2 sandstones and conglomerates. Feldspathic greywacke clasts are locally abundant, especially towards the base of the package. Mudstone, metaquartzite, quartz-mica schist, unmetamorphosed quartz arenite and dolomite fragments are present in variable amounts throughout the

package. Whole rock chemistry and chromites indicate that the MUC are is the likely source of mafic detritus, and this is mixed with a compositionally mature siliciclastic source and/or a felsic volcanic source

Suite 3 rocks involve a broad range of compositions which do not correspond directly with any single source terrain. They are the most widespread in the Dundas region, with data collected from western, central and eastern areas. Samples which were included in this petrographic study were fine- to medium-grained lithic arenites, greywackes and pebble conglomerate. Sandstones contain low to high abundances of lithic fragments and a monomineralic grain component dominated by quartz. Rock fragments include 'cherty' material, mudstone, protoquartzite, carbonate, quartzose- and less commonly feldspathic-greywacke fragments. Metamorphic lithic fragments include metaquartzite, phyllite and 'ribbon quartz'. The diversity and abundance of volcanic fragment-types increases towards the east.

Both sandstones and mudstones are broadly intermediate to acidic in composition. Unlike the dominantly mono-genetic source signatures characterised by suites 1 and 2, the provenance of suite 3 appears more complex with significant contribution from two or more source terrains. Evidence from petrographic studies suggests input of detritus from: i) mature siliciclastic sources ii) basaltic source terrains and iii) minor acid to intermediate volcanic sources.

Suite 4 involves compositionally and texturally mature, sandstones, mudstones and fine-grained meta-sedimentary rocks. Suite 4 samples were collected from the Moores Pimple-Comet Maestries region , a fault bounded block which crops out in the Ring River and the Farrell Rivulet 'quartzwacke'/conglomerate package. The stratigraphic position of some of these units has been the focus of controversy for some years. For instance, the Concert Schist at Moores Pimple have been traditionally interpreted as a basement inlier comprising correlates of the Precambrian Oonah Formation and metasediments of the White Schist (Elliston, 1954; Turner, 1979; Brown, 1986).

The petrographic features of sandstones from all areas are remarkably consistent. Quartz comprises the bulk of the framework component. Feldspar grains are uncommon and include untwinned albite and K-feldspar. Apart from these grains, unstable mineral assemblages such as ferromagnesians are absent. The micaceous component includes muscovite flakes ranging in thickness from <0.01mm to 0.05mm in their shortest dimension and rare books of biotite which have been partially altered to chlorite. Sedimentary rock particles comprise the bulk of the lithic fraction. The heavy mineral assemblage is ultra-mature and includes yellow-green and blue-green euhedral to rounded tourmaline, rounded zircon, minor rutile and rare skeletal opaques.

There is a good chemical correlation between the Oonah Formation and sandstones and mudstones of the Comet area. An additional basic component is indicated

for the Concert Schist, and is also tentatively suggested for the Stitt Quartzite and correlates. The provenance approach failed to convincingly discriminate between suite 4 sandstones of different ages.

Contribution of detritus from sources of mafic composition is apparent in all suite 1-3 samples. The chemistry of those sediments which contain a significant mafic component (ie. suite 1 and suite 2 sandstones) is strongly dependant on the composition of the mafic source(s). Sediments which have most faithfully recorded the compositions of their mafic precursor involve suites 1A and 1B. These all show SiO_2 values $\leq 62\%$ and possess a geochemical signature which can be closely approximated with volcanic facies and volcanogenic sediment of the Crimson Creek Formation. The most distinctive Crimson Creek Formation signature is the high values of Ti (>11000 ppm) and Nb ($\geq$21ppm) relative to other incompatible element abundances.

Identification of MUC-sourced detritus from whole rock geochemical data alone is less effective. This problem is manifested in coarse-grained sandstones from Black Hill and in particular the Que River member (suite 1A). Despite evidence from petrographic features and chromite composition for a significant MUC input in these sediments, incompatible element enrichment has caused the MUC signature to be masked. Although mudstones are less likely to be effected by heavy mineral concentration, MUC signatures are masked in cases where mixing with a more 'felsic' component has occurred. Incompatible/compatible element ratios such as Nb/Ni, Nb/Sc or Th/Sc provide useful indicators of an MUC source. Contribution from mature basement siliciclastics and felsic volcanic sources of the MRV is best established from petrographic analysis.

The provenance data produced some important results for stratigraphic and structural interpretations. Suite 1B siliciclastics are distinguished from other CCF-derived suite 1 members by their textural and compositional immaturity. These features could possibly be explained by derivation from a proximal CCF source which was dominated by coherent volcanic facies but are interpreted here as evidence these rocks are inliers of Crimson Creek Formation. If this interpretation is correct, then other units located in the structurally complex eastern domain may also comprise uplifted slices of basement material (eg quartz-rich siliciclastics of suite 4 may be Oonah Formation).

The western-most exposures of the Dundas Group involve petrographically and chemically similar conglomerate-greywacke-mudstone successions which crop out at Dundas and at Que River to the north (Suite 1A). These are derived principally from basement sources (CCF and mature siliciclastic basement), however minor input from a felsic volcanic source is indicated from the presence of euhedral quartz grains. Contribution from the MUC in the Black Hill and Que River members is evident from low-Ti Cr-spinels, boninitic lava fragments and anomalously low Zr/Cr values. The most volumetrically significant suite 1A deposits include the Brewery Junction, Fernfields and Que River members. These range in age from latest Middle Cambrian to probable Late

Cambrian and represent a marked change in basin geometry characterised by rapid basement uplift. This phase of tectonism and associated sedimentation is slightly older than, to coeval with, the onset of Denison Group deposition further to the east. The Black Hill member is anomalous in that it is appears to be older than other suite 1A siliciclastics.

Deposition of suite 3 siliciclastics occurred during the middle Middle Cambrian in the western domain, but continued into the latest Middle Cambrian in the central domain. During this latter period, suite 1A sediments were being deposited along the western margin of the basin, whereas coeval finer-grained suite 3 sediments occupied central or eastern portions of the basin. This asymmetry in lithofacies distribution from west to east probably reflects proximal derivation of suite 1A conglomerates and sandstones from rapidly uplifted basement sources to the west, with either reworking and mixing of slope sediments or supply of thoroughly mixed sediment along basin axial drainage systems (suite 3) to the east.

6.4 Structural relationships

The earliest deformation (D_1) is characterised by pre-lithification structures including coherent slides along bedding parallel surfaces, chaotic zones of liquefaction, brittle fault zones and folds which contain no axial planar fabric. Regional cleavage development and upright, open to tight folding are associated with the most important deformational event (D_2), which is correlated with the earliest phase of Middle Devonian orogenesis.

The S_2 cleavage is the dominant penetrative fabric developed throughout the Dundas region. It is a moderately to steeply-dipping mesoscopic foliation spaced between 0.1-3mm. Mesoscopic folds related to the S_2 cleavage are rare The folds are upright to moderately inclined and shallowly to moderately plunging, however the trend of hinge lines is quite variable, ranging from NNW-SSE to NE-SW . Folds have both cylindrical and non-cylindrical geometries and the S_2 cleavage (striking between NW to N) is almost always non-axial planar. Despite the spread of S_2 data, the transection of individual folds by S_2 when viewed perpendicular to the hinge is consistently in an anticlockwise sense. The cleavage transection is interpreted to be the result of superposition of temporally distinct, non-colinear fold generations. The earliest fold generation is interpreted to have originally possessed and NNE to NE trend and preceded the D_2 event. Pre-D_2 mesoscopic folds may relate to D_1 pre-lithification slumping, but are best explained a tectonic folding phase prior to D_2.

There are localised zones of gentle refolding (D_3) with or without a weak crenulation cleavage. The regional structure is cut by a large number of faults which have been multiply reactivated.

The macroscopic structural geometry of the Dundas region was analysed in terms of three broad structural domains.

Dundas township domain

The macroscopic structure of the Dundas township domain is relatively simple, with the bulk of the data positioned on the eastern limb of a major D_2 syncline which plunges shallowly towards the SSW and verges to the E. Throughout the Dundas township domain there is evidence of pre-D_2 'irregularities' in S_0 orientation effecting the morphology of the major F_2 syncline (shown mainly in the variable plunge of L_2^0). I suggest that sub-area DT1 (which comprises Middle Cambrian to earliest Late Cambrian strata) records an early phase of deformation (D_1 or at least pre-D_2) which did not involve, or was at best only weakly developed in younger (Upper Cambrian) strata positioned in sub-areas DT2 and DT3. Although unexposed, the boundary between sub-areas DT1 and DT2 is therefore interpreted as an angular unconformity.

Black Hill Domain

The Black Hill domain contains Dundas Group strata of Middle to early Late Cambrian age. The northern boundary with Serpentine Hill MUC is generally faulted, however an erosional contact involving a basal conglomerate package of the Dundas Group is preserved. The southern margin is defined by a sheared contact with the Dundas MUC and an inferred faulted contact with sediments contained in the Dundas township domain. An overall E-W structural grain, defined by the orientation of bedding, distinguishes this domain from the Dundas township domain. Stratigraphic facing is dominantly towards the south, with poles to S_0 spread slightly about a F_2 fold axis which plunges moderately to the SSW. Little evidence exists for post-D_2 folding as indicated by the relatively consistent orientation of S_2. The increase in plunge of F_2, compared to the Dundas township domain, is most likely a primary geometric feature resulting from folding of inclined strata.

Northeast Dundas domain

The structural grain of the northeast Dundas domain has a N to NE trend. This structural grain is manifested by the inferred axial traces of close to tight macroscopic folds. The orientation of the S_2 cleavage does not coincide with major fold axial surfaces however, and on average, strikes anticlockwise of N to NE-trending D_2 hinge lines. Both the tightness of folds and the density of faulting increases towards the east of the domain, where fault-bounded slivers of basement lithologies (MUC and Crimson Creek Formation) are tectonically intermingled with Cambrian strata.

The western margin is defined by a faulted contact with the Serpentine Hill MUC. Strata are closely folded about a series upright closures which plunge shallowly to moderately to the SSW. Projection of the same closure between successive exposures reveals sinuous fold traces. This non-cylindrical geometry of folds indicated from field observations is confirmed by the plot of poles to S_0. Macroscopic folds deviate further

from a simple cylindrical geometry towards the east, where evidence exists for superimposed fold generations. Despite the rather random distribution of S_0 data in the eastern parts of the northeast Dundas domain however, the NNW to NNE strike of S_2 remains comparable with that observed in the west , indicating that post-S_2 deformation (either brittle faulting or folding) cannot account for the geometry of bedding. In the footwall of the Rosebery Fault, strong tectonic dismemberment of upright folds during movement on syn- to late-D_2 NNW to NE striking faults and ductile shear zones has resulted in the annihilation of hinge regions and shearing out of limbs. The Ring River melange represents one of these ductile shear zones and was examined in detail.

The departure from simple fold morphologies is most evident in the northeast Dundas domain. The complex macroscopic cleavage-fold relationships within this domain are also reflected in the geometry of mesoscopic folds. If the mechanism of superimposed fold generations interpreted to explain mesoscopic fold morphology is applied to the macroscopic structural geometry of the northeast Dundas domain, a large-scale pre-D_2 NNE-trending fold generation, previously unrecognised in the Dundas region, can be interpreted. The most likely regional event associated with this early folding is the Late Cambrian E-W compressive phase described in Berry (1994).

Although the pre-D_2 rotation axis associated with late Middle Cambrian to earliest Late Cambrian strata in the Dundas township domain (ie. package 3) roughly coincides with the pre-D_2 NNE-SSW fold trend interpreted within the northeast Dundas domain, the structural geometry in the former domain is unlikely to have resulted from a regional folding event. The confinement of pre-D_2 "deformation" to package 3, coupled with a distinct "fanning" pattern of bedding traces are best explained by primary lateral thickness variations or slumping related to syn-depositional basin-floor rotation, possibly associated with extensional block tilting and half graben development.

6.5 Ring River Melange

Structural relationships in the Dundas region are most complicated towards the east and culminate in tightly folded and disrupted strata positioned within the footwall of the Rosebery Fault. The macroscopic geometry of these rocks is characterised by the dissection of a N-S trending generation of presently upright folds by an anastomosing array of steeply dipping faults . Faulting out of major hinges has resulted in abrupt facing changes between adjacent blocks and in many instances, obscured the original geometry of large scale folds.

The most conspicuous of these 'anomalous' structural elements involves zones of intense disruption in which sedimentary layering is annihilated. These zones range between 5-150 m in width and in most cases have been recognised at the margins of fault bounded blocks. The dominant cleavage in this region (S_2 in this study) is sub-vertical and strikes roughly parallel to the trend of minor folds.

Domains of melange-type deformation are well exposed in the Ring River, approximately 300 m east of the Ring Valley Mine. Although more than 80% of the 400m thick sequence in the Ring River is disrupted, stratally coherent domains are locally preserved and provide the best insight into the lithological character of the unit prior to deformation. The original sedimentary lithologies are interpreted to have been predominantly mudstone with subordinate thickly bedded massive sandstone and thinly bedded sandstone-mudstone multilayers.

The dominant texture common to all disrupted units is partially to completely fragmented sedimentary layers enclosed within a fine-grained and frequently fissile matrix. This 'block-in-matrix' texture is developed at both microscopic and mesoscopic scales, with isolated fragments ranging in size from discrete sand grains to elongate inclusions with cross-sectional areas exceeding 2 m^2. Matrices are always argillaceous and range in coarseness from extremely fine-grained, homogeneous black mudstone to dark grey silty mudstone. All of these lithotypes are represented in the neighbouring coherent domains and there is no evidence to suggest that material foreign to the unit has been incorporated into the disrupted domains. As such, the latter are considered to reflect disaggregation of a single, initially intact sedimentary sequence. This style of deformation has been referred to as broken formation (Hsu, 1974) or Type I melange (Cowan, 1985). The Ring River disrupted zone represents a domain of significant, but localised accumulation of bulk non-coaxial strain resulting from layer-parallel shear.

In areas of low strain, inclusions of roughly equal dimensions and similar composition are commonly arranged in semi-continuous trains. The enveloping surface of these inclusions represents 'bulk' sedimentary layering S_e. Oriented at low to moderate angles to S_e and S_B (generally less than 35°) is a sub-vertical, NNW to N-striking mesoscopic composite foliation. This has two morphologically distinct continuous cleavages forms. The first of these, S_{SL}, is pervasively developed in fine-grained lithotypes, but only crudely developed in coarse-grained, matrix-poor sandstones. S_{SL} is a closely spaced slaty cleavage defined by the moderate to strong preferred alignment of both detrital and recrystallised grains. S_{SL} correlates with the regionally developed Devonian cleavage (S_2). The second continuous cleavage S_{SP} (spaced cleavage) was observed in narrow zones of high strain and cross-cuts S_{SL} with an anticlockwise sense in horizontally oriented thin sections and with a clockwise sense in northerly facing, vertically oriented thin sections.

Ductile shear bands and brittle shear fractures cross-cut S_e, S_{SL} and S_{SP}. In most cases. The shear fractures are commonly polished and slickensided with striations consisting of fine grooves or quartz-chlorite-epidote fibre veins. Two sets of striations were observed on these surfaces, one set plunges shallowly to moderately to the north and the younger set is subvertical.

Folds are rare and characteristically small-scale with wavelengths less than 20cm. There is no evidence for large scale folding within the melange. Commonly only one hinge from a syncline-anticline pair is preserved or was ever developed (usually the synclinal closure). Both S_{SL} and S_{SP} occur as axial planar fabrics to folds.

Partitioning of strain and variation of deformation styles throughout the disrupted domains occurs primarily as a function of the original sedimentary lithotypes. Three broad mesoscopic styles are defined: i) "high strain" phacoid zones , ii) domains of large-scale boudinage and pinch-and-swell structure and iii) chaotic block-in-matrix structure.

The microstructural fabrics of the melange provide valuable information on environmental conditions as well as the physical character of the rock. Inclusions contained within melange domains are characterised by cataclastic textures. Grain breakage is closely related to microstructures formed in response to diffusive mass transfer and crystal plastic processes. Three main styles of cataclastic behaviour have been identified: i) incipient ductile cataclastic flow , ii) brittle failure along extension fractures and shear fractures and iii) transitional brittle-ductile cataclastic flow. The association of deformation processes requires deformation in well consolidated rock with moderate confining pressure and high fluid pressure.

Bulk flattening-type strains in the Ring River melange is indicated by chocolate tablet boudinage structure and development of quasi-synchronous orthogonal extensional vein generations. The favoured interpretation for the development of the Ring River melange involves shearing of tightening and rotated upright, shallowly plunging, NNE to NE trending pre-D_2 folds during oblique imposition of NNW to N striking slaty (S_{SP}) and spaced (S_{SL}) cleavages. The obliquity of these cleavages to bulk sedimentary layering (S_B and S_e) shown in both horizontal sections is interpreted to indicate they transect the axial surfaces of major folds in an anticlockwise sense. The obliquity of sub-vertical fold limbs to the XY plane of the bulk stain ellipsoid during D_2 resulted in the activation of layer-parallel shear zones with a dominant strike-slip component. The S_{SL} cleavage approximated the bulk XY plane during the earliest phase of deformation, but was progressively rotated clockwise due to localised non-coaxial flow within the shear zone. With progressive rotation of tightened folds (hence also the layer parallel shear zones) towards the bulk XY plane, the wrench component of shearing was diminished whereas the dip-slip component was increased. Late in melange development, the S_{SP} cleavage overprinted the S_{SL} cleavage, the latter having become inactive, and a steeply plunging stretching lineation was formed.

Detailed examination of the melange in the Dundas region indicates that the melange textures formed under conditions of intense flattening strains, low effective confining pressure, marked competency contrast and relaxation of along strike boundary constraints to allow stretching in two directions.

6.6 Synthesis

Middle to Late Cambrian sedimentary rocks and minor volcanic rocks of the Dundas Group record a period of vigorous basin activity and marine deposition. Features of the facies architecture, including: i) rapid lateral facies changes, ii) the lack of a coherent vertical stratigraphy, iii) deposition of volumetrically significant, coarse-grained mass flow units within laterally confined channels, iv) numerous chaotic facies associations (ie. debris flows, slides and zones of liquefaction) and v) the abundance soft sediment deformation features indicate that sedimentation occurred, for the most part, on gravitationally unstable basin slopes. Although the association of texturally immature volcaniclastic deposits with the late Middle Cambrian portion of the succession indicate that sedimentation was coeval with the later stages of Mt Read volcanism, the bulk of the detritus contained in sedimentary units was ultimately sourced from proximal, older "basement" terrains. The discovery of an erosional surface between basal Dundas Group conglomerates and underlying basaltic lavas of the MUC refutes the interpretation of Brown (1986) that these two successions are interdigitating. Furthermore, similarities in terms of provenance and sedimentological characteristics between basal and upper parts of the Dundas Group, and the ubiquitous detrital components sourced from autochthonous "basement" terrains, indicates that the suggestion of Berry and Crawford (1988) that the 'lower' Dundas Group was exotic, is erroneous.

Petrographic and geochemical provenance analyses of siliciclastic has been an effective tool in aiding stratigraphic correlation and highlighting both lateral and vertical variation in sediment dispersal systems. The combination of these techniques together with facies and structural analysis reveals a complex basin evolution. Critical interpretations include: i) lack of litho- and/or chemo-stratigraphic correlation between western and central part of the Dundas region during Undillan and Mindyallan stages, and ii) vigorous basin activity and basin-floor tilting during the deposition of package 3 (latest Boomerangian - Mindyallan stage) in the western Dundas region, which culminated in the influx of chaotic facies at the Mindyallan-Idamean stage boundary. These findings form the basis of the basin evolution model shown in Figure 6.1, which interprets the Dundas Group as having formed in series of meridionally-trending sub-basins, now distinguished as western, central and eastern parts of the Dundas region. Only the western and central regions are included in Figure 6.1, as tectonic disruption has obscured the original facies architecture in the eastern region. Although facies analysis has proved largely ineffective in determining basin evolution in the eastern region, four lines of evidence support the inference that the boundary between this region and the central region marks the position of sub-basin margin. Firstly, the pervasive soft-sediment deformation contained in strata exposed at the boundary in the Ring River indicates that it was the locus of syn-sedimentary seismic activity and/or gravitational collapse. Secondly, the boundary can be traced both north and south of the Dundas region where it forms the western limits of

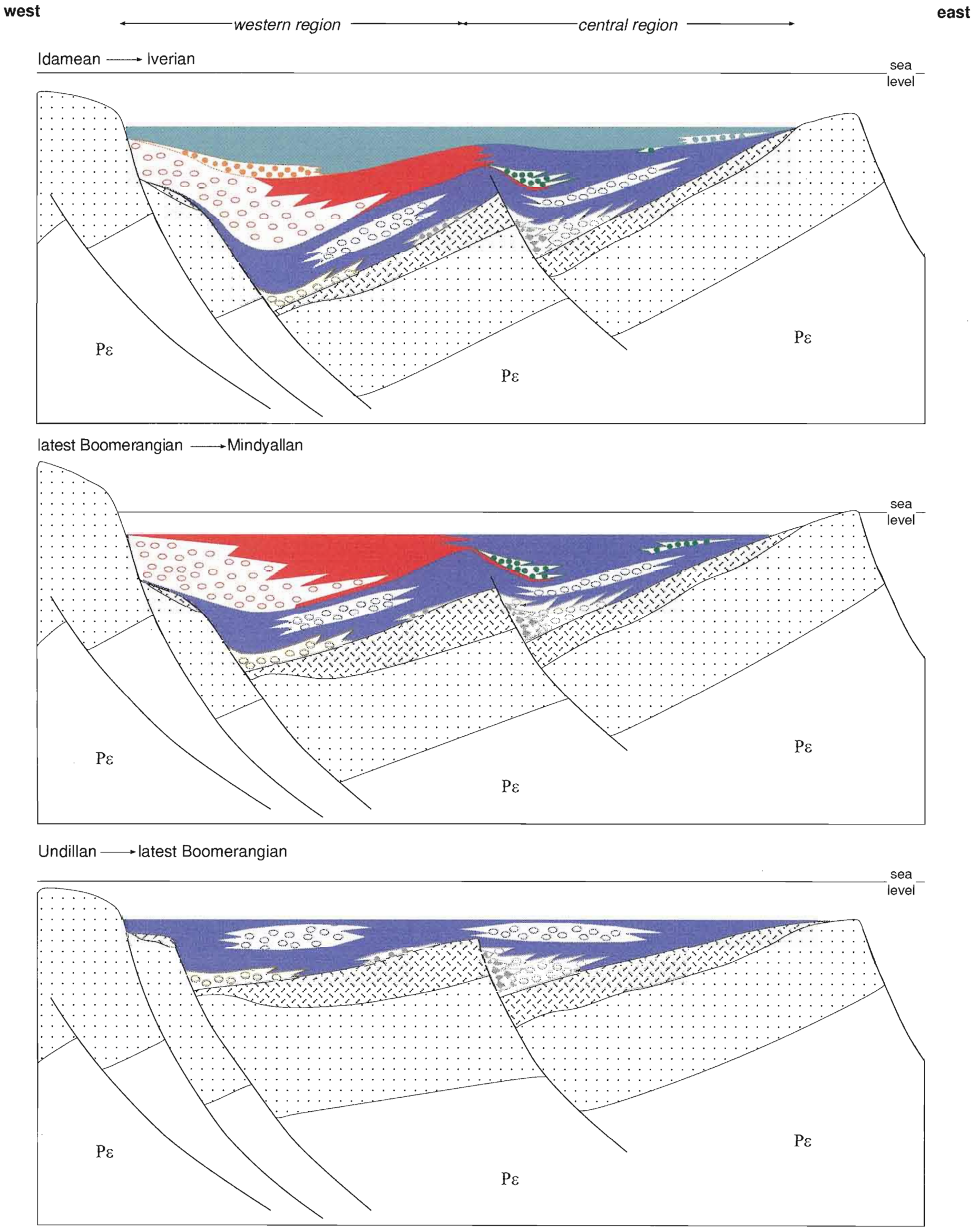

Figure 6.1. Middle to Late Cambrian basin development and facies architecture in western and central parts of the Dundas region.

fault-bounded basement inliers. Thirdly, sub-facies 5A volcaniclastic units, which potentially represent litho-stratigraphic correlates of the Tyndall Group, were recognised only in the eastern domain. Tyndall Group correlates represent a particularly voluminous and widespread succession at higher levels of the western volcano-sedimentary sequence in the east of the Dundas trough, and their absence at similar chrono-stratigraphic levels to the west suggests that westward-directed sediment dispersal was inhibited by a major topographic structure. Finally, the boundary effectively separates western volcano-sedimentary sequence correlates which are underlain to the west by "basement", but to the east, are underlain by, or interfinger with lavas and of the Central Volcanic sequence.

The earliest evidence of sub-basin development is manifested by the difference in provenance and thickness of proximally-derived basal conglomerates (?Undillan) of the Dundas Group. Whereas basal conglomerates exposed in the western region were derived from a mixed Crimson Creek Formation - MUC source, chrono-stratigraphic equivalents in the central region form a considerably thicker interval of conglomerate which was sourced primarily from the MUC, with minimal detrital input from the Crimson Creek Formation (Fig. 6.1). Moreover, the conglomerates in the central region involve an association of MUC-derived breccias, interpreted as talus spalled from a fault scarp, a facies not recognised further to the west. From Undillan to latest Boomerangian stages, sedimentation is interpreted to have transgressed the western region - central region boundary (Fig. 6.1). Strata deposited during this period, possess a complicated and mixed provenance which included both intrabasinal and extrabasinal "basement" sources. The lack of a distinctive provenance signature, coupled with evidence of contourite sedimentation is tentatively interpreted to indicate along basin-axis sediment dispersal patterns which resulted in thorough mixing of several sources. The bulk of volcaniclastic facies, which are most voluminous to the east, were also deposited at this time and correlate with final stages of felsic explosive volcanism associated with the Mt Read volcanic belt.

The latest Boomerangian - Mindyallan stage records the major period of sub-basin activity during deposition of the Dundas Group. Rapid uplift of basement sources to the west was heralded by the massive influx of Crimson Creek Formation-derived material in the western region. In sedimentary rocks of the central region, however, this dominant Crimson Creek Formation signature is largely absent, with a mixed source signature persisting at least until the uppermost Mindyallan. This contrast in provenance characteristics is interpreted to indicate that sub-basins had effectively become separated, each of which was sourcing material from confined sediment dispersal systems. The final stage of "basement" uplift occurred at the Mindyallan-Idamean stage boundary and is marked by deposition of intrabasinally-derived mass flow units and slide sheets in the western region and corresponds with the inferred unconformity between packages 3 and 4.

In terms of the broader picture of Dundas trough development, the Mindyallan stage records the onset of molasse-type Owen Conglomerate sedimentation to the east and the cessation Mt Read volcanism (Seymour and Calver, 1995). According to the models of Berry (1994) and Lees and Wright (1994), deposition of the Owen Conglomerate corresponds to a phase of E-W directed compression and uplift of the Tyennan region along the eastern margin of the Mt Read volcanic belt. Uplift of basement sources in the Dundas region potentially relate to inversion of earlier sub-basin bounding growth faults, as suggested by Selley (1994), however the transition to quiescent marine sedimentation during the Iverian stage, indicated by the thick interval of mudstone-dominated facies in the western region, suggests that sub-basins to the west continued to subside during Owen Conglomerate deposition in the east. Furthermore, there is little evidence to suggest that drainage systems were sourcing uplifted terrains to the east during the Mindyallan stage, as the thickest accumulation of strata of this age occurs along the western margin of the Dundas region. An extensional model, as shown in Figure 6.1, is therefore preferred, in which basement sources were actively uplifted and eroded in response to block rotation on listric normal faults.

Continued subsidence in the west of the Mt Read volcanic belt during Idamean and Iverian stages is interpreted to have submerged local "basement" source areas and starved basins of significant clastic input. This apparent basin deepening probably corresponds to down-flexuring in front of the incipient fold and thrust belt to the east. This interpretation is supported by change from a local Crimson Creek Formation provenance to that of a diluted, compositionally mature basement source signature in Iverian mudstone facies. Although palaeocurrent data is lacking, the fine-grained Iverian succession probably represents a distal marine equivalent of the molasse-type facies depositing in front of the emerging Tyennan region to the east. With subsequent basin closure at the end of the Late Cambrian event, local basement sources again became emergent, with the onset of coarse-grained molasse-type sedimentation in western parts of the Mt Read volcanic belt.

Evidence for probable Late Cambrian compression in the Dundas region has been revealed from analysis of Middle Devonian (D_2) fold geometries. Examination of fold-S_2 cleavage relationships has demonstrated imposition of an ENE-WSW directed D_2 shortening axis on a pre-D_2, NNE- to NE-trending fold generation. Evidence of this fold interference geometry is best developed in central and eastern parts of the Dundas region. Evidence of pre-D_2 folding in the western region may have been obscured due to added complexities related to late Middle Cambrian block rotation. Alternatively, the effects of pre-D_2 folding in strata to the west may have been minimal and accordingly have had little influence on the geometry of macroscopic folds nucleated during D_2. The most dramatic manifestation of obliquity between pre-D_2 and D_2 strain axes occurs in the footwall of the Rosebery Fault, where very tight, upright macroscopic folds have been dissected by N-

to NNE-trending shear zones. Where these shear zones have developed in strata which possessed a well-developed primary stratification and marked competency contrast, domains of melange-type deformation have formed. Conditions of melange-type deformation involve intense flattening strains and low effective confining pressures and are common in accretionary environments, but are not restricted to them. Similar conditions can occur in other upper crustal locations and produce melange from well-consolidated ancient rocks. The spatial relationships in the Ring River and throughout the eastern part of the Dundas region provide no support for the model that this melange was developed in an accretionary environment as suggested by Corbett and Lees (1987).